# Analytical Calibration of the Airborne Photogrammetric System Using *A Priori* Knowledge of the Exposure Station Obtained from Kinematic Global Positioning System Techniques

by

Commander Lewis A. Lapine, NOAA

**Report No. 411**

**Department of Geodetic Science and Surveying**
**The Ohio State University**
**Columbus, Ohio 43210-1247**

**October 1991**

To My Parents
Jack and Selma Lapine
Who Gave Me The Start

and

My Wife and Children
Maryann, Cynthia, and Meghann
Without Whom, I Could Not Have Finished

**ABSTRACT**

The airborne photogrammetric system is a complex combination of measuring tools which form a system used predominantly in most modern mapping programs. Classic aerial photogrammetry relies on the projective transformation of known object space coordinates into the photo coordinate system, enforcing the condition of collinearity, in order to solve for the six unknown parameters of exterior orientation for each photograph. Errors due to the imperfect determination of the system calibration, particularly those errors related to the interior orientation elements of the camera lens system, propagate into the exterior orientation parameters due to the high correlation between the orientation parameters. Three of the exterior orientation parameters are the object space coordinates of the camera exposure station.

In the future, the position of the exposure station will be determined by very accurate navigation systems such as the NAVSTAR Global Positioning System (GPS). Direct measurement of the exposure station position has the potential of minimizing or totally eliminating the requirement for signalized control in the object space. The positions of object space points can be extrapolated from their image coordinates through the known position of the exposure station. The extrapolation accuracy will be highly dependent on the precise calibration of the entire airborne system under normal operating conditions.

Kinematic GPS techniques provide the means to accurately position the airborne system over a dense set of signalized geodetic control points so that the entire airborne can be calibrated in the environment which it normally operates. This research instrumented the calibration technique, analyzed obvious sources of systematic error, and demonstrated the technique by calibrating an airborne system. The lens system, as well as aircraft induced systematic errors, were modelled and verified. Certain systematic errors would not otherwise have been determined by normal laboratory calibrations.

The airborne calibration improved the overall performance of the system. Relative positional accuracies of 5 cm were achieved for targeted object space points. These accuracies were achieved from photography obtained at an altitude of 2100 m above the ground at speeds in excess of 80 meters per second without any knowledge of the object space coordinates.

## PREFACE

This report was prepared by Commander Lewis A. Lapine, NOAA, while a graduate student in the Department of Geodetic Science and Surveying at The Ohio State University. It was submitted to the Graduate School of The Ohio State University in the Autumn of 1990 in partial fulfillment of the requirements for the Doctor of Philosophy degree.

Funding for this research was provided by the National Oceanic and Atmospheric Administration (NOAA), Offices of NOAA Commissioned Personnel, Coast and Geodetic Survey, and Aircraft Operations.

**ACKNOWLEDGEMENTS**

I wish to express my sincere appreciation to Professor Emeritus Dean C. Merchant for his understanding, guidance and constant attention provided throughout the research. Warm appreciation is extended to the other members of my advisory committee, Drs. Clyde Goad and Urho Uotila, for their teaching enthusiasm, suggestions and comments during the research. I wish to thank the Professors and Staff of the Department of Geodetic Science and Surveying who have given me an outstanding education over the past 22 years.

I am grateful to the National Oceanic and Atmospheric Administration (NOAA) for providing the opportunity to perform the research by assigning me to full time university training. I wish to express my appreciation for the aircraft and photogrammetric resources extended to me by Rear Admiral Wesley V. Hull and Captain Christian Andreasen of the NOAA Office of Charting and Geodetic Services. Gratitude is also expressed to the Ohio Department of Transportation, Division of Aerial Engineering for their surveying expertise and support. The technical assistance of James Lucas, Dr. Gerald Mader, David Crump, David Conner , Dennis Hoar, Lloyd Herd, and the NOAA pilots and photographers, is gratefully acknowledged.

To my wife, Maryann, I offer sincere thanks for your loving understanding, unshakable confidence, endless favors and patience during the most trying times of my research. To my children, Cynthia and Meghann, I thank you for giving up your friends in Maryland, your trust and long peaceful bicycle rides.

TABLE OF CONTENTS

LIST OF TABLES

LIST OF FIGURES

# CHAPTER I
# INTRODUCTION

## Overview - Statistical Control

The calibration of any measuring system is achieved through the statistical control of all the processes which make up the system. Statistical control is a rather ambiguous term which may take on many interpretations. For the purposes of this research, statistical control will be defined as the achievement of confidence in a particular result or value obtained through direct or indirect measurement. Even measurements are not necessarily the basic building block of a result or value. Measurements may be composed of a series of observations whose combination yields a single measurement. Confidence is achieved by performing repetitive and redundant observations in the normal operating environment of the airborne photogrammetric system, unbiased by the measuring technique, procedure, or standard.

Three error types can occur when performing measurements of physical quantities: blunders, systematic errors and random errors. One must consider the operating environment in which the measuring process takes place and develop a measuring system to determine, as nearly as possible, the true value of a physical quantity. A valid measuring system will facilitate the repetition of the measurement (precision), detect blunders, model or eliminate systematic, and minimize biases in the remaining random errors.

Statistical control often requires the use of expensive instrumentation with a limited availability (such as the NOAA aircraft) and may have to be obtained from a limited set of observations. Statistical control can be obtained even with the above-mentioned limitation if the observing technique will ensure against systematic errors (leaving a proper mathematical model) and blunders. **Statistical control of the photogrammetric system calibration will be defined as the refinement of all physical measurement processes to a state where measurement errors resulting from blunders are eliminated, systematic errors are modeled, and any remaining random errors will belong to a defined probability density function.** The measurements necessary for the calibration will take place in the operating airborne environment of an airplane, even if the operating environment is seldom conducive for isolating all of the individual error sources.

The airborne photogrammetric system is a complex combination of measuring tools which form a system used predominantly in most modern mapping programs. The calibration of the airborne system is generally accomplished by calibrating only the optical components of the camera subsystem in a laboratory environment. The subsystem approach has two major drawbacks. First, the laboratory environment is quite different from the airborne environment both in terms of the atmospheric conditions and the signal to noise ratio of the measured quantities. Second, the subsystem approach to calibration does not consider the correlated effects that may occur when subsystems interact.

Classic aerial photogrammetry is based on projective transformation of signalized geodetic ground coordinates into the photo coordinate system, enforcing the condition of collinearity in solving for six parameters of exterior orientation (three exposure station coordinates and three rotation angles). Errors due to the imperfect determination of the system calibration are compensated by an effect known as projective

compensation. Projective compensation occurs when high correlation exists between the interior and exterior camera orientation. That is, errors in interior orientation are compensated for by the free parameters of exterior orientation.

In the future, the position of the exposure station will be determined by very accurate navigation systems such as the NAVSTAR Global Positioning System (GPS). Direct measurement of the exposure station position has the potential of minimizing or totally eliminating the requirement for geodetic ground control. Systematic errors in the photogrammetric system will no longer be compensated for in the projective transformation because the image coordinates will be extrapolated to the ground, through the exposure station of the photogrammetric system. The exposure station coordinates will not be treated as free parameters in this case. The extrapolation accuracy will be highly dependent on the precise calibration of the entire airborne photogrammetric system under normal operating conditions.

The ideal method of inflight calibration has met with limited success due to the inability to eliminate the correlation (projective compensation) between the interior and exterior components of the camera orientation. The dependency can be eliminated by accurately determining the exposure station of the camera independent of the photogrammetric solution. Unfortunately, considering the velocity and altitude of the aircraft, the positioning of the exposure station had been beyond the practical capabilities of the current technology.

GPS now offers such an opportunity. This report will describe in detail a complete airborne photogrammetric system calibration combining the GPS positioning technology with modern analytical photogrammetry.

Research Objective

The objective of the research is to use well-established scientific investigative procedures to attain statistical control (defined on page 2) of all the observations in order to study the spatial relationships between the photogrammetric mapping system and the Global Positioning System (GPS) kinematic positioning of the exposure station, define and integrate yet-to-be-determined timing and positional biases between photogrammetry and GPS, and develop numerical models to correct for systematic errors particular to the combined system which effect the *a priori* knowledge of the camera exposure station and the camera's interior orientation as determined in the laboratory situation.

The research objective is verified by calibrating a complete airborne photogrammetric system as installed in the National Oceanic and Atmospheric Administration (NOAA) Cessna Citation II jet aircraft during actual flight conditions over a calibration range at the Transportation Research Center (TRC) in Marysville, Ohio. The TRC is owned by Honda Corporation (managed by The Ohio State University), but formerly established by the Ohio Department of Transportation (ODOT). The calibration is performed by photographing carefully designed and precisely positioned photo targets situated on flat terrain using near vertical photography.

Previous Attempts at Airborne System Calibration

The introduction of GPS information for the exposure station eliminates the correlation between the parameters of camera interior orientation and the parameters of camera exterior orientation in a least-squares adjustment. In the past, two significant attempts have been made to uncorrelate the orientation parameters. Merchant (1971) developed the calibration method of mixed ranges which was accomplished by establishing a calibration range using a combination of flat and

mountainous terrain. The large elevation differences between signalized geodetic control reduce the mathematical dependency between the flying height and camera constant. The location and construction of a mixed range calibration field makes this technique difficult to instrument. The environmental factors may also be significantly different from those encountered in the operational area. Tudhope (1988) developed a technique for use over flat terrain using a combination of vertical and high oblique photography.

This method relies less on the terrain configuration, but requires that the photographs be taken at an attitude which is not normally encountered in most photogrammetric operations. The strain on the camera when inclined to the vertical by 45 degrees may become a dominant contribution to the system calibration. For the purpose of the current research, a calibration range is required over flat terrain as in Tudhope's case. The photography is taken at the normal attitude, flying height and aircraft velocity. The calibration range is designed to facilitate its construction in most normal operating areas. Appendix A contains an unpublished report prepared by the author describing the establishment of such a range. A summary of this report was recently published by the author (Lapine 1990).

GPS Technology

The GPS/photogrammetry calibration is not without its own special considerations. The GPS kinematic positioning technique requires constant carrier phase lock on a minimum of four satellites by two receivers throughout the photo mission. The photo mission cannot begin until the integer number of cycles between each receiver and the visible satellites are determined. This requirement can be satisfied only if a precise geodetic baseline can be instrumented at the airport which will accommodate the aircraft parked over one end of the baseline and the reference ground receiver over the other end. The sparsity of the GPS satellites at the time of the research (1988) confined operations to a two-month period (October-November) during which a minimum of four satellites are above the horizon during periods of adequate sun angle for aerial photography. The four satellite configuration also had to have sufficient geometric strength to allow adequate three dimensional positioning accuracy. By August 1990, nearly four hours of five or more satellite coverage is available from mid-July to late October.

Kinematic GPS Positioning

The NAVSTAR Global Positioning System is a U.S. Department of Defense (DOD) navigation system currently (10/89) comprised of eight Block 1 satellites orbiting the earth in near circular orbits having a radius of approximately 20,000 km from the earth's center of mass. The present constellation provides coverage of 4 or more satellites for a period of approximately 6 hours. The complete constellation of 18 satellites will enable 24-hour three-dimensional world-wide coverage. The GPS navigation system was designed to provide instantaneous positioning with a precision of 10 m, assuming the receiver could decode a protected navigation message. A study by Lucas and Mader (1988) suggested that a positional accuracy of 1 m for the exposure station would be necessary to satisfy accuracy requirements for NOAA's charting program which consists of chart manuscripts at scales of 1:20,000 or smaller produced from 1:50,000 scale photography.

The accuracy required for the exposure station position is obtained by post processing the GPS information from two receivers, one static over a known geodetic position and the other in the aircraft. The technique is known as kinematic GPS positioning. The positional accuracy is obtained from the ability to eliminate certain systematic timing and orbital errors through a double-difference carrier phase solution. The

solution involves solving three double difference observation equations for the three unknown parameters of position for the mobile receiver. This solution depends on *a priori* knowledge of the double-difference integer cycle counts obtained from observations over a fixed baseline or from a procedure known as an antenna swap. The double-difference technique does not depend on the knowledge of the protected message but requires a continuous carrier phase lock on four or more satellites by both receivers during the entire photo mission, including pre- and post-flight calibration. The pre- and post-calibration periods are used to determine, and verify the integer number of double-difference cycles (wavelengths) between the receivers and satellites, respectively. Appendix A contains an unpublished report by the author which describes the kinematic technique in greater detail. Separate studies by Remondi (1984) and Goad (1989) indicate that kinematic GPS positioning using ground vehicles to transport the mobile receiver yields positional precision of 1 cm for unknown marked points relative to a known point. To test the above-mentioned studies, the geodetic control for the photo targets was established by the author using a combination of static and kinematic GPS positioning. A comparison of the kinematic results against selected classic geodetic measurements confirms the findings by Remondi (1984) and Goad (1989). Again, the reader should refer to Appendix A for a more complete discussion. Based on the results of the ground survey, the potential for kinematic positioning of the airborne GPS antenna to an equivalent precision is realistic. In fact, if the total error budget for the exposure station is increased to 3 cm, the determination of principal point coordinates to a precision of 2.5 microns using 1:12,000 scale photography would be possible (refer to Section 6.3.2.a Linear Dependencies). This precision would be most acceptable for a laboratory calibration.

Systematic Errors

The kinematic positioning of the aircraft yields a position for the airborne GPS antenna on a fixed time interval throughout the photo mission. It is necessary to consider several systematic errors which would otherwise contaminate the transformation of the antenna position to the exposure station position. The systematic errors include timing bias between the GPS navigation information and camera exposure station time tags, timing bias between shutter status pulse and actual lens opening, bias in the determination of the spatial offsets between the GPS antenna and camera reference frame, and bias in the interpolation model used to compute the antenna position at the moment of exposure.

In addition to the biases between GPS and the exposure station, aircraft induced biases caused by the optical flat between the camera compartment and exterior of the fuselage, atmospheric refraction, interior camera orientation and film deformation must be identified and modeled. The discussion of systematic errors will consume the major portion of this report.

Previous GPS/Photogrammetry Experiments

Mader (1986) demonstrated kinematic GPS positioning techniques by transporting a GPS receiver and laser altimeter in an Orion P-3 airplane. The elevation obtained by GPS was compared to the laser altimeter readings obtained over Assateague Bay corrected for tides. A 20 cm comparison was obtained. Lucas and Mader (1988) demonstrated the feasibility of the combined GPS/Photogrammetry technology in a test conducted with the Texas Highway Department in 1985. A second practical test was performed by Lucas and the Washington State Department of Transportation. These tests were all performed over flat terrain, targeted for highway mapping projects. The photography was flown at large scale (1:3,000) with the majority of horizontal control centered on the highway route. The tests enabled the development of new software

for processing the GPS using kinematic double-difference techniques and GPS controlled aerotriangulation. Lucas's (1989) and Mader's (unpublished) software were used extensively by the author in testing the results of the system calibration.

Lucas's and Mader's tests, although extremely important for demonstrating the technique of GPS/photogrammetry had their unique problems (hardware deficiencies and control problems) and were not designed for an analytical calibration of the airborne photogrammetric system. NOAA traditionally maps at much smaller scales (1:20,000) using very sparse horizontal and vertical control. In order to test the application of analytical calibration of the airborne photogrammetric system with *a priori* knowledge of the exposure station, a new target field was desired that had well-designed and precisely positioned targets equally distributed across the test field to enable a thorough analysis of the methodology.

At every step of the research, application of accepted principles of instrument calibration were followed. All assumptions were based on sound statistical theory, and tested to ensure that the system would function predictably in the circumstances likely to be found in practice.

Conclusions and Significant Contributions

The discussion of any system calibration should yield conclusions which will improve the overall performance of the measuring process. As mentioned earlier, systems are generally composed of parts, the whole system being made up of the sum of its parts. Likewise, the following report is composed of parts which discuss the system calibration of an airborne photogrammetric system. The parts will be presented in the chronological order of the research project. The discussion will end with an amalgamation of the parts and the manner in which they fit into the system. The calibrated system can then be used for improving the overall performance of the photogrammetric measuring process.

The following items are the most important findings of the research:

1. Definition of Systematic Errors Related to the GPS/Photogrammetry System

    a. Shutter opening to horizon pulse timing bias
    b. Spatial relationship of antenna position to the camera reference frame
    c. Propagate the covariance of the antenna position to the camera exposure station
    d. Interpolation modeling of aircraft trajectory between GPS sampling periods

2. Definition of Systematic Errors in Photogrammetric System

    a. Modeling of aircraft induced systematic errors
    b. Statistical detection of outliers in image coordinate observations
    c. Derivation of an atmospheric refraction model for a pressurized camera compartment independent of atmospheric observations

3. Practical Application of System Calibration

    a. Removal of linear dependency between image-space and object-space coordinates through application of GPS positions for the exposure station

b. Demonstrated camera calibration for nine interior orientation elements
c. Demonstrated sub-decimeter accuracy for aerotriangulation without survey control for block photography

4. Solution for GPS Integer Cycles in the Aircraft Situation

# CHAPTER II
# GEODETIC SURVEY CONTROL

## 2.1 Introduction

The Transportation Research Center (TRC) operated by The Ohio State University was selected as the site for the camera calibration range. The TRC had a previously-established set of photo targets already in place. The targets were established by ODOT and OSU for camera calibration and were previously used by Tudhope (1988). The Union County Airport was selected as the base for aircraft operations. Union County Airport is the nearest airport to the TRC, limiting flight operations to less than 40 km from the ground receiver, and the airport facilities could support the NOAA Citation.

The first step in the calibration process was to select a datum and a point of beginning for the geodetic control to be used for the GPS initialization and positioning of the photo targets. The chosen datum is the North American Datum of 1983 (NAD83). The selection of NAD83 is based on its close approximation to the World Geodetic System of 1984 (WGS84) which defines the GPS reference datum. NAD83 and WGS84 are three-dimensional right-handed rectangular coordinate systems using the conventions defined for the Conventional Terrestrial System (CT). Both systems are earth centered and define semi-major axis and flattening for a reference ellipsoid. The origin of the system is at the center of the Earth's mass. The Z axis is oriented towards the Conventional International Origin (CIO). The X and Y axes are in the plane of the equator. The X axis is aligned with the Greenwich meridian. A slight difference for the two datums lies in the definition of flattening. For distances up to thousands of kilometers, the difference in flattening is negligible. Since all survey control will be defined relative to the point of beginning, the difference between the two datums is of no consequence to the relative accuracy between survey points.

The point of beginning for all geodetic surveys will be established on NAD83 datum. Union County Airport has a geodetic station, MARYPORT 1986, established by the National Geodetic Survey using GPS. The station coordinates are published on the NAD83 datum. The point of beginning, therefore, is satisfactory for initializing the GPS receivers prior to flight operations as well as serving as the point of beginning for all survey operations.

## 2.2 Airport Survey

The following information was contained in an unpublished draft report by the author to the ODOT Bureau of Aerial Engineering.

### 2.2.1 Purpose

The purpose for the survey is to provide geodetic control within the boundary of the Union County Airport for combined GPS and photogrammetry operations. Three new stations were established. One new station was established on the centerline of the East taxiway and used for pre and post-flight initialization of the airborne GPS receiver. Two other stations were located 30 m east of the East taxiway and used for locating up to two different ground based GPS receivers. Precise knowledge of the spatial relationship between these stations was necessary for resolving the GPS baseline components between the aircraft and ground receivers. The baseline components enable the determination of the double-difference integer cycle counts for the four GPS satellites.

2.2.2 Origin

The origin for all navigational and geodetic control for the aircraft and photo targets is located at the Union County Airport. The selected point of beginning is MARYPORT 1986, previously positioned by the National Geodetic Survey using GPS methods. The station is part of the National Geodetic Survey ADAM Network established at approximately 1800 airports to provide a uniform datum for aircraft navigation in the United States. At my request, NGS agreed to hold the coordinates for MARYPORT 1986 fixed in subsequent regional adjustments. The following published coordinates for MARYPORT 1986 on NAD83 were held fixed throughout the research:

| | |
|---|---|
| MARYPORT 1986 | Latitude 40/13/29.89678 N |
| | Longitude 83/21/03.28907 W |
| | Ellipsoid Elevation 272.2 M |

Note that the Cartesian coordinates are expressed in the more familiar ellipsoidal elements of latitude, longitude and elevation. The elevation in this case is referenced to the ellipsoid rather than the geoid, the difference being, the geoidal undulation. When comparing ellipsoidal elevations to the more common orthometric elevations obtained from classic spirit leveling, the geoidal undulation must by applied. The computed geoidal undulation for station MARYPORT 1986 is -34.1 meters using the Rapp 360 Model, therefore, the computed orthometric elevation would be 306.3 meters. Since all future work would be done with GPS instrumentation, and since analytical photogrammetry is most adaptable to Cartesian coordinate systems, all elevations are referenced to the ellipsoid.

The initial azimuth control is computed from MARYPORT 1986 to MARYPORT AZIMUTH 1986. The second station was also positioned by GPS as part of the ADAM Network and held fixed in the regional adjustment.

| | |
|---|---|
| MARYPORT AZIMUTH 1986 | Latitude 40/13/32.00595 N |
| | Longitude 83/20/40.59904 W |
| | Ellipsoid Elevation 269.4 M |

2.2.3 Accuracy Requirements

Classic geodetic ground survey methods were used to extend control within the boundaries of the Union County Airport. Third Order Class I Federal Geodetic Control Committee (FGCC) Standards were followed for horizontal control and for the monumentation on the active taxiway. Third Order FGCC Standards were followed for vertical control ties from a First Order bench mark in Marysville, to and within, the Union County Airport. The beginning point of the level line was NGS Bench Mark T37 1933, which is part of a First Order Level Line 101. The ending bench mark was Union County Mark 052, which is part of a Second Order County Network of Vertical Control tied to the NGS First Order Network. Although the leveling forms a loop using orthometric elevations, the orthometric elevations were used only for computing closure. The elevations within the airport are referenced to the ellipsoidal elevation of MARYPORT 1986 and orthometric elevation differences from the leveling. Any error due to a geoid slope relative to the ellipsoid between stations at the airport should be quite small (less than 2 centimeters as predicted from the Rapp 360 Model) considering a maximum horizontal separation of 200 meters between Maryport 1988 and any other station.

The order and classes were chosen based on the relative accuracies required, available equipment, and existing monumentation quality. GPS integer cycles are approximately 19 centimeters in length, therefore, the GPS baseline components necessary to resolve the integer cycle

biases should be known well enough to eliminate any cycle ambiguity. From past experience, cycle ambiguity is suspected at a 0.3 cycle level, or 6 centimeters. Using the published precision for the available instrumentation and a centering tolerance of 2 millimeters, the theoretical horizontal error was propagated through the mathematical model of the designed traverse loops. The largest error ellipse (95 percent) had a semi-major axis of 2.8 centimeters, with a semi-minor axis of 0.4 centimeters at the 3 sigma level. The software used for this determination was previously developed by Uotila (1973) and Lapine(unpublished). All three new points should be determined within a tolerance of 0.15 cycles and within the limits of horizontal standards for Third Order Class 1 of 1:10,000 for survey traverse closure (the traverse length was 390 meters for a projected closure of 3.9 centimeters).

2.2.4 Mensuration

The horizontal survey (Figure 1) was originally performed on October 17, 1988 and repeated on April 24, 1989. New stations established include TAXI, NPT, and SPT. TAXI is PK nail driven in the tarmac centered on a yellow guideline. TAXI is used to initialize the aircraft GPS receiver. A second point, TACK ,a PK nail set in the center of the guideline, marks the geodetic azimuth for the guideline. Any eccentricity between the aircraft antenna and TAXI can be directly related to NAD83 using the azimuth of TACK. Stations NPT and SPT are used to locate the ground GPS receiver and, as such, form one end of the baseline for kinematic GPS aircraft positioning. NPT and SPT were originally marked by survey tacks driven into wooden survey stakes. The marks were subsequently replaced after the April 24 survey with stainless steel rod marks designed for greater three-dimensional stability. The new marks were located on April 26, 1989 and determined to be within several millimeters of the original marks. All reduced observations and positions are listed in Table 1.

Horizontal survey operations began by observing horizontal directions and Electronic Distance Measurements (EDM) from MARYPORT 1986 using a WILD T-2 Theodolite and Hewlett Packard 3808 EDM instrument on October 17, 1988. A Wild T-2000 and DI3000S EDMI were used on April 24, 1989. A check angle was formed by observing a horizontal angle between MARYPORT AZIMUTH 1986 and MARYSVILLE NESTLES FOOD STACK 1933. The observed angle was compared against inverse position computations based on NAD83 positions. A check of 4.0 sec was obtained. This check angle was not repeated on the April 24, 1989 survey. Angles and distances were measured during both occupations to MARYPORT AZIMUTH 1986, TAXI, NPT, and SPT. During the April 24, 1989 and April 26, 1989 surveys, angles and distances were measured at TAXI with the T-2000 and a combination of DI5S and DI3000S EDM instruments to NPT, SPT, and MARYPORT AZIMUTH 1986. Taped distances were measured between NPT and SPT. A single angle from TAXI to TACK was observed on October 17, 1988 and April 24, 1989. The distance was taped on the latter occupation. All directions were observed four times from MARYPORT 1986 and two times from TAXI. All electronically measured distances were measured ten times (same setup) without instrument-applied corrections. Barometric pressure temperature and relative humidity were recorded during electronic distance measuring sessions. All tripod, instrument, reflector, and signal heights were measured before and after observations. Standard NGS recording procedures were followed. During leveling operations, collimation tests were performed daily to ensure the proper operation of the leveling instrument. A Wild N 2 compensator level was used for single-wire leveling between bench marks. Closed loops or direct ties between bench marks of the same line were used for checks.

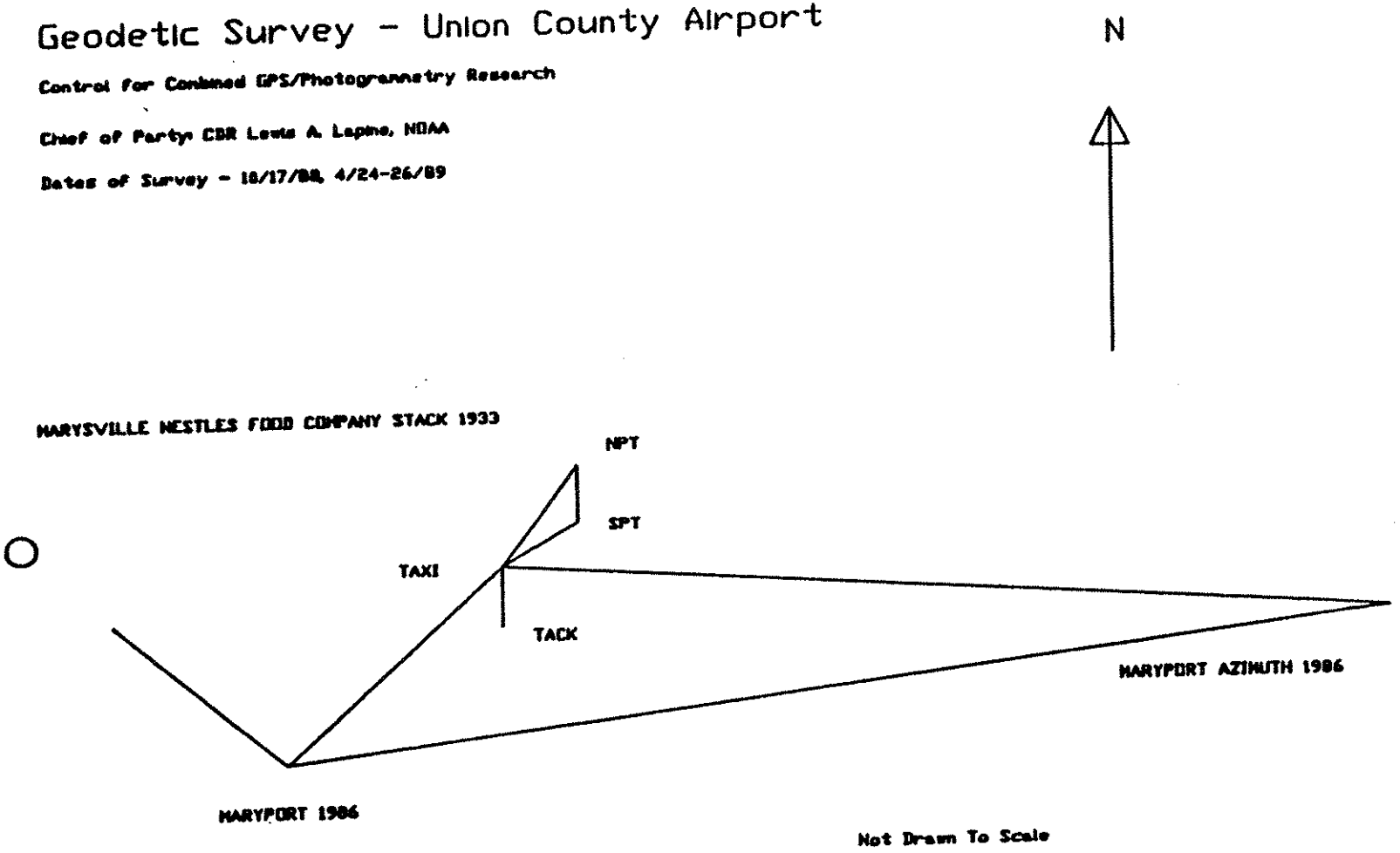


Figure 1

Figure 1. Geodetic Survey - Union County Airport

2.2.5 Computations and Results
All horizontal directions were checked, meaned to a common initial of MARYPORT AZIMUTH 1986. All electronically measured distances were corrected for scale and meteorological conditions and reduced from slope to geodetic distances. The appropriate reduction formulas were obtained from the equipment manufacturer's operating manuals. All taped distances were reduced to geodetic distances. All leveling observations were checked and used without any adjustments.

Three Side-Angle-Side (SAS) computations were computed. The results are shown on Figure 2. The misclosure was less than 2 millimeters for all three SAS computations. As a result of this close agreement, no further mathematical adjustment was made to the data. The above procedures and redundancy are assumed sufficient for attaining statistical control of the survey control within the airport.

All positions were computed from MARYPORT 1986. Elevations for the stations originate from the published ellipsoidal elevation of MARYPORT 1986 with differential orthometric elevations applied directly from the leveling results. The Rapp 360 Model was used to compute the geoidal undulation for MARYPORT 1986. A difference of 0.48 meters was found between the orthometric elevation as determined from the leveling and the Rapp 360 Model. The Rapp 360 Model predicted 0.02 meter geoidal slope throughout the airport.

The positions computed from the October 17, 1989 and April 24, 1989 surveys agree quite well, with the exception of station SPT which differs by 1 cm and which was used on Day 301 for kinematic aircraft positioning. The latest position was accepted because the earlier determination had insufficient redundancy to confirm the position as measured. The latest position also yields slightly improved estimates for the GPS integer biases determined from the known baseline SPT to TAXI, a baseline length of approximately 30 m.

On April 25, 1989, new monumentation was set for NPT and SPT. The monuments consist of stainless steel rods driven to refusal and capped with ODOT rod marks. The rod marks are stamped with the appropriate station designation. The rod marks are surrounded by Poly-Vinyl-Chloride (PVC) cases and topped by an aluminum cover. On April 26, 1989 TAXI was reoccupied with a Wild T-2000. The new monuments were re-surveyed and found to be within 5 mm of the April 24, 1989 survey. New positions were computed for the April 26, 1989 observations. These positions should be adopted for future work.

2.3 Calibration Range and Target Survey
The following information highlights the geodetic control operations performed in order to establish positions for the photo targets at the TRC on NAD 83. For more detailed information on the field work and techniques, the reader is referred to Appendix A.

2.3.1 Survey Design Considerations
The calibration range geodetic control consists of two unique surveys, one employing static and the other employing kinematic GPS technique. The static survey uses static GPS observations from three receivers (one receiver at MARYPORT 1986, two receivers at the TRC) to measure baselines between the Union County Airport and two primary geodetic control stations at the TRC. Two additional static baselines were measured within the TRC to establish a third geodetic station also referenced to MARYPORT 1986. The kinematic survey within the bounds of the TRC established the positions for all the photo targets. The kinematic survey served two purposes. The first purpose satisfies the

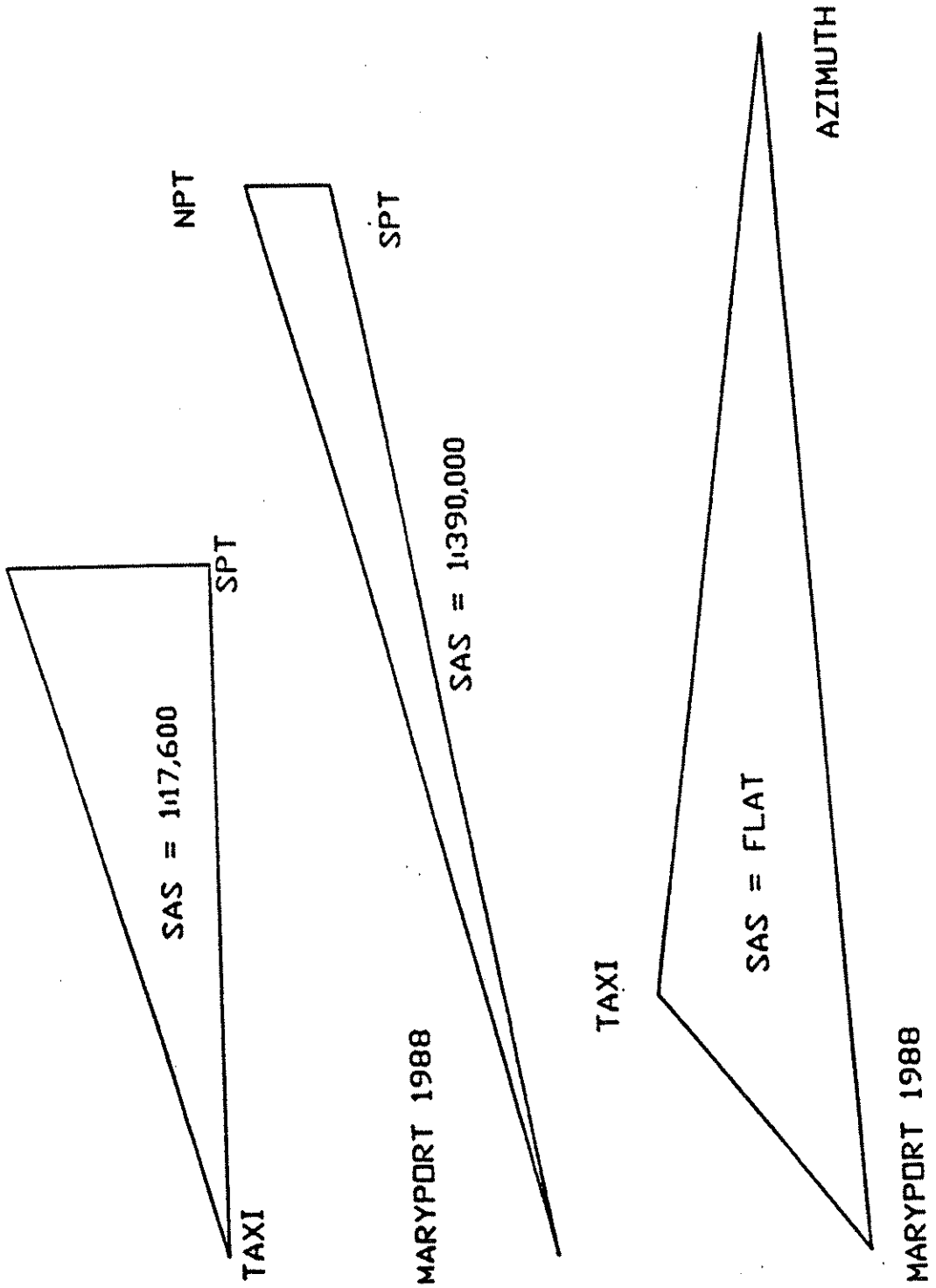


Figure 2. Side-Angle-Side Computations

Table 1 -- Summary of Observations and Results for the Geodetic Survey at the Union County Airport

| | | |
|---|---|---|
| Published Control: | MARYPORT 1986 (NAD 83) | |
| | Latitude: | 40/13/29.89678 N |
| | Longitude: | 83/21/03.28907 W |
| | Elevation: | 272.2 M |
| | MARYPORT AZIMUTH 1986 (NAD 83) | |
| | Latitude: | 40/13/32.00595 N |
| | Longitude: | 83/20/40.59904 W |
| | Elevation: | 269.4 M |
| | MARYSVILLE NESTLES FOOD COMPANY STACK 1933 (NAD 83) | |
| | Latitude: | 40/13/47.61609 N |
| | Longitude: | 83/22/29.64177 W |

| Horizontal Directions | October 17, 1988 | April 24, 1989 |
|---|---|---|
| MARYPORT to MARYPORT AZIMUTH: | 000/00/00.0 | 000/00/00.0 |
| MARYPORT to STACK | 201/54/45.8 | |
| MARYPORT to TAXI | 338/58/47.1 | 338/58/51.6 |
| MARYPORT to NPT | 339/05/59.0 | 339/06/01.6 |
| MARYPORT to SPT | 339/55/10.6 | 339/54/59.7 |
| TAXI to MARYPORT | | 000/00/00.0 |
| TAXI to NPT | | 180/41/06.9 |
| TAXI to SPT | | 185/26/37.8 |
| TAXI to MARYPORT AZIMUTH | | 209/05/54.2 |
| TAXI to TACK | 290/01/40.8* | 290/01/58.4 |
| | | April 26, 1989 |
| TAXI to MARYPORT | | 000/00/00.0 |
| TAXI to NPT | | 180/41/15.8 |
| TAXI to SPT | | 185/26/46.2 |
| TAXI to MARYPORT AZIMUTH | | 209/05/57.9 |

| Geodetic Distances: | October 17, 1988 | April 24, 1989 |
|---|---|---|
| MARYPORT to MARYPORT AZIMUTH | 540.383 | 540.398 |
| MARYPORT to TAXI | 156.167 | 156.170 |
| MARYPORT to NPT | 189.225 | 189.233 |
| MARYPORT to SPT | 188.494 | 188.502 |
| NPT to SPT | 2.800 | 2.789 |
| | April 24, 1988 | April 26, 1989 |
| TAXI to MARYPORT | 156.173 | 156.177 |
| TAXI to MARYPORT AZIMUTH | 398.575 | 398.580 |
| TAXI to NPT ** | 33.070 | 33.074 |
| TAXI to SPT ** | 32.457 | 32.452 |

Table 1 -- Continued

Adopted Coordinates (all work prior to April 25, 1989):

| | | |
|---|---|---|
| TAXI | LATITUDE: | 40/13/32.26874 N |
| | LONGITUDE: | 83/20/57.45324 W |
| | ELEVATION: | 271.48 M |
| NPT | LATITUDE: | 40/13/32.75959 N |
| | LONGITUDE: | 83/20/56.20991 W |
| | ELEVATION: | 271.62 M |
| SPT | LATITUDE: | 40/13/32.67125 N |
| | LONGITUDE: | 83/20/56.18498 W |
| | ELEVATION: | 271.63 M |

Adopted Coordinates (All work subsequent to April 25, 1989):

| | | |
|---|---|---|
| NPT | LATITUDE: | 40/13/32.75969 N |
| | LONGITUDE: | 83/20/56.20957 W |
| | ELEVATION: | 271.54 M |
| SPT | LATITUDE: | 40/13/32.67116 N |
| | LONGITUDE: | 83/20/56.18501 W |
| | ELEVATION: | 271.51 M |

* Computed
** Wild DI5S, all other EDM - Wild DI3000S

---

requirement to position the photo targets using NAD83 as the reference datum. The targets were initially positioned by classical techniques using a local three-dimensional Cartesian coordinate system. The local datum could be transformed to a world reference datum with sufficient statistical control only if a number of the survey points were positioned by GPS. The second purpose satisfies the need to verify that the kinematic GPS technique would yield the required precision of 1 cm as predicted by Remondi (1984) and Goad (1989).

2.3.2 Geodetic Tie to Airport

As we discussed earlier, the survey control consists of two networks connected by GPS static baselines. These networks are located within the Union County Airport and in the vicinity of the TRC. The networks are separated by approximately 19 km. Three static baselines were measured between MARYPORT 1986, TRC8 and TRC31 in June, 1988. The misclosure of the 36 km traverse was 3 mm or 0.1 parts per million (PPM). The baseline between MARYPORT 1986 and TRC8 was re-measured in June, 1989 as a confirmation of the earlier determination made in June, 1988. Both observing sessions lasted approximately 2.5 hours, however the first session had a maximum of five satellites per epoch, while the second session had nearly 40 minutes of seven satellites per epoch. The baseline slope distance is 19358.522 m as determined from the original observation. The second determination of the baseline slope measurement differs by only 0.0014 m! The East, North, and Up components differ by 0.011 m, -0.018 m and -0.007 m, respectively. The normal section azimuths differ by only 0.2" while the vertical angles between the two stations differs by 0.1". The two measurements agree well enough

(1:14,000,000) suggesting that there are no gross errors in the connection of the two networks as a result of the baseline ties.

A third primary station, TRC3, was established by static GPS baseline observations. TRC3 and TRC8 were used exclusively as the starting points for all kinematic GPS traverses used to position photo targets. All photo target positions are connected to the point of beginning by a combination of static and kinematic GPS traverses on the NAD83 datum.

2.3.3 Kinematic GPS Observations

The kinematic survey served the purposes of gaining familiarity with the kinematic techniques which would ultimately be applied to the positioning of the aircraft GPS antenna in flight, gain an estimation of the potential precision of the technique, and obtain sufficient information to transform the local Cartesian coordinates of the existing survey into the NAD83 datum. The kinematic technique was so successful that a transformation between the local datum and NAD 83 was abandoned in favor of re-positioning all 25 existing targets. Eight new targets were also positioned along U.S. Route 33 enlarging the existing calibration range in order to accommodate the operating altitude of the NOAA aircraft.

The photo targets were positioned by transporting the mobile receiver by truck between selected photo targets. Different combinations of traverses and targets were attempted to test the repeatability of the kinematic measurements.

2.3.4 Analysis of Results

The GPS determined positions for the photo targets were used to compute horizontal distances, horizontal angles, and elevation differences between adjacent photo targets. These GPS derived distances, angles, and elevation differences were compared to the adjusted distances, angles and elevation differences obtained from the classical geodetic survey. The classical geodetic survey (performed to Second Order Federal Geodetic Control Committee (FGCC) standards) serves as the standard against which the GPS kinematic results can be compared. The photo targets were spaced at distances of 550 m or 275 m. Tables 18, 19, and 20 in Appendix A give the results of the comparisons. If it is assumed that the standard deviations in the tables are unbiased, they will represent the accuracy estimates for the measurements. It is clear that the kinematic GPS technique yielded a horizontal accuracy of 1 cm as suggested by Remondi (1984) and Goad (1989). It is also apparent from Table 20 in Appendix A, that the determination of elevation has an accuracy of 3 cm. The results are summarized in the following Table 2.

Table 2 -- Comparison of Distances, Angles and Elevations Between the Classic Geodetic Survey and GPS Kinematic Survey of Photo

Control Stations at the TRC

| Measurement | Number of Comparisons | Mean | Sample | Std Dev |
|---|---|---|---|---|
| Distances | | 29 | -0.1 cm | 0.8 cm |
| Angles | | 16 | 1.1 " | 3.3 " |
| Elevations | | 34 | -34.225 m | 2.9 cm |

## 2.4 Aircraft Survey

The "geodetic" control survey within the confines of the aircraft is better defined by the science of metrology. Standard geodetic surveying tools were combined with special measuring devices to determine the spatial offsets between the aircraft GPS antenna, a reference point on the airframe, and the camera reference frame defined by the fiducial coordinate system. As in all other aspects of the research, careful attention was paid to the mensuration techniques to ensure that statistical control was being achieved.

### 2.4.1 Survey Design Considerations

The geometric relationship between the local reference frame of the camera (as defined by the fiducial system and related to the aircraft) and the GPS antenna phase center (as defined in WGS 84 coordinate system) must be established in order to compute the kinematic GPS position of the camera exposure station. The vector between the camera exposure station and antenna phase center can vary as the camera is allowed to rotate in its mount while the GPS antenna is fixed to the aircraft frame. For this research, the camera was leveled and locked in the mount throughout each flight line in the photo mission. A three-dimensional orthogonal transformation between the local (camera) and world coordinate systems can be defined by a set of three rotations and translations. The requirement to define the three rotations can be minimized during the initial measuring process by defining a coordinate system whose axes are parallel to both camera and antenna systems. The resultant coordinate system can be defined relative to the camera or the aircraft, but in either case, the local gravitational vertical is used to relate the coordinate systems. NOTE: WGS 84 rectangular coordinates can be transformed into a local vertical system which closely approximates the local gravity vector. The difference being the deflection of vertical. Two different measurement procedures were used. The first procedure defines the coordinate system relative to the camera fiducial system. The second procedure defines the coordinate system relative to the aircraft. A by-product of both methods is the definition of a vertical offset point on the belly of the aircraft that lies on the local vertical projection of the antenna phase center. The vertical offset of the phase center is used to determine the eccentricity of the aircraft GPS antenna and the baseline initialization point (TAXI).

### 2.4.2 GPS Antenna to Airframe

The NOAA Cessna Citation II jet aircraft has been specially modified to carry two Wild RC-10 metric aerial cameras. The cameras are mounted athwartship of one another just aft of the entrance and emergency hatches to the aircraft. The choice of antenna mount location was left up to the author. It was decided to install the antenna on top of the fuselage as close to the cameras as possible to minimize the length of the spatial offsets between the camera and antenna. The low-wing design of the NOAA Citation ensured that the GPS signal would not be blocked by the wings if banking angles were kept to less than 15 degrees. The vertical stabilizer, although significantly higher than the GPS antenna, did not block the GPS signal. It is hypothesized that the stabilizer is thin enough to allow the GPS signal to "bend" around the obstruction. The selected location for the GPS antenna was compromised slightly to enable the simultaneous observations from two theodolite stations to the antenna phase center, and its vertical projection inside and underneath the aircraft.

After the antenna was installed, the aircraft was flown to Union County Airport. The aircraft was parked on a section of tarmac making the aircraft as level as possible. The leveling was judged satisfactory as indicated by a carpenter's level striding the GPS antenna. The author,

assisted by personnel from NOAA, set up two Wild T-2 theodolites, one on each side of the aircraft. The collimation of each theodolite was checked prior to the measurements. Proper collimation would ensure that the line of sight instrumented by the theodolites would not shift horizontally as the instrument was plunged. The theodolites were positioned forward of the GPS antenna on either side of the aircraft. Furthermore, the theodolites were positioned so that the lines of sight to the antenna intersected at approximately 90 degrees. The theodolite setup accommodated a line of sight through both aircraft hatches to the vertical projection of the antenna center. The theodolites intersected the center of the antenna (as defined in the side view of the GPS antenna, Figure 3), and then were plunged down to intersect the vertical extension of the antenna on the overhead of the interior of the aircraft by sighting through the open hatches. The theodolites were plunged further to intersect the vertical extension of the antenna on the belly of the aircraft. In each sighting, a well-defined target was observed. The antenna center was marked by a pencil point that rested on the indicated antenna phase center. The vertical projections were defined by a plumb bob string stretched tautly by a 16-ounce plumb bob. The vertical extensions were marked by a red indelible marker. The intersections were repeated several times to ensure the precision of the pointings. Both vertical extensions are critical for defining the spatial relationships between the antenna, airframe and camera.

With the aircraft still level, the vertical height from the tarmac to the top of the antenna was determined. A section of a level rod was laid horizontally across the GPS antenna so that the ends projected equal distances over each side of the fuselage. A second section of the level rod was laid horizontally on the tarmac directly below the section laid across the antenna. The second level rod section was used to eliminate the unevenness of the tarmac. The level rod on top of the antenna was made perpendicular to the local vertical by using a carpenter's level. Vertical measurements between the two rod sections were obtained several times. Corrections were made for the eccentricities introduced by the width of the level rods. The difference between the vertical measurements taken on the port and starboard sides of the aircraft is a function of the slope of the tarmac, which was assumed to be linear over the short distance. The vertical measurements from either side were meaned to yield the height of the antenna phase center. The height from the tarmac to the belly of the aircraft on the vertical extension was also measured. The heights could be verified independently due to the cylindrical shape of the fuselage whose diameter can be obtained from drawings, and verified by measuring between the open hatches. These diameters could be compared to the antenna height measurements after removing the eccentricities of the antenna to fuselage and tarmac to belly. Table 3 lists the obtained comparisons:

Table 3 -- Comparison of Three Independent Methods for the Determination of the Aircraft Diameter

| | |
|---|---|
| Aircraft Diameter from Drawings: | 1.624 m |
| Aircraft Diameter from Hatch to Hatch: | 1.625 m |
| Aircraft Diameter from Antenna Height Measurements: | 1.624 m |

Table 3 confirms the accuracy and precision of the determination of the height of the GPS antenna assuming that the engineering drawing is a standard for comparison.

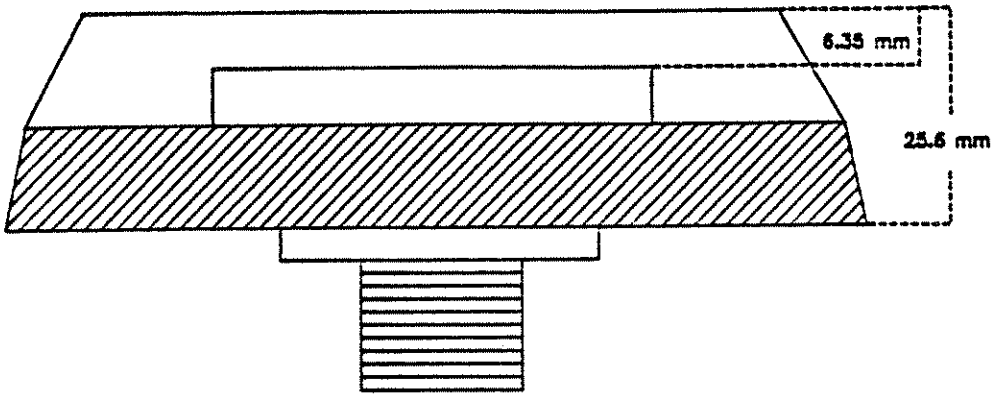


SIDE VIEW OF GPS ANTENNA

Figure 3. Side View of GPS Antenna

2.4.3 GPS Antenna to Camera

The coordinate system chosen for this investigation is an orthogonal right-handed system with the vertical axis parallel to the local vertical as defined by a plumb line. The coordinate system is instrumented after approximately leveling the aircraft frame (+/- $1^0$) and precisely leveling the camera registration frame. The camera registration frame now defines the horizontal plane of the reference system. Any effect of not precisely leveling the aircraft will be discussed later. The camera flight line axis is adjusted nominally parallel to the aircraft frame by setting the camera mount swing angle to zero degrees. The coordinates for the antenna phase center in terms of the camera fiducial marks can now be defined by a set of spatial offsets which are parallel to the common axes (Figure 4).

The spatial offsets defined above are most advantageous for several reasons. First, most aerial photography used for photogrammetric mapping is taken in the near vertical attitude which requires the camera registration frame to be leveled to the local vertical.

Second, the local vertical of the registration frame can be easily instrumented during the measuring of the spatial offsets, and minimizes the requirement for leveling the entire aircraft as might be required for other reference systems. Third, the camera registration frame which contains the fiducial marks will be used during the aerotriangulation process to relate the photo-image coordinates to the survey control. The spatial offsets, therefore, directly relate the world coordinates of the GPS antenna phase center to the fiducial coordinate system.

The GPS antenna was purposefully installed as close to the camera mounts as possible to limit the length of the spatial offsets. In particular, the displacement (0.25 m) of theantenna in the nominal flight direction was minimized as much as possible considering the structure of the aircraft. The displacement thereby minimizes the error in aircraft pitch (phi rotation) on the vertical spatial offset. A pitch correction will be applied based on the pitch angle observed during flight operations, but this measurement can not be determined with certainty to better than $1^0$. A phi angle of $1^0$ amounts to less than 5 mm of displacement between the antenna phase center and the camera exposure station.

$$0.250 \text{ m} * \sin(1) = 0.004 \text{ m}$$

Prior to the start of the measurement process, the aircraft pitch and roll errors (phi and omega rotations) are minimized by selecting a parking spot on a level portion of the tarmac. The aircraft can now be made level by adjusting the tire air pressure. During flight operations the pitch angle can be measured to $1^0$ with an inexpensive hand-held inclinometer, once again minimizing the effect of a small error in the determination of the pitch angle. The inclinometer used during actual flight operations was installed on the aircraft and observed to read $0^0$ while the spatial offsets were being measured and the aircraft was level. Any change in pitch angle recorded in flight represents the change in pitch and a resulting change in the spatial offsets subsequent to their determination.

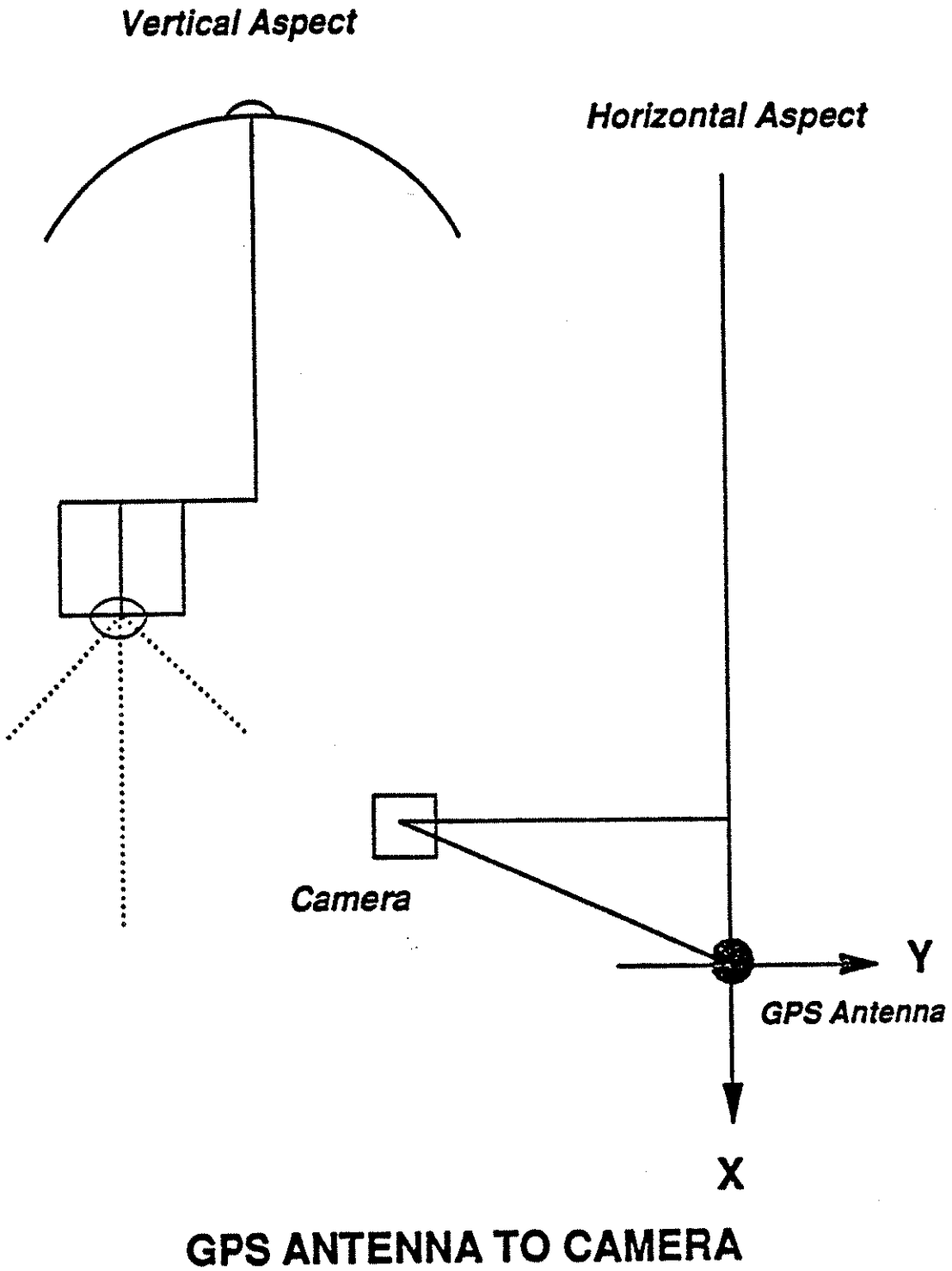


Figure 4. GPS Antenna to Camera Spatial Offsets

The spatial offsets are measured using the following sequence of steps for Procedure 1:

1. The camera mount swing angle is set to zero using the swing angle indicator on the camera mount. This position for the camera nominally orients the camera X axis in the direction of flight. Any backlash in the camera mount was compensated by adjusting the zero setting so that the backlash on either side of the zero indicator was equal. The maximum backlash was 20' introducing a maximum radial error in the horizontal plane to the antenna of 3 mm (the approximate horizontal separation between the antenna and camera is 0.525 m).

$$0.525 \text{ m} * \sin(20') = 0.003 \text{ m}$$

2. The camera registration frame is then made level to the local vertical by adjusting the camera mount while observing a spirit level vial placed across the registration frame. The axis of the vial is set perpendicular to the axis about which the camera was being rotated. The level vial is reversed to compensate for any non-parallelism between the vial and its mount. The camera registration frame now instruments the horizontal plane of the reference system.

3. The vertical separations, between the four gimbals on the camera mount to the top of the mount are measured in order to determine a mean distance about which the mount and, therefore, the registration frame is rotated. This distance will later be combined with the vertical distance between the antenna phase center and the registration frame, as well as the vertical distance between the registration frame and the entrance node of the camera lens system. A combination of these vertical distances will determine the vertical spatial offset of the camera exposure station to the antenna phase center in the camera coordinate system.

4. The antenna phase center, as defined by the manufacturer, and documented in a side view of the GPS antenna (Figure 3) is carefully marked on the upper surface of the antenna structure. The mark is viewed by two theodolites set up so that their lines of sight to the antenna intersect at nearly 90 degrees (refer to Section 2.4.2). These lines of sight will pass through the door and escape hatch of the aircraft. The theodolites are carefully leveled prior to intersecting the antenna. The theodolite sight lines are lowered vertically to the inside of the aircraft. A plumb bob is then suspended from the inside of the aircraft and moved slowly until both theodolites intersect the plumb bob string. The lines of sight are elevated to the cabin overhead while the plumb bob is continuously adjusted to the intersection of the lines of sight. The point at which the intersection of the theodolite lines of sight occurs on the overhead is marked with a red indelible marker. This point represents the local vertical projection of the antenna phase center because the theodolites and aircraft were leveled to the local vertical. Since the camera film plane has also been leveled to the local vertical, the vertical component of the antenna phase center to the overhead mark represents a component of the total vertical spatial offset. This procedure is accurate to 1 mm in the horizontal components (half the diameter of the plumb bob string). With the theodolites still in place, the lines of sight were lowered to the belly of the fuselage. The plumb bob string was once again used as a target to locate the vertical extension of the antenna phase center. This mark will be used for positioning the aircraft over a known geodetic position on the taxiway for pre-flight GPS operations.

5. A 6 mm thick rectangular glass plate measuring 66 cm by 40 cm is placed on the registration frame (film plane) of the camera so that the entire registration frame is covered by the glass plate. The glass plate extends beyond the registration frame through the vertical axis of the antenna phase center as defined by suspending a plumb bob from the previously determined mark on the overhead. Several heavy pieces of steel are placed on the glass to prevent the plate from moving on the registration frame. The glass plate now instruments the horizontal plane of the camera registration frame.

6. The horizontal component of the antenna phase center is transferred to the glass by suspending a plumb bob from the mark on the overhead to the glass. The glass is marked by carefully transferring a waxed circle to the glass. The circle is approximately 2 mm in diameter. The plumb line is repeated to ensure that the circle has been correctly transferred.

7. A 35 power microscope equipped with crosshairs is placed on the glass plate in the vicinity of a fiducial or reseau mark. The microscope mount is constructed to instrument a line of sight perpendicular to the surface being observed. The microscope is focused and carefully centered on a fiducial or reseau mark. A waxed circle is placed in the field of view and brought into focus without changing the horizontal position of the microscope. The circle is transferred to the glass. The microscope is re-focused on the fiducial to ensure that the microscope has not moved. Three non-collinear fiducial or reseau marks are observed and transferred to the glass plate in this manner.

8. The plumb bob is once again suspended from the overhead to ensure that the glass plate has not shifted on the registration frame of the camera. The glass plate now contains sufficient information to trilaterate the horizontal spatial offsets of the antenna phase center in the reference system of the camera. This procedure was performed for both camera mounts in the NOAA aircraft.

9. The vertical spatial offset must be measured as a combination of the following vertical sections:

a. The side view of GPS antenna (Figure 3) is used to measure the vertical separation from the phase center of the antenna micro-strip element to the bottom of the antenna mounting plate.

b. The vertical separation between the bottom of the antenna mounting plate and fuselage flange is measured with a steel tape.

c. The thickness of the fuselage skin in the vicinity of the antenna is obtained from the aircraft engineering drawings and confirmed by measuring the aircraft skin in the vicinity of the hatch.

d. The vertical separation from the inside of the fuselage skin to the cabin side of the overhead covering is measured with a steel tape through an inspection plate located near the antenna.

e. The vertical separation from the overhead to the registration frame is measured with a steel tape with the glass plate still in place on the registration frame.

f. The vertical separation from the registration frame to the top of the camera mount, which references the gimbals, is measured with a steel tape.

The algebraic sum of these vertical separations represents the vertical spatial offset from the antenna to the camera mount gimbals. The vertical separation from the gimbals to the entrance node of the lens system will be discussed in Section 2.4.4. The spatial offsets described thus far are listed in Table 4.

To attain the confidence required for statistical control of the measurement process, a second procedure was used to measure and verify the spatial offsets. In this case, the measurements were referenced to the airframe of the NOAA Citation.

In this procedure, the spatial offsets were measured as follows:

1. A platform is constructed from a heavy cardboard box that was placed in the aisle of the cabin on the aircraft frame in the vicinity of the camera. The platform is adjusted so that its upper horizontal surface is parallel to the bottom surface and at the same height as the leveled camera registration frame. The height is verified by placing a carpenter's level across the box and registration frame of the camera. The level bubble should be centered.

2. The platform is centered on the vertical extension of the GPS antenna phase center by suspending a plumb bob from the mark on the overhead. Herein lies a major source of inaccuracy. The aircraft must be level or a significant error in the horizontal spatial arms can result. A one degree tilt of the aircraft propagated over the vertical distance from the overhead to the platform follows:

$$1.032 \text{ m} * \sin(1^0) = 0.018 \text{ m}$$

3. A second red indelible mark is made on the overhead approximately 2 m aft of the antenna phase center mark. The same lateral offset from the flight axis is used for the second mark.

4. A protractor, 30 cm in diameter, is set on the platform and centered under the antenna phase center by use of a plumb bob. The protractor is rotated until the $0^0$ mark, $180^0$ mark and the aft mark on the overhead form a range. The alignment is performed using the $0^0$ and $180^0$ marks as sights aligned with a plumb bob string suspended from the aft mark. Once again a leveled aircraft is necessary so that the plumb line is truly on the axis of the aircraft. Assuming that the alignment is accurate to half the diameter of the plumb bob string, the alignment is within 2' of arc of the flight line as defined by the aircraft frame.

$$\arctan(2 \text{ m}/.001 \text{ m}) = 1.7'$$

The maximum error in the spatial offsets will be:

$$0.525 \text{ m} * \sin(1.7') = 0.0003 \text{ m}$$

5. A template is placed over the registration frame of the camera. The center of the fiducial system is located by intersecting the corner fiducial marks. This templet is later compared against several diapositives taken with the same camera. The intersection of the corner fiducial marks on the templet agrees with the intersection of the corner fiducial marks on the diapositives within 0.0005 m.

6. A steel tape is used to measure the horizontal radial distance from the center of the protractor (vertical extension of the antenna phase center) to the center of the fiducial system as marked on the templet. The intersection of the steel tape and the protractor scale is also noted. It is also necessary to measure the horizontal distances and angles from the center of the protractor to several fiducial marks if the horizontal spatial offsets are required in the fiducial coordinate system. If it is assumed that the fiducial system has been aligned with the flight axis, the extra measurements are not required.

7. The radial distance and angle of intersection can be used to compute the horizontal spatial offsets in the reference system of the aircraft.

8. The vertical spatial offset is measured in the same manner as described in the other measurement procedure. The distance from the overhead to the platform is measured instead of the distance from the overhead to the glass plate.

Table 4 is a comparison of the results. The difference in vertical separation between the registration frame and overhead is insignificant. The difference in horizontal spatial offsets is most likely caused by a combination of the less accurate leveling of the aircraft, determination of the fiducial center, and the alignment of the platform with respect to the airframe in procedure 2. Procedure 1 values were accepted. The internodal separation has been determined by methods described in Section 2.4.4. The values for Procedure 1 were determined on November 11, 1989. The values for Procedure 2 were determined on October 17, 1988.

The techniques developed above represent the first significant contribution of the research.

2.4.4 Film Plane to Entrance Node

Modern aerial cameras have a lens system composed of many individual lens elements. The optical behavior of the light rays passing through the system of lenses is described by the laws of thick lenses. In theory, a thick lens has the same refractive characteristics as the composite of the individual lenses. A thick lens has 2 points of focus or nodes on the optical axis such that when all object distances are measured from one point (entrance node) and all image distances are measured from the other (exit node), they satisfy the simple lens relation expressed by the conjugate-foci formula ($1/f = 1/I + 1/O$) (ASP 1980). The entrance node represents the location of the exposure station in the three-dimensional object space coordinate system used for the aerotriangulation solution. The vertical separation between the GPS antenna and entrance node is, therefore, one component of the spatial reference frame that must be determined. The vertical separation between the antenna and film plane has already been determined. The vertical separation between the film plane and entrance node has yet to be determined. The separation is slightly different for each lens. For the purpose of this research i.e., determining the flying height of the exposure station, a precision of 1 cm will be tolerated. This tolerance is one order of magnitude below the threshold of determining the flying height of the GPS antenna (currently thought to be 10 cm).

The most precise method of determining the nodal separation is to use a nodal slide; unfortunately, one large enough to accommodate the aerial camera lens could not be found. The author employed two other methods. First, the author contacted Wild-Heerburg. Wild-Heerburg provided an 8.5 x 11.0 inch cross-sectional drawing of the lens. The drawing (Figure 5) noted the intersections of the extreme entrance and exit-rays

Table 4 -- Spatial Offsets Between the GPS Antenna and Camera Exposure Station

| | Procedure 2 | Procedure 1 |
|---|---|---|
| Vertical Spatial Offset | | |
| Antenna Element to Shim | 0.019 m | 0.019 m |
| Antenna Mount Shim | 0.003 m | 0.003 m |
| Aircraft Skin | 0.004 m | 0.004 m |
| Overhead to Skin | 0.084 m | 0.084 m |
| Film Plane to Overhead | 1.029 m | 1.025 m |
| Nominal Camera Constant | 0.153 m | 0.153 m |
| Internodal Separation | 0.130 m | 0.130 m |
| Total Vertical Spatial Offset | 1.422 m | 1.418 m |
| Horizontal Spatial Offsets | | |
| Photo X | 0.207 m | 0.210 m |
| Photo Y | -0.525 m | -0.534 m |
| Vector Distance Antenna Phase Center to Exposure Station | 1.530 m | 1.530 m |

with respect to the film plane and the objective lens. The rays were extended into the lens system to the points where they intersected. These intersections were assumed to be the entrance and exit nodes for the lens system. Knowing the nominal camera constant, the print could be scaled by measuring the exit-ray intersection to film plane distance on the print. The entrance-ray intersection to exit-ray intersection distance was then measured from the print. This distance was scaled and added to the camera constant to yield a reasonable estimation of the film plane to entrance node separation. This first approximation was 274 mm. Second, the author contacted the U.S. Geological Survey, Calibration Laboratory in Reston, Virginia. They suggested a method which should yield a precision of 0.5 cm. The method is documented in Appendix B. The distance from the film plane to the entrance node by this method was 283 mm for both NOAA G and B Cones. The internodal separation would be 130 mm (283 mm minus a focal length of 153 mm). This distance was accepted for the measuring system.

The separation, if any, between the entrance node and the center of the gimbals must also be determined. Due to the symmetry of the camera mount and gimbal construction, it is assumed that the optical axis of the camera coincides with the center of the gimbals. The distance from the film plane to the entrance node was determined to be 0.283 m. The measured separation from the film plane to the center of the gimbals was 0.259 m. The difference in vertical separation of the gimbals to entrance node is 0.024 m. Assuming that the roll and pitch angles seldom exceed 2° the maximum error which can occur by assuming that the gimbals intersection and entrance node coincide can be expressed as follows:

$$\text{horizontal error (m)} = 0.024 * \sin(2^\circ) = 0.0008 \text{ m}$$

The maximum rotation angle encountered during the missions flown for this research (based on the aerotriangulation solution) was a phi rotation of 1.2°. Therefore the maximum difference between the center of gimbals and entrance node would be:

$$\text{horizontal error (m)} = 0.024 * \sin(1.2^\circ) = 0.0005 \text{ m}$$

The error is considered to be insignificant for this research, therefore the entrance node and gimbal center are assumed to be the same.

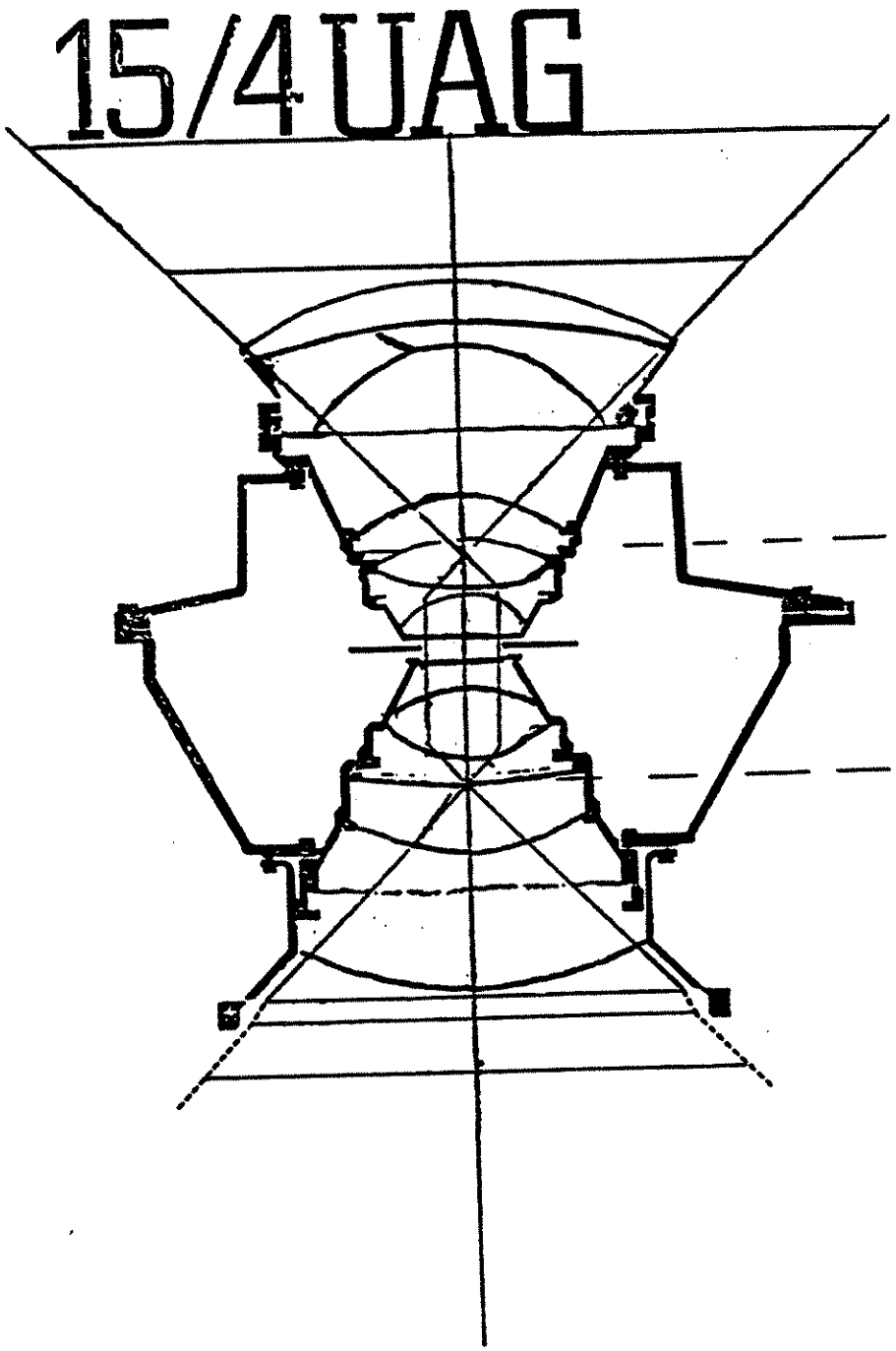


Figure 5. Internodal Separation

# CHAPTER III
# PHOTO MISSION PLAN

Two entirely successful photo missions were accomplished on October 25, 1988 (DOY 299) and October 27, 1988 (DOY 301). Successful mission implies that the weather and flying conditions were suitable for obtaining photographic images with less than 5 microns of image smear and free from cloud patches. On those two missions, the GPS also performed in an acceptable manner, with only small, but easily correctable, cycle slips. The findings of this research are based entirely on these two missions.

## 3.1 Instrumentation

Up to this point of the research, the author was able to dictate the environment in which the observations were collected. Individual measurements were isolated and brought under statistical control, as defined in the Introduction. From this point on, the author was forced to consider multiple sources of systematic effects, situation-dependent variables, and the influence of considerable human interaction. The success of this research is founded upon the boundless energy and professionalism provided by the personnel from OSU, ODOT, and of course, NOAA. The following section describes the instrumentation used to collect the data and is provided for completeness, but without explanation.

### 3.1.1 Aerial Camera System

As mentioned earlier, the NOAA Cessna Citation II aircraft was used to carry the instrumentation. The aircraft was equipped with a Wild Heerburg Model RC-10 camera system which included the following components:

1. Remotely controllable camera mount
2. Intervalometer
3. Navigation sight with leveling mount for remote camera control
4. RC-10 15/4 UAG NOAA B Cone with eight fiducial marks
5. RC-10 15/4 UAG NOAA G Cone with film plane reseau
6. Infrared Filter
7. Kodak Plus Pan X roll film

### 3.1.2 GPS Receiver System

The aircraft and ground reference station were equipped with Motorola Eagle GPS receivers. The receivers have the capability of receiving information simultaneously from four satellites. Although four satellites are sufficient for the solution of position, the lack of redundancy made it difficult, if not impossible, to recover cycle slips in the data. The ground station had a standard Motorola antenna preamplifier and ground plane micro-strip antenna. The aircraft had a specially modified antenna preamplifier to accommodate a 2 m separation from the antenna. The aircraft antenna was an FAA approved ground plane micro-strip navigation antenna (manufacturer unknown). The aircraft receiver was equipped with an optional Pulse Per Second (PPS) signal generator. Each receiver was interfaced to a Compact 286 or 386 portable computer. Raw data from the receivers were collected by the computers and stored on high-density (1.2 Megabyte) floppy disks. Disk storage capacity limited flight operations to a maximum of 80 minutes at a one-second data collection rate.

3.1.3 Exposure Timing Apparatus

The RC-10 camera lens cone contained a shutter status device which generated a pulse to synchronize the RC-10 exposure to an optional horizon camera. The pulse referred to as the horizon pulse was connected to a "start port" of a Hewlett Packard frequency counter. The PPS from the Motorola GPS receiver was connected to the "stop port" of the frequency counter. The frequency counter had a precision of 10 micro-seconds for a single timing event. A Hewlett Packard desk-top calculator was interfaced to a crystal clock (synchronized to GPS time) and the frequency counter. The horizon pulse cleared and triggered the start of the timing sequence. The next PPS from the GPS receiver stopped the timing sequence and triggered the recording of the crystal clock and elapsed time between exposure and PPS. The inherent precision of the system was 0.01 msec, or 3 mm at an aircraft velocity of 200 miles per hour (89.4 m/sec).

The timing system contained many systematic errors which had to be discovered and modeled. This effort became one of the major contributions of the research.

3.2 Flight Design

The goal of the design for the photo mission was to obtain a block of 15 photographs composed of three strips of five photos which covered the entire TRC calibration range. The block would have 80 percent forward overlap and 60 percent sidelap. The physical limits of the calibration range, the design of the targets, and the minimum operating limits for the NOAA aircraft had to be carefully considered. The normal photo scale for NOAA mapping is 1:30,000. Considering a nominal camera constant of 6 inches, this requires a flying height of 15,000 ft. At this altitude, image smear, caused by the aircraft velocity, is also minimized. The physical limits of the TRC calibration range precluded the use of 1:30,000 scale photography. In fact, the previously established target size was optimized for 1:10,000 scale photography (Appendix A). The NOAA aircraft minimum flying height and velocity are 6000 feet (1:12,000 scale) and 200 miles per hour, respectively. Below these limits, the aircraft begins to porpoise and looses the ability to maintain a constant heading, adversely affecting the photo images. To accommodate the aircraft and photo target size, the calibration range was enlarged by establishing a fourth set of 8 photo targets along U.S. Route 33 which parallels the other sets of photo targets. A compromised scale of 1:12,000 was chosen. Figure 6 is the NOAA flight plan based on the author's recommendation. The compromised operating conditions did not adversely affect the ability to calibrate the airborne system.

3.3 GPS Initialization

Many references have been made thus far concerning the initialization of the GPS receivers before the flight began and to confirm the initialization after the flight ended. The initialization is used to determine the integer number of cycles between the two receivers (ground reference and aircraft) and the four satellites being tracked at some selected starting epoch. Once the integer cycles are determined for the starting epoch, the changes to the integer values are computed from the accumulated cycle count recorded by the receivers as the Space Vehicles (SV) and receivers change position with respect to one another (satellites are often referred to as Space Vehicles). The integer counts are actually the double-difference integer value between the two receivers and two of the four SV's. One SV is normally selected to be common between all double-difference integer values. The total number of integer counts is, therefore, reduced to three values. As an example, the three combination integer values for the two receivers and SV 9, 11 ,12, and 13. would be:

Difference 1 = SV 9, SV 13, Reference and Aircraft Receivers Difference 2 = SV 9, SV 12, Reference and Aircraft Receivers Difference 3 = SV 9, SV 11, Reference and Aircraft Receivers

The SV 9 is the common SV in the above example. The common SV is usually the SV which has the highest elevation above the horizon throughout the tracking period and generally is tracked without loss of signal lock throughout the mission. It is known (Goad 1989) that high SV elevations reduce the effect of atmospheric refraction by reducing the path length for the signal through the atmosphere.

### 3.3.1 Baseline Method

The baseline method for initialization was used on DOY 299 and DOY 301 to determine and confirm the integer values. This method uses the knowledge of the baseline components between the two receivers to solve the double-difference equations for the integer cycle values. The double-difference equations involve terms of station coordinates, SV coordinates and integer cycle values. The station coordinates are all known if the baseline is known. The SV coordinates are computed from the satellite broadcast ephemeris. The only unknowns are the integers and they can be solved for using the double-difference observation equations. Once the integers are known, the aircraft antenna can be moved off the baseline because in this situation, the only unknowns will be the aircraft coordinates. In principle, only one set of observations is required in order to determine the integers. In practice, the aircraft remains on the baseline for up to 5 minutes. The data collected during the 5-minute initialization are processed and reviewed for any drift in the baseline. A drift in the initialization is indicative of incorrect baseline components. The aircraft returns to the baseline subsequent to the mission and an additional 5 minutes of data are collected. The ending data set is processed and analyzed. The baseline components should equal the beginning values. Any difference or drift is indicative of cycle slips (Appendix A). Periods of less than 5 minutes may not be long enough to detect a drift in the baseline components.

One might ask how to maneuver a jet airplane directly over the end of the baseline. The author devised a method which uses a Radar Maneuvering Board commonly found on commercial and military ships. The maneuvering board is a 13 in paper square with a 10 in diameter protractor printed on it. The protractor has concentric circles spaced at 0.5 in increments and radial lines every 10 degrees. The radial plot of objects such as antenna eccentricities is facilitated by the device. The center of the maneuvering board is placed over the baseline mark and oriented to a known azimuth by magnetic compass or other known reference point (TACK at Union County Airport). The maneuvering board is 10 inches in diameter, so the aircraft need only be guided within 5 inches of the mark. This tolerance is easily achieved with minimal practice. A plumb bob is suspended from the antenna phase center reference point on the belly of the aircraft. The plumb bob point indicates the eccentricity from the baseline to the horizontal position of the antenna phase center. The North and East eccentricities can be determined from the offset and orientation angle as noted on the maneuvering board.

### 3.3.2 Antenna Swap Method

The antenna swap method discussed in Appendix A can also be used for determining the integer values. This method is quicker and as precise as the baseline method without the need for a known baseline. The problem with this method is the need to exchange the receiver antenna positions. The aircraft antenna cannot be removed, necessitating the movement of the entire aircraft! The author, consulting with Dr. Goad devised a new antenna swap method specifically for this situation. The

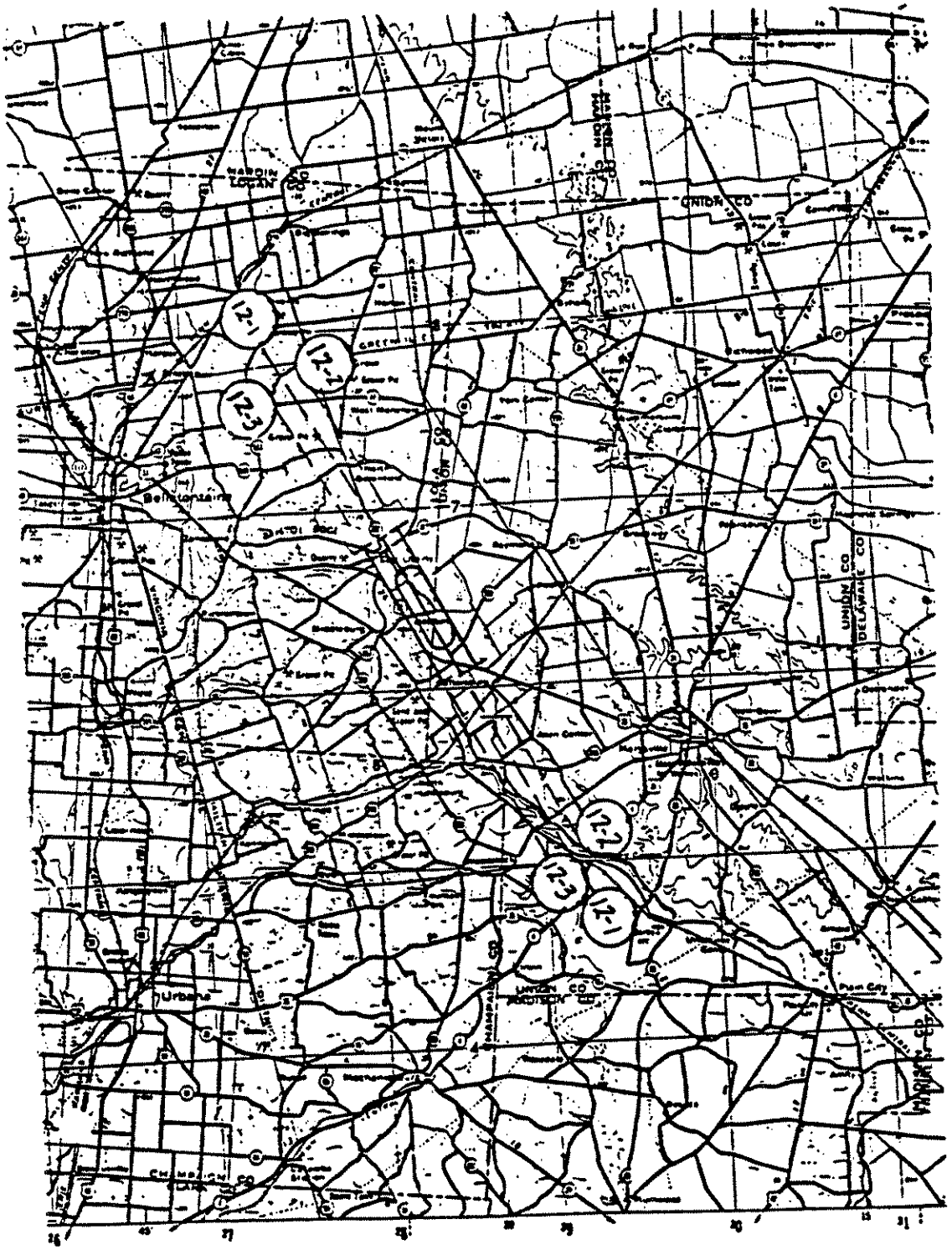


Figure 6. Flight Plan

integer values can be determined by an antenna swap without *a priori* knowledge of the baseline or antenna locations because the double-differences resulting from antenna swap cancel out the coordinate difference information in the observation equation, leaving only the unknown integer value. A baseline must be instrumented on the aircraft such that the aircraft antenna is located at the baseline midpoint. The baseline need only be about 2 m in length. The specified length is more for convenience so that the two antennas are not brought so close together as to cause a blocked satellite signal. The antenna swap begins with the reference receiver on one end of the baseline. Several epochs of data are collected by both receivers in this position. The reference receiver is then moved to the other end of the baseline. A few additional epochs are collected by both receivers in this position. Sufficient information now exists to compute the integer values between the receivers and satellites through the normal double-difference equations. The equations, however, are set up as if both antennas were moved between the midpoint point and beginning end of the baseline. The reference receiver is now used to perform a kinematic survey as its antenna is moved to the reference station. Once the reference receiver is on the reference point, the coordinates for both ends of the baseline between the reference station and the aircraft are known, as are the integers. The aircraft can now become the mobile station. This method is one of the significant contributions resulting from the research.

### 3.4 Mission Scenario

The current limiting factors for GPS controlled photogrammetry are satellite availability and inflight data storage capacity. At the present time, both limitations allow for normal mission lengths of approximately 80 minutes. A well-planned mission is the only way of insuring that the human, mechanical and electronic interactions will function together. In order to maximize the length of the photo mission, ground-based activities must be made as efficient as possible. Table 5 is a time table for a 90- minute photo mission.

The following inflight observations and restrictions are required in addition to the GPS observations, exposure timing, and photo images:

a. Cabin pressure and temperature
b. Exterior barometric pressure and temperature
c. Exposure interval
d. Drift setting
e. F-stop and shutter speed
f. An estimate of image smear
g. The camera mount may be adjusted for level and drift prior to the first flight line.
h. The camera mount cannot be changed thereafter.
i. Ground barometric pressure and temperature

Table 5 -- A Typical 90-Minute Mission Time Table

| | |
|---|---|
| T-90 min | Mission briefing at airport |
| T-60 min | Maneuver aircraft over calibration point<br>Set up reference GPS receiver |
| T-45 min | Begin GPS receiver warmup (30-second epochs) |
| T-15 min | Begin engine warmup/pre-flight checkouts |
| T- 5 min | Switch to 15-second epochs<br>Perform antenna swap |
| T- 0 min | Switch to 1-second epochs<br>Perform baseline initialization |
| T+ 5 min | Begin taxi and takeoff operations |
| T+65 min | Begin final approach and landing operations |
| T+70 min | Position aircraft over calibration point<br>Preform baseline verification |
| T+75 min | Switch to 15-second epochs<br>Perform antenna swap |
| T+80 min | Begin post mission shut down |
| T+85 min | Return to hanger area |
| T+90 min | End of mission |

NOTE: The Mission Time Table allows for both antenna swaps and baseline initialization.

# CHAPTER IV
# KINEMATIC GPS PROCESSING

Although kinematic GPS positioning plays an extremely important role in the research project, it is not the author's intent to discuss the technical aspects in great detail. Instead, this chapter will be devoted to a description of the various systematic errors identified during the GPS processing. The resolution of all errors in the measuring system is, after all, the goal of the research.

The research is based on two different flight missions. On Day of Year (DOY) 299 the aircraft was equipped with the NOAA G Cone Reseau Camera. SV 8, SV 9, SV 11, and SV 13 were tracked continuously by the reference and aircraft receivers for approximately 70 minutes. Figure 7 is the actual flight pattern for DOY 299 drawn from the processed GPS positions of the aircraft. On DOY 301 the aircraft was equipped with the NOAA B Cone Camera, with an 8 fiducial mark reference frame. SV 9, SV 11, SV 12, and SV 13 were tracked continuously by the reference and aircraft receivers for approximately 55 minutes. Figure 8 is the flight pattern for DOY 301 drawn from the processed GPS positions of the aircraft.

The final values for the kinematic double-difference positions of the aircraft are obtained from NGS program OMNI. The positions are expressed as time-tagged NAD83 coordinates for the aircraft antenna phase center. This file is known as the antenna ephemeris file. The time tags are expressed as corrected GPS time.

The final version of each antenna ephemeris file is the result of many attempts to resolve all possible error sources. Confidence in the solution required for statistical control was not attained until November, 1989, nearly 13 months after the data had been collected. Idiosyncracies with the particular GPS receivers and omissions in the field notes had to be resolved. The greatest single contribution to the successful completion of the computations resulted from lectures presented by Goad at The Ohio State University, Spring Quarter, 1989. The following list contains improvements for the final kinematic double-difference solutions found in both antenna ephemeris files:

a. Selection of the SV with the highest elevation and without cycle slips as the common SV for double-difference solutions and computation of the integer values (Goad 1989).

b. Discovery that the GPS time tags were not corrected for SV clock error. This improvement was verified by the author after several telephone conversations with Motorola engineers and verified through the use of the OMNI software. A complete description will be presented in Section 4.1.

c. Time Shifting the GPS observations for both receivers to the nearest integer second. The shift then synchronized both receivers and the PPS from the aircraft receiver to GPS integer time. The time shift in all instances was less than 3 msec. Again, a complete discussion will be contained in Section 4.1. The processing of the GPS data using an integer time for each epoch eliminated two important sources of timing errors.

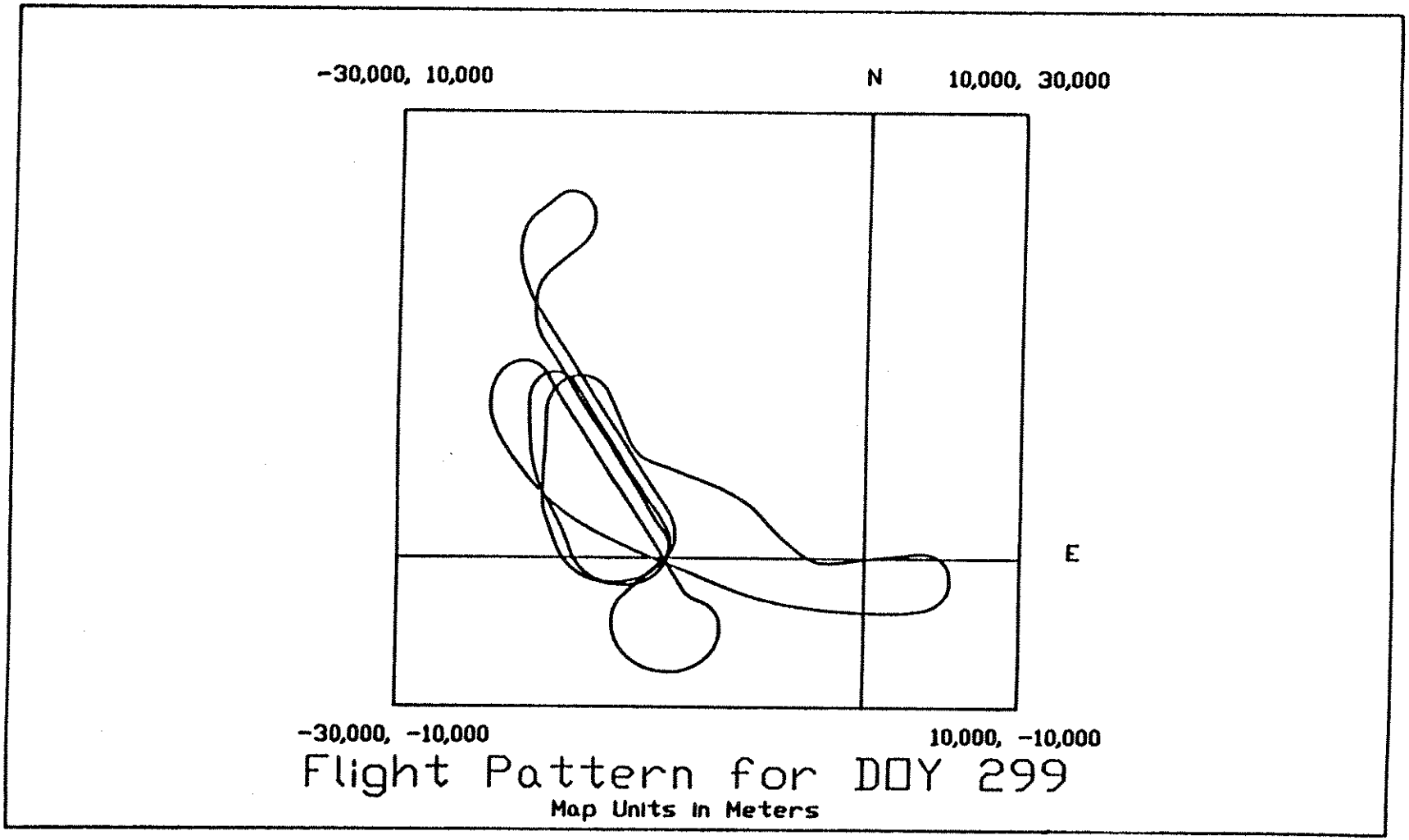


Figure 7. Flight Pattern for DOY 299

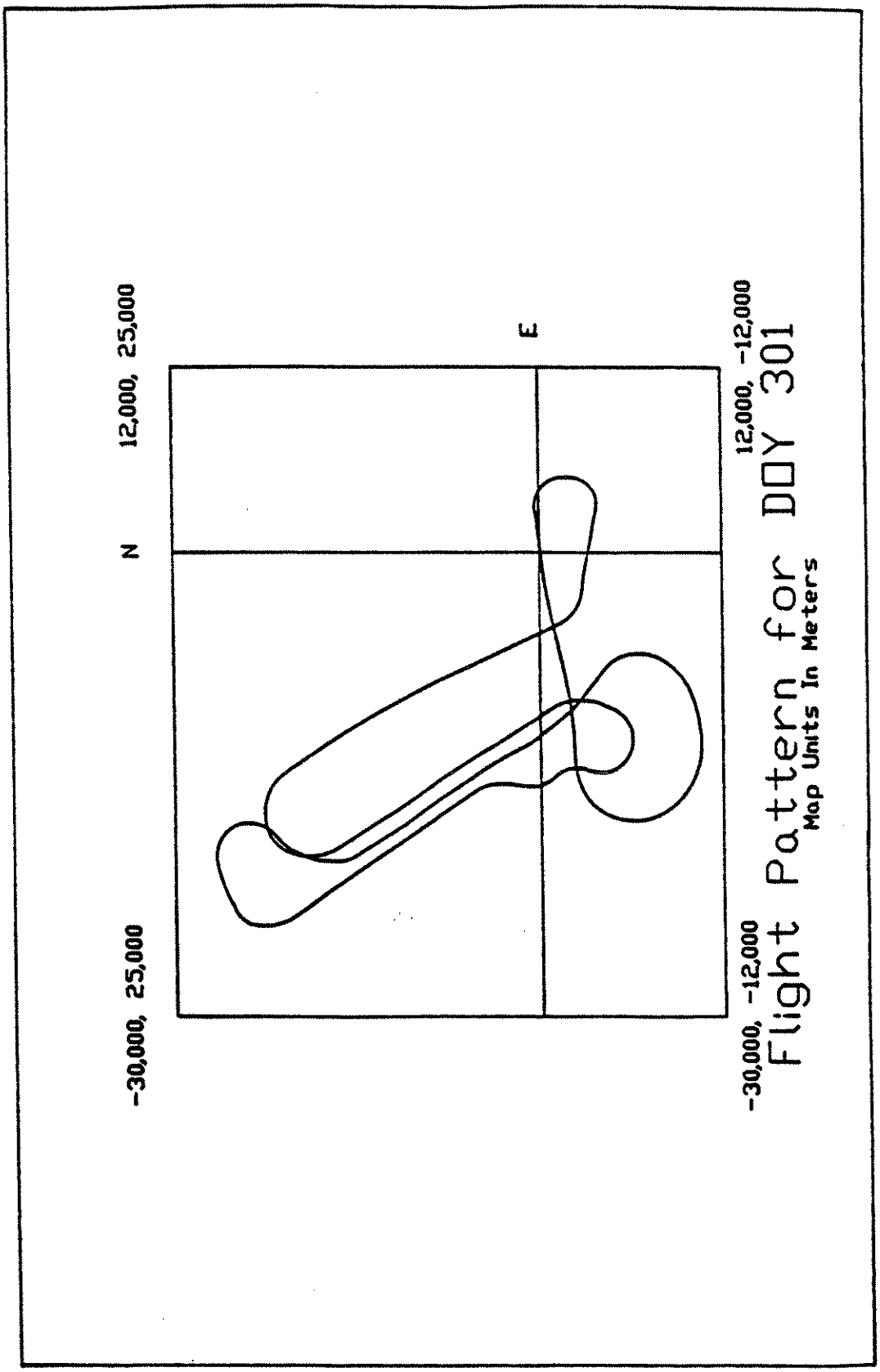


Figure 8. Flight Pattern for DOY 301

1. The first source of error results from an epoch time-tag ambiguity. The antenna ephemeris file displays time to nearest 1/100 second, when in fact the time of epoch might have been several msec after the displayed time. This error will eventually be corrected in OMNI.

2. The use of integer time in processing also removes any timing bias resulting from small instantaneous shifts in the receiver time tags which cause the time intervals between epochs to become unequal. Interpolation routines developed by the author and Lucas (1989) are based on equal-time interval interpolation algorithms.

d. Resolution of the timing bias between the receiver time and the PPS time tag. It was not clear if the same time tag was shared by the observed carrier phase values and the PPS signal considering that both quantities were based nominally on a one second interval. The resolution of this investigation required numerous telephone conversations between Motorola technical representatives and the author. It was finally determined that the PPS was generated by the receiver's most recent (less than one-second old) determination of GPS time (King 1988). The design of the PPS signal circuit ensures that the signal will be generated within 1 micro second of integer or rollover time. As a result of Items c and d, the GPS position file for every second of the aircraft antenna's trajectory is now time tagged to rollover time, and in agreement with the PPS time tag to within 1 micro second.

e. The 5-minute initialization period was scanned to identify the most noise free period of observations. This period normally begins several minutes into the initialization period after the receiver electronics stabilized and personnel inside the aircraft are settled into pre-flight preparations.

f. Processing the kinematic GPS double-differences in chronological and reverse-chronological order to confirm the beginning and ending integer cycle ambiguity values are the same.

g. Application of the appropriate eccentricities to the coordinates of the aircraft and reference receiver antennas. The horizontal and vertical eccentricities resulted from the imperfect centering of the GPS antennas over the baseline ends. The author devised a method for determining the aircraft antenna horizontal eccentricities as follows:

1. The aircraft was maneuvered as closely as possible over the mark.

2. A maneuvering board (described in Section 3.3.1) was centered on the mark and oriented into the geodetic azimuth previously determined and marked on the taxi-way guide line.

3. A plumb bob was suspended from the vertical extension of the GPS antenna as marked on the belly of the aircraft. The plumb bob point then indicated the eccentricity of the GPS antenna to the mark on the maneuvering board.

4. The North and East offsets could be obtained graphically from the maneuvering board.

5. The vertical eccentricity was measured from the mark to the belly of the aircraft. This value was added to the other previously determined vertical spatial offsets.

h. Derivation of an improved tropospheric refraction model for program OMNI which updated the estimates for atmospheric pressure and temperature at the aircraft antenna based on the previously computed altitude during the kinematic processing. The following equations express the change in pressure and temperature as a function of altitude:

$$T_a = T_g + (H_g - H_a) * B$$

$$BP_a = BP_g * (T_a / T_g)^{-34.11/B}$$

Where:

$BP_a$ = Barometric Pressure (mb) exterior to the aircraft
$BP_g$ = Barometric Pressure (mb) at the initialization point
$H_g$ = Elevation (m) of the aircraft antenna at the initialization point
$H_a$ = Elevation (m) of the aircraft antenna in flight
$T_g$ = Temperature (C) at the initialization point, and
$B$ = The temperature lapse rate in $^{o}C/Km$

The temperature and pressure at the initialization point are assumed constant for the entire flight. The constant 34.11 represents the standard atmospheric change in barometric pressure in mb/100 m change in elevation as a function of pressure, temperature, water vapor, and gravity. The temperature lapse rate B is a constant, 6.5, which represents the temperature lapse rate of a standard atmosphere in $^{o}C$ per Km in elevation. This algorithm was submitted by the author for incorporation in a future version of OMNI.

The particular details for each antenna ephemeris file is highlighted in the following two sections.

4.1 Day of Year 299

The data set for DOY 299 had some problems right from the start of processing. Several epochs of raw data were not recorded properly by the aircraft's computer disk drive. These epochs were removed from the data set. Fortunately, the epochs occurred prior to the start of the first flight line and were not required for interpolation of any exposure station positions. Once the data set was edited, the raw data sets from both receivers were converted to the NGS ARGO format (Chin 1988) and pre-processed for cycle slip detection by ARGO. No cycle slips were detected. The data sets from both receivers were then merged by OMNI into a single data set. A decision had to be made whether or not to apply the satellite clock (SV Clock) correction to both the pseudo-range and phase data. The pseudo-range data will be used later to estimate the station clock corrections. Some manufacturers apply the SV Clock correction during data collection. A decision not to apply the SV Clock correction was made based on a statement in the Motorola User's Manual (1987) that the receiver time tags were corrected by the Kalmin Filter to GPS time. The merging process was executed. Upon examination of the SV clock-residual plot generated by OMNI, it was found that each SV clock-residual plot was displaced parallel to one another. This indicates that the SV Clock correction was improperly applied. In the normal case the SV Clock corrections would have traced a single overlapping curve assuming the *a priori* station position coordinates were correct and no cycle slips had occurred. The fact that the individual curves appeared to be parallel to one another indicates that the SV Clock drift was negligible compared to the receiver clock drift but shifted by a constant amount of time (perhaps due to the poling sequence used by the receiver electronics). The data were re-merged

with the SV clock correction function applied. The clock residual plot showed a single curve which meant that the SV clock drift had been applied correctly. At this stage of the processing, the carrier phase and pseudo-range information for both receivers is mathematically shifted to integer time. The author chose to investigate if the shift could be correctly applied to the moving receiver's data. The time-tag shift capability was originally implemented in OMNI so that receivers of different manufacturers could be combined despite their method of time tagging. The technique had only been used for static receivers where it could be assumed that the shift was time dependent and not related to the negligible motion of the receiver. It was suspected that the shifts for mobile receivers may be in error due to the imperfect knowledge of the aircraft velocity components. The time tags from the mobile receiver were visually inspected and found to be within +/- 0.5 msec of integer time. The data were merged two ways. The first merging used integer time tags. The second merging used time tags having a fractional component of 0.0005 sec. The two double-difference solution files were compared. The static positions (during pre- and post-flight initialization were within 2 mm of each other based on a sample mean of approximately 35 epochs spaced 5 sec apart. Individual samples within the kinematic portion of the double-difference (during periods when photography was being collected) were compared. Differences as great as 2 cm were found in this portion of the data set. Considering the velocity of the aircraft (67 m/sec) differences of up to 3.4 cm (67 m/sec * 0.0005 sec) should have been noted. The error in time shifting the data 0.0005 sec will therefore be less than 1.5 cm. The magnitude of the difference is not significant at the level of precision expected for the positioning system. The author chose to use integer time for the time tags and SV Clock corrections. All data are now related to a single set of integer time tags. A final small improvement to the solution came from the selection of SV 11 (highest elevation) as the common satellite for double differences. The solution for cycle ambiguity values yielded fractional biases which were very close to integers (+/- 0.05 cycles), giving confidence that the correct integer values before and after the mission were determined.

The difficulty in processing resulted mainly from incorrect assumptions concerning the receiver time tags, noisy starting portion of the initialization period (first several minutes), and inappropriate application of eccentricities to the antenna heights. The difference between the computed ending position of the antenna and the observed eccentricity between the aircraft antenna and TAXI was less than 2 cm. The final data set is assumed free of cycle slips, and represents the aircraft antenna location for every integer second of time during the mission. The processing for DOY 301 was not to be any less difficult.

4.2 Day of Year 301

The field notes indicated that the reference receiver was positioned over station NPT. The determination of integer values before and after the mission had fractional biases of 0.30 cycles. Not only were the biases not close to integers, but a significant drift was detected in both beginning and ending initialization periods.

A possible problem with the baseline positions was suspected. The beginning and ending initialization differed by nearly the difference in position between NPT and SPT. Substituting SPT for NPT in the solution for integer values caused the biases to approach integers (+/- 0.1 cycles). The field records were checked to confirm the possibility of that the reference receiver was set up over SPT. No conclusions could be drawn from the records, but checking with several personnel from ODOT confirmed that the antenna was, in fact, set up over SPT.

A second improvement resulted from a combination of selecting SV 13 (highest elevation) as the common satellite for double differences and using the improved position (second ground survey) for SPT. The combination of the above factors yielded fractional biases of 0.05 cycles, thereby increasing the probability that the integer values before and after the mission were determined accurately.

A final improvement in the processing resulted from the elimination of cycle slips detected during the preprocessing phase for SV 3 at the reference site, and SV 12 on the aircraft. These cycle slips are detected by differencing the pseudo-range observable from the phase observable (using similar units). Although there will be a bias between the two quantities, the assumption is that the bias will remain fairly constant between epochs unless a cycle slip occurs. An instantaneous change of 20 meters between the pseudo range and phase solutions sets a cycle-slip flag which is displayed on the final printout from ARGO. The cycle slip at the receiver site was confirmed by a note in the field log which stated that one of the personnel involved in the ground operations was standing very close to the antenna at the time of cycle slip. The magnitude of the cycle slips were resolved by computing the integer biases before and after the flight. The same integer bias was computed for the SV 13/SV 11 combination from both static periods supporting the cycle slip detection provided by the NGS ARGO software. Cycle slips of 2 and 1 were computed for SV 3 and SV 12, respectively. Such small slips are possible considering the operating mode of the Motorola Eagle Receivers. The receivers were designed to be used as an integral part of a real-time navigation system. The receiver software design includes a Kalman Filter for predicting the phase and pseudo-range during periods of signal absence. The Kalmin Filter was used to predict (extrapolate) the correct cycle count accumulation subsequent to short periods of loss of phase lock.

The beginning and ending static antenna positions for the aircraft agreed quite well after the cycle slip repair. Since the detected cycle slips occurred prior to the first flight line, it would be possible to compute the exposure station positions using only the ending static period, thus entirely ignoring the cycle slips. The difference between the computed ending position of the antenna and the observed eccentricity between the aircraft antenna and TAXI was 0.007, 0.080, and -0.015 meters, in X, Y, and Z, respectively. The final data set is assumed free of cycle slips, and represents the aircraft antenna location for every integer second of time during the mission.

The GPS navigation files represent the final NAD83 coordinates for the aircraft GPS antenna phase center. From this point on, these coordinates will be used as a basis for determining the exposure station coordinates.

# CHAPTER V
# IMAGE PROCESSING AND MENSURATION

The discussion, from this point on, will be centered on the photogrammetric aspects of the airborne system calibration.

## 5.1 Processing and Printing

The exposed negative film was cut from the roll of Kodak Plus Pan X film and removed from the camera magazine at the end of each day and transported to Precision Photo Service Inc., Dayton, Ohio. The film was processed on their automated facility according to NOAA specifications (Appendix C) for maximizing film density and resolution. Several test exposures were taken prior to the mission photography so that the processing equipment could be adjusted for the specific conditions under which the photography was obtained. The ability to maintain statistical control of the system calibration is weakest at this point of the calibration process. To ensure the highest quality control over the developing stage, one of the two NOAA photographers always accompanied the film to Precision Photo. The film was processed on the night shift, which has better (but more expensive) quality control.

The ODOT, Bureau of Aerial Engineering (BAE) facility was used by the author to make diapositives. The diapositives were printed on a Log-E-Tronic, Model IV, printer using Agfa-Gevaert Avitone P3p film. Film deformation was minimized in the printing process by following a technique developed for this particular printer by Merchant (1990). The negative and positive emulsions were placed between two optically-flat, 6 mm thick plates of glass and pressed against the printer stage using 12 pounds of pressure. The pressure was tested by pulling the printer mechanism closed using a precise tension device. The tension device is commonly used for precise steel tape measurements. The specifications were developed for ODOT to limit distortion in the printing process to less than 5 microns throughout the format after removal of the uniform component. The combination of glass plates and pressure setting suppresses the flexure of the printer optical stage and ensures complete contact between the emulsions. The diapositives were developed at the ODOT facility using their automated developing techniques under the author's supervision.

Fifteen photos were selected from each mission flown on DOY 299 and DOY 301. The photo coverage provided stereo imagery of all the photo targets in the calibration range. Each set was comprised of 3 strips of 5 photos each with 80 percent forward overlap and 60 percent side overlap.

## 5.2 Image Coordinate Observations

The image coordinates taken on DOY 299 and 301 were measured on Wild BC-1 analytical plotter located at the OSU. The image coordinates for DOY 301 were later re-measured on the NOAA Integrated Digital Photogrammetric Facility, Personal Work Station 1 (IDPF/PWS1) based on an Ottico Meccanica Italiana (OMI) analytical plotter. In order to maintain statistical control, both analytical plotters were tested against a known standard before the observations were performed. The BC-1 was also checked before and after each day of observations.

### 5.2.1 BC-1 Observations

The BC-1 was used in the mono-comparator mode for measuring image coordinates from the diapositives generated from each photo mission. The BC-1 was allowed to warm-up for a minimum of three hours before any work was performed. The room in which the instrument is kept is

temperature and humidity controlled. The instrument was not used by anyone else during the measuring process.

Once the equipment stabilized, a test calibration program was executed. The test calibration consisted of measuring nine von Gruber grid points on the measuring stage. The BC-1 software was used to compute an isogonal affine transformation based on the measurements and the known (+/- 1 micron) coordinates of the grid points. The residuals of the measurements were generally less than 3 microns, which is the stated measuring precision of the BC-1 (User's Manual (1984)). The check calibration was used only as a check on the latest calibration performed on the BC-1. The results of the test calibrations agreed quite well with Tudhope's (1988) more complete Rigid Body Transformation test using a Jena test grid (+/- 1.5 microns).

The image coordinates were measured using a right-handed system defining the direction of flight to coincide with the direction of the positive X photo axis and the positive X axis of the plotter. The positive Y photo axis points towards the port side of the aircraft and is coincident with the positive Y axis of the analytical plotter. The above convention agrees with the normally accepted convention for analytical photogrammetry. The diapositives were inserted in the BC-1 emulsion down and flattened by glass plate. The measurements contain no comparator applied corrections for lens distortion or atmospheric refraction. The measured coordinates are transformed from raw stage to comparator coordinates but not transformed to the photo coordinate system. Careful notes were taken during this measuring process to eliminate any questions, after the fact, as to the nature of the measuring process (attain statistical control).

Thirty photos covering missions for DOY 299 and DOY 301 were measured during a single effort covering a five day period beginning on March 7, 1989. The BC-1 comparator was turned on and left undisturbed to reach thermal equilibrium for three hours prior to the start of observations and never turned off throughout this period. At the beginning and end of each day the check calibration program (as noted above) was used to ensure the BC-1 was still operating properly and maintaining a constant calibration. The room temperature was carefully monitored to maintain an even operating temperature.

The first step in the measuring process for each photograph was to observe the eight fiducial marks on each photo. The marks were measured twice in the following sequence: 1-5-3-7-2-6-4-8. These points exist on both the B and G Cone photography and are identified for completeness in Figure 9.

The photos obtained on DOY 299 were taken with the NOAA G Cone camera equipped with a focal plane reseau. The fiducial marks are located on the reseau. The image measurements for this set of photos also include measurements of the nearest 4 reseau points measured in the following sequence:

Pointing #1 - Ground image
Pointing #2 - Upper left reseau
Pointing #3 - Upper right reseau
Pointing #4 - Ground image
Pointing #5 - Lower right reseau
Pointing #6 - Lower left reseau
Pointing #7 - Ground image

Figure 9
Fiducial Mark Map
(Diapositive Plane)

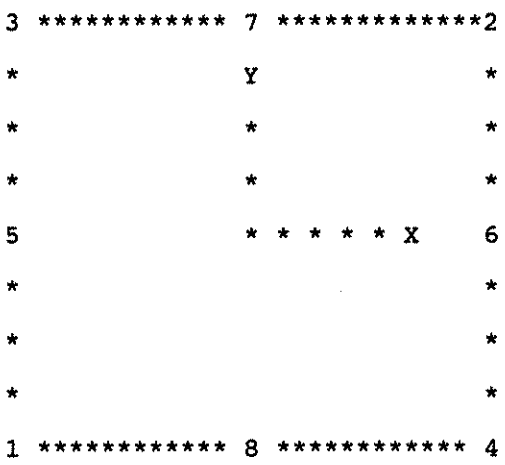


If any coordinate of the ground image varied by more than 5 microns from the mean (of pointings 1, 4 and 7), the particular pointing was rejected from the data set and re-observed.

The photos obtained on DOY 301 were taken with the NOAA B Cone camera which was equipped with the standard eight corner and edge fiducial marks. The measurements for this set of photos included two independent sets of observations on all fiducial marks before and after the measurement of ground images. All ground images were measured twice. One complete pointing on all ground images was made and then re-measured a second time. If the second observation of either coordinate varied by more than 5 microns, the observations for that ground point were repeated. This measuring process was augmented by using the ability of the BC-1 to automatically return to previously measured points.

The final product of the observations was two data sets of X and Y coordinates, unbiased by BC-1 applied corrections, oriented in a conventional two-dimensional right-handed system. These image coordinates were then transformed into the photo coordinate system. The transformation corrects the observed image coordinates for distortions caused by differential film shrinkage. Lens distortions as given in the laboratory camera calibration reports (Appendix D) were also applied to the transformed image coordinates. The corrected photo coordinates were then used in an aerotriangulation least-squares adjustment to compute unbiased estimates for exterior orientation of the camera based on the known survey control (Case 3 Solution, see Section 6.2). The corrected photo coordinates will eventually be used for aerotriangulation least-squares adjustment with *a priori* knowledge of the exposure station obtained from the GPS antenna ephemeris file in order to perform a system calibration (Case 4 Solution). The Case 4 mathematical model will contain nine terms of interior orientation to model any additional contributions of lens distortion caused by the installation of an optical flat installed in the fuselage of the aircraft. The computation of these terms is made possible by eliminating the correlation between the terms of interior and exterior orientation by the introduction of GPS observations for the exposure station. The computed parameters for interior orientation should reflect the additional influences of the complete airborne system on the laboratory calibration. The computed corrections for interior orientation will be tested on a different camera system in an attempt to prove that their contribution is truly

related to the aircraft. The justification for the selected mathematical model will be discussed more completely in Chapter 6.

5.2.2 IDPF Observations

The IDPF is a production-based analytical photogrammetry system designed by OMI for NOAA. Within the IDPF is an analytical stereo comparator, data archive system, and digital processing system. The IDPF provides the capability for super-imposition. Super-imposition allows the simultaneous viewing of imagery and the digital mapping data base.

The IDPF was used to measure the diapositives obtained on DOY 301. More pass-point observations were made since it was felt that an insufficient number of pass point images had been measured on the BC-1.

The IDPF uses a self-check calibration which is automatically performed on system start-up. Like the BC-1, the IDPF is kept in an environmentally-controlled room. Unlike the BC-1, there is no prescribed warm-up period prior to its use.

The imagery is measured in stereo with automatic pointing for all ground point images entered or previously measured within the format. The IDPF applies lens distortion (see Appendix D - Laboratory Calibration Reports), differential film deformation and transforms the image coordinates into the photo coordinate system. The parameters for these corrections are obtained from the data base or can be user supplied. The output from the IDPF is photo coordinates which can be directly used for aerotriangulation or compilation. The instrument applied algorithms for the corrections and transformations agreed with the author's.

5.3 Coordinate Transformation

The image coordinate observations in terms of the comparator coordinate system are transformed to the photo coordinate system using a general affine, six-parameter transformation. The six parameter model imposes the condition that parallel lines will transformed into parallel lines. Non-orthogonality and scale differences between the coordinate axes will be accommodated by six parameters. The transformation of comparator coordinates also compensates for linear film deformation.

5.3.1 Film Deformation

The placement of eight fiducial marks along the edges of a standard aerial photograph does not permit the accurate modeling of non-linear film deformation within the central portion of the photograph and may, in fact, be the limiting factor for a system calibration. For this reason, the G Cone reseau photography will be used from this point forward in the system calibration. The B Cone photography will be used later to test the conclusions of the system calibration.

The transformation parameters are computed from known reseau coordinates within a 1 cm region of each set of image coordinates in the G Cone photography. Although only linear film deformation is modeled, non-linear film deformation can be approximated quite well due to the close proximity of known reseau point coordinates to the image being measured.

5.3.2 General Affine Transformation

The following models represent the general affine six parameter transformation in linear form (Merchant 1988):

$$X = ax + by + c$$

$$Y = dx + ey + f$$

X and Y are observed reseau coordinates in the comparator system

x and y are known reseau coordinates in the photo system as obtained from a stellar calibration

a,b,c,d,e, and f are the linear form of the unknown transformation parameters, where:

$$a = C_x * \cos(a)$$
$$b = C_y * \sin(a)$$
$$c = dx$$
$$d = -C_x * \sin(a+q)$$
$$e = C_y * \cos(a+q)$$
$$f = dy$$

$C_x$ is the constant scale factor in the x axis
$C_y$ is the constant scale factor in the y axis
a is right-handed rotation between the x and X axes
q is the right-handed rotation angle of non-orthogonality between the x and y axis
dx is the separation component along the X axis between the x and X axis
dy is the separation component along the Y axis between the y and Y axis

NOTE: Due to the linear nature of the transformation equations which results in constant scale factors in x and y only linear film deformation can be compensated.

A solution for the six unknowns depends on a non-zero determinate expressed by the following equation:

$$a*e - b*d$$

The transformation was based on observations of the nearest four reseau points to the image. Eight observation equations of six unknowns can be formed from the observations of the four reseau points. The statistical detection of outliers from the reseau observations is weak due to the small number of degrees of freedom (8-6=2) and the lack of redundancy in the measurement of the individual reseau points. Therefore, a four parameter isogonal affine transformation of the following model was also used to examine the residuals for the reseau observations (Merchant 1988):

$$X = ax + by + c$$

$$Y = -bx + ay + d$$

The four-parameter transformation imposes the condition of conformality. A common scale and orthogonality of axis is assumed. The six parameters of the general affine transformation are reduced to four parameters as follows:

$$q = 0, \text{ and } C_x = C_y$$

since orthogonality of axes and constant scale are assumed

$$a = e, \text{ and } b = -d$$

The higher number of degrees of freedom (8-4=4), increases the statistical probability for the detection of outliers in the reseau observations. While the four-parameter model may yield more degrees of

freedom, it may not model the transformation of reseau coordinates as well as the six-parameter model. The four-parameter mathematical model imposes more conditions on the solution which may not be entirely valid for the population being sampled.

The four-parameter transformation was used first for each set of reseau coordinates. The observations were assigned an accuracy 3 microns as stated accuracy BC-1 User's Manual (1984) for a single observation. The accuracy is based on an assumed linear scale error of one micron combined with other residual errors (some of which may be systematic) caused by the non-orthogonality of the comparator axes and uncompensated drift in the BC-1 measuring system. The effect of systematic errors for a single observation is assumed negligible because comparator scale and non-orthogonality will be compensated for during the transformation of raw stage coordinates into comparator coordinates. An *a priori* variance of unit weight of 1 was assumed when determining the weights for the observations.

The *a posteriori* variance of unit weight for each image point transformation was tested using the Chi Square statistic at a 90 percent single tail uncertainty level. If the *a posteriori* variance of unit weight exceeded the 90 percent single-tail test for four degrees of freedom (2.3 statistic), the comparator coordinates for that image were rejected from the final data set. The remaining image coordinates were transformed using the six-parameter transformation model. In actuality, little difference (if any) was to be gained by using the six-parameter model. The six-parameter model is used by NOAA and since the calibration was being performed for NOAA, the same model was employed. The use of an accepted model helps attain statistical control over the measuring and processing systems. This procedure was not used for the B Cone imagery because of all image coordinates were transformed using the same set of measured fiducial marks.

Additional G Cone image coordinate observations were removed from the data set based on a Case 3 (mathematical model treats survey coordinates as weight constrained parameters) aerotriangulation using survey control but not GPS control of the exposure station. A rejection criteria of 3 sigma (99 percent confidence level) for the image coordinate residuals (where sigma was the assumed standard deviation for an image coordinate observation) was used in these cases. The following observations were removed by the Case 3 aerotriangulation:

507 - all photos - only 2 sets of image observations and one of those sets was rejected by the above criteria
508 - all photos - only 1 set of image observations after the transformation
542 - all photos - only 1 set of image observations after the transformation
543 - all photos - only 2 sets of image observations and one set of those sets was rejected by the above criteria
927 - rejected in photos 21 and 23 by the above criteria
929 - rejected in photo 24 by the above criteria
998 - rejected in photo 32 by the above criteria
5135 - rejected in photo 35 by the above criteria

The selected set of image coordinates transformed into the photo system is now ready for further processing to remove known systematic errors. The following standard errors are accepted for the image coordinate data set thus far:

a. BC-1 single observation 3 microns
The standard deviation of a mean observation can be computed by dividing the standard deviation of a single pointing by the square root of the number of independent observations. Since there were three independent pointings for each ground image, the standard deviation of the mean pointing is:

$$3.0/(3^{1/2}) = 1.7 \text{ microns}$$

b. BC-1 mean observation (3 samples) 1.7 microns

A full discussion of the standard error for an image coordinate will be given in Section 6.2.2.b.

The *a posteriori* standard error of adjusted observations for the reseau points seldom exceeded 2 microns. In the several instances when the standard error exceeded 3 microns, the measured reseau points were greater than 1 cm apart suggesting less accurate modeling of film deformation. These few cases occurred when the incorrect reseau points were observed or the bracketing reseau were not useable due to the poor resolution of the image.

# CHAPTER VI
# DATA ANALYSIS

## 6.1 Identification of Systematic Errors

The goal of the GPS/photogrammetry system calibration is to design a measuring system which will minimize the sources and magnitude of errors, enable the detection of remaining error sources and model the imperfect measuring system. If the goal is obtained, then the measuring system will have achieved statistical control as defined in the beginning of this document.

Assuming that blunders can be reliably detected and random errors are minimized by the measuring technique, known sources of systematic error must be removed from the observations by modeling their effect. The difference between precision and accuracy is based on the magnitude of systematic error (Mikhail and Ackerman (1976)) which remains after all other sources of error have been identified and removed from the observations. Precision includes only random effect while accuracy is a combination of random and systematic effects (biases).

A measure of accuracy proposed by Gauss (Mikhail and Ackerman, 1976) is the Mean Square Error (MSE) which follows:

$$\text{MSE} = \text{population variance} + (\text{systematic error})^2$$

which can be approximated by

$$\text{MSE} = \text{sample variance} + (\text{systematic error})^2$$

when the sample variance is an unbiased estimator of the population variance.

As the systematic errors are identified and removed, the MSE will approach the unbiased estimate of the sample variance. In this special circumstance the results of the system calibration can be assigned a measure of accuracy which represents its uncertainty.

The measuring system associated with GPS controlled photogrammetry has various sources of systematic errors which occur due to the measuring environment and instrumentation. The remainder of the section will be devoted to an in-depth analysis of each systematic error considered for the measuring system.

### 6.1.1 Timing

The general relationship between the survey coordinates of the GPS aircraft antenna phase center and the exposure station of the camera is a function of space and time. The spatial relationship is defined by the vector between the GPS antenna phase center and the camera lens entrance node. The antenna phase center is the point within the antenna's electrical field where the received signals are assumed to converge. The entrance node of the camera lens (1st node) is defined as a point within the lens system where all light rays from the object space will pass as they travel towards the film plane. The object space is assumed to end at the entrance node and, therefore, this point is also considered to be the exposure station of the camera defined in terms of the survey coordinate system. This relationship was presented in Section 2.4.

Time also plays an important role in relating the GPS position of the aircraft's antenna to the camera exposure station. Generally, it is not

practical to synchronize the collection of GPS information with the instant of exposure. The collection of GPS information is synchronized to uniform intervals of GPS time while the aerial film is exposed according to a desired overlap dependent on the instantaneous and continuously varying velocity of the aircraft. It will be shown in Section 6.1.2 that it is not necessary to synchronize the two events if the timing offset can be kept to less than 0.5 sec, requiring the design of the GPS receivers to collect data as frequently as once a second. At ground speeds of 150 mph, the aircraft travels 67 meters per second! The GPS time of the exposure must be determined to an accuracy of 0.5 msec (3 cm @ 150 mph) in order to ensure the positioning of the exposure station to an accuracy of 10 cm, i.e., the predicted precision obtainable from kinematic GPS positioning. The following discussion will begin with the assumption that the aircraft motion can be adequately modeled within intervals of less than one second. Proof of this assumption cannot be verified directly since GPS receivers with a faster sampling rate are not available. The excellent agreement between GPS and aerotriangulated positions for the exposure stations gives credibility to the assumption. Section 6.1.2 will present a study of the effect of less frequent sampling intervals on the accuracy of interpolating the aircraft's trajectory.

6.1.1.a An Example of System Timing Techniques

The experiments conducted on DOY 299 and DOY 301 employed Wild Heerburg RC-10 camera systems and Motorola Eagle GPS receivers. The time delay between the exposure and GPS events was determined and recorded by a Hewlett Packard (H/P) 100 Mhz Universal Counter and H/P desk-top calculator. A typical exposure event proceeded as follows:

a. The RC-10 camera system intervalometer triggers an exposure sequence.

b. The RC-10 shutter control opens the capping shutter which generates an electronic pulse to trigger a horizon camera.

c. The horizon pulse triggers the start of the H/P frequency counter (a sophisticated stop watch).

d. The next electronically generated Pulse Per Second (PPS) from the Eagle GPS receiver stops the frequency counter.

e. The H/P desk-top calculator records the elapsed time interval accumulated by the universal counter and time tags the interval by recording the displayed time of a digital clock synchronized to GPS time.

The time interval between horizon pulse and PPS will always be less than one second. The position of the exposure station based on the measured time difference will be affected by the following factors:

a. The aircraft travels through a non-homogeneous medium which results in abrupt changes in an otherwise uniform trajectory of the aircraft. Prediction of these changes would be difficult, if not impossible, if the sampling rate of the trajectory were not frequent enough. Using a previous GPS/photogrammetry experiment conducted by Lucas, where every other GPS epoch was removed, (thus increasing the time interval between fixes to two seconds), it was demonstrated that the standard deviation for a sample of survey point positions (aerotriangulated minus survey control) increased from approximately 5 cm to 41 cm. Although this demonstration was a limited sample, the result of increasing the time between GPS samples is clear.

b. A uniform timing interval enables the use of efficient equal interval interpolation algorithms or finite differencing techniques.

c. Even sampling intervals will make the detection of biases easier. This point is most clear when one examines the GPS navigation data set. During periods of nearly straight-line trajectory, a constant rate of change (velocity in cardinal directions) of the coordinates will be noted. Any deviations can be efficiently and predictably found through the double differences of the sequential GPS coordinates representing the position of the aircraft antenna.

d. The longer the interval between epochs, the greater the demand for long-term stability of the frequency counter. The universal counter selected for the experiment had a published stability of 0.1 micro-seconds over one second time spans. This stability estimate is degraded when starting and ending timing biases are added. A better estimate for complete timing events of less than one second is 1 micro-second.

The time interval between the horizon pulse and PPS signal was investigated for the following time-related biases:

a. Horizon camera timing pulse to center of exposure.

b. True exposure time to shutter midpoint of opening.

c. Timing biases in the timing circuit.

d. GPS epoch time to output of a one pulse per second (PPS) timing signal.

6.1.1.b Horizon Camera Pulse to Center of Exposure

The RC-10 camera generates an electronic pulse to trigger a horizon camera through an electra-mechanical process. The timing of this pulse is directly related to the shutter speed in order to generate the horizon pulse reasonably close to the actual transmission of light through the open shutter. The timing sequence for shutter opening begins with a command from the intervalometer to the camera. This pulse enables a circuit to open the capping shutter for a given time span (longer than the shutter opening). The actual capping shutter open command signal is generated by the closing of a reed switch. This switch is drawn closed by a magnet (situated on one of the shutter blade timing gears) as it passes beneath the reed switch. The magnet then passes underneath a second reed switch and the closing of this reed switch generates the horizon pulse. These pulses are logically "AND" together so that the capping and horizon pulses only occur when combined with the intervalometer command. The actual exposure will occur sometime after the capping shutter pulse when the rotating shutter blades are properly aligned and the capping shutter is still open.

The transmission of light through the lens system to the film occurs sometime after the closing of the capping shutter reed switch but not necessarily before the closing of the horizon camera reed switch. Three different RC-10 cameras were tested and three different timing biases for horizon pulse to shutter opening were found. A simple experiment was devised by the author to determine the timing bias for each camera. The bias is dependent on shutter speed and can be accurately modeled only if a well distributed set of shutter speeds is sampled. Two of the cameras exhibited a constant timing offset between horizon pulse and center of shutter opening while the third camera exhibited a timing bias which was linearly proportional to the shutter speed. To the author's knowledge, this is the first time the shutter to external pulse timing bias has been this thoroughly investigated for an aerial camera. Taylor

(1962 and 1964) reported that the midpoint of shutter opening on a Wild BC-4 satellite tracking camera which also uses a rotating disk shutter could be determined with an accuracy of 100 micro-seconds using an electronically generated timing pulse, a similar but not identical shutter timing measurement process. Subsequent investigations by the University of Texas Applied Research Laboratory (Coker 1989) revealed results similar to the author for a Wild RC-20 aerial camera.

The shutter timing bias was detected in the first place because the flight line design included flight lines in opposite directions. A shutter to horizon pulse timing bias of approximately 3 msec was predicted from the data. Once again, this is the first GPS/photogrammetry experiment to involve flight lines in opposite directions. The problem was exacerbated by using different cameras to photograph the same test area.

6.1.1.c Testing the NOAA G Cone

The first independent determination for the timing bias of the horizon pulse relative to the midpoint of shutter opening, was performed in a laboratory setting using the NOAA G Cone. The midpoint of shutter opening was assumed to agree with the instant of exposure. The bias between the midpoint of shutter opening and the actual chemical reaction between the incoming photons of light through the lens system and the emulsion of the film is assumed to be negligible. The experiment was conducted with the assistance of Frank Huffman, an electronic engineer in the OSU Department of Geodetic Science and Surveying. For the initial test, only the lens cone assembly was available. A small electronic circuit was designed to simulate the intervalometer. Figures 10 and 11 illustrate the test layout while Figure 12 is a schematic of the circuit which simulated the intervalometer.

A two channel oscilloscope was used to display the horizon pulse and shutter-open signal once triggered by the intervalometer. The electronic circuit mentioned above produced a pulse similar to the intervalometer which activated the capping shutter and horizon pulse circuitry contained within the lens cone. The shutter open/close signal for the oscilloscope was produced by light passing through the lens system which in turn illuminated a photo diode that generated an electric current. Several light sources were used to trigger the photo diode. Florescent lighting produced the highest current by the photo diode. The higher current created a well defined step function on the oscilloscope display, indicating a very low signal to noise ratio and, therefore, more accurately determinable pulse width. Incandescent light caused a weaker and sightly delayed reaction compared to florescent light. The horizon pulse triggered the start of the oscilloscope sweep while the shutter-open signal was displayed sometime thereafter, depending on the shutter speed. This test was used to model the timing bias of the horizon pulse with respect to the shutter opening and the effective shutter speed. A 75 percent efficiency level of the shutter opening (see Figure 13) was assumed by measuring from midway up the slope of the shutter opening to midway down the slope of shutter closing. Varying the light intensity in subsequent tests proved that nearly all the slope was due to the reaction time of the photo diode. Every attempt was made to maximize the light intensity prior to the measurements. The combined effect of the slope on both ends was reduced to less than 0.2 msec by using a sufficiently bright light source and by carefully positioning the photo diode in the plane of focus. Shutter speeds between 1/400 and 1/1000 sec were sampled a minimum of ten times, on two different days. For the first test, the lens and shutter mechanisms were allowed to run at a shutter speed of 1/500 sec (the nominal speed used by NOAA) for approximately 30 minutes prior to sampling to allow the camera to reach thermal equilibrium (an average

warm-up time used by NOAA). The first test took a total of 1.5 hours to complete. A second test was performed the following day with no warmup time. The results agreed with the previous day within the resolution of the oscilloscope of 0.1 msec. The conclusion drawn from the second test is that the shutter system is not temperature sensitive within a reasonable operating range ($60^0$-$80^0$).

The timing bias, however, was shutter-speed dependent. The G Cone was subsequently tested a third time in the NOAA aircraft using the system's intervalometer. The results of the third test verified the previous laboratory experiment, thus confirming that the laboratory environment was not significantly different from the actual operating environment of the measuring system. Once again, confidence was gained in the measuring process, enforcing the fact that statistical control was being achieved. As will be discussed later, the G Cone was the only camera lens cone to exhibit a timing bias dependent on the shutter speed.shutter speed of 1/500 sec (the nominal speed used by NOAA) for approximately 30 minutes prior to sampling to allow the camera to reach thermal equilibrium (an average warm-up time used by NOAA). The first test took a total of 1.5 hours to complete. A second test was performed the following day with no warmup time. The results agreed with the previous day within the resolution of the oscilloscope of 0.1 msec. The conclusion drawn from the second test is that the shutter system is not temperature sensitive within a reasonable operating range ($60^0$-$80^0$).

The timing bias, however, was shutter-speed dependent. The G Cone was subsequently tested a third time in the NOAA aircraft using the system's intervalometer. The results of the third test verified the previous laboratory experiment, thus confirming that the laboratory environment was not significantly different from the actual operating environment of the measuring system. Once again, confidence was gained in the measuring process, enforcing the fact that statistical control was being achieved. As will be discussed later, the G Cone was the only camera lens cone to exhibit a timing bias dependent on the shutter speed.

The electronic device designed by Frank Huffman to replace the intervalometer could be used to measure the effective shutter speed as well as the timing bias. The shutter speed is regulated by voltage supplied to the shutter motor. Under actual operating conditions, the shutter motor is supplied 24 volts (nominal) but the voltage is interrupted by a tachometer feedback circuit to control the shutter motor speed. In the laboratory tests a constant voltage from a variable regulated power supply was used. The shutter system is designed to provide a continuously variable shutter speed from 0 to 1/1000 sec as the voltage is varied from 0 to 15 volts. The voltage and shutter speed are dependent. The test was designed to check the shutter speed voltage against the effective shutter speed and determine the timing bias at the same time. Figure 14 illustrates the measurements recorded by the oscilloscope. Referring to the figure, the beginning of the sweep indicates the horizon pulse trigger. The points $T_1$ and $T_2$ represent the 75 percent efficiency level. The actual oscilloscope trace was used to measure the time differences between the horizon pulse, opening, and closing events. Each shutter speed determination was performed ten times.

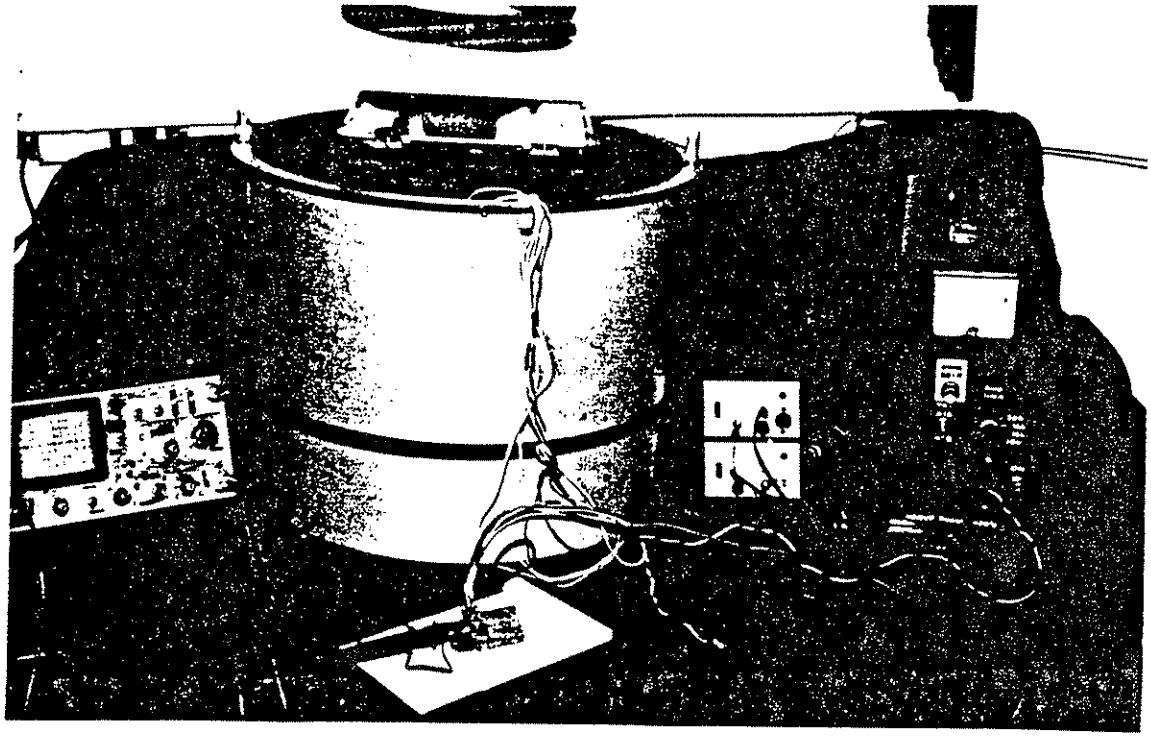

Figure 10 - Equipment Test Set-Up For Shutter Timing

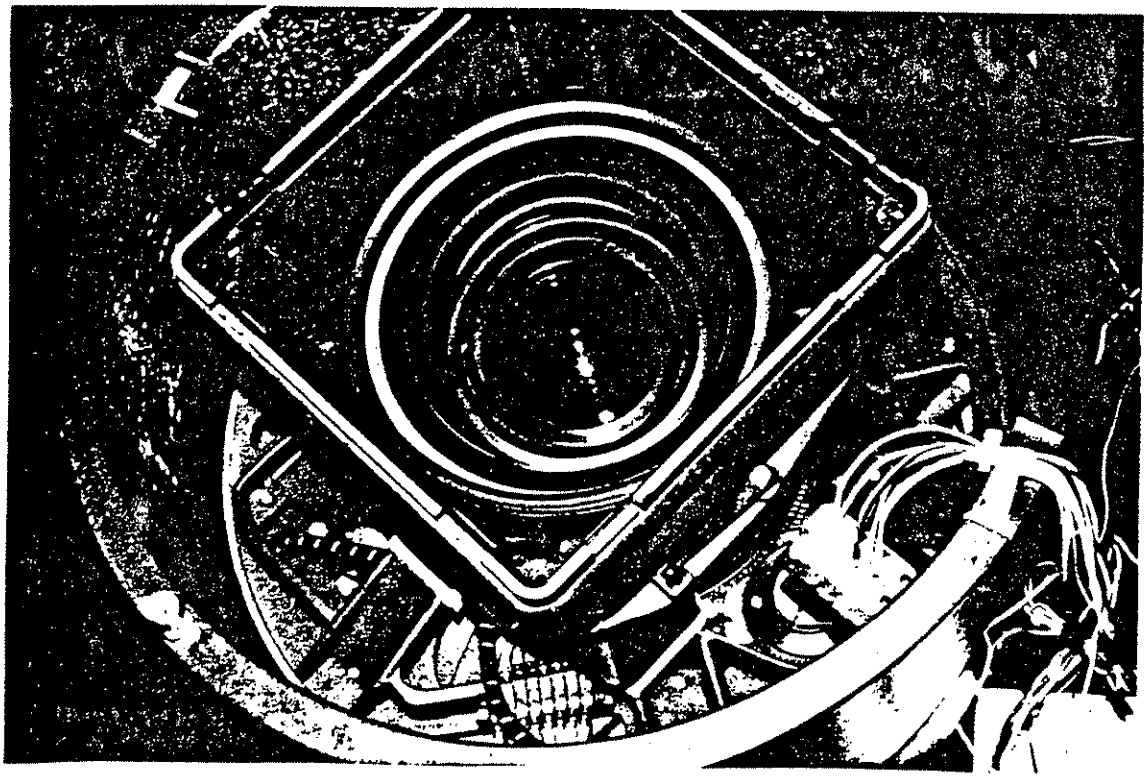

Figure 11 - Wiring Set-Up For Shutter Timing Test

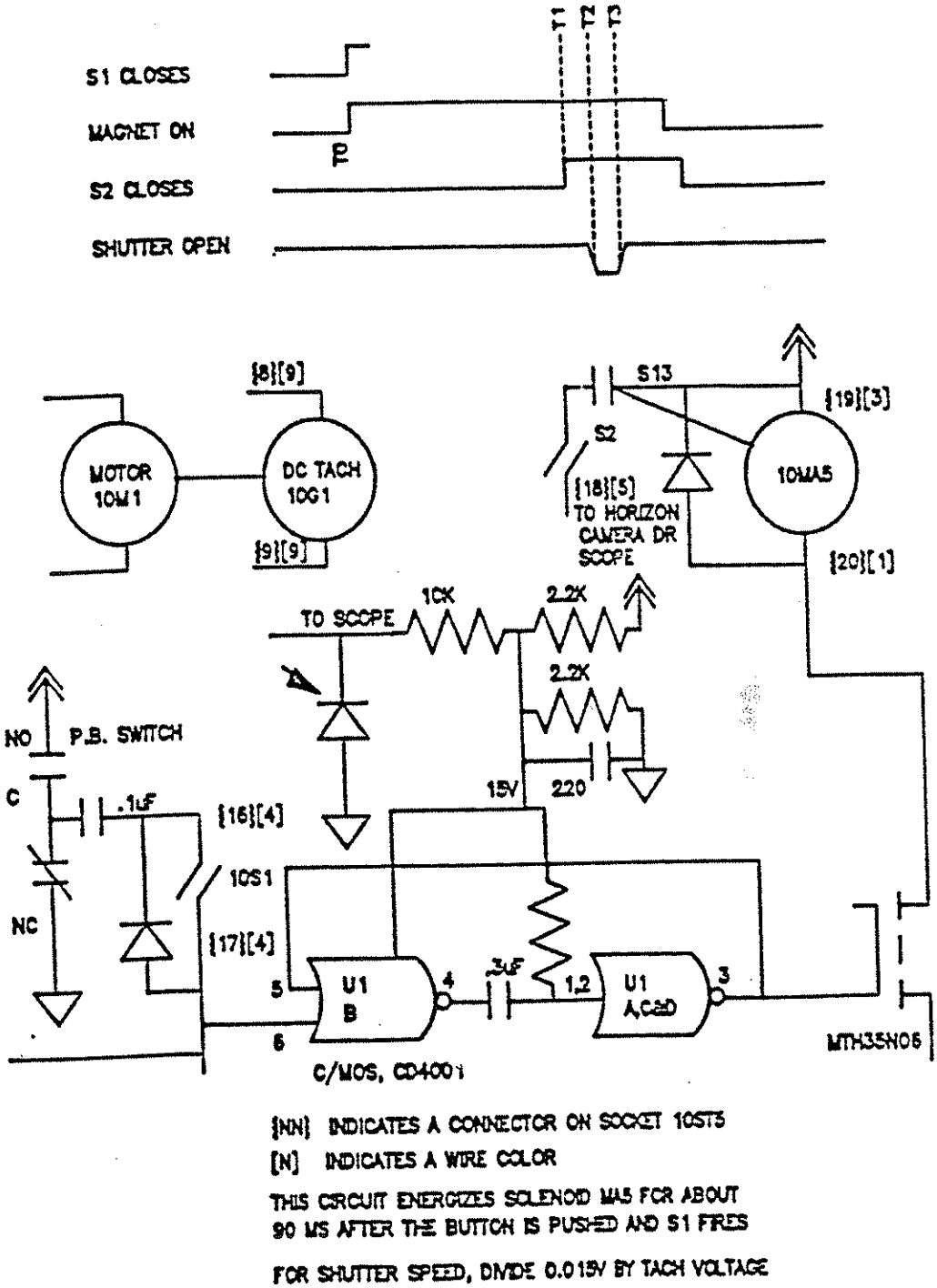


CIRCUIT SCHEMATIC OF INTERVALOMETER SIMULATOR

Figure 12. Circuit Schematic of Intervalometer Simulator

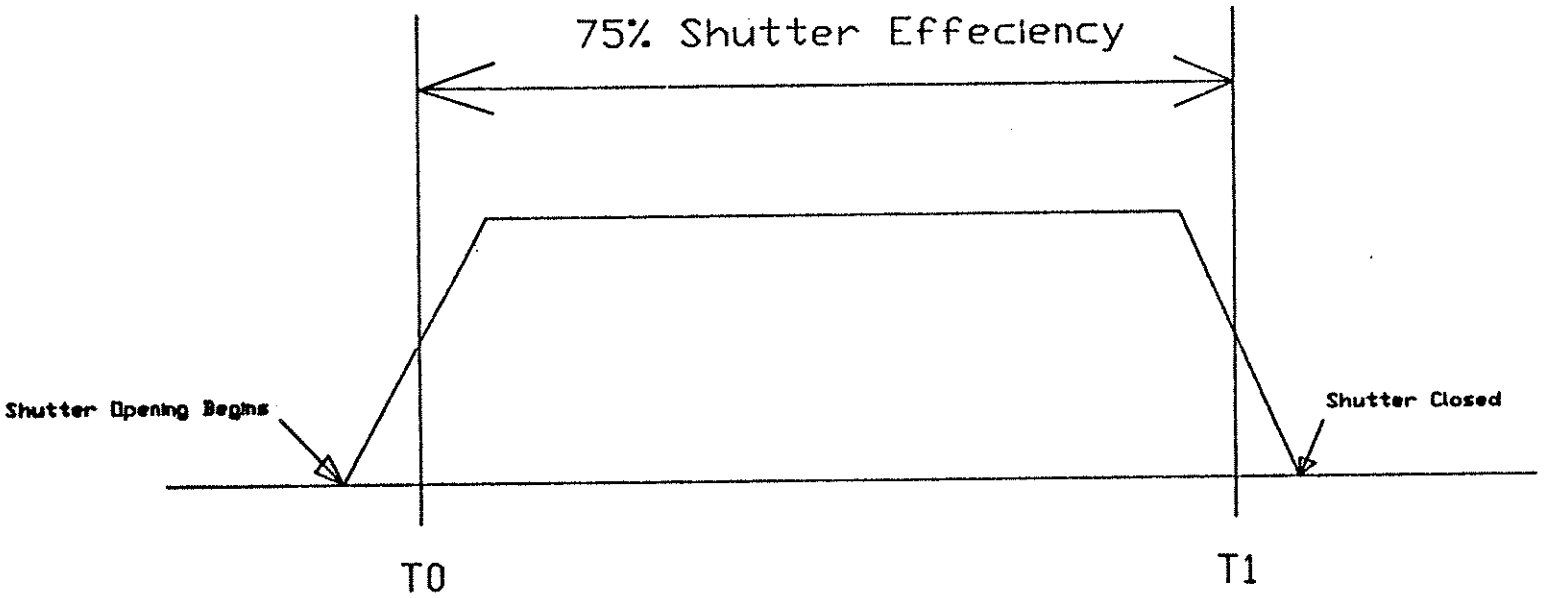


Figure 13. 75 Percent Efficiency of Shutter Opening

In addition to measuring the three events, the voltage supplied to the shutter motor was also recorded. The midpoint of the shutter opening as well as the timing bias were mathematically modeled by the following equation:

$$T2 - T1 = 15*B/C$$

where T1 = shutter opening
(opening event - horizon pulse event)
T2 = shutter closing
(closing event - horizon pulse event)
B = scale factor for voltage readings
C = volts monitored at the shutter motor

The scaling factor B was included in the model to account for any scaling error in the volt meter used to monitor the shutter motor voltage and scale factor correction for the assumed ratio of 15 volts to 1/1000 sec shutter speed relationship. A least-squares solution was used to compute the unknown parameter B and adjust the observed values T1, T2 and C. The arithmetic mean of the adjusted pairs of T1 and T2 yields the horizon pulse timing bias from the center of shutter opening for a given shutter speed. The shutter speed for a given pair of adjusted T1 and T2 values is the inverse of their absolute difference.

The same model expressed slightly differently can be used to compute adjusted shutter speeds for a given supply voltage to the shutter motor. The following model was used:

$$A = 15*B/C$$

where A = shutter speed in msec (T2-T1)
B = scale factor for voltage readings
C = volts monitored at the shutter motor

In this model the unknown parameter is the scaling factor B, while the observed quantities are A and C. The shutter speeds from this model will of course be the same as from the previous model. With the latter model, there is no need to trigger the scope with the horizon pulse.

The *a posteriori* variance of unit weight from the first model was 1.006 with 19 degrees of freedom. The Chi Square ($X^2$) Test supports that the variance is a valid estimate of the *a priori* variance of unit weight at the 95 percent confidence interval as follows:

$H_0$ : $Sigma^2$ equals 1.0; vs $H_1$ : $Sigma^2$ not equal 1.0

$$P(X^2_{(19,0.025)} > X^2 > X^2_{(19,0.975)}) = 0.95$$

where $X^2 = 19*1.006/1.000 = 19.114$

$X^2(19,0.975) = 8.91$

$X^2(19,0.025) = 32.85$

so it can be seen that

$$P(32.85 > 19.114 > 8.91) = 0.95$$

and the Null hypothesis not rejected.

Figures 15 and 16 and Tables 6a and 6b summarize the results of this investigation.

6.1.1.d Timing Bias Tests of the NOAA B, G, and Z Cones

Armed with the results of the timing bias test from the G Cone, it was assumed that all camera cones would have the same timing bias. Data reduction was started for the two missions , one involving the G Cone and the other involving the B Cone camera (DOY 299-G Cone, DOY 301-B Cone). Initial data processing with the G Cone and GPS data went according to plan, but the B Cone data would not correlate well with the GPS information. There appeared to be a 2 or 3 msec timing bias between lines flown in opposite directions. The magnitude of the bias was equal to, but of opposite sign, to the horizon pulse bias modeled for the G Cone. In order to resolve the problem, a new test was conducted which included all NOAA camera cones. The B and Z cones were in operational status and could not be shipped to The Ohio State University. A new test was devised to determine the timing bias while the various cameras were installed in the NOAA aircraft. The experiment was moved to the operational site of the aircraft. These tests did not require the special electronic circuit because the Wild Heerburg intervalometer was used to operate the shutter. The oscilloscope was triggered directly by the horizon pulse, while the output from the photo diode used in the previous tests was displayed by the sweep. A point was made to use as much of the same equipment as possible to minimize any new timing biases into the measuring system. As predicted by processing the flight lines flown in opposite directions with the B Cone, the timing bias for the B Cone proved to be at the center of exposure a timing difference of 3 micro-seconds! The G Cone was re-installed in the aircraft and tested. The results agreed exactly with the laboratory experiment. This gives strong proof that there is no difference between the two experiments or environments. While the equipment was assembled, a third NOAA camera cone (designated as the Z Cone) was tested and modeled for future work.

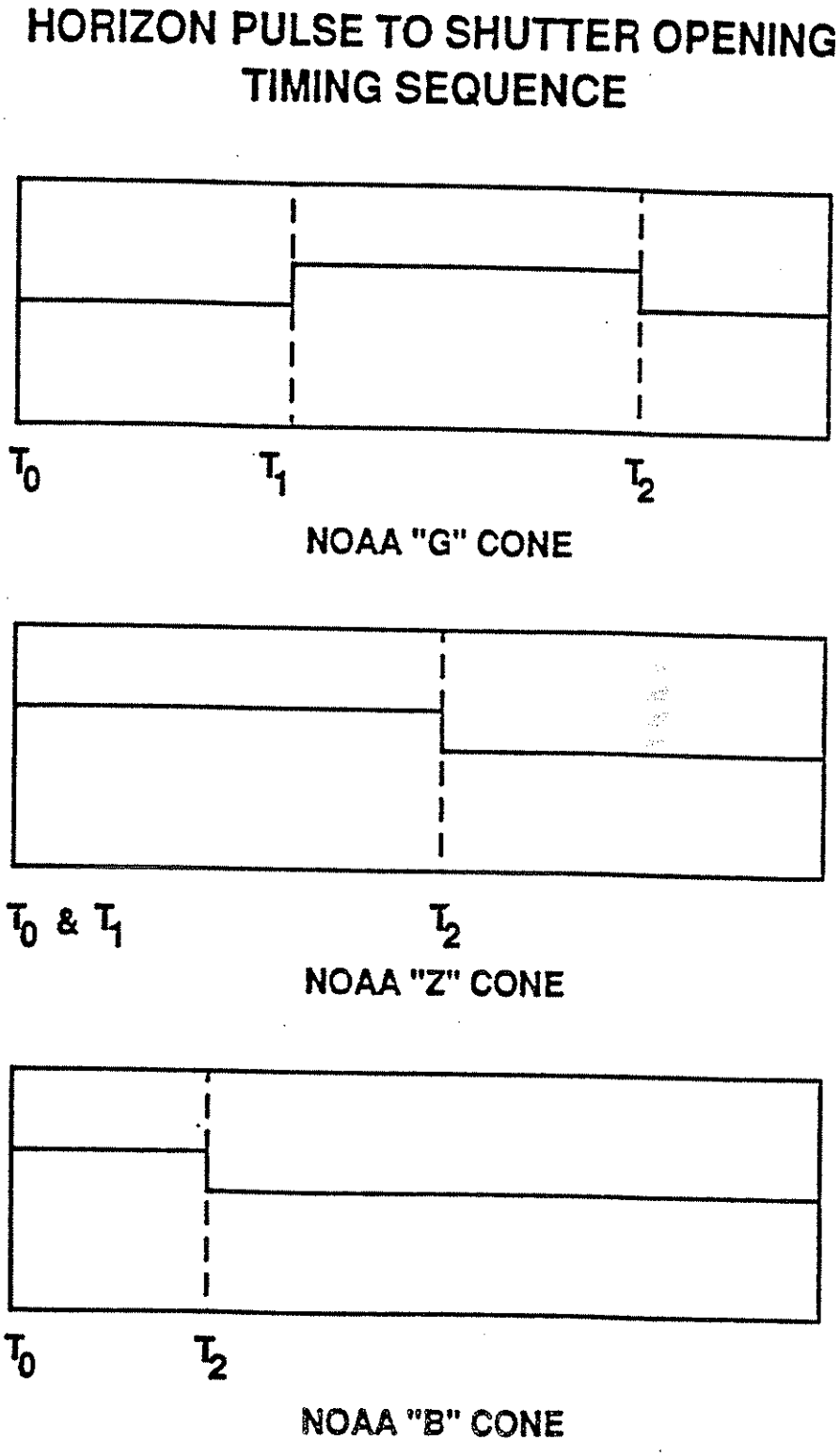


Figure 14. Horizon Pulse to Shutter Opening Timing Sequence

Table 6a -- Delay in Milliseconds Between the Horizon Pulse and Shutter Midpoint of Opening

Wild RC-10 Geodetic Lens Cone Shutter Calibration

Mathematical Model: T2 - T1 = 15*B/C
T1 = Shutter Opening in Milliseconds
T2 = Shutter Closing in Milliseconds
B= Scale Factor Correction for Voltage Readings
C = Voltage Monitored at the Motor Drive Tachometer
Delay = T1 + (T2 - T1)/2

| C volts | Adjusted T1 msec | T2 msec | Delay msec |
|---|---|---|---|
| 15.096 | 1.228 | 2.222 | 1.725 |
| 15.189 | 1.186 | 2.174 | 1.680 |
| 13.300 | 1.371 | 2.499 | 1.935 |
| 11.995 | 1.575 | 2.825 | 2.200 |
| 12.097 | 1.545 | 2.785 | 2.165 |
| 12.097 | 1.545 | 2.785 | 2.165 |
| 12.028 | 1.541 | 2.789 | 2.165 |
| 12.114 | 1.561 | 2.799 | 2.180 |
| 10.517 | 1.812 | 3.238 | 2.525 |
| 9.091 | 2.175 | 3.825 | 3.000 |
| 8.946 | 2.162 | 3.838 | 3.000 |
| 9.041 | 2.050 | 3.710 | 2.880 |
| 9.008 | 2.132 | 3.798 | 2.965 |
| 8.994 | 2.166 | 3.834 | 3.000 |
| 7.456 | 2.644 | 4.656 | 3.650 |
| 5.795 | 3.506 | 6.094 | 4.800 |
| 6.094 | 3.319 | 5.781 | 4.550 |
| 6.094 | 3.319 | 5.781 | 4.550 |
| 6.164 | 3.283 | 5.717 | 4.500 |
| 6.144 | 3.194 | 5.636 | 4.415 |

V'PV = 19.240 $\quad \text{Sigma}_0^2 = 1.006$ Degrees of Freedom = 19

B = 1.000050

Table 6b -- Shutter Speed as a Function of Shutter Motor Voltage

---

Wild RC-10 Geodetic Lens Cone Shutter Calibration

Mathematical Model: A = 15*B/C
A = Shutter Speed in Milliseconds
B= Scale Factor Correction for Voltage Readings
C = Voltage Monitored at the Motor Drive Tachometer

| C volts | Shutter Adjusted Speed msec |
|---|---|
| 15.096 | 0.994 |
| 15.189 | 0.988 |
| 13.300 | 1.128 |
| 11.995 | 1.251 |
| 12.097 | 1.240 |
| 12.097 | 1.240 |
| 12.028 | 1.247 |
| 12.114 | 1.238 |
| 10.517 | 1.426 |
| 9.091 | 1.650 |
| 8.946 | 1.677 |
| 9.041 | 1.659 |
| 9.008 | 1.665 |
| 8.994 | 1.668 |
| 7.456 | 2.012 |
| 5.795 | 2.589 |
| 6.094 | 2.461 |
| 6.094 | 2.461 |
| 6.163 | 2.434 |
| 6.145 | 2.441 |

V'PV = 18.879 $\quad Sigma_0^2$ = 0.997 Degrees of Freedom = 19

B = 1.000051

---

# HORIZON PULSE TIMING BIAS
## NOAA "G" Lens Cone

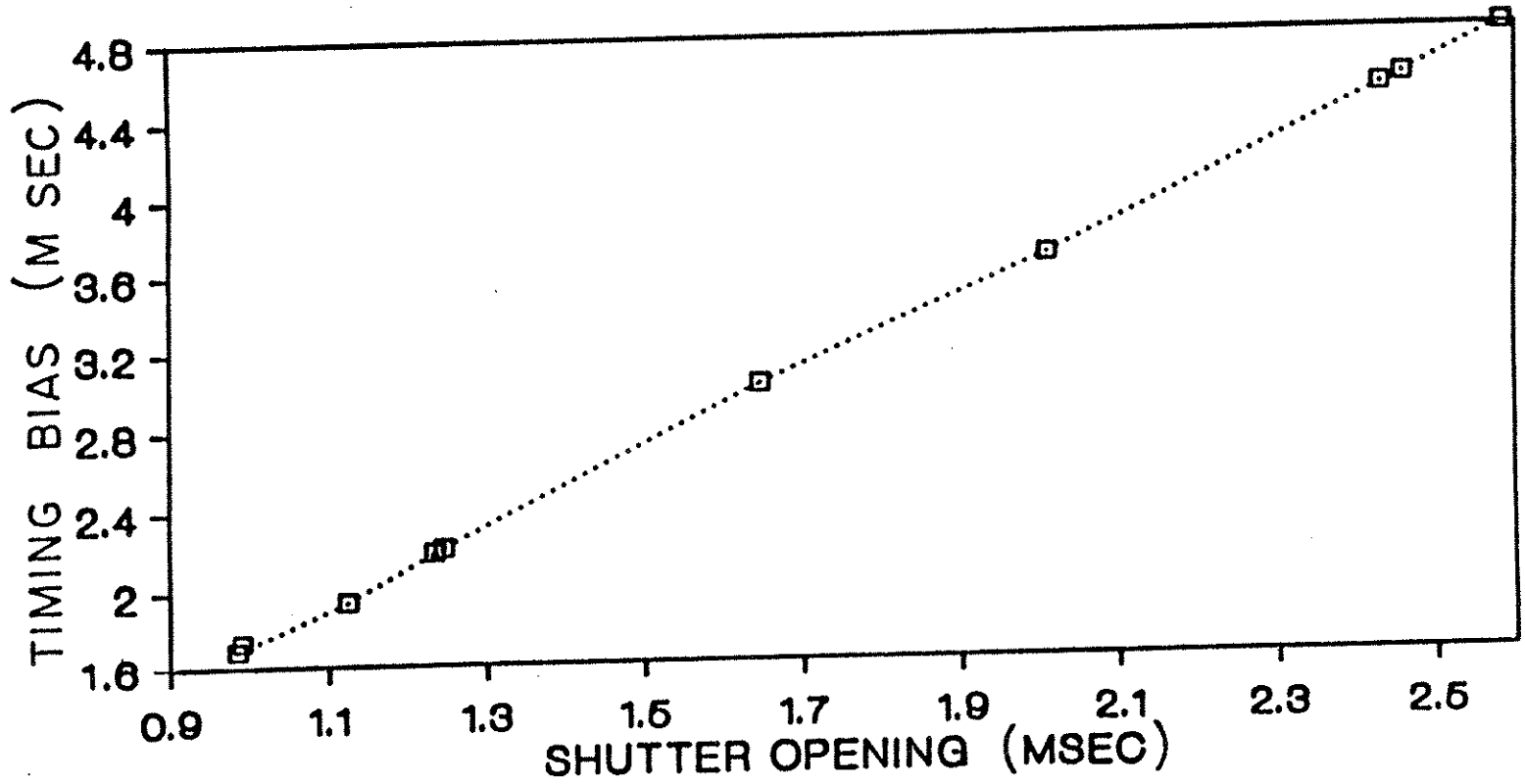


Figure 15. Horizon Pulse Timing Bias - NOAA G Lens Cone

# VOLTAGE VS. SHUTTER OPENING
## NOAA "G" Lens Cone

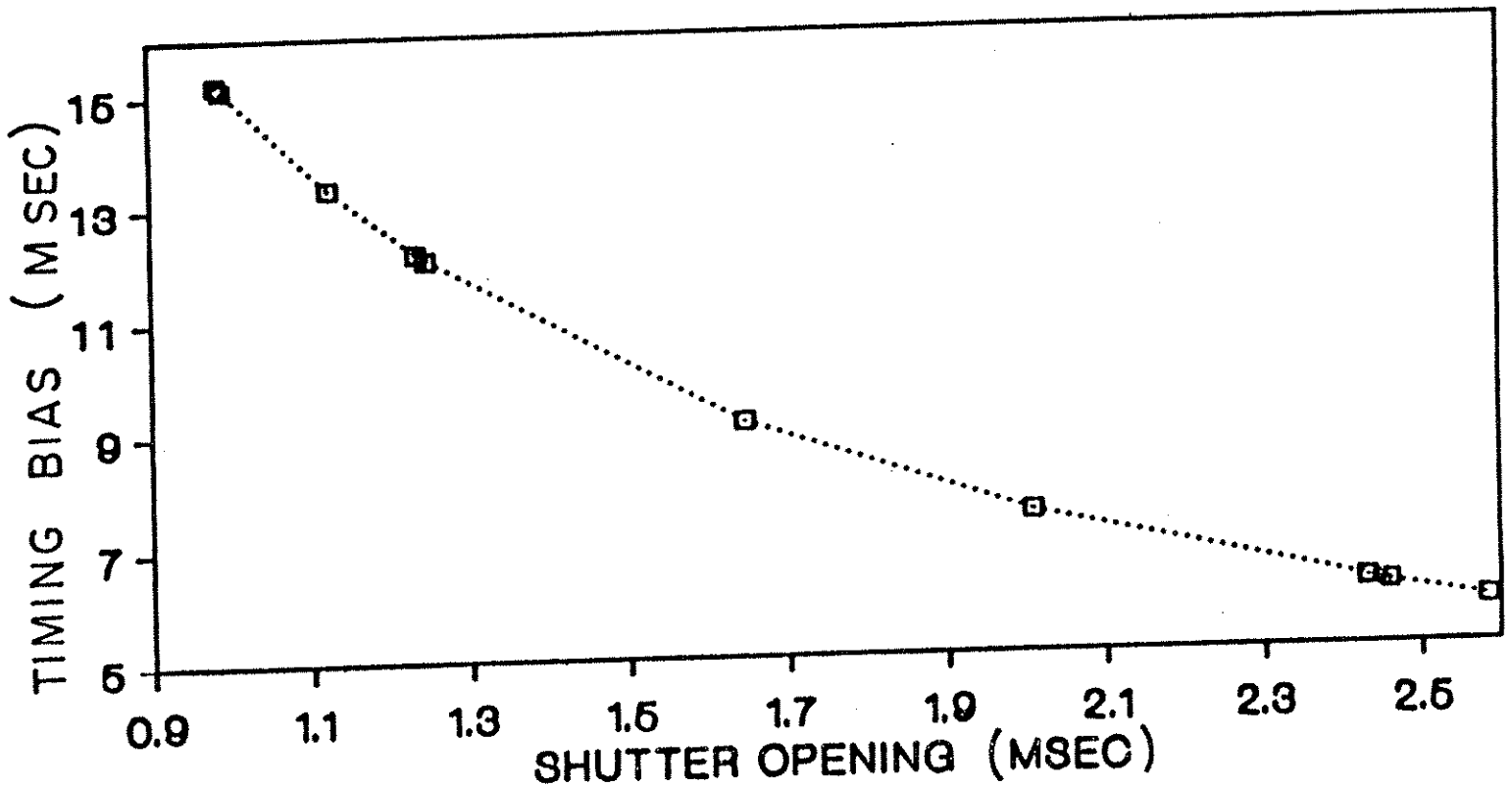


Figure 16. Voltage Vs. Shutter Opening - NOAA G Lens Cone

For the B and Z Cones, the horizon pulse is generated at or during the shutter-open sequence so, it was not possible to observe the complete shutter opening and closing events (T1 and T2). Although it was still possible to determine the offset, the shutter speed could not be directly determined. The shutter speed in these cases came from the indicator on the intervalometer. Since the intervalometer was calibrated by USGS in May, 1989 and since the results of the G Cone agreed, it is assumed that the intervalometer controlled the shutter opening as calibrated. An attempt was made to capture the shutter-open sequence by manually triggering the oscilloscope. It proved difficult to observe the full shutter opening with any regularity. In the future, a tap on the capping shutter reed switch should be devised to trigger the oscilloscope display during shutter calibration. Once the shutter is calibrated to the intervalometer, the test could proceed with more confidence.

The determination of the shutter bias in the laboratory and aircraft situation, as well as by use of aerotriangulation, represents the second significant contribution to the research.

6.1.1.e True Exposure to Indicated Exposure Time

A secondary conclusion, inferred from the above tests, is that higher shutter speeds will result in less timing bias due to the uncertainty of the exact instant of the "chemical reaction" which creates the image in the negative emulsion. The image is created from a chemical reaction precipitated by the incoming light energy and the chemical composition of the emulsion. The exact moment of "chemical exposure" is difficult, if not impossible, to determine. Any assumption based on the exact time of exposure will, therefore, be biased by this uncertainty. Some undocumented tests were performed by NOAA using a Wild BC-4 camera and stellar images in the early 1960s. These tests suggest that the instant of exposure occurs 60 percent of the way through the shutter opening sequence. The tests, however, were concerned only with a monochromatic light source from stars. In the case of aerial photography, a broader light spectrum and, therefore, a more complicated energy spectrum must be considered. One way to minimize this problem and at the same time minimize image motion is to use the highest possible shutter speed thereby shorting the lens opening. The difference between shutter midpoint and 60 percent opening will become smaller as the shutter speed increases.

6.1.1.f Timing Biases in the Timing Circuit

Timing biases were also discovered in the H/P timing circuit composed of the Hewlett Packard universal counter and desk-top calculator. Subsequent to the experiment, it was discovered that none of the recorded time intervals (Horizon Pulse to PPS) ever exceeded 0.5 sec even though it was logical to expect timing intervals from zero to one second. It was found that nearly half of the GPS positions for the exposure stations were in gross error (greater than 35 meters) relative to the exposure station positions obtained strictly from survey-controlled aerotriangulation. The photogrammetric exposure station positions were used to determine the time of exposure by reverse interpolation of the navigation file of one second positions. In every case where there was a suspected gross error, the interpolated time differed from the timing circuit time by almost exactly 0.5 sec. A timing circuit error of 0.5 sec was suspected. The intervalometer was set to generate exposures of equal 80 percent end lap (not necessarily equal time separation) so that the time intervals between exposures were not quite equal (+/- 0.1 sec). The difference between the times of exposure was, however, close enough to accurately predict 0.5 sec timing biases through a double-difference technique. The exposure timing information (PPS-Horizon Pulse) for a complete mission was assembled

into a single file. The adjacent times were subtracted from one another (single differences) resulting in a new file having nearly uniform time differences except at the boundaries between flight lines. The single differences were subtracted from one another (double differences). The new double-difference file contained values of zero, one, or large values. Zero differences infer correct timing differences between adjacent samples. Differences of one second infer the transition between 0.5 sec timing errors. The large differences once again represent the boundaries between adjacent flight lines. To test this conclusion, the predicted 0.5 sec timing errors from the double differences were compared against the differences detected between photogrammetry and GPS determinations of exposure station positions from the interpolation technique. A perfect agreement was found between these methods of detection. Future missions were pre-processed by the double-difference technique to eliminate the 0.5 sec timing biases. A programming error in the H/P universal counter is suspected to have caused this problem.

6.1.1.g Timing Biases from the GPS Receiver

The PPS signals generated by the Motorola GPS receiver used in the experiment were also found to contain timing biases between this signal and the GPS epochs. In this case, it was assumed from the information contained in the User's Manual (1987) that all timing was coincident with the GPS time tag for the epoch. The PPS should have the same time tag as the GPS data (the time tags were not uniformly spaced because of receiver clock drift). Again, the processing of lines flown in opposite directions, appeared to have timing biases of approximately 1.5 msec. The timing biases varied line to line and mission to mission. Although most noticeable on the comparison of flights in opposite directions, this bias adversely affected the incorporation of the center flight line in combination with the side strips. Upon further consultation with Motorola, it was determined that the timing circuit for the PPS was designed to produce the pulse on the GPS "rollover" or integer second. The timing for the pulse generation is based on and corrected for the most recent epoch of GPS information. It is very important to realize that the initial GPS navigation files were not based on integer time. The timing bias between the navigation file and PPS was eliminated by reprocessing the navigation information using program OMNI to shift all time-tagged information to the GPS integer second. Figure 17 illustrates the potential problems when proceeding from relative time of the timing device and absolute time ($T_K$) of the navigation file.

$$T_{EXP} = (T_{K+1} - dT) + (T_{PPS} - T_{K+1}) + (T_{EXP} - T_{HP})$$

In the above equation the time interval ($T_{EXP} - T_{HP}$) represents the horizon pulse to shutter midpoint of opening as determined from the shutter timing experiments. ($T_{PPS} - T_{K+1}$) is the GPS time difference between the PPS and the nearest integer second. In the case of the Motorola Eagle, this time interval is zero seconds. The time span for interpolation can be obtained from the following equation:

$$\text{Interpolation Time Span} = T_{FIX} - T_{EXP} + T_K$$

6.1.2 Exposure Station

The GPS receiver collects the carrier phase and pseudo-range information pertaining to the trajectory of the aircraft throughout the photo mission. The raw data are processed by OMNI into trajectory information consisting of GPS time-tagged geocentric positions for the GPS antenna phase center which is correlated to the exposure station through time and orientation of the spatial offset system described earlier. The antenna position at the time of exposure can be computed by interpolating the trajectory based on the time of exposure. The camera

# CAMERA TO GPS TIME SCENARIO

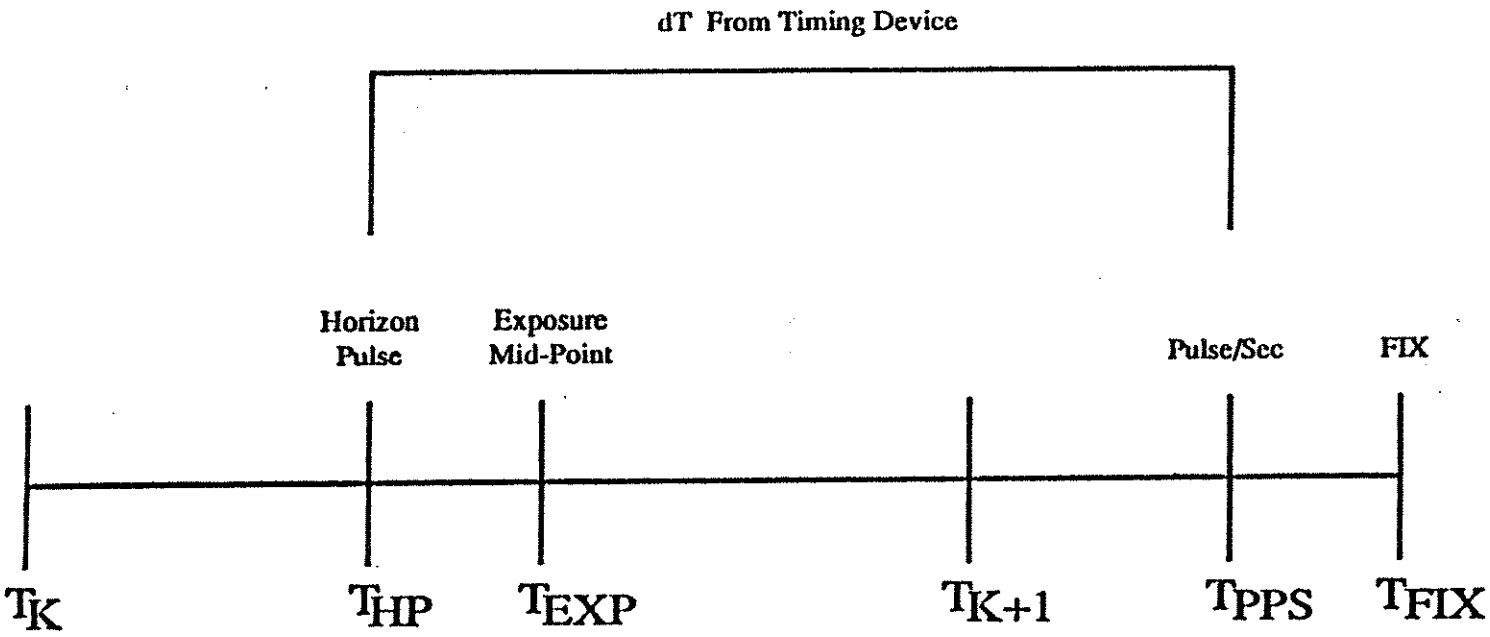


$$T_{EXP} = (T_{K+1} - dT) + (T_{PPS} - T_{K+1}) + (T_{EXP} - T_{HP})$$

Position Interpolation Time = $T_{FIX} - T_{EXP} + T_K$

K = Seconds

Figure 17. Camera to GPS Time Scenario

exposure station position can then be computed using an orthogonal three-dimensional transformation incorporating the spatial offsets and a *priori* estimates for the elements of exterior orientation. The error of the individual component observations can be propagated during this process to yield a covariance matrix for the camera exposure station. Since it is not practical to control the GPS collection by the exposure event. The antenna phase center position at the time of exposure must be computed by interpolating the aircraft trajectory after the appropriate timing biases have been added to the observed exposure time.

The GPS signals are sampled on a nearly uniform time interval affected only by a very small (1 micro-second/sec) drift in the receiver clock. The signals, subsequent to being processed by OMNI, have receiver clock drift removed and have been time shifted so that all antenna positions are equally spaced in time. The interpolation becomes simplified since the data points are evenly spaced in time. The length of the uniform interval (time between successive epochs of data) is governed by the GPS receiver hardware and may be the limiting factor for the accurate interpolation of the exposure station position from the aircraft trajectory. A one-second data collection rate is currently found to be most acceptable. Shorter intervals may be more desirable from the standpoint of interpolation accuracy, but are not obtainable by the available hardware. Longer time intervals degrade the interpolation as suggested in the following study conducted by the author.

The study was performed using GPS data collected at a one-second rate and then thinned to two-second and four-second rates by removing the appropriate sample points. The thinned data sets were interpolated for the missing midpoint samples. The intent was to test the ability to interpolate antenna positions over intervals of two and four seconds. The GPS data sets used for this test came from two sets of Motorola Eagle receiver data collected aboard the NOAA Citation and one set of Ashtech receiver data collected aboard the Texas Highway Department King Air. Comparison of the interpolated positions with the observed positions indicate a standard deviation about the mean difference as great as 41 cm (similar to Lucas' prediction in Section 6.1.1.a). The number of samples whose position difference was greater than 20 centimeters was recorded for each data set and reported in Table 7.

The sample standard deviations for the various populations suggest a degradation in position as the interval of interpolation becomes greater. It is interesting to note that the magnitude of the standard deviations associated with the NOAA Citation are different from the Texas King Air. The population variances were tested for equality using the F statistic.

Hypothesis: Citation and King Air Population variances are equal, a Two-sided Test.

$H_0$ : $Sigma_1^2$ equal to $Sigma_2^2$; vs $H_1$ : $Sigma_1^2$ not equal to $Sigma_2^2$

Alpha significance level of 1 percent.

Reject if $F > F_{99.5}(1038,872)$ or if $F > F_{0.5}(2085,1502)$

| 4 second sample | 2 second sample |
|---|---|
| F = 0.170/0.085 = 2.0; | F = 0.015/0.007 = 2.1 |
| 2.0 > 1.00 and 2.0 > 0.01 | 2.1 > 1.00 and 2.1 > 0.01 |

Thus: Accept the alternative that $s_1^2$ not equal to $s_2^2$
Considering the large Degrees of Freedom, this test has a high power (Hamilton 1964).

Table 7 -- Evaluation of 2 and 4-Second Sample Rates for GPS Phase Information During a Photo Mission

| Aircraft Type | Number of Interpolations | Sample Rate | Position Difference of > 20 cm | % of Sample | Mean/Std Dev of Sample(m) X,Y, and Z |
|---|---|---|---|---|---|
| King Air | 2086 | 2 Sec | 316 | 15 | 0.000/0.055<br>-0.001/0.122<br>0.001/0.114 |
| King Air | 1039 | 4 sec | 605 | 58 | -0.002/0.270<br>0.004/0.412<br>-0.007/0.409 |
| Citation | 1715 | 2 sec | 64 | 4 | 0.000/0.031<br>0.000/0.063<br>-0.001/0.055 |
| Citation | 1503 | 2 sec | 82 | 5 | 0.000/0.032<br>0.001/0.084<br>0.000/0.063 |
| Citation | 873 | 4 sec | 293 | 33 | 0.000/0.292<br>-0.002/0.261<br>0.002/0.281 |
| Citation | 748 | 4 sec | 256 | 34 | 0.001/0.286<br>0.000/0.274<br>-0.002/0.261 |

The differences between the two and four-second populations is most likely caused by the inability to model the aircraft trajectories over a time span greater than two seconds. The difference between the Ashtech and Motorola populations may result from the same inability to model the trajectories or may be caused by a larger signal-to-noise ratio in the Ashtech data set. The trend indicates that the shorter the interpolation interval, the higher the probability one has of determining the true antenna position (assuming that the one second data set represents the true value) at the time of exposure. The logical conclusion, until further analysis can be performed on aircraft stability, is that a one second sample rate is most desirable.

An interesting alternative to the above timing situation would be to activate the camera shutter with the one second timing pulse generated by the GPS receiver. In this procedure one may be able to entirely eliminate the time difference between GPS fix information and exposure. Interpolation of the GPS navigation file would be eliminated except possibly for a constant time offset between the timing signal and the camera response to the signal. The NOAA photographers were consulted about this possibility. Their response was that a single exposure taken on demand could vary from 0 to 1 second from the time the shutter release was pressed. A quick test by the author aboard the NOAA aircraft indicated that the time delay would be on the order of 0.1 sec. The Wild RC10 service manual states that the maximum time delay between rotating shutter blade opening and capping shutter delay is less than 70 msec. The time delay depended on the shutter speed, position of the rotating shutter blades at the time the pulse was initiated, and the vacuum status. The Wild shutter schematics were investigated by the author and Frank Huffman to determine if a circuit could be built to activate the shutter without the variable delay. It appeared that such a circuit could be developed for certain shutter speeds, but would require the disabling of the intervalometer, sensing the vacuum state and establishing a different power supply and tachometer control for the shutter motor, a proposition found unfavorable by NOAA at this time. One major problem with this procedure would be the inability to accurately control overlap as is the case with the current drift sight. Some timing bias might still exist in any event. New receiver technology accommodates the direct input of the shutter pulse into the receiver memory. The shutter pulse is time tagged to the recorded GPS time. The new technology eliminates all the timing apparatus used in this research. Until new camera technology is developed to enable a GPS driven intervalometer, the author is content with the current timing methods. The objective of the interpolation is to compute, using a limited portion of the navigation file, a position for the antenna phase center at the time of exposure which is within 0.5 sec of the central time of the limited data set. The interpolation algorithm uses a second order polynomial whose three coefficients are solved for by least-squares method. The polynomial represents a curve which fits the aircraft trajectory over a five second period. A different curve is fit to each coordinate axis. The coefficients represent the aircraft position offset, velocity and acceleration in each coordinate direction. The coefficients are computed from a sample of five consecutive time-tagged data points most nearly centered about the exposure time.

The following models are used for interpolating the antenna phase center coordinates:

$$\begin{aligned} X_1 &= a_x + b_x t_1 + c_x t_1^2 \\ X_2 &= a_x + b_x t_2 + c_x t_2^2 \\ &\cdot \quad\quad \cdot \quad\quad \cdot \quad\quad \cdot \\ &\cdot \quad\quad \cdot \quad\quad \cdot \quad\quad \cdot \\ X_i &= a_x + b_x t_i + c_x t_i^2 \end{aligned}$$

where $t_i = time_i - time_3$; when i = 1,5; and

$time_3$ = the central time

$t_1 \ldots t_5$ are the five consecutive time tags of GPS antenna phase center positional data

Similar equations could be written for the other two models:

$$\begin{aligned} Y &= a_y + b_y t + c_y t^2 \\ Z &= a_z + b_z t + c_z t^2 \end{aligned}$$

The unknown parameters for each model are:

a = distance
b = velocity
c = twice the acceleration

The observation equations are:

$$v_x = a_x + b_x t + c_x t^2 - X = 0$$

$$v_y = a_y + b_y t + c_y t^2 - Y = 0$$

$$v_z = a_z + b_z t + c_z t^2 - Z = 0$$

The coefficient matrix elements for all three models are the partial derivatives of the model with respect to the unknowns. The coefficient matrix is the same for all three models, as follows:

$$A = \begin{bmatrix} 1 & t & t^2 \\ 1 & t & t^2 \\ 1 & t & t^2 \\ 1 & t & t^2 \\ 1 & t & t^2 \end{bmatrix}$$

The observation vectors composed of the observed coordinate values for each GPS epoch are:

| for X; | for Y; | for Z; |
|---|---|---|
| $-x_1$ | $-y_1$ | $-z_1$ |
| $-x_2$ | $-y_2$ | $-z_2$ |
| $-x_3$ | $-y_3$ | $-z_3$ |
| $-x_4$ | $-y_4$ | $-z_4$ |
| $-x_5$ | $-y_5$ | $-z_5$ |

A least-squares solution minimizing the function

PHI = V' P V

is used to solve for the unknown parameters. The P matrix is the scaled inverse of the covariance matrix (Sigma $L_b$) for the observed quantities.

The scaling is represented by $Sigma_0^2$, the variance of unit weight, which in this case has the value of 1. The solution for the unknown parameters begins with the normal equations noted as follows:

$$V_x = AK_x + X$$
$$V_y = AK_y + Y$$
$$V_z = AK_z + Z$$

where;

$$K_x = -(A'PA)^{-1}(A'PX)$$
$$K_y = -(A'PA)^{-1}(A'PY)$$
$$K_z = -(A'PA)^{-1}(A'PZ)$$

where the ' symbol represents the transpose matrix, assume for the moment P = I (identity matrix);

$$A'PA = A'A = \begin{bmatrix} 5 & 5t & 5t^2 \\ 5t & 5t^2 & 5t^3 \\ 5t^2 & 5t^3 & 5t^4 \end{bmatrix}$$

$$A"PX = A'X = \begin{bmatrix} x_1 + x_2 + x_3 + x_4 + x_5 \\ x_1t + x_2t + x_3t + x_4t + x_5t \\ x_1t^2 + x_2t^2 + x_3t^2 + x_4t^2 + x_5t^2 \end{bmatrix}$$

similar equations can be written for A'PY and A'PZ.

The covariance matrix, P, is used to weight the contribution of each observation considering the span of time between the central observation point and the camera exposure station. The assumption is made that the five observations are independent and, therefore, the covariances between observations are zero. Several different choices for the variances were considered. The first choice was equal weights. This choice was not considered appropriate considering possible non-uniformity of the trajectory. A second choice was to compute the variances by giving more weight to the center value of the interpolation, a central weight scheme. The justification for this decision is based on the increasing difficulty to accurately model a trajectory as the distance between data points increases. This fact was confirmed by the test used to determine the need for a one-second data collection rate for GPS observations. The weight for the central values is, therefore, greatest with decreasing weights for the other data points as the time span from the data point to the central value increases. Several central weight systems were tried. The final scheme weights the data points using a binomial expansion technique. The central variance was chosen to be 1.0 $cm^2$. The following formula for the variances of the weight matrix follows:

$$Sigma_{Lb} = \begin{bmatrix} 2^2 * 0.01\ m^2 & 0 & 0 & 0 & 0 \\ 0 & 2^1 * 0.01\ m^2 & 0 & 0 & 0 \\ 0 & 0 & 2^0 * 0.01\ m^2 & 0 & 0 \\ 0 & 0 & 0 & 2^1 * 0.01\ m^2 & 0 \\ 0 & 0 & 0 & 0 & 2^2 * 0.01\ m^2 \end{bmatrix}$$

Thus the time separation from the central observation is inversely proportional to the weight. Again, no correlation was considered

between observations. Therefore, the P (weight) matrix is a diagonal matrix with the following elements:

$$P_{11} = 1.0 \;/\; Sigma^2_1 = 1/(2^2 * 0.01\ m^2)$$
$$P_{22} = 1.0 \;/\; Sigma^2_2 = 1/(2^1 * 0.01\ m^2)$$
$$P_{33} = 1.0 \;/\; Sigma^2_3 = 1/(2^0 * 0.01\ m^2)$$
$$P_{44} = 1.0 \;/\; Sigma^2_4 = 1/(2^1 * 0.01\ m^2)$$
$$P_{55} = 1.0 \;/\; Sigma^2_5 = 1/(2^2 * 0.01\ m^2)$$

The *a priori* variance of unit weight is 1.0. The validity of this weight system is supported by using a Chi Square test of the *a posteriori* variance of unit weight against the *a priori* variance of unit weight. The test indicated equal variances in 43 of 45 interpolations. The validity must be tempered by the knowledge that the degrees of freedom for the test is only 2 (number of observations - number of unknowns, 5 - 3 = 2).

The interpolated values for the antenna phase center at the time of the exposure are expressed as follows:

$$X_{exp} = K_x(1) + K_x(2)*(time_3 - time_{exp}) + K_x(3)*(time_3 - time_{exp})^2$$

$$Y_{exp} = K_y(1) + K_y(2)*(time_3 - time_{exp}) + K_y(3)*(time_3 - time_{exp})^2$$

$$Z_{exp} = K_z(1) + K_z(2)*(time_3 - time_{exp}) + K_z(3)*(time_3 - time_{exp})^2$$

The interpolated geocentric position of the antenna phase center at the exposure time can now be transformed through the previously determined system of spatial offsets to the position of the exposure station.

The errors due to the observed quantities and interpolation can be propagated through the above system of interpolation equations if the variances for the unknown parameters, position, and time can be estimated. Estimates for the covariance matrix for the parameters is obtained from the inverse of the normal equation matrix scaled by the *a posteriori* variance of unit weight. The estimate for timing error is obtained empirically from the knowledge of the precision for the GPS time tags, timing delay between the camera and GPS, and the shutter timing offset measurement. The first two error sources are insignificant considering the velocity of the aircraft and the stability of the receiver and timing clocks. The largest contributing factor is, therefore, the shutter timing offset. As reported earlier this error is estimated to be 0.0005 sec. The error estimate for the GPS position is given by Mader (personal communications) as 2 cm in planimetry and 4 cm in elevation. These values have been accepted as true. Assuming that there is no correlation between the position, timing and unknown parameters, a combined covariance matrix can be formed as follows:

$$S_{XT} = \begin{bmatrix} S_{11} & S_{12} & S_{13} & 0 & 0 \\ S_{12} & S_{22} & S_{23} & 0 & 0 \\ S_{13} & S_{23} & S_{33} & 0 & 0 \\ 0 & 0 & 0 & S_t^2 & 0 \\ 0 & 0 & 0 & 0 & S_p^2 \end{bmatrix}$$

$S_{YT}$ and $S_{ZT}$ can be formed in similar manner.

The variances $S_T^2$ and $S_p^2$ represent the estimates of variances for time and position, respectively.

The partial derivatives with respect to the interpolation equation are:

$$dF/da = 1$$
$$dF/db = t$$
$$dF/dc = t^2$$
$$dF/dt = b + 2ct$$
$$dF/dp = -1$$

The partial derivatives differ for X, Y, and Z because the polynomial coefficients (b and c) are different for each coordinate. The covariance matrix is also different for all three coordinates since the covariance matrix for the parameters is scaled by the *a posteriori* variance of unit weight for each solution of the parameters. The partial derivatives of the interpolation equations with respect to the coefficients, position, and time form the "G" coefficient matrix of one row by five columns.

The propagation of covariances for each coordinate is computed as follows:

$$(G*S_{XT}*G^T),\ (G*S_{YT}*G^T),\ \text{and}\ (G*S_{ZT}*G^T)$$

The resulting scalers represents the estimate of the precision for the interpolated antenna position in each coordinate.

Several assumptions are made about the camera and aircraft attitudes and the resultant contribution to the error in the exposure station position:

a. The exposure station will be defined as the entrance node to the lens system of the camera.

b. The rotational elements for the exterior orientation of the camera can be determined from aerotriangulation using survey control only. A slightly less accurate transformation can be obtained by assuming vertical photography and a swing angle equal to the azimuth between two consecutive antenna positions.

c. The pitch and drift angles are measured between the aircraft and the camera. The pitch and drift angles were zero when the spatial offsets were measured.

d. The covariance matrix for the exposure station can be obtained through the various models using *a priori* estimates of the precision for the observations.

The antenna and camera coordinate systems are right-handed as are the three rotations about the camera axes. The relationship is generalized in Figure 18. The following three rotations and three translations are used in the transformation:

1. The antenna coordinates at the time of exposure are converted from WGS84 rectilinear to ellipsoidal latitude, longitude and elevation. The latitude (lat) and longitude (lon) are then used to rotate the WGS84 coordinates into an East, North, local vertical system.

2. The propagated covariances are similarly obtained through the above matrices to obtain covariances in the local vertical system.

3. The spatial offset components between the camera and antenna are then rotated into the local coordinate system using the standard gimbal form. The rotation elements of Kappa and drift are combined into a single rotation. Rotational elements of Phi and pitch are also combined. No determination of roll was made during the flight so, Omega is treated independently. The combined rotation matrix is an orthogonal matrix with the property that the transpose is equal to the inverse. Since the standard gimbal form transforms from the survey coordinate system to the photo coordinate system, the transpose will transform the spatial offsets in the photo system to the local vertical survey system. These transformed spatial offsets can then be algebraically added to the antenna coordinates at the time of exposure to produce the survey coordinates of the exposure station.

4. No error results from the transformation (photo - survey) because the angular quantities (latitude and longitude) are assumed error free (at least in theory). The product of the gimbal form rotation matrix by its transpose is equivalent to the product of the rotation matrix by its inverse because the rotation matrix has the property of orthogonality. This property causes the product to equal an identity matrix.

The three rotation matrices which make up the gimbal form follow:

$$R1 = \begin{bmatrix} 1 & 0 & 0 \\ 0 & \cos(\text{omega}) & \sin(\text{omega}) \\ 0 & -\sin(\text{omega}) & \cos(\text{omega}) \end{bmatrix}$$

$$R2 = \begin{bmatrix} \cos(\text{phi+beta}) & 0 & -\sin(\text{phi+beta}) \\ 0 & 1 & 0 \\ \sin(\text{phi+beta}) & 0 & \cos(\text{phi+beta}) \end{bmatrix}$$

$$R3 = \begin{bmatrix} \cos(\text{kappa+gamma}) & \sin(\text{kappa+gamma}) & 0 \\ -\sin(\text{kappa+gamma}) & \cos(\text{kappa+gamma}) & 0 \\ 0 & 0 & 1 \end{bmatrix}$$

It may be argued that the camera rotates about a set of mechanical gimbals whose rotational center may or may not be coincident with the exposure station. If there is any eccentricity between the gimbal rotational center and the exposure station (discussed in Section 2.4.4), then the angles of exterior orientation cannot be algebraically summed with the observed angles of pitch and swing. The eccentricity discussion will begin with the particular situation encountered in this research in which pitch and swing angles are small (less than $2^{\circ}$). A more general explanation will follow.

By design of the RC-10 camera mount, the optical axis, about which swing is measured also coincides with the vertical axis of the mount, therefore swing and kappa angles can be combined without an eccentricity correction. Such is not the case for the pitch angle. The exposure station has a vertical separation of approximately 27 mm from the gimbal origin (the gimbal center is probably at the camera's center

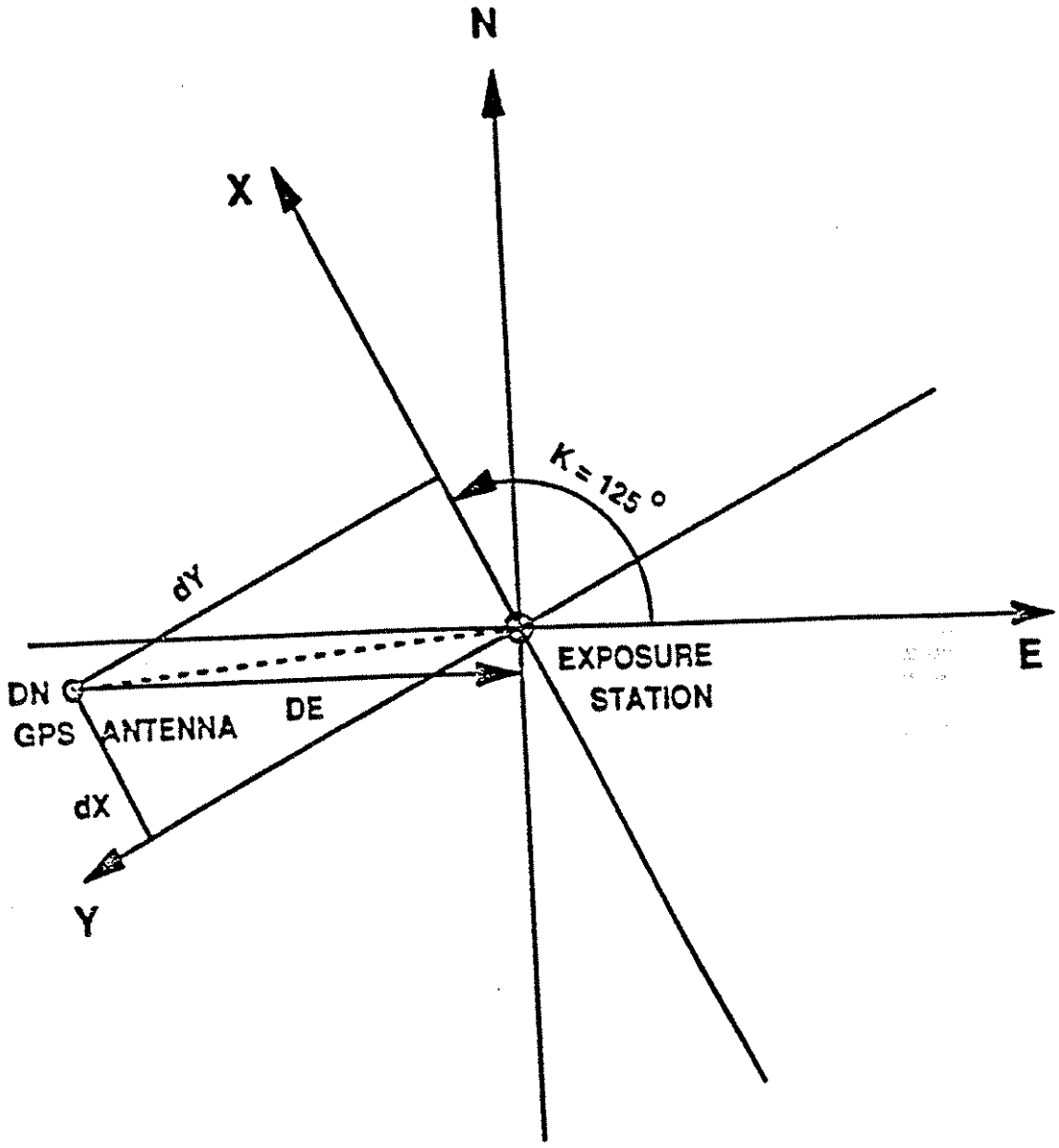


GEOGRAPHIC REPRESENTATION
OF
THE SPATIAL OFFSETS

Figure 18. Geographic Representation of the Spatial Offsets

of gravity). The aircraft pitch relative to the camera mount was measured during actual flight conditions and is referenced to the gimbals. A maximum pitch angle of $1.5^0$ was measured and occurred at the lower limit of the Citation's operating speed. The consequences of not taking the eccentricity into account are as follows:

$$\text{Maximum pitch error} = 0.027\text{m} * \sin(1.5^0) = 0.0007\ \text{m}$$

A displacement error of the exposure station of less than 1 mm in the direction of flight will occur by neglecting the eccentricity correction. Since the Citation tends to porpoise (oscillate between a nose up and down attitude) at the lower speeds which were used in the research, this error would tend to be frequently less than the maximum value computed above and was, therefore, not considered a significant correction. This decision was further reinforced by the fact that the horizontal reference plane instrumented by the inclinometer used for the pitch measurement was probably accurate to no better than $0.5^\circ$ and the pitch observations were only taken once per flight line. In the future, NOAA has procured digital inclinometer for the pitch and roll axes which are accurate to $0.1^\circ$.

In the most general case, a camera mount consists of a double concentric two orthogonal axis gimbal. The mechanical design of the gimbals and the magnitude of the rotation angles may dictate a more thorough investigation of the effect of the eccentricity.

The gimbal form rotation matrix is formed by the product of R1, R2, and R3 matrices. The order of multiplication is important only in the general case mentioned above. The order of rotation for the specific case is not critical, considering, the design of the camera mount, magnitude of the angles (generally less than $2^\circ$), and since the rotations are being treated in a purely analytical application.

The combined rotation matrix would transform survey coordinates to photo coordinates. Since the spatial offsets are measured in the photo system, the transpose of the combined matrix is required. The product of the transposed matrix times the spatial offset vector yields values for the spatial offsets in the survey system. The spatial offsets may now be algebraically added to the interpolated position of the antenna position at the time of exposure. The result is a set of GPS coordinates for the exposure station and the associated estimates for the position precision.

### 6.1.3 The Environment - Atmospheric Refraction

The first order theory in photogrammetry employs the condition of collinearity. Simply stated, the condition of collinearity implies that a ray of light travels undisturbed in a straight line from the object space point, through the exposure station and terminates at the film plane of the camera. Light waves only travel in straight lines when passing through a medium of constant density. In the case of aerial photogrammetry, the light rays from the object space travel through a medium of diminishing density as they approach the camera. The change in atmospheric density causes rays of light to refract (bend) in a concave manner towards the center of the object space. The refraction effect is further complicated by introducing an optical flat (window) in the fuselage which separates the camera environment from the outside atmosphere. The Earth's atmosphere is very uniform, with an average temperature lapse rate (gradient) of $-6.5^\circ$ C/Km up to 11 Km and an average pressure gradient of -100 mb/Km. These gradients suggest a decrease in atmospheric density with altitude and, therefore, a decrease in the index of refraction. The standard atmospheric models used to correct for atmospheric refraction in the object space are based on the

generalized gradients for pressure and temperature gradients mentioned above. The atmosphere exterior to the camera compartment will generally be less dense and, therefore, have a different index of refraction from the atmosphere within the pressurized camera compartment. Assuming that the optical flat (window) is perfectly ground as a parallel plate, object rays entering the glass will be refracted away from the center of the object space as they pass through the denser medium of the glass, but will be refracted an equal amount towards the center of the object space as they exit the glass into an atmosphere identical to that on the exterior of the optical flat. The angular change and shift can be determined from Snell's Law of Refraction as follows (refer to Figure 19):

$$n1 * \sin a1 = n2 * \sin a2 = n3 * \sin a3$$

Where:

n1 = the index of refraction of air outside the aircraft (~1.0003)
n2 = the index of refraction of Crown Glass (~ 1.52)
n3 = the index of refraction of air inside the aircraft
a1 = the angle of the incident ray
a2 = the angle of the refracted ray
a3 = the angle of the exiting ray

The above equation can then be rewritten assuming equivalent atmospheric conditions inside and outside the aircraft as:

$$n1 * \sin a1 = n2 * \sin a2 = n1 * \sin a3,$$

since

$$n1 * \sin a1 = n1 * \sin a3,$$

$$a1 = a3.$$

The light rays on either side of the window are parallel. The shift occurs in the object space. The consequences of the shift will be discussed in greater detail in Section 6.1.5.

The atmosphere of the camera compartment is generally pressurized and heated resulting in a denser atmosphere than exterior to the aircraft. The denser atmosphere in the Citation camera compartment will cause the light rays emerging from the window to refract less towards the center of the image space so that the light ray will no longer be parallel to its path prior passing through the window. The interior atmospheric refraction combined with the refraction of the window tends to have a canceling effect on the exterior atmospheric refraction.

The NOAA Citation II is equipped with a window in the fuselage which isolates the camera from the environment exterior to the aircraft. The cabin of the aircraft is pressurized to the nominal atmospheric pressure at ground level up to an altitude of 2750 m above MSL, above this altitude the cabin pressure is slowly decreased until a pressure equivalent to 2750 m is reached at the maximum operating altitude of 12,200 m.

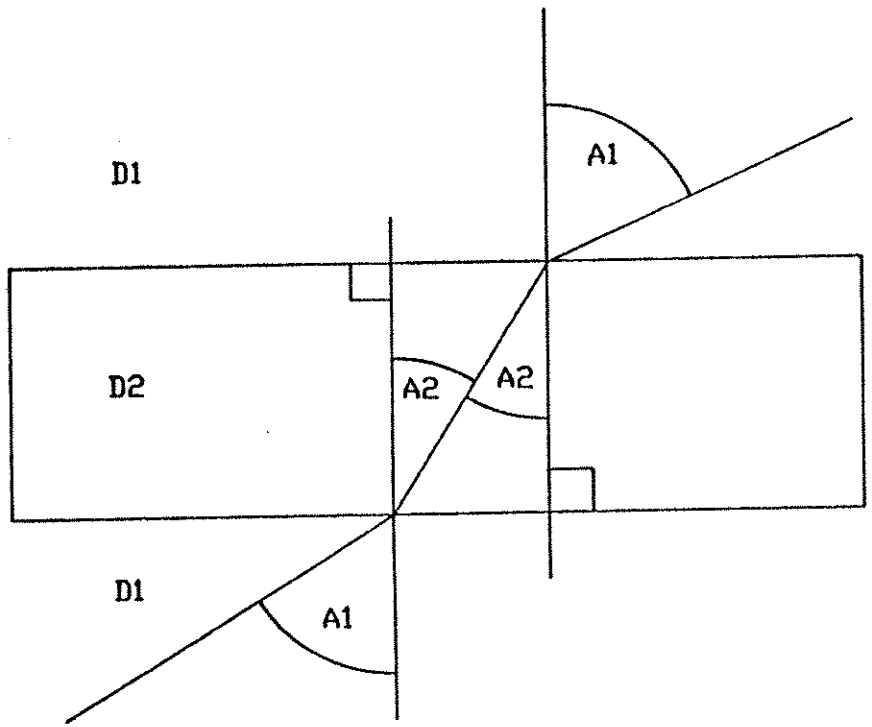


Figure 19. Snell's Law of Refraction

The following atmospheric model was derived by Saastamoinen (1974) to accommodate this situation:

Saastamoinen Model for a Pressurized Cabin

$$K_r = -2.316*((P_1 - P_0)/(Z_0 - Z_1) - 34.11*P_a/T_a)*10^{-6}$$

where:

$K_r$ = constant of photogrammetric refraction

$P_1$, $P_0$ and $P_a$ = atmospheric pressure (mb) at the ground, exterior of the aircraft, and within the aircraft, respectively

$T_a$ = absolute temperature (Kelvin) within the aircraft

$Z_0$ and $Z_1$ = are the elevation of the exposure station and elevation of the ground, respectively

The constants 2.316 and 34.11 accommodate the standard atmospheric gradients for temperature, pressure, water vapor and gravity. This model requires knowledge of meteorological quantities not measured at the time of the experiment and which may be impractical to measure under most operational conditions.

The atmospheric pressure at the exposure station (assuming an unpressurized camera compartment) was computed as described in Chapter 4 but will be repeated here for completeness.

$$T_a = T_g + (H_g - H_a) * B$$

$$BP_a = BP_g * (T_a / T_g)^{-34.11/B}$$

Where:

$BP_a$ = Barometric Pressure (mb) exterior to the aircraft
$BP_g$ = Barometric Pressure (mb) at the initialization point (airport)
$H_g$ = Elevation (m) of the aircraft antenna at the airport
$H_a$ = Elevation (m) of the aircraft antenna, and
$T_g$ = Temperature (C) at the airport
$B$ = The temperature lapse rate in $^oC/Km$

The temperature and pressure at the airport are assumed constant for the entire flight. The constant 34.11 represents the standard atmospheric change in barometric pressure in mb per 100 m change in elevation as a function of pressure, temperature, water vapor, and gravity. The temperature lapse rate B is a constant, 6.5, which represents the temperature lapse rate of a standard atmosphere in $^oC$ per km in elevation. The above model also depends on accurate observations of atmospheric temperatures and pressures on the ground and within the aircraft. Unfortunately, accurate records of the barometric pressure at the airport (assumed ground level) were not taken. The altitude of the aircraft and the temperature exterior to the cabin were, however, recorded in flight. An unbiased estimate of the aircraft altitude was also determined from the GPS observations. From the above observations, the ground pressure and temperature could be computed as follows:

1. The computed altitude of the aircraft based on the GPS observations was 2060 m. The recorded altitude from the aircraft's altimeter which was set at the airport based on the known airport elevation was 2164 m.

2. The difference between these values can be used to determine the difference in local barometric pressure at altitude and the ground.

3. The altitude difference of 104 m is approximately 10 mb when computed from a simplified standard pressure gradient of .1 mb/m. The nominal value for atmospheric pressure at MSL used by aircraft pilots when setting their altimeter is 1013 mb.

4. The pressure at the airport, therefore, might have been 1013 mb - 10 mb or 1003 mb. The correction was subtracted because the altimeter reading was high, reflecting a lower pressure.

5. The ground temperature can be computed from the above equations by solving for Tg instead of Ta. The computed ground temperature would be 7.4 $^{o}$C.

6. As a check, the atmospheric pressure at 2060 m (the GPS determined elevation) is now computed from the above equations based on the computed ground temperature and observed exterior temperature at altitude. The computed atmospheric pressure at altitude is 806.8 mb.

7. Once again, using the simplified pressure gradient of 0.1 mb/m, the atmospheric pressure at MSL would be:

$$806.8 \text{ mb} + 0.1 \text{ mb/m} * 2060 \text{ m} = 1012.8 \text{ mb}$$

versus the nominal assumed value of 1013 mb. Thus supporting the previous assumptions.

Unbiased estimates for the unknown ground temperature and atmospheric pressure have now been computed. The atmospheric pressure in the aircraft was assumed to be at ground level pressure, 1003 mb (as computed in step 4 above) because the aircraft was operating below 2750 m.

The accuracy of cabin temperature and pressure are subject to some degree of speculation if it is assumed that the cabin pressure remained at ground level throughout the flight and that the cabin was heated evenly to 60$^{o}$ F. The regulation of the aircraft interior, however, is carefully controlled and any deviations will be assumed insignificant. In the spirit of maintaining statistical control, an independent check on the effect of atmospheric refraction must be developed. A new model for atmospheric refraction will be derived which combines the refraction effects from the ground to the window and from the window to the camera. The new model will also be independent of the precise knowledge of the ground level meteorological parameters. The model has the form:

$$K_r = R + dR;$$

where:

R is the refraction caused by the atmosphere external to the camera compartment
dR is the refraction caused by the pressurized camera compartment

Schut (1969) and Bertram (1966) used a similar summation of various contributing sources for the computation of atmospheric refraction based on a standard atmosphere. Saastamoinen (1974) used their model to compute the average index of refraction from the ground to the flying height minus the index of refraction at flying height (nm - n1). This model is equal to the photogrammetric refraction (R). Olsen (1984) showed that the refraction caused by the pressurized cabin could be

computed from Snell's Law if knowledge of the indexes of refraction on both sides of the window and the angle of the incident ray are known. Employing certain assumptions about the difference of refraction and the angular change between the incident and exit rays, Olsen showed that the change in refraction dR is equal to n1 - n3, the indexes of refraction outside and inside the aircraft, respectively.

A new atmospheric refraction model based on a standard atmosphere can be derived from Saastmoinen's and Olsen's models as follows:

$$K_r = (nm - n1) + (n1 - n3) = nm - n3.$$

where:

n1 is the index of refraction at the flying height
nm is the mean atmospheric refraction
n3 is the atmospheric refraction inside the camera compartment

The similarity of this model with Saastamoinen's model for a pressurized cabin is easily recognized. The difference between the average index of refraction and the index of refraction at the flying height can be computed from any standard atmospheric model. The indexes of refraction n1 and n3 can be computed as follows:

$$(n3 - 1) * 10^6 = 79.0 * (p3/t3)$$

$$(n1 - 1) * 10^6 = 79.0 * (pa/ta)$$

where:

pa is the atmospheric pressure at the flying height
ta is the air temperature at the flying height
p3 is the atmospheric pressure in the aircraft
t3 is the temperature in the aircraft

Remember pa and ta can be conveniently observed during the mission. Table 8 compares the difference between Saastamoinen's pressurized camera compartment model and the

Table 8 -- Comparison of Atmospheric Refraction Models

| Radial Distance from Principal Pt. from PP (mm) | Saastamoinen Pressurized Cabin (microns) | R+dR Mean Atm. (microns) | Difference (microns) |
|---|---|---|---|
| 0 | 0.0 | 0.0 | 0.0 |
| 15 | 0.2 | 0.2 | 0.0 |
| 30 | 0.5 | 0.4 | 0.1 |
| 45 | 0.8 | 0.6 | 0.2 |
| 60 | 1.0 | 0.9 | 0.1 |
| 75 | 1.4 | 1.2 | 0.2 |
| 90 | 1.9 | 1.6 | 0.3 |
| 105 | 2.4 | 2.0 | 0.4 |
| 120 | 3.0 | 2.6 | 0.4 |
| 150 | 4.5 | 3.9 | 0.6 |

combination of the ARDC Model (standard atmosphere model) and the computation of dR from direct observations.

Table 8 shows little difference between the models, thereby verifying the accuracy of the computation of atmospheric parameters from observations of the exterior temperature and altimeter during flight operations.

The total atmospheric refraction correction was very small (less than 5 microns) even for the images at the extreme distances from the perspective center. The systematic correction $K_r$ based on the newly derived combined model was applied to the image coordinates of the vertical photograph in the following manner:

$$da = K_r * \tan(a) = K_r * r/c$$

where: da is the change in nadir angle
a is the nadir angle
r is the radial distance from the principal point to the image
c is the camera constant

$$r = c * \tan(a)$$

$$dr/da = c * \sec^2(a) = c * (r^2 + c^2) / c^2$$

$$dr = (c * (r^2 + c^2) / c^2) * K_r * r/c$$

$$dr = K_r * (r + r^3/c^2) = K_r * (1 + r^2/c^2) * r$$

where:

dr is the radial distortion in the plane of a vertical photograph caused by atmospheric refraction. The radial distortion can be expressed in terms of the photo coordinate system as follows:

$$dx = x_{image} * dr/r$$

$$dy = y_{image} * dr/r$$

substituting in the equation for radial distortion,

$$dx = K_r * (1 + r^2/c^2) * x_{image}$$

$$dy = K_r * (1 + r^2/c^2) * y_{image}$$

The derivation was performed assuming vertical photography. The actual photography was within 2 degrees of vertical for all photographs. The deviation from vertical will not introduce any measurable systematic error. The corrections dx and dy can now be applied to the transformed photo coordinates.

6.1.4 The Camera

The nine interior orientation elements for the camera describe the equivalent camera constant, the principal point coordinates, and lens distortion. The six parameters of lens distortion include: three coefficients of radial (aberration) distortion, and three coefficients of tangential (decentering) distortion.

The equivalent focal length is the linear distance from the rear nodal point, measured along the lens axis, to the plane of best average

definition across the entire photo plane. Often, a calibrated camera constant is given which represents an adjusted value of the equivalent focal length computed to distribute the effect of lens distortion across the entire photo plane.

The principal point coordinates represent the location of the perpendicular intersection of the optical axis with the film plane in terms of the fiducial coordinate system.

As was mentioned earlier, camera calibrations are normally performed in a laboratory where it is possible to separate the linear dependency between interior and exterior orientation elements. Laboratory calibrations performed in the United States by the U.S. Geological Survey do not duplicate the actual operating conditions because the laboratory and operating environments can be significantly different. The laboratory calibration does not attempt to duplicate any of the disturbing effects which occur naturally during the taking of photographs. The limiting ability to simulate actual flight conditions will effect the ability to accurately determine the interior orientation parameters. The stellar calibration for the G Cone and a laboratory calibration for the B Cone were used as a first order approximation to correct the image coordinates for the systematic errors induced by radial and tangential lens distortion components.

Radial Lens (Seidel Aberration) Distortion Model

$$dx = (K_1*r^2 + K_2*r^4 + K_3*r^6)*(x - x_0)$$

$$dy = (K_1*r^2 + K_2*r^4 + K_3*r^6)*(y - y_0)$$

where:

dx and dy are the components of radial distortion
$K_1$, $K_2$, and $K_3$ are the coefficients of Seidel Aberration distortion
$x_0$ and $y_0$ are the principal point coordinates
x and y are the image point coordinates

Tangential Lens (Decentering) Distortion
Conrady-Brown Model (Brown 1966)

$$dx = (P_1*(r^2 + 2x^2) + 2P_2xy)(1 + P_3*r^2)$$

$$dy = (2P_1xy + P_2(r^2 + 2y^2))(1 + P_3*r^2)$$

where:

dx and dy are the components of tangential distortion
$P_1$, $P_2$, and $P_3$ are the coefficients of decentering distortion
x and y are the image-point coordinates

The components of radial and tangential distortion can be combined to form a model for systematic lens distortion as follows:

System Distortion Model - Based on a camera calibration

$$dx = (K_1*r^2 + K_2*r^4 + K_3*r^6)*(x - x_0) + (P_1*(r^2 + 2x^2) + 2P_2xy)(1 + P_3*r^2)$$

$$dy = (K_1*r^2 + K_2*r^4 + K_3*r^6)*(y - y_0) + (2P_1xy + P_2(r^2 + 2y^2))(1 + P_3*r^2)$$

The Calibration Sheets for the G and B Cones are contained in Appendix D.

6.1.5 The Aircraft

The effect of the optical flat separating the interior and exterior atmospheric environments and the resulting cabin pressure were mentioned in section 6.1.3. The optical flat becomes part of the camera lens system when calibrating a complete measuring system. The following discussion of the effects of the optical flat begins with a first order theory which assumes an optical flat with perfectly parallel surfaces and progresses to a second order theory where parallel surfaces are not assumed.

A first order theory would assume that the optical flat is represented by a plate of high quality glass of uniform density whose major surfaces are ground flat and parallel to each other. If these conditions are met, any light ray passing through the glass would be refracted by a density change at the entrance and exit interfaces of the glass surfaces. The incident and exit rays would remain parallel to each other if the atmospheric density were the same on either side of the glass (atmospheric pressure differences are compensated by the Saastamoinen Model for a Pressurized Cabin).

The optical flat in the NOAA Citation is a 40 mm thick plate of crown glass with a refractive index of 1.52. The shift and distortion in the object space can be computed from the following equations (ASP 1980):

$$P_1 = \sin(Phi_{air}) * A_{air} / A_{glass}$$

$$Phi_{glass} = \arcsin(P_1)$$

$$D_1 = A_{air} * \cos(Phi_{air})$$

$$D_2 = A_{glass} * \cos(Phi_{glass})$$

$$D_3 = 1 - (D_1/D_2)$$

$$D = T * \sin(Phi_{air}) * D_3$$

$$C = T * ( 1 - (A_{air} / A_{glass})$$

$$DIS = T * (\tan(Phi_{air}) - \tan(Phi_{glass}) - C * \tan(Phi_{air})$$

where:

$Phi_{air}$ is the angle of incidence
$Phi_{glass}$ is the angle of refraction in glass
$A_{air}$ is the refractive index of air (1.0)
$A_{glass}$ is the refractive index of glass (1.5)
T is the thickness of the glass plate
D is the radial shift of the exiting ray away from the center of the glass

C is the vertical shift towards the camera of the optical ray
DIS is the radial distortion which results from the combination of D and C

Table 9 lists some refractive shifts and distortions in the object space caused by the NOAA Citation's optical flat, assuming the flat is perpendicular to the optical axis of the camera.

In the second order theory (ASP 1980) an optical flat introduces three types of aberrations, a displacement of the image plane, radial distortion accompanied by astigmatism, and disturbance of the resolving power. If the flat is placed between the object space and the first lens vertex (Figure 20), as in the case of a window installed in an airplane, the radial distortion will be outward from the center of the lens system. The thickness of the window will determine the displacement of the object plane. The displacement is approximately one-third the thickness of the window. The effect on image resolution is hard to determine in advance. It is advisable to consider the requirement for an optical flat at the time the lens is being designed.

It is important to understand the effect of the optical flat on the interior orientation elements of the lens cone. The introduction of the glass plate will not change the focal length, because, the location of the entrance and exit nodes are not shifted with respect to the film plane or positive plane. Lens distortion is, however, introduced. The distortion occurs in the form of astigmatism, barrel distortion and spherical aberration. These three aberrations in combination cause both radial and tangential distortion. The full extent of these distortions is hard to determine because the window is not included in the laboratory calibration.

The window will be treated as a component of the lens system in the final system calibration and it's effects will be modeled by tangential and radial distortion components discussed previously.

The second order theory does not make any assumptions about parallel and/or flat surfaces for the optical flat. The plate may, in fact, deform due to the cabin pressure. The optical flat in the NOAA Citation is 56 cm long by 48 cm wide, and 40 mm thick with a total surface area of 2688 $cm^2$.

A cabin pressure of approximately 3 psi (interior - exterior atmospheric pressure) exerts 1250 pounds of force on the optical flat. The optical flat is mounted on a rubber gasket in a frame which prevents side-to-side movement but does not constrain vertical movement. The mounting arrangement prevents the glass from breaking under pressure by allowing it to distort. If the optical flat is approximated by a circular plate of area equal to it's true rectangular shape, Reuleaux's Formula (Oberg and Jones 1935) can be used to determine that the deflection of the center of the plate would be approximately 0.1 mm assuming the glass has a modulus of elasticity of 25,500,000. The deflection is small because of the plate thickness. The plate, under pressure, would become very slightly concave on the cabin side and thinner at the center where the most pressure and least support exists. Considering the small change in the radius of curvature caused by the deformation and considering that both inner and outer surfaces would deform the same amount due to the mounting design, a differentially small cross-section of the plate would still have parallel surfaces.

Table 9 -- Refractive Shift of a 40 mm Thick Optical Flat

| $Phi_{air}$ degrees | $Phi_{glass}$ degrees | D mm | C mm | Distortion mm |
|---|---|---|---|---|
| 0 | 0.0 | 0.0 | 13.3 | 0.0 |
| 5 | 3.3 | 1.2 | 13.3 | 0.0 |
| 10 | 6.6 | 2.3 | 13.3 | 0.0 |
| 15 | 9.9 | 3.6 | 13.3 | 0.1 |
| 20 | 13.2 | 4.9 | 13.3 | 0.3 |
| 25 | 16.4 | 6.3 | 13.3 | 0.7 |
| 30 | 19.5 | 7.8 | 13.3 | 1.3 |
| 35 | 22.5 | 9.4 | 13.3 | 2.1 |
| 40 | 25.4 | 11.2 | 13.3 | 3.4 |
| 45 | 28.1 | 13.2 | 13.3 | 5.3 |

The effect of the refraction caused by the deformed optical flat would be extremely small and difficult to determine with any confidence. Since the plate cannot be expected to deform in a perfectly uniform manner, the distortion cannot be defined as strictly radial or tangential distortion. Instead, the overall effect of the distortion will be considered as contribution to the other second-order effects described next.

Another deviation from the first order theory would be to assume that the optical flat and/or the airspace between the optical flat and first lens vertex may not have parallel surfaces. Considering the airspace first, the optical flat in the NOAA Citation (Figure 21), is located within 6 cm of the first objective lens of the camera system. Realizing that the NOAA aircraft generally flies in a slight nose up attitude and the camera is level, the close proximity between lens and optical flat may induce a systematic distortion caused by a differential change in atmospheric refraction across the field of view. The airspace in this case would approximate a thin prism. Considering an optical flat which does not have parallel major surfaces, the optical flat would also approximate a thin prism. Ray tracing through a thin prism forms the basis for the Conrady-Brown model (Merchant 1973) for tangential lens distortion.

It is impractical to confirm the existence of parallel surfaces or parallel air space by direct measurement. The distortions caused by these effects, however, are similar to radial and tangential lens distortion. The effect of such systematic errors can be modelled in the system calibration by incorporating the Conrady-Brown lens distortion model. As stated earlier, the observed image coordinates have been corrected for lens distortion based on a previous laboratory calibration. The Conrady-Brown mathematical model will be used to determine the combined effect of the optical flat and differential atmospheric refraction on the combined lens system for the mission flown on DOY 299. If the systematic effect determined is not related to the

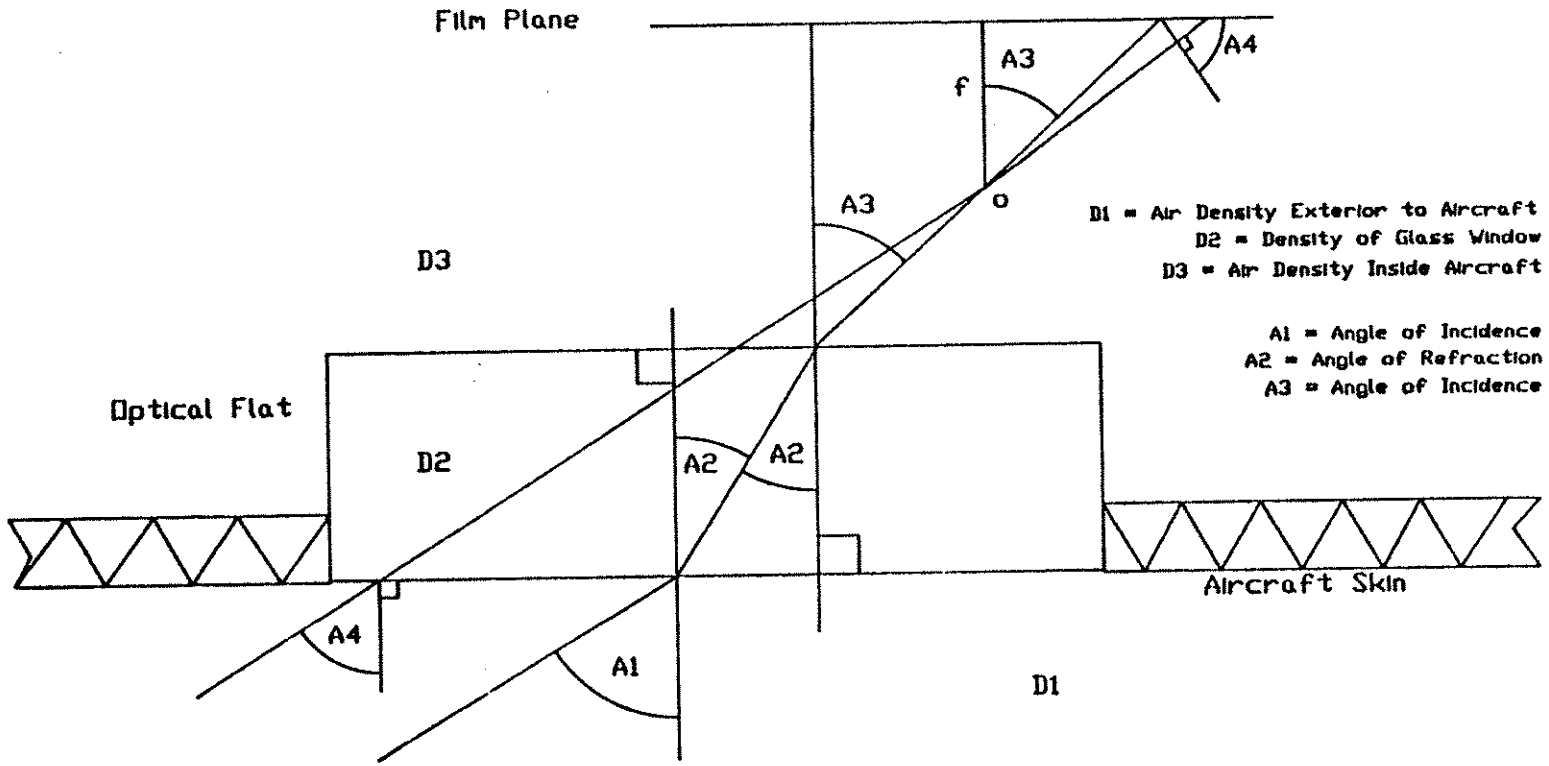


Figure 20. Camera to Window Relationship

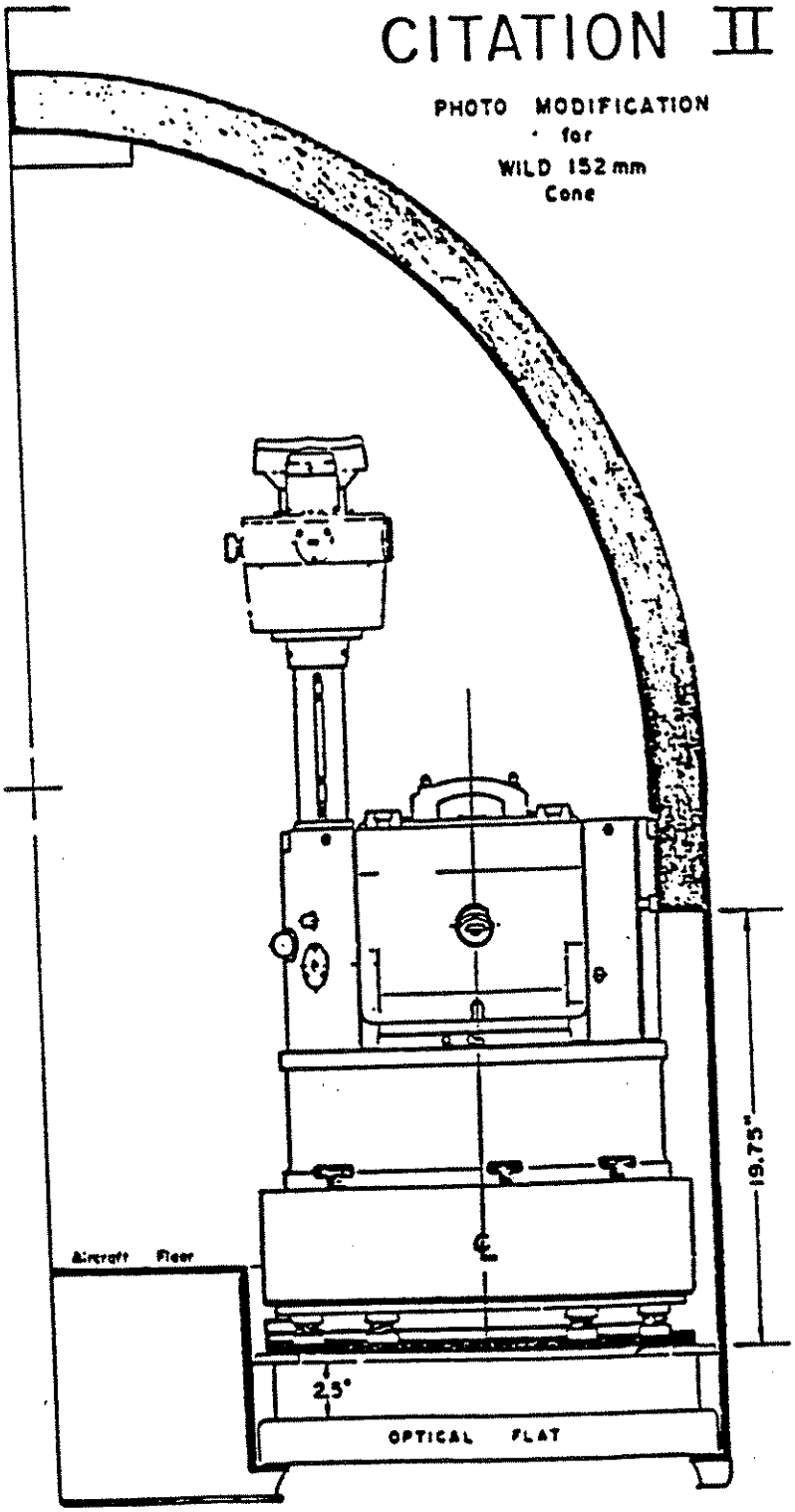


Figure 21. Camera to Optical Flat Proximity in NOAA Citation

G Cone lens system or the GPS control of the exposure station, then the model should be transferrable to the B Cone mission flown on DOY 301.

6.1.6 The Ground Survey Control

Ideally, the photogrammetric targets positioned in the survey control system should be free of blunders, corrected for systematic errors, and have reliable estimates for the random error. The survey control used in this measuring system was determined by kinematic GPS control surveys. The precision estimates are discussed in the Chapter 1 and Appendix A.

Conventional survey control established for photogrammetry is separated into ellipsoidal coordinates for location and orthometric heights for elevation. The transformation of these coordinates to a three-dimensional rectangular coordinate system consistent with the projection equations cannot be done without introducing some error. An assumption must be made that the orthometric heights can be converted to ellipsoidal heights by applying accurate values for the local geoid undulation. A local-vertical reference system is most preferable because the exterior orientation parameters contain rotational elements which relate the photo coordinate system to the local-vertical reference system. Both reference systems are three-dimensional rectangular coordinate systems. The earth-centered GPS reference system can be mathematically transformed into a local-vertical system without introducing any error because orthometric heights are not used.

To highlight the potential problem of using orthometric heights, the author compared the orthometric heights obtained from the conventional survey at the TRC to the ellipsoidal heights obtained from the GPS survey. A slope between the heights along the longitudinal axis of the test track of 6.5" was computed. The slope was 3.2" as determined by the RAPP 360 Model. The slope amounts to 10 centimeters over the 3.2 km length of the track if left uncorrected. This source of error was avoided by using geocentric rectangular coordinates for the signalized control and exposure stations in lieu of the necessity of determining more accurate local geoidal variations. All elevations are referred to the ellipsoid in lieu of the geoid.

All of the systematic errors discussed thus far have been removed from the observations during the various processing stages. Table 10 lists the identified error sources, their model, and the manner in which the correction was verified.

This concludes the discussion of systematic errors.

Table 10 -- Systematic Errors Associated with the GPS/Photogrammetry Calibration

| | Systematic Error | Model | Verification |
|---|---|---|---|
| | | GPS Control | |
| 1. | Union County Airport | By Design | Re-survey |
| 2. | Photo Targets | By Design | Comparison to Conventional Control |
| 3. | Exposure Stations | By Design | Pre and Post-Mission Comparison Integer Cycle |
| | | Imagery | |
| 1. | Film Distortion | 6 Parameters | Significance Level Test |
| 2. | Lens Distortion | 6 Parameters of Radial & Tangential Lens Distortion | System Calibration |
| 3. | Atmospheric Refraction | Pressurized Camera Compartment | Comparison to ARDC Model |
| | | Antenna to Camera | |
| 1. | Spatial Offsets | By Design | Determined from 2 Different Methods |
| 2. | Interpolation | 3 Parameters/Coordinate | Comparison to GAPP |

Table 10 -- Continued

| | | |
|---|---|---|
| | Timing Biases | |
| 1. Horizon Pulse to Exposure Center | 3 Parameters | Direct Observations |
| 2. GPS to PPS | OMNI | Eliminated by Software Shifting of Phase and Pseudorange observations to Integer Time |
| 3. Camera to GPS | Design | Double-Difference Exposure station Times |

## 6.2 Photogrammetric Solution

The observed image coordinates can be transformed into object-space coordinates if the elements of exterior orientation and interior orientation are known. The usual photogrammetric aerotriangulation solution depends upon a certain number of image coordinate measurements of objects with known coordinates in the object space. The elements of interior orientation are assumed known and the elements of exterior orientation are treated as unknown parameters that are solved for in an over-determined system of observation equations. The observation equations are derived from a three-dimensional projective transformation of object-space coordinates to image-space coordinates.

The condition of collinearity is normally imposed on the observation equations. The condition of collinearity assumes that if a ray of light is allowed to pass undisturbed through the atmosphere and lens system to a location in the film plane, this path will be a straight line. The straight line is defined by the object-space coordinates, entrance node, and image coordinates. The condition of collinearity forms the "First Order Theory" of photogrammetry, as described by Bender (1971).

The "Second Order Theory" of photogrammetry assumes that the collinearity condition is violated since the image coordinates are distorted by the systematic effects of film deformation, atmospheric refraction, and lens distortion. The Second Order Theory incorporates corrections for the distorting influences. The research, thus far, has reached the Second Order Theory.

The "Third Order Theory" of photogrammetry assumes that additional distorting influences are identified and modeled in the observation equations. Brown ((1969) and Gruen (1978) are two prominent researchers who have developed polynomial models to describe various effects not otherwise removed by the Second Order Theory. Two factors they have considered are film platen flatness and thermal gradients within the camera optics. The polynomials may accurately model real conditions, but those conditions do not necessarily occur all the time or in every measuring system. The polynomial models generally improve the results of the aerotriangulation solution because all unknown error sources, identified or otherwise, tend to be absorbed by the polynomials. Some of the errors absorbed by the polynomial may be time or situation dependent, therefore, the polynomial would not accurately model the measuring system at a different place or time.

For this research, only the First and Second Order Theory mathematical models are adopted. The observation equations are derived from a projective transformation, imposing the collinearity condition, and containing parameters of interior orientation used to model the effect of the optical flat on the airborne system. The effect of the optical flat is, therefore, assumed to be independent of time and place. Proof of this statement will come from the application of the optical flat distortion model derived from the G Cone photography to correct photo image coordinates obtained by the B Cone installed over the optical flat, but on a different photo mission.

### 6.2.1 Observation Equations

The observation equations incorporating First and Second Order Theory assume that the systematic effects of film deformation and atmospheric refraction have been removed from the observed image coordinates. These corrections were applied during the transformation of comparator coordinates to photo system coordinates.

The film deformation was eliminated by transforming the comparator coordinates using a six-parameter general affine transformation based on observations of the closest four reseau points. The details of this transformation were discussed in Section 5.3. The transformation will also eliminate linear scale distortions in the comparator system as well. The localized nature of the transformation made possible by reseau photography enhances the ability to accurately model film and comparator distortions. Although non-linear effects are not directly modelled, their effect is minimized by the close proximity of known reseau coordinates. The photo coordinates were corrected for the effects of atmospheric refraction using a pressurized cabin model. The model was discussed in Section 6.1.3.

The photo coordinates were then corrected for lens distortion, as determined from a stellar calibration. The photo coordinates are now assumed to have been corrected according to the Second Order Theory. If no further disturbing effects exist, the condition of collinearity has been achieved.

The research will use a modified version of the Third Order Theory of photogrammetry by assuming that the optical flat has had a disturbing effect that can be modeled by the same elements of interior orientation used in the Second Order Theory.

The derivation of the observation equations begins with the General Projective Equations (Gimbal Form) (GPE). The GPE are used to transform object-space (survey) coordinates into image-space (photo) coordinates. The transformation requires the solution of six parameters (3 rotations and 3 translations). The transformation assumes right-handed Cartesian coordinate systems for the photo and survey coordinate systems. The rotations in this solution are right-handed rotations of Kappa about the Z survey axis, Phi about the Y survey axis, and Omega about the X survey axis (in the general case, the rotations can be defined in any consistent convention). The rectangular coordinates $X_0$, $Y_0$, and $Z_0$, define the location of the entrance node (exposure station) in terms of the survey coordinate system.

The three rotation matrices which make up the gimbal form follow:

$$R1 = \begin{bmatrix} 1 & 0 & 0 \\ 0 & \cos(\text{omega}) & \sin(\text{omega}) \\ 0 & -\sin(\text{omega}) & \cos(\text{omega}) \end{bmatrix}$$

$$R2 = \begin{bmatrix} \cos(\text{phi}) & 0 & -\sin(\text{phi}) \\ 0 & 1 & 0 \\ \sin(\text{phi}) & 0 & \cos(\text{phi}) \end{bmatrix}$$

$$R3 = \begin{bmatrix} \cos(\text{kappa}) & \sin(\text{kappa}) & 0 \\ -\sin(\text{kappa}) & \cos(\text{kappa}) & 0 \\ 0 & 0 & 1 \end{bmatrix}$$

The three translations which are used in the gimbal form are:

$$DX = (X - X_0)$$
$$DY = (Y - Y_0)$$
$$DZ = (Z - Z_0)$$

where: $X_0$,$Y_0$, and $Z_0$ are the coordinates of the exposure station.

The GPE can now be written as:

$$\begin{bmatrix} x - x_0 \\ y - y_0 \\ z - z_0 \end{bmatrix} = [R1 * R2 * R3] * \begin{bmatrix} DX \\ DY \\ DZ \end{bmatrix}$$

The coordinates x, y, and z represent a three-dimensional right-handed coordinate system of the photo system whose origin is at the exposure station. The coordinates $x_0$ and $y_0$ define the principal point in a fiducial centered system. The coordinate difference $z-z_0$ represents the camera constant, because the z is coordinate is always zero in the two dimensional photo coordinate system!.

The condition of collinearity is now applied to the GPE. Using similar triangles and vertical photography (Figure 22) the following relationships can be developed:

$$x' / X' = c / Z'; \text{ or } \quad x' = c * X' / Z'$$

$$y' / Y' = c / Z' \text{ or } \quad y' = c * Y' / Z'$$

The coordinates x' and y' are the photo coordinates of an object-space point whose survey coordinates are X' and Y' and c is the camera constant (labeled f in Figure 22) defined as $z - z_0$.

The mathematical model based on the GPE becomes:

$$f(x) = (x - x_0) - c * X' / Z'$$

$$f(y) = (y - y_0) - c * Y' / Z'$$

The values for X', Y', and Z' being obtained from the matrix multiplication R1*R2*R3.

In summary:

| | |
|---|---|
| x, y | = photo coordinates in the reseau system |
| $x_0$, $y_0$, and c | = principal point coordinates in the reseau system, with c defined as the camera constant |
| $X_0$, $Y_0$, and $Z_0$ | = exposure station coordinates in the survey system |
| X, Y, Z | = object-space coordinates in the survey system |
| Kappa, Phi, Omega | = Gimbal angle rotations relating survey and photo system |

In the general case the six parameters of exterior orientation (Kappa, Phi, Omega, $X_0$, $Y_0$, and $Z_0$) are unknown. The kinematic GPS solution, however, provides *a priori* knowledge of the exposure station coordinates $X_0$, $Y_0$, and $Z_0$. It will be shown that the *a priori* knowledge can be used to eliminate certain linear dependencies between parameters of the combined Third Order Theory model. The elimination of the linear dependence makes possible the analytical calibration of the airborne photogrammetric system.

The next step in the development of the mathematical model is to add the model for combined lens distortion. The combined lens distortion model derived in section 6.1.4 is repeated below.

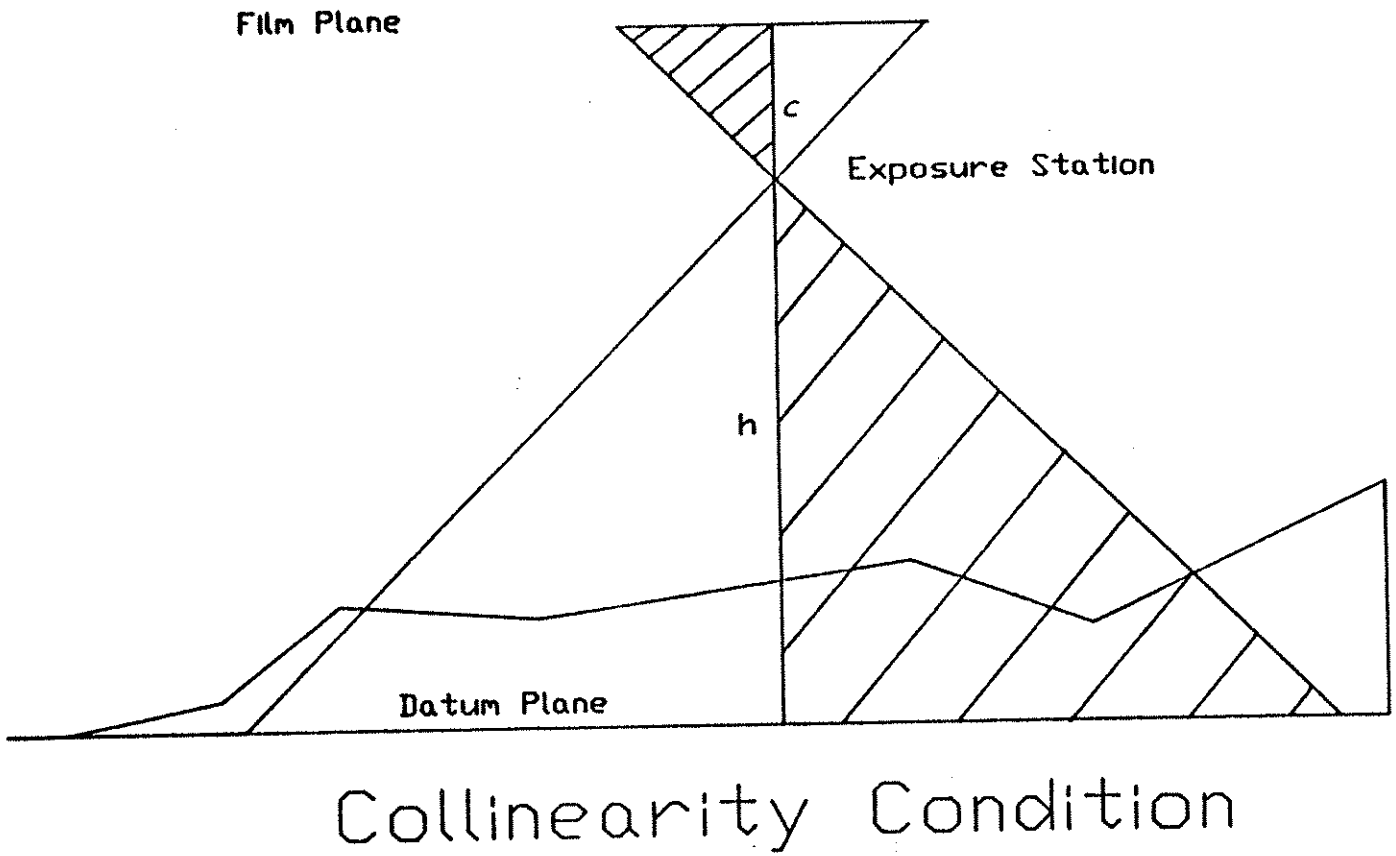


Figure 22. Condition of Collinearity

$$dx = (K_1*r^2 + K_2*r^4 + K_3*r^6)*(x - x_0) + (P_1*(r^2 + 2x^2) + 2P_2xy)(1 + P_3*r^2)$$

$$dy = (K_1*r^2 + K_2*r^4 + K_3*r^6)*(y - y_0) (2P_1xy + P_2(r^2 + 2y^2))(1 + P_3*r^2)$$

The mathematical model based on the GPE become:

$$f(x) = (x - x_0) - c * X' / Z' + dx = 0$$

$$f(y) = (y - y_0) - c * Y' / Z' + dy = 0$$

$x_0$, $y_0$, c, $K_1$, $K_2$, $K_3$, $P_1$, $P_2$, $P_3$, Kappa, Phi, and Omega will be treated as unknown parameters in a least-squares solution.

The above set of equations are known as the mathematical model which relates the unknown parameters to the observed quantities (Merchant 1973). The various parameters involved in the solution can be treated differently, leading to the definition of four cases for the solution.

Case 1 considers the photo coordinates as the only observed quantity. The survey coordinates and interior elements of orientation are given as correct. The exterior elements of orientation are computed by least squares.

Case 2 considers the photo coordinates and exterior elements of orientation as observed quantities. The survey coordinates are given as correct. The interior elements of orientation are assumed correct. The exterior elements of orientation are adjusted by least squares. For this research the exterior elements $X_0$, $Y_0$, and $Z_0$ are directly observed. The following mathematical models must be included in the solution:

$$F(Kappa) = Kappa_0 - Kappa_a = 0$$

$$F(Phi) = Phi_0 - Phi_a = 0$$

$$F(Omega) = Omega_0 - Omega_a = 0$$

$$F(X_0) = X_{00} - X_{0a} = 0$$

$$F(Y_0) = Y_{00} - Y_{0a} = 0$$

$$F(Z_0) = Z_{00} - Z_{0a} = 0$$

Kappa, Phi, and Omega are assigned a weight of 0 (infinitely large standard error).

Case 3 considers the photo coordinates, exterior elements of orientation, and survey coordinates as observed quantities and treated as weight constrained parameters. The survey coordinates of the pass points which do not have geodetic positions are still considered as observed quantities. The interior elements of orientation are assumed correct. Adjusted values for all observations are computed by least squares. The following additional mathematical models for observations of survey coordinates must be added to the Case 2 Solution:

$$F(X_j) = X_{j0} - X_{ja} = 0$$

$$F(Y_j) = Y_{j0} - Y_{ja} = 0$$

$$F(Z_j) = Z_{j0} - Z_{ja} = 0$$

The sub-script j identifies a particular control point. A total of 3 * j equations must be included in the solution.

Case 4 considers photo coordinates, interior and exterior elements of orientation, and survey coordinates as observed quantities. Adjusted values for all observations are computed by least squares. The following additional mathematical models must be added to the Case 3 Solution:

$$F(x_0) = x_{00} - x_{0a}$$

$$F(Y_0) = Y_{00} - Y_{0a}$$

$$F(c) = c_0 - c_a$$

$$F(K1) = K1_0 - K1_a$$

$$F(K2) = K2_0 - K2_a$$

$$F(K3) = K3_0 - K3_a$$

$$F(P1) = P1_0 - P1_a$$

$$F(P2) = P2_0 - P2_a$$

$$F(P3) = P3_0 - P3_a$$

The Case 4 solution can only be used if the correlation between Z and c can be removed. As discussed earlier, Merchant (1972) experimented with mixed ranges, Tudhope (1988) experimented with convergent photography, this research uses the *a priori* knowledge of $X_0$,$Y_0$, and $Z_0$ as did Brown who experimented with the USAF's USQ-28 Geodetic Sub-system in 1969. The correlations are discussed in Section 6.3.2.a.

The mathematical model based on the GPE contains non-linear terms. The model is approximated by using the linear terms of a Taylor's Series Expansion to approximate the model. The non-linear terms of the Taylor's Series Expansion are dropped. The observation equations may be expressed according to the following notation (Merchant (1973):

$$AV + B^eX^e + B^sX^s + B^iX^i + E = 0$$

$B^e$, $B^s$, $B^i$ are the design matrices which represent the partial derivatives from the Taylor's Series Expansion with respect to the exterior orientation, survey and interior orientation parameters respectively. The A matrix is the identity matrix composed of the partial derivatives with respect to the image coordinates. All partial derivatives can be found in Merchant (1973).

The observation equations for the rest of the mathematical models follow:

$$v^e - x^e + E^e = 0$$

$$v^s - x^s + E^s = 0$$

$$v^i - x^i + E^i = 0$$

The combined set of observation equations becomes:

$$V + B^e x^e + B^s x^s + B^i x^i + E = 0$$

$$v^e - x^e + E^e = 0$$

$$v^s - x^s + E^s = 0$$

$$v^i - x^i + E^i = 0$$

A discussion of the formation of the normal equations and exploitation of the normal equation pattern is presented by Merchant (1973) and will not be repeated here.

6.2.2 Weighting System

In Cases 1, 2, 3, and 4, it is assumed that covariance estimates are available for the observed quantities. For this research, it will also be assumed that there is no correlation between the observation types. In fact, all the observations within each type are assumed to be uncorrelated and, therefore, all weight matrices will contain only the diagonal elements of the observation variances. The variances represent accuracy estimates for the observations. An individual weight can be expressed as follows:

$$w_{ij} = \text{sigma}^2_0 \; / \; \text{sigma}^2_{ij}$$

or

$$w_{ij} = 1 \; / \; \text{sigma}^2_{ij}$$

when: $\text{sigma}^2_0 = 1$

All the weight matrices are therefore scaled by a common *a priori* variance, $\text{Sigma}_0$ having unit weight. A value of unit weight assumes that the inverses of the observational weights are true estimates of the accuracy of the measurements themselves. The *a posteriori* variance of unit can be computed from the weighted squared sum of the observational residuals divided by the degrees of freedom. The variance of unit weight is useful for assessing the results of the adjustment. The statistical $\text{Chi}^2$ Test can be used after the adjustment to compare the *a priori* to the *a posteriori* variance to see if both variances could be equal with a certain probability. If the test passes, one can assume that the *a priori* estimates for the observation accuracies were reasonably correct, and unbiased assuming a normal distribution. One may also draw a conclusion that the mathematical model was correct. If the test fails, it must be ascertained first if the computations were performed correctly, second if all systematic errors were accounted for, third if the proper number of condition and/or constraint equations were determined, fourth if the actual functional relationship of the equations is correct, finally if the proper stochastic model was assumed.

6.2.2.a Survey Coordinates

The standard errors for the survey control coordinates are estimated from the kinematic GPS survey by comparison with the conventional survey. The conventional survey served as a standard for comparison of distances, angles and height differences because the standard errors for the adjusted coordinates are on the order of 2 mm. The comparison of GPS to the conventional survey adjusted distances, angles, and elevation differences are listed in Table 2 in Section 2.3. A standard error of 1 cm is estimated for each coordinate based on the comparison. The coordinates are assumed to be uncorrelated. It is acknowledged that some correlation might exist between kinematic GPS coordinates as correlation exists between all survey coordinates, the author does not believe that the omission of correlation would seriously bias the results of the adjustment. The estimate was checked by computing the sample variance for each coordinate based on repeated observations. The sample standard deviations were also close to 1 cm in magnitude.

6.2.2.b Photo Coordinates

The standard error for the photo coordinates is obtained from a combination of sources which include the BC-1 measuring system, the operator's pointing ability (personal equation), and image sharpness. The standard error of a BC-1 observation is 3 microns as stated by the manufacturer. This estimate will be degraded by the operator's familiarity with image mensuration (almost none in my case), and image quality. The G Cone camera is optically tuned to the orange spectrum while the targets at the TRC were white on black, somewhat degrading the image sharpness. In fact, the low altitude targets could not be observed unless the image was near the center of the photo. This was not the case with the B Cone photography. Since there is no statistical basis for estimating the contribution of the operator's ability and image sharpness, standard errors used in other projects such as the Ada County, Idaho photo-geodesy project, Tudhope's camera calibration thesis and NOAA IDPF were compared.

The *a posteriori* standard error for image coordinates obtained from the Ada County Photo-Geodesy Project was 2.7 microns for G Cone imagery. This estimate is based on six observations of each image point along with six reseau points for each image. The targets for this project were painted orange to take maximum advantage of the optical system resolution. An estimate for the standard error based on three observations per point (the number of observations taken on the BC-1) would be:

$$2.7 \text{ microns} * 6^{1/2} / 3^{1/2} = 3.8 \text{ microns}$$

Tudhope used a standard error of 3 microns for his work performed on the same BC-1 but with imagery obtained from a camera unbiased for the black and white targets. NOAA uses a standard error of 5 microns for all image coordinates measured on the IDPF, regardless of the number of pointings. Based on the above comparisons, a standard error of 4 microns for all image coordinates was adopted.

6.2.2.c Elements of Exterior Orientation

The standard errors for the rotation and translation elements of exterior orientation will be treated differently. The rotational elements will have an infinite standard error so that the rotations will be solved for as free parameters in the adjustment. The translation elements (exposure station coordinates) are treated as observations. The standard error for exposure station coordinates was computed during the interpolation and transformation of antenna coordinates to exposure station coordinates. The error propagation technique is explained in Section 6.1. The standard error for $X_0$ and $Y_0$ is 5.0 cm for flight

lines 1 and 3 which are flown against the wind (i.e., lower ground velocity). The standard error for $X_0$ and $Y_0$ is 6.5 cm for flight line 2 which is flown with the wind (higher ground speed). The standard error for all $Z_0$ coordinates is 4.0 cm (nearly constant velocity). It should be noted that the standard errors depend on the aircraft velocity, thus, the reason for slightly larger estimates for flight lines flown in the direction of the wind.

6.2.2.d. Elements of Interior Orientation

The standard errors for the elements of interior orientation will be infinity. The elements will be treated as free parameters in the Case 4 adjustment. The elements are initially assigned standard errors of zero to stabilize the solution during the first two iterations. This procedure is used to separate the influence of interior orientation parameters on the exterior orientation parameters and is fully discussed by Tudhope (1988).

6.2.3 The Least-Squares Solution

Ten photographs were selected from the block of three strips of five photos each. Four photos were selected from the center strip. The three center photos were selected from each side strip. The block maintained 80 percent overlap and 60 percent sidelap and adequately covered the entire set of photo targets. The ten photos contain 152 measured image points. Table 11 summarizes the various quantities involved in the solution.

The direct observations include the x and y image coordinates which are measured on the BC-1 analytical plotter. GPS provides observations of the unknown translation parameters of exterior orientation. The survey coordinates have been directly measured at the phase center of the GPS antenna by kinematic GPS observations. The survey coordinates are introduced to the solution as weight constrained parameters. The solution has

$$n + r - u = \text{degrees of freedom}$$

or

$$292 + 120 - 159 = 253 \text{ degrees of freedom}$$

Table 11 -- Observations and Parameters Involved in the System Calibration Least-Squares Adjustment

| | Direct Observations (n) | Observed Parameters (r) | Unknown Parameters (u) |
|---|---|---|---|
| **Image Points** | 292 | 0 | 0 |
| **Exterior Orientation** | | | |
| **Rotations** | 0 | | 30 |
| **Translations** | 0 | 30 | 30 |
| Interior Orientation | 0 | 0 | 9 |
| Survey Points | 0 | 90 | 90 |

The linearized observation equations of a non-linear model require reasonably good estimates for the unknown parameters. The unknown rotational parameters are estimated from a Case 3 solution. The parameters of interior orientation are initially assigned estimates of zero because the lens distortion contribution (from the stellar

calibration) has been applied during the process of transforming comparator coordinates to photo coordinates, leaving only the small effect of the optical flat. The calibration solution will yield estimates for the unknown terms of interior orientation resulting from the optical flat. A second calibration solution is performed with image coordinates left uncorrected for the laboratory calibration of interior orientation elements. The difference between the two solutions for interior orientation elements was the values of the laboratory calibration. The contribution of the optical flat on interior orientation has therefore been isolated from the total interior orientation values. This fact is important because it demonstrates that both solutions provided unbiased estimates for the interior orientation. Proof of this statement will be accomplished by transferring the interior orientation model for the optical flat to a second camera system and determine if the aerotriangulation results are improved.

6.3.2.a Linear Dependencies

If a design matrix contains two or more rows or columns which are scaler multiples of one another or if a linear combination of rows or columns are equal, the condition of linear dependence is said to exist. In this situation, the matrix fails to have full rank. Provided that the design matrix combines with the weight matrix in the formation of the normal matrix, the normal matrix will also lack full rank and will have a determinant of zero. It is not possible to compute the Cayley Inverse of a matrix which has a determinant of zero and, therefore, a unique solution for the unknown parameters is not possible and an infinite number of solutions will exist for the observation equations. The point of the research is to eliminate known linear dependencies by employing GPS positioning in the first place.

Until now, great importance was attached to the need to reach a state of statistical control in order to calibrate the measuring system. Even if the state of statistical control has been reached, it is possible that certain unknown parameters in the solution are highly correlated or linear dependent. The solution of one unknown may depend on another unknown. In the classic sense of a least-squares solution, linear dependency prevents a unique solution of the unknown parameters for the system calibration.

As an example of the linear dependence which exists in the analytical calibration using vertical photography over flat terrain (this research), consider the relationship between the flying height $(Z-Z_0)$ and camera constant (c) in the application of the condition of collinearity. The mathematical model can be expressed as follows:

$$f(x) = (x - x_0) - c * m / q = 0$$

$$f(y) = (y - y_0) - c * n / q = 0$$

assume vertical and crab-free photography, so

$$\text{Kappa} = \text{Phi} = \text{Omega} = 0,$$

and therefore,

$$R1 = R2 = R3 = 1$$

$$m = X - X_0$$

$$n = Y - Y_0$$

$$q = Z - Z_0$$

assume flat terrain, so

$$q = Z - Z_0 = \text{a constant}$$

$$f(x) = x - x_0 - c * (X - X_0) / (Z - Z_0) = 0$$

and;

$$f(y) = y - y_0 - c * (Y - Y_0) / (Z - Z_0) = 0$$

$$x_0 = x - c * (X - X_0) / (Z - Z_0)$$

$$dx_0 / dX_0 = c / (Z - Z_0) = \text{constant}$$

similarly

$$y_0 = y - c * (Y - Y_0) / (Z - Z_0)$$

$$dy_0 / dY_0 = c / (Z - Z_0) = \text{constant}$$

and

$$c = (x - x_0) * (Z - Z_0) / (X - X_0)$$

$$dc / dZ_0 = - (x - x_0) / (X - X_0) = - (y - y_0) / (Y - Y_0);$$

using similar triangles;

$$dc / dZ_0 = - c / (Z - Z_0) = \text{constant}$$

It can be seen that it is not possible to separate the unknown parameters of interior and exterior orientation. It also cannot be assumed that the Kappa rotation will be zero. Similar dependencies can be developed as noted by Tudhope (1988) and derived by Kenefick (1971). GPS control for the exposure station coordinates eliminates the linear dependency by direct observation of $X_0$, $Y_0$, and $Z_0$. If *a priori* knowledge of the exposure station is not available, the dependency can be eliminated by using orthogonal Kappa rotations for the various photographs. Tudhope (1988) used such a procedure in combination with convergent photography for calibrating the aerial camera.

Secondary dependencies also exist between $x_0$ and Phi and between $y_0$ and Omega when Kappa is very small as follows:

$$dx_0 / dPhi_i = (c^2 + x^2)/c = c + x^2/c$$

$$dy_0 / dOmega_i = (c^2 + y^2)/c = c + y^2/c$$

The above equations indicate that changes in Phi and Omega can partially compensate for errors in $x_0$ and $y_0$. As x and y become relatively small compared to c, as in the case of narrow angle cameras used in terrestrial systems, perfect projective compensation is approached. That is:

$$dx_0 / dPhi_i = (c^2 + x^2)/c = c + x^2/c \quad \rightarrow \quad c$$

as $x^2/c \rightarrow 0$

$$dy_0 / dOmega_i = (c^2 + y^2)/c = c + y^2/c \quad \rightarrow \quad c$$

as $y^2/c \rightarrow 0$

# CHAPTER VII
# RESULTS

The results of the calibration for the NOAA photogrammetric system based on the G Cone as its major component will be presented in the form of tables and figures. Each table or figure will be followed with a brief discussion of the results. The chapter will conclude with the results of aerotriangulation utilizing the B Cone with, and without, the system calibration derived from the G Cone information. Chapter VIII, the final chapter, will attempt to summarize some of the more unique results.

## 7.1 NOAA G Cone Camera Calibration

Table 12 represents the results of the system calibration based on *a priori* knowledge of the exposure stations determined during inflight GPS kinematic positioning of the aircraft.

Table 12 -- Final Values from the Case 4 Least-Squares System Calibration Solution

| Parameter | Initial Value | Final Value | Std Error |
|---|---|---|---|
| $x_0$ | -0.0087 mm | 0.0105 mm | 0.0057 mm |
| $Y_0$ | -0.0153 mm | 0.0260 mm | 0.0059 mm |
| c | 153.2970 mm | 153.2200 mm | 0.0051 mm |
| K1 | $0.26\ 10^{-7}$ | $0.11\ 10^{-7}$ | $0.13\ 10^{-7}$ |
| K2 | $-2.22\ 10^{-12}$ | $0.34\ 10^{-12}$ | $1.51\ 10^{-12}$ |
| K3 | $58.50\ 10^{-18}$ | $-14.36\ 10^{-18}$ | $53.4\ 10^{-18}$ |
| P1 | 0.00 | $-0.28\ 10^{-6}$ | $0.17\ 10^{-6}$ |
| P2 | 0.00 | $-0.36\ 10^{-6}$ | $0.16\ 10^{-6}$ |
| P3 | 0.00 | $-0.38\ 10^{-4}$ | $8.96\ 10^{-5}$ |

| | Std Error |
|---|---|
| $X_0$ | 0.044 m |
| $Y_0$ | 0.044 m |
| $Z_0$ | 0.025 m |

| | *A Priori* | *A Posteriori* |
|---|---|---|
| $Sigma_0^2$ | 1.00 | 0.87 |
| Degrees of Freedom | | 253 |

The Table 12 represents only a summary of the results. The final iteration is contained in Appendix E. Included in the final iteration is a portion of the covariance/correlation coefficient matrix for the adjusted parameters of interior and exterior orientation. The initial values for lens distortion were obtained from a stellar lens calibration of the G Cone camera performed in 1985 (Appendix D). The final values for lens distortion are significantly different from their initial values which reflects the effect of the optical flat, in particular, and the system performance, in general, on the lens system. The standard error for the exposure station coordinates before and after the adjustment agree well in $X_0$ and $Y_0$ (4.4 cm vs 5.0 cm). The $Z_0$ standard error after the adjustment is slightly smaller than the *a priori* standard error (2.5 vs 4.0 cm). No significance is attached to these standard error differences. The assumptions being made are:

1. All major sources of systematic error have been carefully determined and eliminated prior to the adjustment.
2. Any remaining systematic errors were modelled and solved for during the adjustment or are insignificant at the achieved level of accuracy for the calibration.

3. All other sources of error are assumed to be random and normally distributed (although a normal distribution is not required for a least-squares solution). Making the above assumption, it will be assumed that the standard errors approximate the true errors.

If a normal distribution is assumed, then the *a posteriori* variance of unit weight can be tested to see if it could be equal to the *a priori* estimate using the $Chi^2$ statistic.

$Chi^2$ = d.f.* *a posteriori* variance/*a priori* variance

= 253 * 0.87 / 1.00 = 220

for alpha = 0.5

$Chi^2_{0.5} = 199$; $Chi^2_{99.5} = 316$

or even for alpha = 5.0

$Chi^2_{2.5} = 208$; $Chi^2_{97.5} = 297$

Thus the *a posteriori* variance of unit weight could be equal to the *a priori* variance of unit weight, then it can also be assumed that the *a priori* estimates for the standard errors of the observations are valid.

The new terms for interior orientation are the summation of the stellar and system calibration values (which agree with the second calibration solution performed with image coordinates uncorrected for the laboratory calibration) as follows:

$X_0$ = 0.002 mm; $Y_0$ = 0.011 mm; CC = 153.220 mm

K1 = $0.37\ 10^{-7}$; K2 = $-1.88\ 10^{-12}$; K3 = $44.14\ 10^{-18}$

P1 = $-0.28\ 10^{-6}$; P2 = $-0.36\ 10^{-6}$; P3 = $-0.38\ 10^{-4}$

The above values for interior orientation can be directly computed from the Case 4 solution if the transformed image coordinates are not first corrected lens distortion as determined from the stellar calibration. The tangential distortion terms are the same as in Table 12 because the stellar calibration did not include terms for tangential distortion. Therefore, it can be assumed that the stellar calibration can be separated from the system calibration.

The presence of the tangential distortion terms in Table 12 suggest that the optical flat and/or the air gap between the optical flat and the entrance node introduce the effect of a thin prism as discussed in Section 6.1.5.

Figures 23 through 27 illustrate the magnitude and distribution of the combined radial and tangential distortions as a function of radial distance from the principal point.

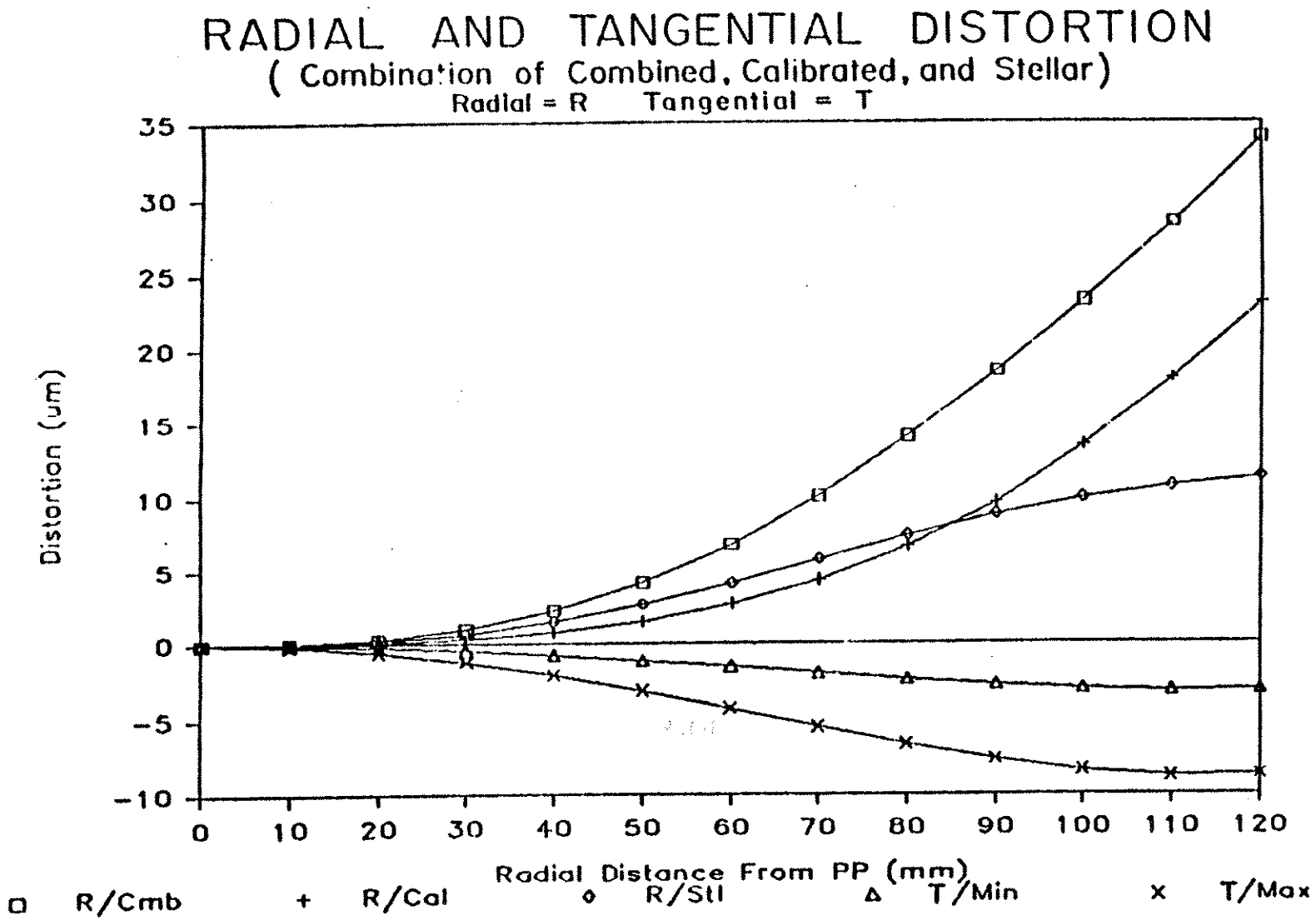


Figure 23. Radial and Tangential Distortion

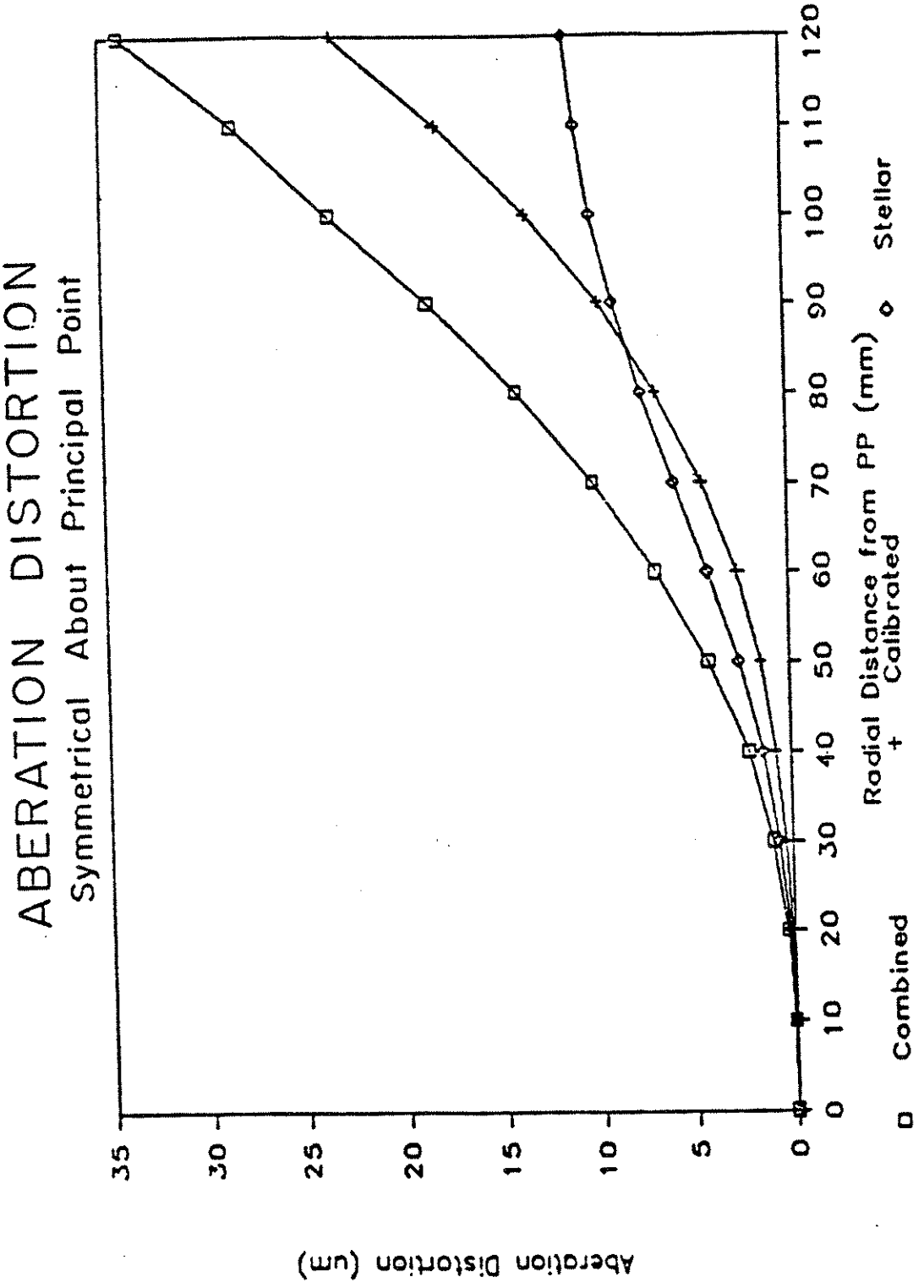


Figure 24. Aberration Distortion

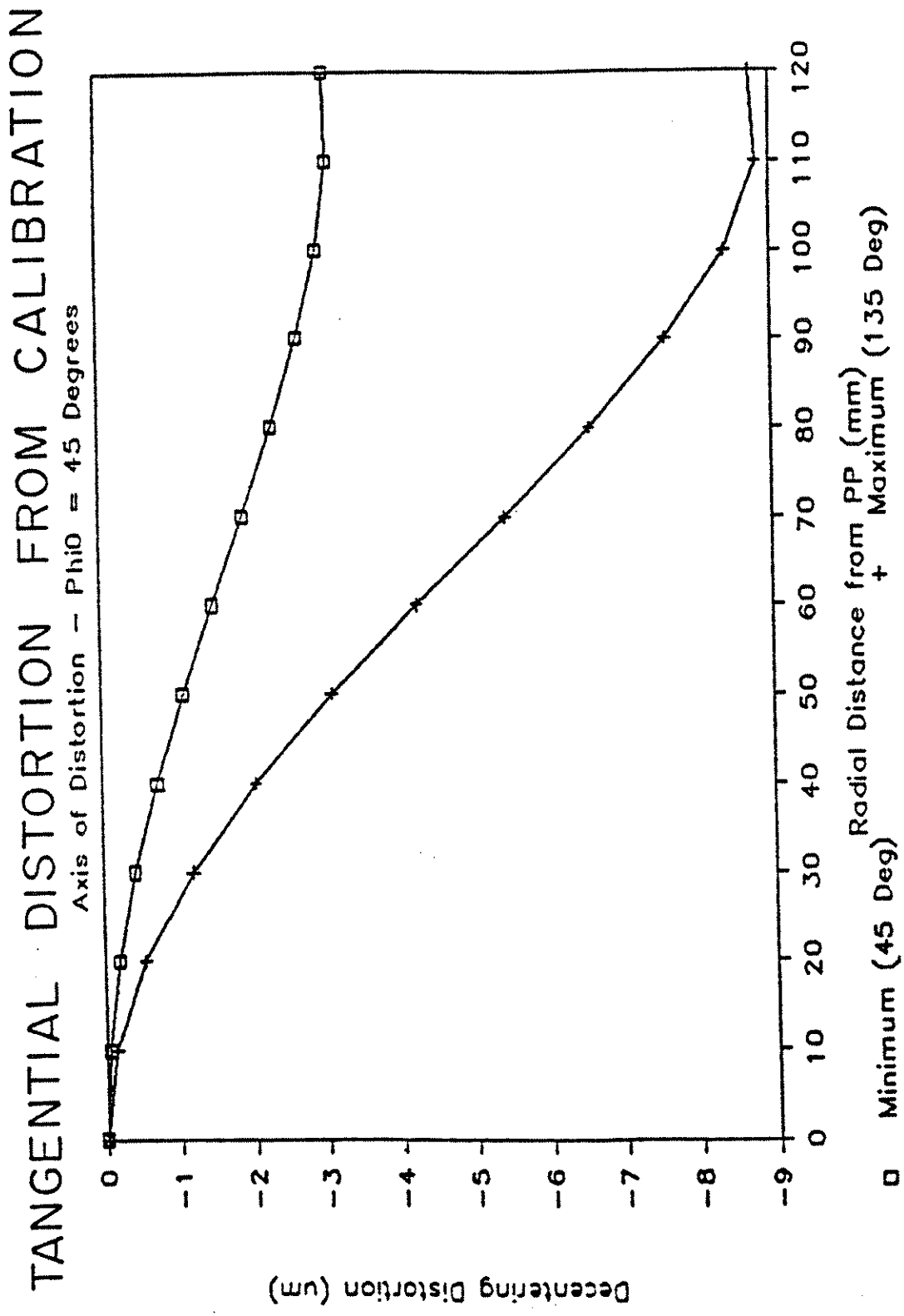


Figure 25. Tangential Distortion from Calibration

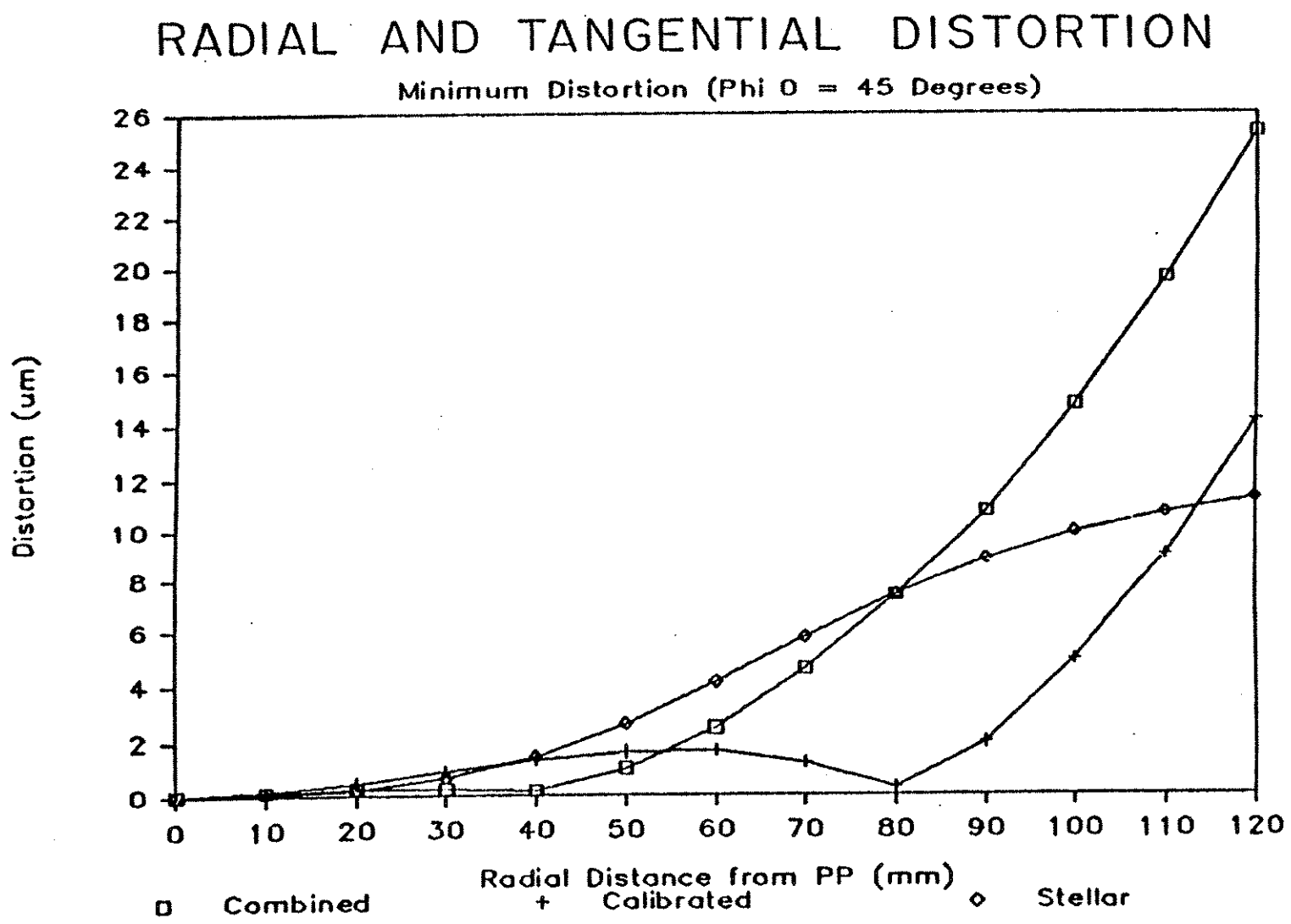


Figure 26. Radial and Tangential Distortion at 45 Degrees

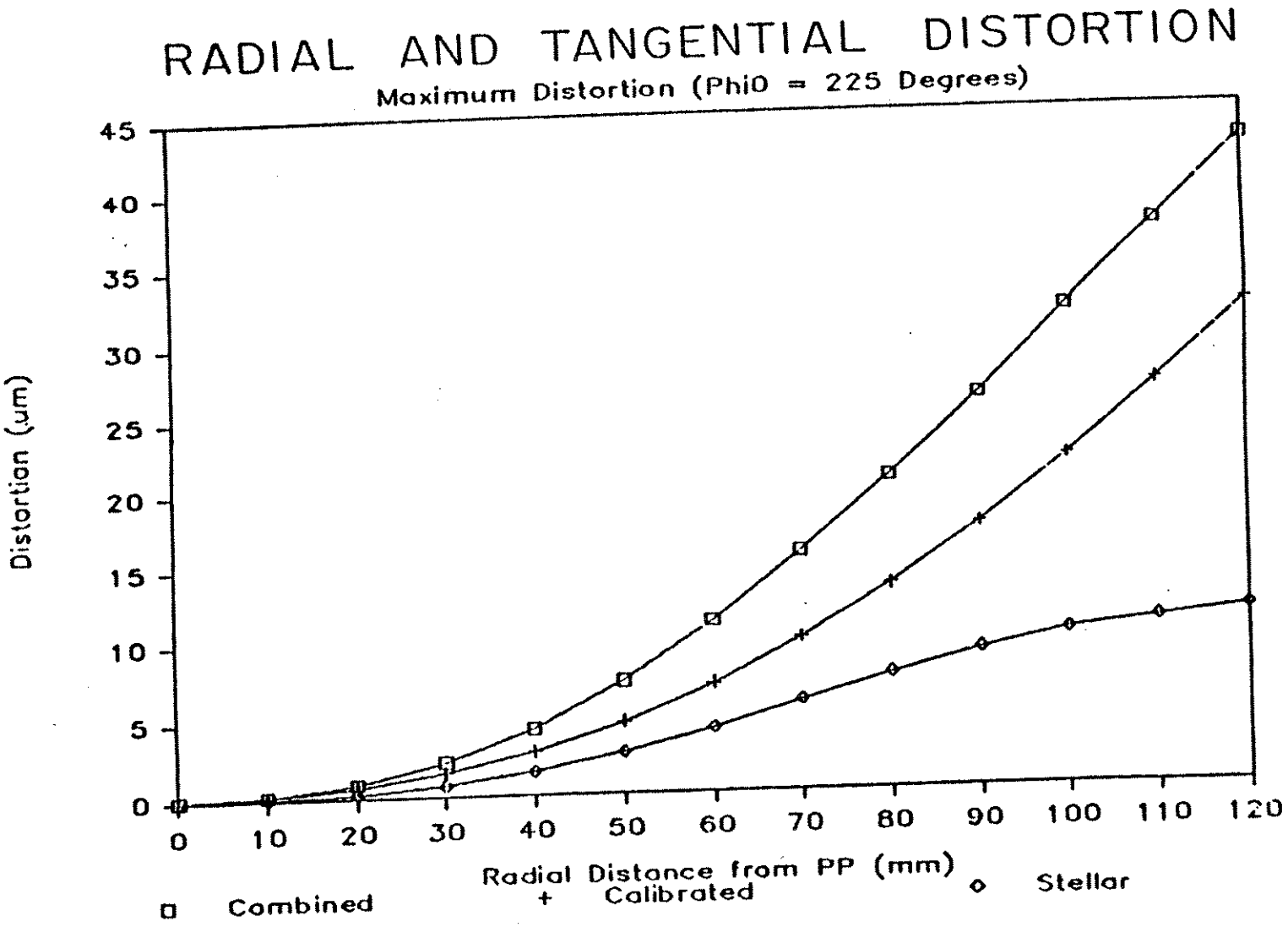


Figure 27. Radial and Decentering Distortion at 225 Degrees

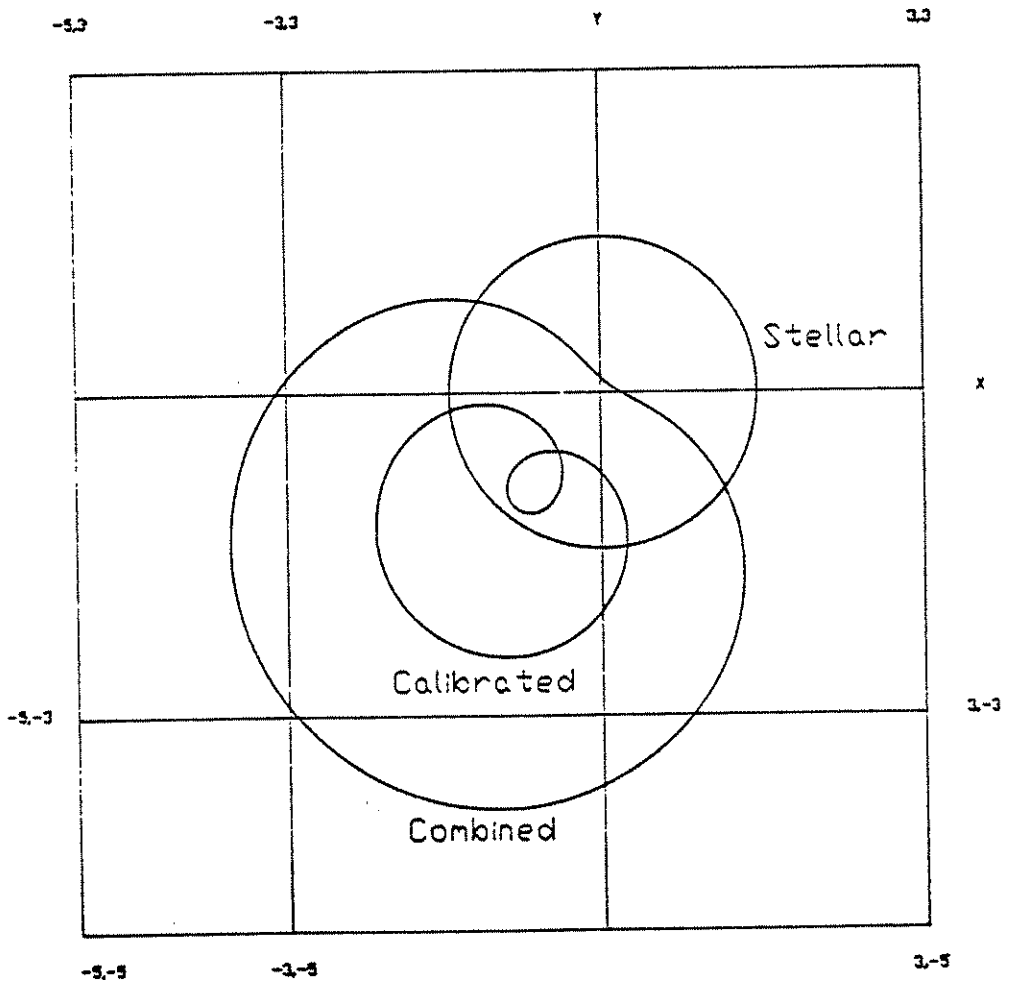


Figure 28. G Cone Lens Distortion Correction at 40 mm from the Principal Point

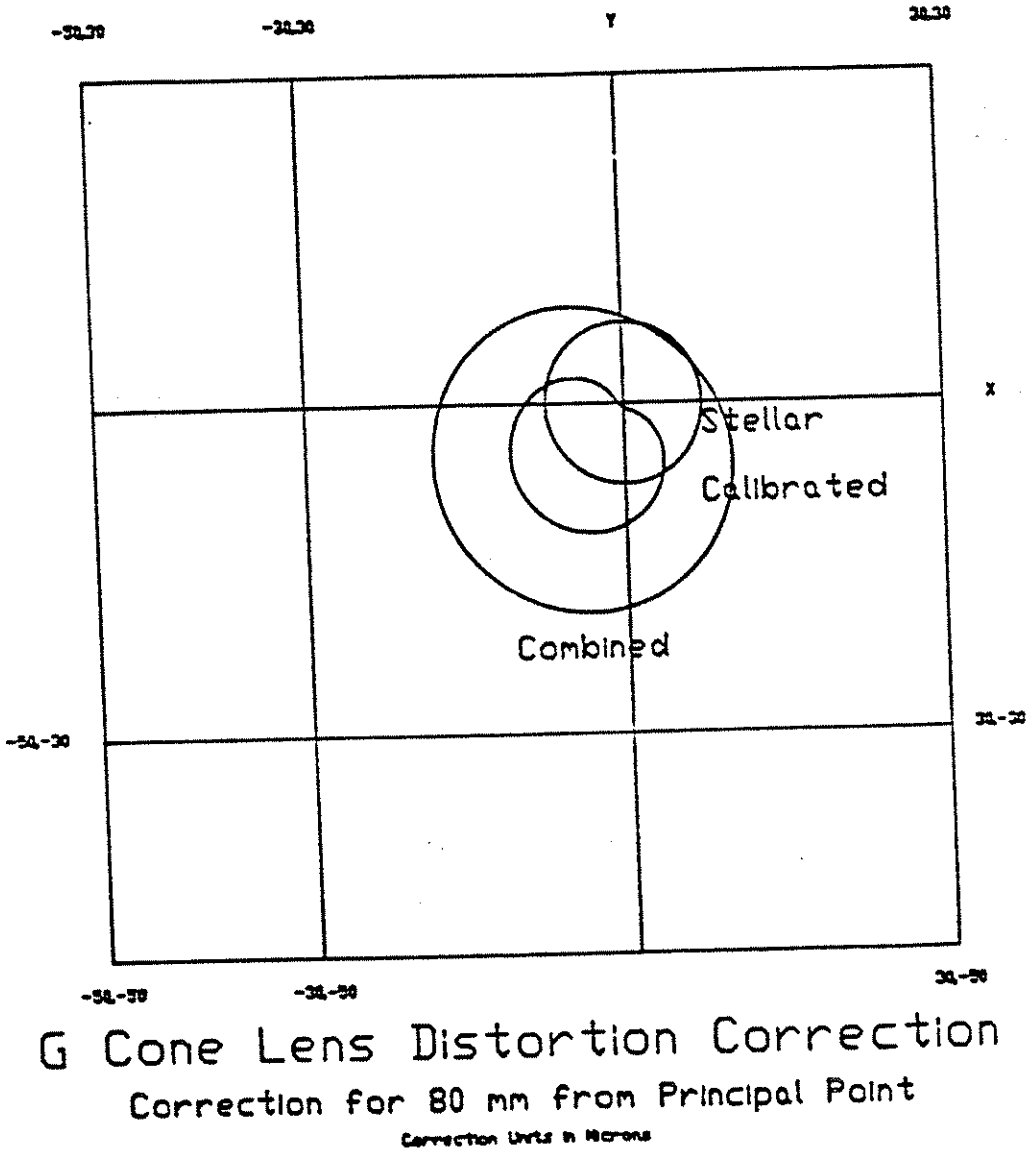


Figure 29. G Cone Lens Distortion Correction at 80 mm from the Principal Point

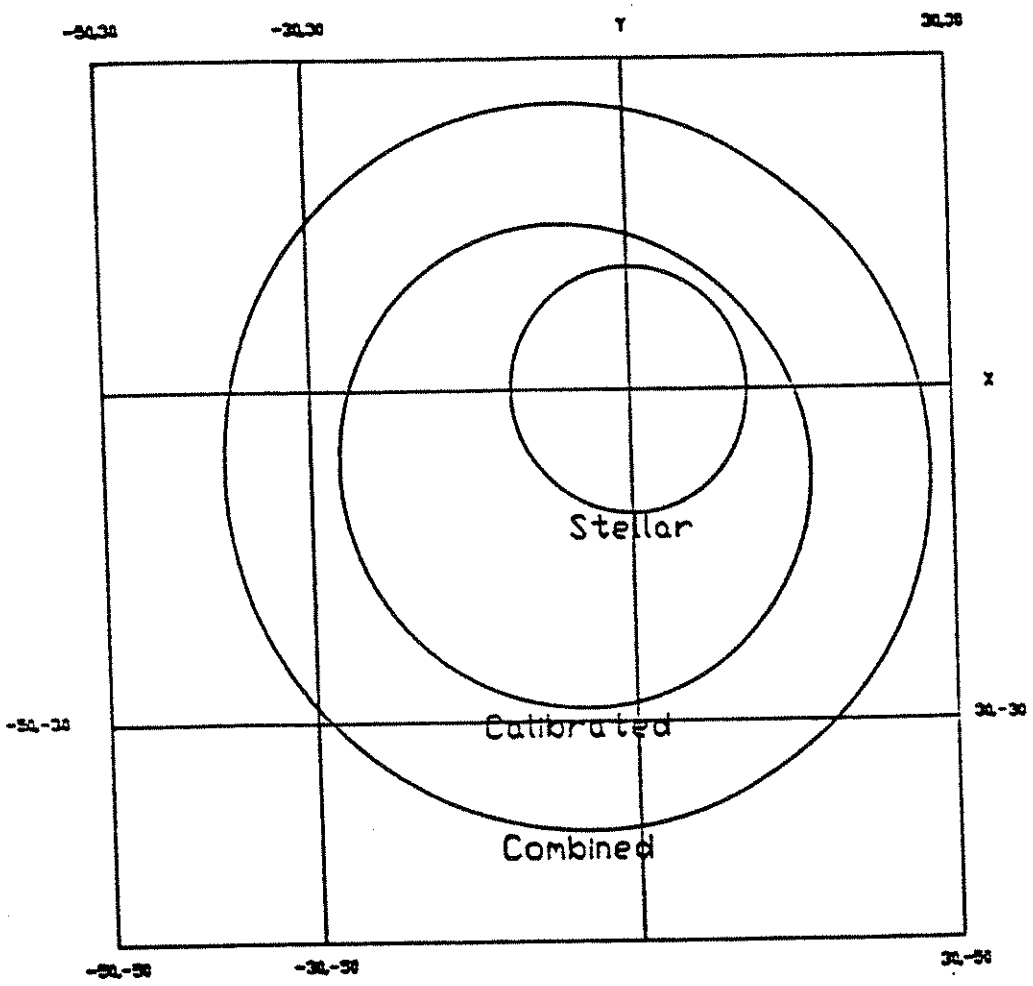


G Cone Lens Distortion Correction

Correction for 120 mm from Principal Point

Figure 30. G Cone Lens Distortion Correction at 120 mm from the Principal Point

Figures 23 through 27 portray lens distortion components in the traditional manner representing only the magnitude of the distortion. Figure 23 represents the maximum and minimum radial (aberration) and tangential (decentering) distortion. Distortions for the stellar calibration, system calibration (effects of the optical flat only) and combined effects are shown. The maximum and minimum tangential distortions are oriented at 135° and 45°, respectively, from the positive x photo axis and refer only to the system calibration. Figures 24 and 25 separate the components of radial and tangential distortion. Figures 26 and 27 illustrate the minimum and maximum combined distortions.

Figures 28 through 30 illustrate the same distortions but are plotted for all directions about the principal point for radial distances of 40, 80, and 120 mm, respectively. Note that the shape of the distortion plot suggests radial distortion, but shifted relative to the principal point due to the domination of the tangential distortion.

Once again, in the spirit of obtaining statistical control, the theory and accuracy of the author's algorithms were tested by an independent method. The combined distortion model along with the combined model for photogrammetric refraction for a pressurized camera compartment was used to correct the raw image coordinate observations obtained on DOY 299. The corrected image coordinates combined with the *a priori* exposure station coordinates interpolated from the GPS antenna positions were used as the only input to aerotriangulation program GAPP (Lucas 1989). The output from GAPP is survey coordinates for the targeted points. The comparison of aerotriangulated survey control against the kinematic GPS ground survey control values serve as a basis for evaluating the accuracy of the system calibration. The comparisons are contained in Table 13.

The Root Mean Square (RMS) values are computed by the from the following equation:

$$RMS = SQRT\ (d^2/n)$$

where: d is the difference between survey and aerotriangulated coordinates
n is the sample size

A mean of zero is assumed instead of the sample mean.

The significance of these comparisons has far reaching consequences on the way photogrammetric surveys can be conducted in the future. Lucas (1988) demonstrated the potential for photogrammetry without ground control; the above results support the concept and represent a very significant contribution of this research.

Three other solutions were performed with the G Cone imagery using GAPP. The first two solutions use the image coordinate corrections as before. In the first solution, eight survey control stations were constrained with no GPS information of the exposure stations introduced. The second solution used the same eight constrained survey points, but also introduced the GPS information for the exposure stations. The third solution uses only GPS information for the exposures stations and the image coordinates are corrected using the stellar calibration and Saastamoinen's photogrammetric refraction model for a pressurized cabin. The means and standard deviations are given in Table 14.

Table 13 -- Comparison of Aerotriangulated Survey Control Utilizing GPS Positions for the Exposure Stations Without *A Priori* Knowledge of Ground Control, to the Known Survey Control Using the NOAA G Cone Camera Lens

| Point | East (m) | North (m) | Elevation (m) |
|---|---|---|---|
| 501 | -0.002 | 0.000 | -0.045 |
| 502 | 0.014 | 0.052 | -0.075 |
| 503 | -0.007 | 0.019 | -0.062 |
| 504 | 0.028 | 0.023 | -0.139 |
| 505 | 0.056 | 0.017 | -0.116 |
| 506 | 0.074 | -0.019 | -0.250 |
| 511 | -0.007 | 0.026 | -0.017 |
| 512 | 0.003 | 0.011 | -0.018 |
| 513 | 0.004 | 0.016 | -0.094 |
| 514 | -0.008 | 0.002 | -0.074 |
| 521 | -0.023 | -0.006 | -0.088 |
| 522 | -0.029 | 0.018 | -0.140 |
| 523 | 0.002 | -0.024 | -0.043 |
| 524 | 0.003 | -0.007 | -0.038 |
| 525 | 0.008 | -0.022 | -0.039 |
| 526 | 0.015 | -0.041 | -0.038 |
| 527 | -0.096 | 0.016 | 0.104 |
| 528 | -0.036 | -0.037 | 0.071 |
| 543 | 0.014 | 0.075 | 0.164 |
| 544 | 0.057 | -0.004 | -0.033 |
| 545 | 0.003 | -0.016 | -0.095 |
| 546 | -0.027 | -0.031 | -0.106 |
| 547 | 0.006 | 0.007 | -0.129 |
| 548 | -0.028 | 0.064 | -0.241 |
| 5125 | -0.009 | 0.001 | -0.081 |
| 5135 | -0.029 | 0.004 | -0.045 |
| 5225 | 0.027 | 0.017 | -0.088 |
| 5235 | -0.028 | -0.020 | -0.058 |
| Mean | -0.001 | 0.005 | -0.065 |
| Std Dev | 0.033 | 0.028 | 0.085 |
| RMS | 0.032 | 0.028 | 0.106 |

Table 14 -- Survey Control Differences for the NOAA G Cone Camera Lens (Aerotriangulation - Ground Control)

| Solution | Mean (m) | Std. Dev. (m) |
|---|---|---|
| 8 Constrained Survey Points | | |
| East | -0.010 | 0.027 |
| North | -0.005 | 0.032 |
| Elevation | -0.002 | 0.103 |
| 8 Constrained Survey Points + GPS | | |
| East | 0.001 | 0.026 |
| North | -0.010 | 0.026 |
| Elevation | -0.025 | 0.054 |
| GPS Only without the contribution of the System Calibration | | |
| East | 0.081 | 0.371 |
| North | 0.090 | 0.429 |
| Elevation | 0.704 | 0.180 |

Note that the constrained solution without GPS positions for the exposure stations matches the GPS Only solution given in Table 13 very well. The constrained solution with GPS improves the solution for elevation slightly. The GPS solution without system calibration (contribution of the optical flat) is significantly worse, however it would still meet NOAA's criteria for 1 m precision of survey control.

7.2 NOAA B Cone Camera Tests

The calibrated system parameters in terms of interior orientation are based on the G Cone calibration. The system calibration may, in fact, be no more than a form of self-calibration where the model for lens distortion acts as a polynomial to absorb situation dependent variables. In order to test the validity of the system calibration, the B Cone camera was installed in place of the G Cone camera in the NOAA Citation and a second mission was flown on DOY 301. To make the test as independent as possible (in the spirit of statistical control) a different set of GPS satellites was used. The system calibration parameters (effect of the optical flat) for aberration and decentering distortion were applied to the B Cone camera imagery along with the combined photogrammetric refraction model and laboratory lens distortion parameters. Table 15 lists the comparison of aerotriangulated survey control to ground survey control.

Table 15 -- Comparison of Aerotriangulated Survey Control Utilizing GPS Positions for the Exposure Stations Without *A Priori* Knowledge of Ground Control, to the Known Survey Control Using the NOAA B Cone Camera Lens

| Point | East (m) | North (m) | Elevation (m) |
|---|---|---|---|
| 502 | 0.130 | 0.163 | -0.069 |
| 503 | 0.116 | 0.084 | 0.031 |
| 504 | 0.153 | 0.005 | -0.018 |
| 505 | 0.160 | -0.031 | 0.036 |
| 506 | 0.097 | -0.031 | 0.157 |
| 511 | 0.057 | 0.068 | 0.089 |
| 512 | 0.056 | 0.037 | -0.065 |
| 513 | 0.016 | -0.007 | -0.071 |
| 514 | 0.077 | -0.025 | -0.154 |
| 521 | 0.054 | 0.055 | 0.008 |
| 522 | 0.003 | 0.028 | -0.180 |
| 523 | -0.009 | -0.028 | -0.163 |
| 524 | 0.012 | -0.049 | -0.279 |
| 525 | 0.067 | -0.071 | -0.257 |
| 526 | 0.079 | -0.066 | -0.068 |
| 527 | 0.042 | 0.002 | -0.026 |
| 528 | 0.059 | 0.140 | 0.144 |
| 543 | 0.071 | 0.008 | -0.009 |
| 544 | 0.039 | -0.112 | -0.266 |
| 547 | -0.101 | -0.014 | -0.279 |
| 548 | -0.001 | 0.065 | 0.039 |
| 5125 | 0.035 | 0.027 | -0.053 |
| 5135 | 0.024 | -0.013 | -0.099 |
| 5225 | -0.026 | 0.004 | -0.220 |
| 5235 | -0.026 | -0.055 | -0.241 |
| Mean | 0.047 | 0.007 | -0.081 |
| Std Dev | 0.059 | 0.064 | 0.131 |
| RMS | 0.075 | 0.063 | 0.151 |

The results for the B Cone are also very good. The fact that the standard deviations for East, North, and Elevation are larger than the same G Cone values is most likely due to the effect of non-linear film deformation which cannot be adequately modelled by the eight fiducial marks in the B Cone. The three additional solutions performed for the G Cone were repeated for the B Cone and the results are given in Table 16 below. Once again, there is not much difference between solution 1 and the above results. Solution 2 shows a similar improvement in the elevation determination. Most significant is the obvious degradation of the results when the system calibration parameters are removed. It becomes very obvious that the system calibration is not merely a self-calibration of the G Cone lens. It should also be noted that the solution without the system calibration parameters became so unstable that certain exposure station coordinates were rejected during the GAPP solution.

Table 16 -- Survey Control Differences for the NOAA B Cone Camera Lens (Aerotriangulation - Ground Control)

| Solution | Mean (m) | Std. Dev. (m) |
|---|---|---|
| 8 Constrained Survey Points | | |
| East | -0.023 | 0.029 |
| North | 0.014 | 0.086 |
| Elevation | 0.020 | 0.121 |
| 8 Constrained Survey Points + GPS | | |
| East | -0.021 | 0.033 |
| North | 0.001 | 0.077 |
| Elevation | 0.006 | 0.098 |
| GPS Only without System Calibration | | |
| East | 0.101 | 0.508 |
| North | 0.274 | 0.602 |
| Elevation | 1.427 | 0.265 |

As a final test, the ARDC model without compensation for the pressurized compartment was substituted for the combined refraction model. The results for both data sets were degraded, thus confirming the relevancy of a need for a pressurized cabin atmospheric refraction model.

The results of the system calibration are the most significant contribution of the research. Inflight calibration of the entire aerial system has been successfully demonstrated. Moreover, the operational practicality of aerotriangulation without ground control has been conclusively demonstrated.

# CHAPTER VIII
# Conclusions

## 8.1 Summary of Results

The integration of precise GPS positioning for the exposure station used as the only source for object-space control in aerotriangulation requires very accurate knowledge of the interior orientation of the airborne measuring system. No longer can projective compensation be tolerated in order to compensate un-modeled systematic error sources into the unknown parameters of exterior orientation. Instead, systematic errors will propagate into the very survey control being established by aerotriangulation. To eliminate the systematic errors, the airborne photogrammetric system will be calibrated through the use of GPS control of the exposure station combined with known survey control to determine valid *a priori* values for a system calibration. Any standard aerotriangulation solution can be used once the interior orientation parameters are properly modeled in the solution.

Once the system is calibrated, GPS positions for the exposure stations will be the only source of object-space control for the photogrammetric process. A vector defined by the exit node of the lens system and the image coordinates of a point in the film plane will be projected into a vector in the object-space solely on the strength of the interior geometry of the camera and measurable disturbances in the object space. The object-space vector will be defined by the entrance node of the lens system and the object-space coordinates of the point whose image was measured in the plane of the photograph. The ratio of these vectors is nearly equivalent to the nominal scale of the photographs. The large ratio between image and object-space vectors necessitates very accurate knowledge of the measuring system parameters. The solution for three-dimension object-space coordinates depends on an intersection of object-space rays from several photos. The effect of un-modeled systematic errors on the point of intersection is not easily predicted, because the intersection error will depend on the geometric relationship of the various object-space rays. The obvious solution is to avoid systematic error influences in the first place by a rigorous analytical calibration process.

## 8.2 Major Contributions

The following items are the most significant findings of the research and which contribute to the successful calibration of the NOAA Citation II airborne photogrammetric system by eliminating significant sources of systematic error:

1. Definition of the spatial relationships between the GPS position of the antenna phase center to the photogrammetric exposure station which include the following:
    a. Mid-point of shutter opening to the horizon pulse timing bias
    b. Spatial relationship of antenna phase center to the camera reference frame
    c. Covariance error propagation of antenna phase center position to camera exposure station
    d. Interpolation modeling of the aircraft trajectory between successive GPS positions
    e. Establishing credible rationale that the maximum time interval between GPS position information should be 1 second

2. Determination of the following systematic errors in the photogrammetric system:

   a. Modeling of the aircraft induced systematic errors related to the optical flat
   b. Statistical detection of outliers in image coordinate observations by using a combination of general and isogonal affine transformations of observed reseau points
   c. Derivation of an atmospheric refraction model for a pressurized camera compartment independent of atmospheric observations

3. Practical application of system calibration

   a. Removal of the linear dependency between image-space and object-space coordinates through application of weight constrained GPS positions for the exposure station
   b. Demonstrated inflight calibration of the airborne photogrammetric system through the determination of the nine interior orientation elements
   c. Demonstrated sub-decimeter accuracy for aerotriangulation without survey control for block photography

4. Solution for GPS integer cycle ambiguity in the aircraft situation

--- The End ---

# APPENDIX A
# KINEMATIC GLOBAL POSITIONING SYSTEM SURVEY REPORT

# KINEMATIC
# GLOBAL POSITIONING SYSTEM
# SURVEY PROJECT*

OHIO TRANSPORTATION RESEARCH CENTER

Marysville, Ohio

by

Commander Lewis A. Lapine, NOAA

* Portions of this unpublished report have subsequently been published in *GPS World* Magazine, May/June 1990.

**U.S. Department of Commerce**

National Oceanic and Atmospheric Administration

National Ocean Service

Office of Charting and Geodetic Services (C&GS)

Nautical Charting Division

NOAA Charting Research and Development Laboratory

and

**Ohio Department of Transportation**

Bureau of Aerial Engineering

**KINEMATIC GLOBAL POSITIONING SYSTEM SURVEY PROJECT**
Ohio Transportation Research Center
Marysville, Ohio

The Survey Purpose
The purpose for this survey is to prepare a facility for ground and airborne kinematic GPS experiments by establishing high-quality three-dimensional geodetic control based on the WGS84 reference system. The network will be used for primary research as partial fulfillment of a Doctoral candidacy for Commander Lewis A. Lapine, NOAA.

The Transportation Research Center (TRC)
The TRC was built by the State of Ohio in 1972 to encourage transportation research studies. The entire facility was recently deeded over to the Honda Motor Corporation, but remains under the management of the Ohio State University. The site offers many advantages for the research project. The physical layout of the TRC is compatible with the need for continuous expanses of the horizon to provide adequate satellite visibility. The facility already has an existing high-quality network of photo-control points ideally suited for the kinematic GPS applications both by ground vehicles and aircraft. The TRC is secure enough to allow valuable equipment to be left unattended for several hours duration, is not congested by traffic, and contains an on-site runway for the aircraft operations. The survey area is located entirely inside the boundaries of the Ohio Transportation Research Center in Marysville, Ohio. The major feature within the facility is a four-lane, seven-mile long, high-speed, oval test track (refer to Figure 31). The track has parallel, two-mile long, straightaways and 1.5-mile long, steeply banked, 180-degree turns. The existing TRC photo control, once converted to the GPS datum, can be used to provide a high-precision position for the aircraft by conducting a well-planned photogrammetric survey. GPS kinematic positions of the airborne camera exposure stations can then be compared and their precision evaluated. A combination of aerial triangulation and kinematic aircraft positioning by GPS may lead to a method for simultaneously calibrating the entire airborne photogrammetric system. This type of research fits well with the intended use of the facility and NOAA's need for GPS controlled photogrammetric mapping in areas of sparse geodetic control. The requirement to re-define the existing local control datum fits well with the additional requirement of implementing ground-vehicle kinematic GPS applications for FAA airport survey projects conducted by NOAA. Although direct coordinate comparisons would be difficult, chord distances and derived angles can be easily computed for checking the GPS measurements against the existing geodetic control.

The Existing Photo Control
Along the inside edge of the high-speed track is a blacktopped low-speed lane. It is on this lane that 25 photo target points had been established by a 1983 conventional ground survey. The centers of the photo targets are marked by PK nails. A service road runs down the central portion of the oval and has 10 similarly targeted points. These points, as well as approximately 15 other higher precision points, form the framework for the ground-vehicle kinematic survey. The target locations are generally free of any obstructions to the horizon above approximately 20 degrees elevation. The high-speed banks are steep enough to obstruct the horizon to 22 degrees at their centers. A single overpass over the track prevents a complete circuit of the track during kinematic operations. Fortunately, the overpass can be avoided by going up the bank and across to the other side!

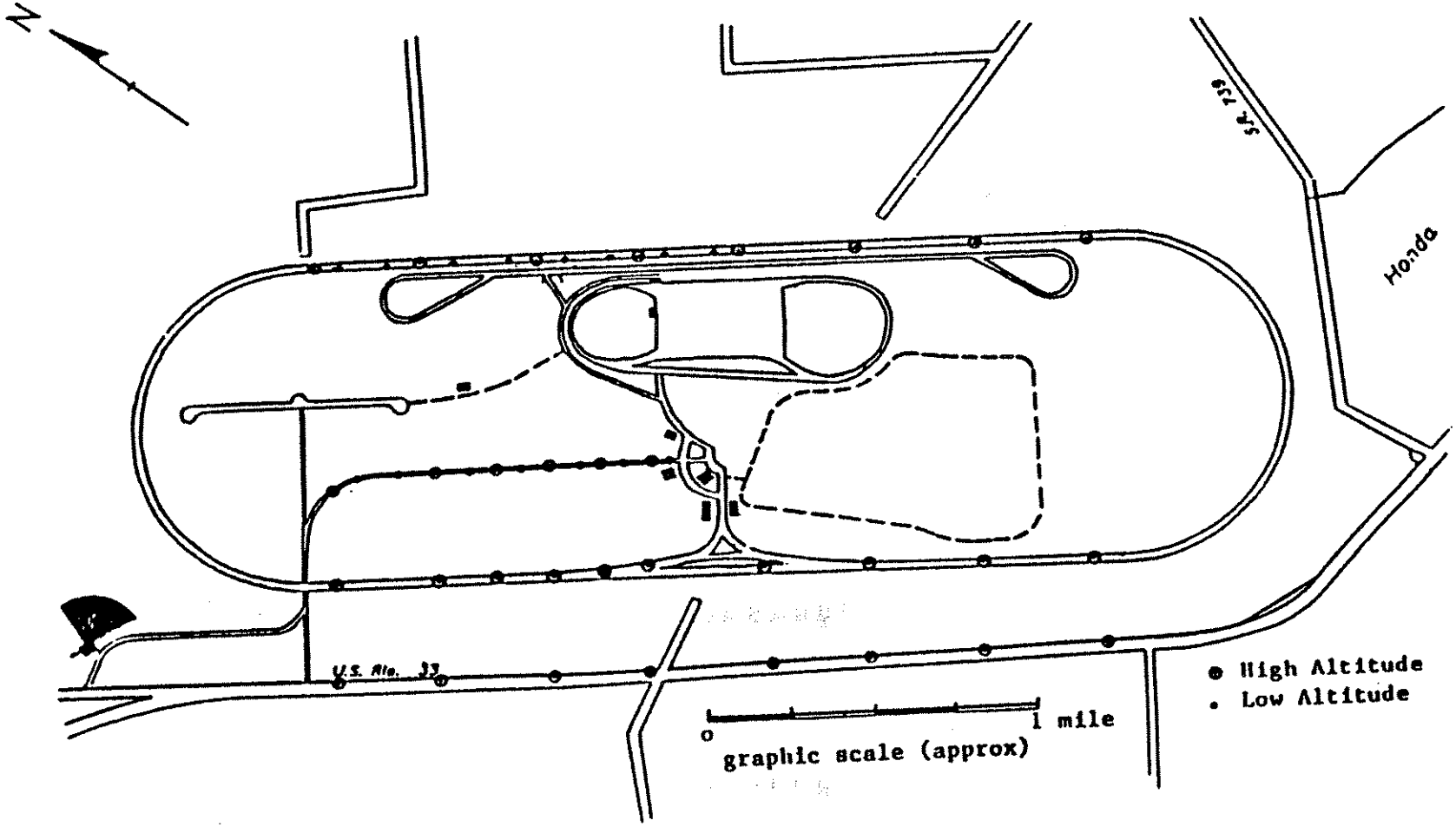


Figure 31. Transportation Research Center, Marysville, Ohio

The photo targets are of two types, low-altitude targets spaced approximately 225 meters apart, and high-altitude targets generally spaced 550 meters apart. The targets are composed of an inner circle painted white with an outer concentric black circle. The outer circle diameter is three times the diameter of the inner circle. The design of these targets provides for high-contrast images on the aerial photographs. The white center portion of the low and high-altitude targets are 28 cm and 49 cm in diameter, respectively. These sizes are chosen for 800 meter above ground level (AGL) and 1500 meter AGL flying heights in order to yield 50 micron photo images. In certain instances the two types are intermixed. The targets all lay in straight lines along the track straightaways and service road. A third strip of high-altitude targets has subsequently been added to the test area along U.S. Route 33 which runs parallel to the test track straightaways. This control was required in order to use the NOAA Cessna Citation II jet which must fly at higher altitudes. The survey was performed entirely by kinematic GPS procedures.

The Terrestrial Survey

The horizontal and vertical control surveys were performed in 1983 by personnel from the Ohio State University, Department of Geodetic Science and Surveying and the Ohio Department of Transportation (ODOT), Bureau of Aerial Engineering. The network was designed to function as a photogrammetric calibration test range to be used by ODOT, Bureau of Aerial Engineering. The 1983 survey project report states that first order horizontal-control techniques were used for angular and distance measurements. Although the documented procedures do not follow strict Federal Geodetic Control Committee Specifications, the adjusted horizontal control coordinates yielded an average standard error a posteriori of 3.1 mm in the x coordinate and 4.0 mm in the Y coordinate. These values are presumed for the primary monuments only. In addition, secondary control and photo-target positions have also been established by classical geodetic techniques. Single-run leveling was also accomplished to all primary and secondary stations. The primary station marks are three-dimensionally stable, sleeved rod marks similar to the NGS design. A cluster of four sleeved marks have been re-surveyed periodically to monitor any motion. The marks have a design stability of 4 mm despite seasonal variations including frost heave. The secondary monuments are un-sleeved deep rod marks, which appear undisturbed by mowing operations and frost heave. The photo-target centers are marked by PK nails driven into asphalt.

All coordinate computations are reduced to a plane elevated at 330 meters above sea level. The chosen datum is strictly local in nature and could not be used for the kinematic GPS/ photogrammetry experiment due to transformation difficulties. A more complete description of the survey is contained in a draft report entitled, Aerial Photo Test Field at the Transportation Research Center (TRC) of Ohio, prepared by Professor Dean Merchant, Department of Geodetic Science and Surveying, OSU, August, 1983.

The Kinematic GPS Survey

The kinematic GPS survey was performed using some of the same marks and photo targets established in the terrestrial survey. The purpose of this survey was to experiment with kinematic GPS techniques, gain an estimation of the potential precision of such methods, and obtain sufficient information to transform the plane coordinate system used in the terrestrial survey into a new local plane coordinate system based on the WGS84 System. The kinematic GPS positions of the NOAA aircraft could then be similarly transformed into the local system for comparison purposes. The photo targets would then be used by a NOAA aircraft/photo

system equipped with GPS for photogrammetric mapping missions. The transformation of photo-target positions into the WGS84 System would hopefully eliminate datum ambiguities during system calibration while the new local system simplifies the transformation of photo coordinates into geodetic coordinates. The field work was completed according to the schedule in Table 17.

Once the GPS survey was computed, it became apparent that an excellent and consistent agreement existed between the two coordinate systems. The comparison was based on computed distances and angles obtained from the corresponding coordinate systems. The agreement was so good, in fact, that a transformation of the original terrestrial coordinates was not necessary. Instead, the kinematic survey was expanded to include all required photo targets. Closures of several millimeters obviated the need for any adjustment. Repeat observations were combined by a weighted mean based on the number of observations.

The Ground Vehicle Kinematic Equipment
The survey was conducted using three Trimble 4000 SX, 5-channel, GPS receivers. These receivers are of the single L1 frequency phase comparison type. Data were sampled at a 15-second epoch rate and recorded on Kaypro 2000 portable computers. A specially equipped NGS field truck was used to transport the kinematic GPS receiver and antenna. The truck utilized shock-mounted racks for the receiver and an antenna mount. The antenna was mounted atop a rigid pole attached to the vehicle by a three-degree-of-freedom support mechanism. The mount enabled the transport of the antenna and it's vertical placement over the survey mark without ever being detached from the vehicle. The unique feature of the mount is that the pole could be made vertical over the mark despite the tilt of the vehicle (Figure 32). The antenna was always supported at the same height above the mark. The antenna mount worked so well that only weight reduction of the pole could improve the system's original design.

The Survey Operations
The first survey priority was to connect the TRC network to the national network. The operations, therefore, began with static baselines being observed from the Union County Airport (MARYPORT 1986) to TRC8 and TRC31. MARYPORT is a National Geodetic Survey GPS station established as part of the FAA airport survey program and is directly determined on the National Geodetic Reference System of 1983. TRC8 is one of 12 three-dimensional marks set during a high-precision survey performed and adjusted by Professor Dean Merchant. TRC31 is a supplemental horizontal-control monument but also part of the same survey. A fourth static baseline was later observed between TRC8 and TRC3. TRC3 is one of the 12 three-dimensional network marks.
Station MARYPORT was held fixed (NAD83) for all subsequent computations.

MARYPORT 1986
Latitude 40/13/29.89678 N
Longitude 83/21/03.28907 W
Ellipsoidal Height 272.2000 m

The first three baselines had a total misclosure of three millimeters over the 36 kilometer length. The baseline between TRC3 and TRC8 checked the adjusted 1983 value by 1 millimeter. The baseline between TRC8 and 31 checked the adjusted value by 5 mm.

Table 17 -- Daily Survey Progress

| Day of Year | Observations | Stations |
|---|---|---|
| 195 | Static | MARYPORT,TRC8,TRC31 |
| 201 | Static | TRC8, TRC3 |
| 201 | Kinematic | 524,523,522,521,528,527 526,525 |
| 203 | Kinematic | 511,512,512.5,513,513.5 514,207,206,205,204 203,202 |
| 208 | Kinematic | 514,513.5,513,512.5,512 511,207,206,205,204 203,202 |
| 209 | Kinematic | 225,226,504,227,228,505 506,507,528,527,526 525 |
| 210 | Kinematic | 524,523.5,523,522.5,522 505,506,507,508,528,527 526,525 |
| 215 | Kinematic | 524,523.5,523,522.5,501 502,503,504,505,506,507 508,528,527,526,525 |
| 216 | Kinematic | 514,513,220,501,221,222 223,224,225,226,227,228 505 |
| 218 | Kinematic | 220,501,221,222 |
| 235 | Kinematic | 220,501,221,222,223,224 225,226,227,228,505 |
| 245 | Kinematic | 531,532,533,534,535,536 537,538 |


Figure 32. GPS Kinematic Survey Vehicle

Once computed, TRC3,8, and 31 were held fixed as follows:

TRC8
Latitude 40/18/03.62946 N
Longitude 83/33/20.43478 W
Ellipsoidal Height 297.0496 m

TRC3
Latitude 40/18/59.09640 N
Longitude 83/33/56.12589 W
Ellipsoidal Height 304.0561 m

TRC31
Latitude 40/18/35.74241 N
Longitude 83/32/34.40455 W
Ellipsoidal Height 301.1056 m

During kinematic operations at least one Trimble receiver was operating on TRC3 or TRC8 simultaneously with the kinematic receiver. Both receivers collected information at a 15 second epoch rate from the same four or five satellites. This procedure enabled the relative double differencing reduction of data. A static sampling interval of 90 seconds yielded seven epochs of data which appeared satisfactory as long as at least two runs are accomplished per session. A shorter sampling interval may be adequate, but a longer sampling interval or longer epoch (i.e., 30-second rate) would be inefficient and should only be used in open-traverse (no position check) type operations.

The Antenna Swap Procedure
Prior to the start of kinematic surveying an "antenna swap" was performed between the kinematic receiver and the base station receiver. It should be made clear that there is no electronic or hardware difference between the receivers. The base station receiver simply does not move from traverse point to traverse point as does the kinematic receiver. The antenna swap enables the quick and sure determination of integer cycles between the base station location and the satellites being monitored at the time (see Section A.1 for a discussion on integer cycles). To perform an antenna swap one simply exchanges the position of the base station antenna with the kinematic antenna (Figure 33). In the case when the base station was located at TRC3, the kinematic antenna was initially set up over TRC14; a distance of 4.0633 m as measured in 1983, 4.065 m as measured by this survey crew in 1988, and 4.066 m as measured by the antenna swap! A full antenna-swap procedure normally consisted of 1 minute in the normal antenna positions, followed by 1 minute in the swapped positions, followed by another minute in the normal positions. In each position the antennas were oriented magnetic north to avoid possible eccentricity due to antenna-phase center ambiguity. **Do not proceed until a complete antenna swap has been performed free of cycle slips!** Upon completion of the swap, the kinematic antenna was installed on the vehicle. Throughout the antenna-swap process careful attention was paid to the computer displays to make sure that there was no interruption in continuity of data recordings. The personnel moving the antennas were careful to keep their heads below the antenna-ground plane and to avoid any large tilts to the antenna. Another antenna swap was performed each time the kinematic receiver completed traverse loop.

In fact, antenna swaps need to be done only if there is a change in satellites, or if there are cycle slips since the last antenna swap, and it is only necessary to obtain integers for each satellite once during the survey, if no cycle slips occur.

The Cycle Slip

The occurrence of cycle slips can be detected if the continuous epoch-count display on the computer is reset to zero. In this situation the satellite signal has been momentarily interrupted, that is, the signal has been blocked from reaching the antenna by some physical obstruction (a head, tree, building, or severe meteorological phenomena such as lightening). Considering the speed at which the satellite is traveling, the fact that the kinematic receiver position is also changing, and that a cycle is only 19 centimeters in length, many cycles can be lost in just a fraction of a second. Cycle slips can cause minor inconveniences in processing to a total loss of the traverse. Based on this experiment, generally, only one satellite will suffer cycle slips during a traverse, if care is exercised. The greatest source of cycle slips encountered in this survey resulted from getting too close to trees along the service road or travelling through the high-banked turns when Space Vehicle 8 was below 20 degrees altitude. Survey operations were normally conducted only when all satellites were at least 25 degrees elevation above the horizon.

The data logging program gives the current elevation and azimuth for each satellite (Space Vehicles as they are often called). One need pay attention only that the line of sight is clear at those azimuths and altitudes.

The Kinematic Traverses

Three kinematic traverses were performed (Figure 34). In each case, the base or home station for the traverse was TRC3 or TRC8. A traverse, in this case, only refers to the route of the kinematic survey. Each station along the route is positioned by a three dimensional vector from the base station. There is no limiting speed at which the receiver must be transported. In this survey, speeds up to 70 miles per hour were recorded in the high-speed turns. It is most important to avoid tilting the truck to avoid satellite blockage by the antenna-ground plane or objects above the horizon. Therefore, the high-bank turns were avoided as much as possible, as were steeply sloped berms.

The first traverse covered all marks on the service road. This survey was used to work out the details for kinematic operations. The second traverse connected 17 of 18 high-altitude targets on the high-speed track. One high-altitude target, 521, was not connected due to its close proximity to the overpass. This traverse covered the entire seven-mile circuit of the high-speed track. The third traverse connected the low-altitude targets on one side of the high-speed track to several of the high-altitude targets on the same side of the track and to two targets on the service road. This traverse cut across the center of the track and proceeded half way around the track. Several of the targets were positioned from different base stations as a check on the consistency of the base network. Each traverse route was attempted at least twice during a single session and repeated on different days. On July 19th and 21st the kinematic sites were occupied for two minutes each. This observation time was reduced to 90 seconds without any detrimental effects for the rest of the survey. By reducing the static time from 120 to 90 seconds, it became possible to run even the longest traverses twice in a single-satellite session.

The average time from becoming static at one target until the time the antenna was again static on the next point was 3 minutes. Upon arriving at each point the truck was stopped and the engine stopped. The driver and front-seat passenger got out and plumbed the antenna over the mark. The antenna was then aligned to magnetic north. Once the antenna was motionless the driver informed the recorder, who then waited for the next satellite epoch and recorded the displayed UTC time of the epoch.

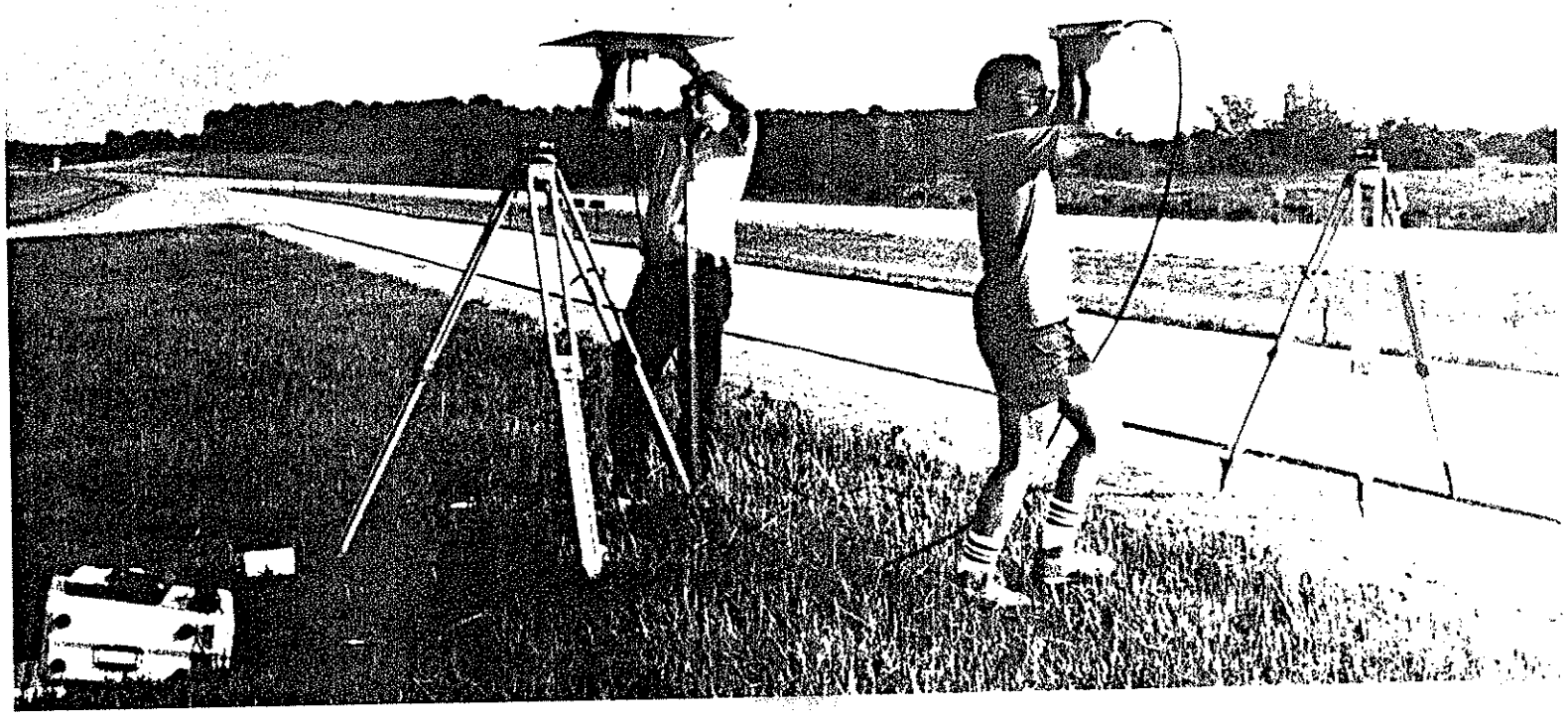

Figure 33. GPS Antenna Swap

The person recording the time remained in the back jump seat monitoring the data collection throughout the kinematic portion of the survey. Ninety seconds were added to the beginning time, and when this new time was displayed by the computer, the antenna was returned to the transport position on the truck. The beginning and ending times denote that portion of time when the antenna remained motionless on the survey marker. In all, seven 15-second epochs were recorded in the static mode. A special form (Figure 35) was devised for record keeping purposes. With certain simple modifications to the antenna rack, the operation could easily be handled by two people, a driver/antenna tender and a recorder. The recorder need never leave the vehicle.

The Computations
All GPS data, both static and kinematic, were reduced using Trimble Navigation Limited software TRIMVEC - GPS Relative Positioning Solution, Version 88.080MB. Routines for converting between three-dimensional Cartesian coordinates to geodetic latitude, longitude and ellipsoidal height, and space inverse solutions were taken from NOAA Technical Memorandum NOS NGS-13, Class Notes for Geometric Geodesy Part 1. Mathematical Projections by Richard H. Rapp were used for converting geodetic coordinates to a local plane coordinate system. Several customized routines were written by the author for comparison purposes. Kinematic processing techniques will be discussed at length in Section A.2.

The Results
Since the terrestrial survey was computed on a plane elevated 330 meters above sea level, it was not possible to make a coordinate-by-coordinate comparison with the GPS coordinates. The results of the kinematic survey were, therefore, compared against the terrestrial work in three ways. First, the horizontal chord distances between adjacent targets (either high or low-altitude) were computed from the GPS three-dimensional coordinates and compared against plane distances computed from the adjusted "plane coordinates" from the terrestrial adjustment. The three-dimensional horizontal-chord distance was determined from GPS vector by correcting the space vector between adjacent targets for the elevation difference between the two marks. The average difference in distance was -1.0 mm with a mean standard deviation of 8 mm for 29 comparisons (Table 18).

The second comparison was made between horizontal angles computed from the GPS coordinates and the "plane angles" computed from the adjusted terrestrial control. The average difference was 1.1 sec with a mean standard deviation of 3.3 sec for 16 comparisons (Table 19). Table 21 contains the final photo target coordinates as computed in NAD83 three-dimensional Cartesian coordinates, latitude, longitude, ellipsoidal height, and local three-dimensional coordinates.

The third comparison was made between the ellipsoidal heights and vertical elevations from the terrestrial control (Table 20). The average difference is -34.225 m with a standard deviation of 0.029 m for 34 samples. The predicted geoid height from Rapp's 360 model is -34.150 m.

The Personnel
Commander Lapine is extremely grateful to the Bureau of Aerial Engineering for the tremendous support offered throughout the survey operations. In particular, much thanks to the Bureau Chief, Mr. Edward Smith, who authorized the overtime and interruption of normal duties of the Bureau survey crew. My gratitude is extended to the Survey Chief, James Hadley, for his foresight and understanding of the value of this new technology. Most important, I wish to thank the survey crew

composed of Greg Gerst, Steve Arter, Jeff Arter, Paul Reed, and Jim Villacres. It was their sweat and surveying expertise which produced such fine results. I would also like to thank David Conner , the National Geodetic Survey Geodetic Advisor to Ohio, who devoted many valuable hours to the survey, most of which he could not afford to spare. Thanks to Professor Clyde Goad, whose boundless energy and devotion to teaching got me interested in kinematics to begin with, who wrote and re-wrote software based on my suggestions and reviewed this report. Lastly, I would like to thank Mr. Walt McPherson, Madeline Grey and Milt Dunlop who, being responsible for the Operations and Safety of the TRC, went along with an operation which I am sure stretched the limits of the operating guidelines for the high-speed track. Thanks is also extended to GRH, a great surveyor and friend, who did not want to be officially recognized.

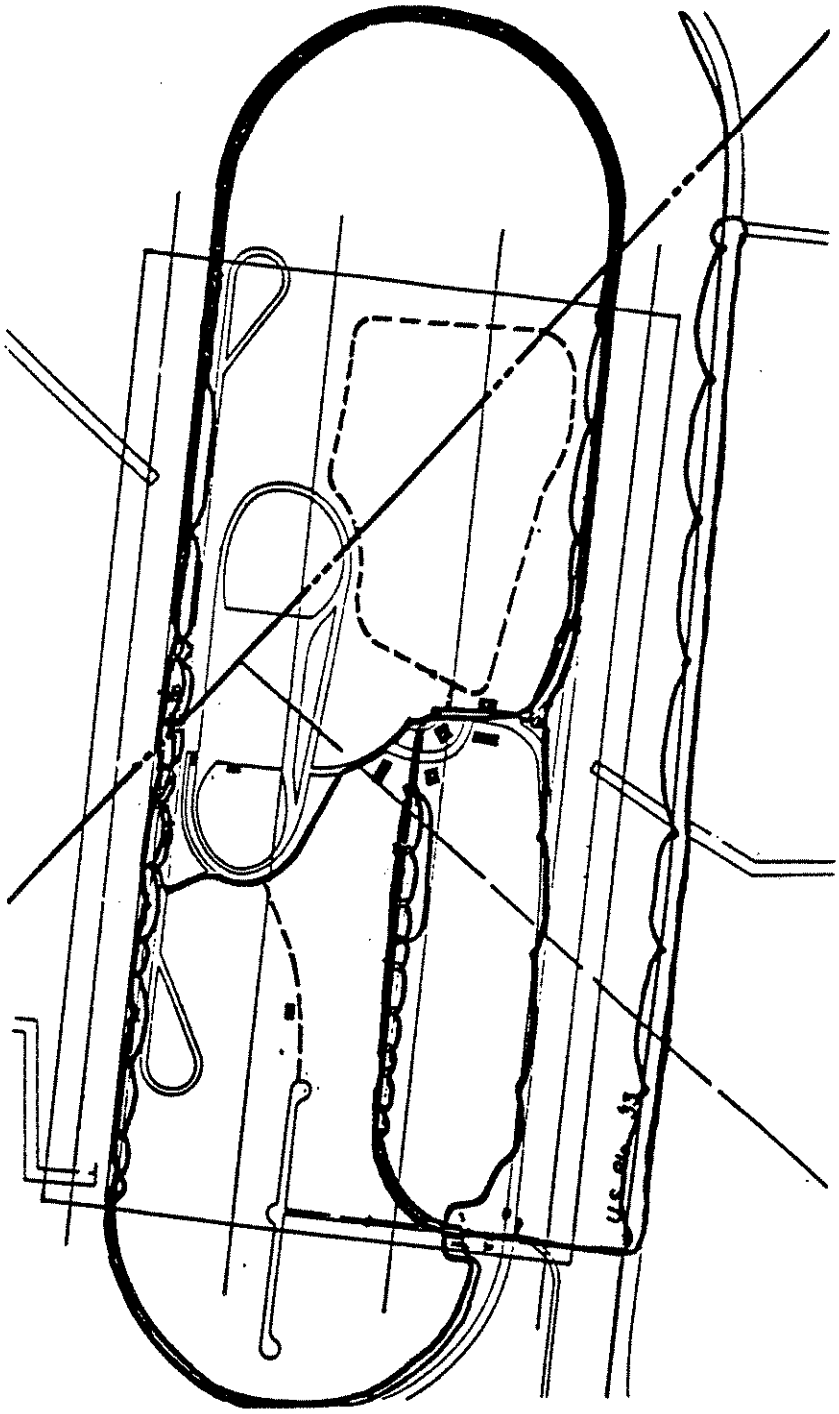

Figure 34. GPS Kinematic Survey Routes

| LOCATION | START | STOP | COMMENTS |
|---|---|---|---|
| | | | |
| | | | |
| | | | |
| | | | |
| | | | |
| | | | |
| | | | |
| | | | |
| | | | |
| | | | |
| | | | |
| | | | |
| | | | |
| | | | |
| | | | |
| | | | |
| | | | |
| | | | |
| | | | |
| | | | |
| | | | |
| | | | |
| | | | |

Figure 35. Kinematic Observation Form

Table 18 -- Comparison of Distances GPS Minus Terrestrial
(meters)

| Stations | Number of Observations | Difference |
|---|---|---|
| 202-203 | 219 | +0.0079 |
| 203-204 | 282 | -0.0143 |
| 204-205 | 339 | +0.0008 |
| 205-206 | 334 | +0.0063 |
| 206-207 | 273 | +0.0063 |
| 501-502 | 291 | -0.0085 |
| 502-503 | 214 | -0.0026 |
| 503-504 | 203 | -0.0038 |
| 504-505 | 305 | +0.0087 |
| 505-506 | 479 | -0.0059 |
| 506-507 | 437 | +0.0043 |
| 511-512 | 262 | -0.0023 |
| 512-513 | 382 | +0.0055 |
| 513-514 | 447 | -0.0084 |
| 521-522 | 339 | -0.0125 |
| 522-523 | 415 | -0.0085 |
| 523-524 | 408 | +0.0111 |
| 524-525 | 386 | -0.0094 |
| 525-526 | 348 | -0.0029 |
| 526-527 | 319 | +0.0083 |
| 527-528 | 335 | +0.0030 |
| 220-221 | 197 | -0.0019 |
| 221-222 | 128 | -0.0087 |
| 222-223 | 110 | +0.0133 |
| 223-224 | 89 | -0.0058 |
| 224-225 | 117 | +0.0001 |
| 225-226 | 148 | -0.0062 |
| 226-227 | 148 | -0.0038 |
| 227-228 | 134 | +0.0115 |
| N = 29 | Mean Diff = -0.0014 | Std Dev = 0.0076 |

Table 19 -- Angular Differences GPS Minus Terrestrial
(seconds of arc)

| Stations | Differences |
|---|---|
| 202,203,204 | -11.55 |
| 203,204,205 | -00.22 |
| 204,205,206 | +00.54 |
| 205,206,207 | +03.49 |
| 501,502,503 | -00.20 |
| 502,503,504 | +04.73 |
| 503,504,505 | +06.91 |
| 504,505,506 | +01.92 |
| 505,506,507 | -00.53 |
| 511,512,513 | +04.94 |
| 512,513,514 | -00.79 |
| 521,522,523 | -01.43 |
| 522,523,524 | +00.42 |
| 523,524,525 | -05.12 |
| 524,525,526 | +04.40 |
| 525,526,527 | -04.01 |
| 526,527,528 | +02.71 |

N = 16 Mean Difference = 1.11 Std Dev = 3.3

Table 20 -- Comparison of Elevation Differences, Ellipsoidal Minus Terrestrial Heights (meters)

| Station | Difference |
|---|---|
| 202 | -34.244 |
| 203 | -34.227 |
| 204 | -34.240 |
| 205 | -34.228 |
| 206 | -34.209 |
| 207 | -34.209 |
| 221 | -34.266 |
| 222 | -34.217 |
| 223 | -34.226 |
| 224 | -34.228 |
| 225 | -34.245 |
| 226 | -34.256 |
| 227 | -34.248 |
| 228 | -34.223 |
| 501 | -34.280 |
| 502 | -34.258 |
| 503 | -34.244 |
| 504 | -34.231 |
| 505 | -34.220 |
| 506 | -34.216 |
| 507 | -34.194 |
| 508 | -34.176 |
| 511 | -34.259 |
| 512 | -34.252 |
| 513 | -34.239 |
| 514 | -34.216 |
| 521 | -34.241 |
| 522 | -34.221 |
| 523 | -34.231 |
| 524 | -34.203 |
| 525 | -34.183 |
| 526 | -34.181 |
| 527 | -34.169 |
| 528 | -34.149 |

N = 34 Mean Difference = -34.225 Std Dev = 0.029

Predicted Geoid Height = -34.150

## A.1 Cycles - A Layman's Description

Imagine looking through a narrow vertical slot at a line shaped like a sine wave passing by on the other side of the slot. The height of this slot is adjusted to be only slightly taller than the amplitude of the sine wave. The image one would perceive is that of a small line segment moving up and down the slot. Next assume that the sine wave has no negative component, but that these negative lobes have been inverted so that the sine wave now has all positive lobes. We will adjust the size of the slot accordingly to match the new amplitude of the wave. Again the image as viewed through the slot would be of a small line segment which travels from the bottom of the slot to its top and then back down again.

Given a time $T_0$ the sine wave is just touching the bottom of the slot, we begin counting every time the line segment again touches the bottom of the slot. At time $T_1$ the sine wave is again at the bottom of the slot and we stop counting. The count would represent the number of half cycles which passed the slot. If each of these half cycles was 10 centimeters in length, we could multiply the number of times the line segment touched the bottom of the slot subsequent to time $T_0$ by 10 and obtain the horizontal chord length of the sine wave segment. If we began counting at $T_0$ with some arbitrary integer and increased this value by one each time the wave touches the bottom of the slot, the difference between the starting and ending values would be the number of half cycles which passed the slot.

The above description is basically what happens electronically inside a GPS receiver which operates on a phase measurement process. The sine wave is the carrier phase transmitted by each of the satellites and the slot is an electronic filter. The cycles or phase change, in addition to the oscillator output, because of the relative motion between the receiver and the respective satellite. The relative motion is due to the satellite traveling along its orbit and the earth revolving about its axis. If the receiver is being moved as in a kinematic survey, this motion will also add the relative motion between the receiver and satellite. At the beginning of survey operations there is no way to determine the total number of integer cycles between the receiver and the satellite. However the receiver's electronics is accurately able to keep count of the cycles as they increase or decrease from some arbitrary initial value. This starting value then is increased or decreased according to the relative motion between receiver and satellite (as the satellite gets closer to the receiver the count increases, as the satellite moves away from the receiver the pattern of sine waves reverse and the receiver reduces cycles to the count). Differences in this count over an interval of time represent the total number of accumulated cycles.

A procedure to be known as an antenna swap, is used to determine the integer number of cycles at an initial time between the satellites and the ground receiver.

In addition to the integer number of cycles, the receiver also is capable of resolving the partial cycles between successive integer cycles. The resolving power of partial cycles is generally 1 part per thousand of the half-cycle length, and tenths of millimeters, which are, of course, influenced by many different error sources. With care, these errors can be reduced to an ultimate precision of 2 parts per million over the length of the baseline distance. The discussion of these errors is beyond the scope of this discussion.

One last point, some receivers have the capability of varying the width of the vertical slot. This ability makes it possible to maintain lock on the signal under a variety of conditions. When the receiver is motionless, the slot is very narrow, which reduces signal noise and improves resolution. Under kinematic conditions the slot can be made wider to avoid loss of lock at the expense of more signal noise and slightly less resolution. This capability is very desirable when kinematic operations are considered.

A.2 Kinematic Processing and Cycle-Slip Handling
The Trimble Software, Relative Positioning Version 88.080MB, is specially modified for handling kinematic data as well as providing all the standard static processing capabilities. This version also allows up to 10 base stations and a nearly unlimited data set size by creating a scratch file of data on any IBM compatible PC equipped with a math co-processor, 640K RAM, and a hard disk drive.

NOTE: From this point on I assume the reader knows the basic operating instructions for TRIMVEC Software as this report is not intended to be a Primer.

The processing begins by specifying the two stations to be processed, followed by the standard questions for ephemeris file name and data file names. The data for the first station should be for the base station. Request the display of message files and ensure the antenna heights for the swap stations are correct. The roving antenna height will be input later in the processing.

Next select main menu Item 16, for processing antenna swap data. From the sub-menu, select item to convert recorded UTC times to week-seconds. At this time convert all recorded times from the recording form (Figure 35) to week-seconds.

When asked for the day count, enter the total number of week days that have elapsed beginning with Sunday and including the UTC day before the times listed on the recording sheet. As an example, if the observations began on Wednesday 1350 UTC; the week day number would be 3 for Sunday + Monday + Tuesday. Next begin to convert all the times. If UTC midnight is passed, add 24 hours to the recorded time. Record the week-seconds returned by the program above the recorded time on the form.

Processing Without Cycle Slips
Once all the times have been converted, select sub-menu Item 1 and begin processing the antenna swap data. NOTE: The computer time may be a second later than the actual UTC epoch time. This can be determined if the recorded time differs from the chosen sampling interval (i.e., if a 30-second sampling interval is chosen then all times should end with either 0 or 30 sec). When entering times into the following menus, always correct the beginning, but not ending, recorded times for this difference. This will ensure that all desired epochs are included in processing. **The above note applies to all future time entries.** Process the first swap only by entering the times (week-seconds) into the "Original Station" menu, when the base station and roving antennas were on their respective marks, then select "E" to exit this menu. Next enter the times into the "Swap Station" menu, when the antennas were in the swapped positions, type "E" to exit and save.

Select sub-menu Item 2, to process swap data. Respond "Y" to viewing the observations, select 3 iterations, and 1 for each epoch to be processed. Observe the residual column as the data are processed. At the end of the first iteration, the RMS may exceed the limits of the format statement, but the baseline distance should be very close to the

actual distance between swap and base marks. If not, interrupt the processing by striking the space bar and exit. Check for an incorrect time entry or incorrect conversion. If no mistakes are found, the recorded time may be incorrect. Try to resolve the problem and reprocess. There is a danger that if you continue without resolving the problem, the program may edit away all the data, at which point the program must be reloaded from scratch.

Once the first swap is processed, continue adding new swap times to the original set and reprocess all the data simultaneously. **Exercise extreme care not to introduce cycle-slip contaminated data.** If no cycle slips exist anywhere in the data, all swaps should be processed, yielding a valid baseline for the swap point! The cycle biases thus obtained, can now be converted to integers and held fixed by selecting the appropriate item from the sub-menu.

Return to the main menu, select Item 10 and output the swap baseline. Since only two stations were input, only one baseline will ever exist at a time in the processing. A suggested name for this file is the first four letters of the base station name and Day of Year with the extension "swp" (i.e., TRC3210.swp).

Select Item 15 from the main menu to get the secondary menu. Select Item 4 and reset the antenna height for station 2 to the roving antenna height. Select sub-menu Item 6 and enter the geodetic position for station 1 that you want to be held fixed. Check this input by selecting sub menu Item 11 and view station number 1. Return to the main menu, select Item 16, to return to the kinematic processing.

Assuming there were no cycle slips anywhere in the data, you can begin processing each kinematic baseline by entering all times for which the roving antenna was on the particular mark being processed. These times are entered into the "Original Station" menu of Item 1. The "Swap Station" menu should be empty. Select Item 2, responding as before. Observe the RMS value and baseline length at the end if each iteration. These values usually stabilize by the third iteration. The RMS value should generally be less than 4 centimeters and all residuals less than 0.1 meters. Sometimes the recorded beginning or ending epoch is contaminated by antenna motion. This can be detected by the larger residuals of either the first or last set of observations for a particular interval. This difference may only be detectable during the second iteration. The final RMS may also reflect this condition because all the epochs have been affected. If motion is suspected, exit from the processing and adjust the appropriate time in sub-menu Item 1 and reprocess the data. The precautions for identifying erroneous data, as mentioned during the instructions for processing swap data, are also recommended at this stage of the data processing. If after the second iteration, any of the residuals are greater than 1, cycle slips have occurred in the data. Exit the processing mode and handle the data as outlined in a future section.

Once the solution has stabilized (usually by the third iteration), return to the main menu and select Item 10 to output the baseline. A suggested name for the file is the first six characters of the station name; the extension becomes the Day of Year of the observations.

If any of the observations become edited during the iterations, (an asterisk next to the residual) a few more iterations are recommended until the RMS and base distance stabilize. When all the baselines have been processed TRIMVEC can be exited.

Handling Cycle Slip Data
The processing becomes much more complicated when cycle slips have occurred during data collection. There are several common situations when cycle slips occur:

1. If while conducting a traverse, one or more satellite channels suffer cycle slips, note as best as possible, the UTC times of the occurrence. If the cycle slips occur between traverse stations, return to the previous station, if possible, and re-observe. If by returning the signal will only be obstructed again, continue on to the next station. A more complicated problem is two or more occurrences of cycle slips on the same satellite between antenna swaps. In this situation it is not possible to recover the integers until a new antenna swap is performed. The collected data can still be processed. At the completion of the traverse, return to the base station and perform another antenna swap.

2. If a new satellite has been acquired during a traverse, again note the UTC time and perform an antenna swap after completing the traverse. If possible, the acquisition of a new satellite should be scheduled while the antenna is motionless on a traverse station. Data collection can be extended on a given station to accommodate the change in satellite status. The integers for the new satellite computed from the next antenna swap will automatically be used on all previously collected data. There is a strong possibility that the first few epochs of data will be contaminated and should not be included in the baseline processing.

3. A satellite sets during a traverse, again note the UTC time but an antenna swap is not necessary at the end of the traverse. As noted above, the change in status should be scheduled while motionless at a traverse station. The last few epochs may be contaminated by cycle slips and, therefore, should not be included in the baseline processing for that station.

Antenna-Swap Processing With Cycle Slips
**The first antenna swap must always be free of cycle slips.** Starting from this premise it will always be possible to process the first swap. If all five satellites are included in the swap and no other satellites are involved, in reality, no more swaps are required. Extra swaps, particularly at the completion of the day, however, are very good insurance.

If a second swap is required because of a change in satellite status other than cycle slips, the second swap can be added to the first swap without any special processing. In fact, all swaps prior to the first cycle slip can be added into the swap computation.

Assuming the cycle slips have occurred for a satellite which already has an integer count, the next set of swap data can be added to the processing after deleting the satellite (for the time period of the swap only) which contains cycle-slip data. To accomplish the deletion, return to the main menu, select Item 6, choose the delete option, select all stations ("99"), select only the satellite number you want to delete, select times by week-seconds, and enter the appropriate start and stop times. The start time should be a few seconds early and the stop time a few seconds late. Return to the swap processing menu and continue antenna swap processing. All future baseline processing which involves the satellite with cycle-slip data will be processed in a different manner.

If the cycle slip occurs during the first traverse and several other traverses are completed without further cycle slips to that particular satellite, it may be better to delete the satellite data from the first swap and determine integers from the subsequent swaps. In this manner more uncontaminated data can be processed, but the first set of baseline epochs will require special processing.

The bottom line to processing swap data with cycle slips is to first process the largest amount of cycle-slip free data. Then add in additional swap data which is cycle slip free by virtue of having deleted those satellites which suffered cycle slips. Eventually, integer counts should be calculated for every satellite. It is then important to understand which portions of the various traverses that the integers belong.

Next the processing of baselines can begin. The procedure is much the same as for cycle-slip-free data, but the data ordering may vary. First process as many of the visits to a particular station as possible using cycle-slip-free data and applicable integers. This processing will determine the integers for the baseline. Next, add in the remaining times for the station. Select sub-menu Item 5 to process data using fractional parts only. Process the complete set of station information in the regular manner. Notice in the residual column the words "frac-resid". The integers are not being used. This should not present a problem because the integers were previously computed with cycle slip free data. Be extremely conscious of the residuals because it will be difficult to detect antenna motion from the noise of the fractional biases.

Upon completion of the process you may find that the RMS is higher than usual. What this means is not exactly known at this time. The more cycle-slip-free data available, the more reliable the solution. After output of the baseline, return to the sub-menu, select Item 5 again, but use the integers instead of the fractions. Process the next baseline, again selecting the cycle-slip-free data, and repeat the fractional processing for the remainder of that station's data. Continue until all baselines have been computed.

If all else fails, and you have returned to the previous mark each time cycle slips occurred, it is possible to use the Trimble advanced diagnostic subroutines to locate the slips and correct the slips by adding the appropriate biases to the data. Slips can be identified by comparing the integer portion of the data collected prior to, and after, the slips occurred. The fractional parts should be approximately the same.

Use common sense and exercise patience, the rest will come easy.
**GOOD LUCK!**

Table 21 -- NAD83 Geocentric Coordinates for Targeted Ground Control

| Station | X | Y | Z |
|---|---|---|---|
| 501 | 546905.711 | -4839092.510 | 4105479.046 |
| 502 | 547175.655 | -4839313.303 | 4105183.190 |
| 503 | 547442.952 | -4839535.692 | 4104885.758 |
| 504 | 547709.417 | -4839757.828 | 4104588.725 |
| 505 | 547976.572 | -4839980.279 | 4104291.171 |
| 506 | 548243.461 | -4840202.522 | 4103993.810 |
| 507 | 548510.255 | -4840424.701 | 4103696.503 |
| 508 | 548777.143 | -4840646.979 | 4103399.071 |
| 511 | 546165.661 | -4839539.265 | 4105052.603 |
| 512 | 546434.094 | -4839759.543 | 4104755.526 |
| 513 | 546700.787 | -4839981.535 | 4104457.781 |
| 514 | 546968.009 | -4840206.011 | 4104162.014 |
| 521 | 545685.388 | -4839741.984 | 4104879.952 |
| 522 | 545953.311 | -4839970.014 | 4104575.823 |
| 523 | 546219.938 | -4840192.416 | 4104278.506 |
| 524 | 546493.994 | -4840409.911 | 4103985.608 |
| 525 | 546754.136 | -4840637.017 | 4103683.745 |
| 526 | 547026.093 | -4840856.826 | 4103388.414 |
| 527 | 547288.057 | -4841081.565 | 4103088.917 |
| 528 | 547554.985 | -4841303.654 | 4102791.688 |
| 541 | 547490.378 | -4841746.825 | 4102292.960 |
| 542 | 547166.813 | -4841497.054 | 4102633.820 |
| 543 | 546842.323 | -4841243.831 | 4102969.709 |
| 544 | 546511.375 | -4840988.288 | 4103314.880 |
| 545 | 546172.680 | -4840726.907 | 4103668.769 |
| 546 | 545857.129 | -4840480.752 | 4103992.655 |
| 547 | 545548.520 | -4840227.406 | 4104326.261 |
| 548 | 545261.075 | -4839978.198 | 4104658.533 |
| 202 | 546236.886 | -4839592.135 | 4104980.496 |
| 203 | 546370.304 | -4839702.890 | 4104831.330 |
| 204 | 546503.682 | -4839813.406 | 4104682.277 |
| 205 | 546637.278 | -4839924.253 | 4104533.313 |
| 206 | 546770.830 | -4840035.902 | 4104384.868 |
| 207 | 546904.309 | -4840147.520 | 4104236.499 |
| 208 | 547052.162 | -4840253.149 | 4104097.783 |
| 221 | 546974.988 | -4839146.542 | 4105406.203 |
| 222 | 547109.387 | -4839258.134 | 4105257.038 |
| 223 | 547242.630 | -4839368.986 | 4105108.752 |
| 224 | 547375.944 | -4839480.229 | 4104960.013 |
| 225 | 547509.273 | -4839591.348 | 4104811.417 |
| 226 | 547642.622 | -4839702.478 | 4104662.731 |
| 227 | 547776.168 | -4839813.528 | 4104514.173 |
| 228 | 547909.510 | -4839924.757 | 4104365.381 |
| 2455 | 545995.860 | -4840588.267 | 4103852.346 |
| 2465 | 545701.213 | -4840355.703 | 4104154.558 |
| 5235 | 546356.943 | -4840301.201 | 4104132.046 |
| 5225 | 546086.656 | -4840081.169 | 4104427.254 |
| 5125 | 546567.317 | -4839870.268 | 4104606.307 |
| 5135 | 546834.392 | -4840093.099 | 4104309.491 |
| 515ecc | 547226.306 | -4840460.879 | 4103828.364 |
| 517ecc | 547863.418 | -4840876.947 | 4103250.845 |
| 518ecc | 548179.183 | -4841123.315 | 4102923.937 |

# APPENDIX B

## Determination of Internodal Separation

## Determination of Internodal Separation

The position of the exposure station is defined by the survey coordinates ($X_0, Y_0, Z_0$) of the entrance node of the compound lens system of the aerial camera. The object space ends at this point as all light rays are assumed to converge (at least according to the first order theory of compound lens optics). The image space does not theoretically begin until the light rays begin to diverge at the exit node of the compound lens.

The position of the entrance node must be spatially relatable to the GPS antenna phase center if *a priori* knowledge of the exposure station is to be used to uncouple the correlation between interior and exterior orientation elements. The uncoupling of correlation will accomplish the primary goal of calibrating the airborne photogrammetric system inflight and ultimately enable aerotriangulation without survey control.

The physical location of the entrance node will be assumed to lie on a vector defined by the optical axis of the lens system some measurable distance from the principal point. Since all light rays are assumed to pass through the nodes, a single ray of light entering the lens system will pass undisturbed through the compound lens even if the optical axis is rotated about either nodal point.

### Nodal Slide Bench

A nodal slide bench is classically used for determining the back, front, and equivalent focal lengths, inter-nodal separation, radial and tangential distortions, and resolving power of a lens or lens system by visual methods. The slide bench is constructed in such a manner that the compound lens system and a viewing microscope can be mounted on a precision set of ways. A parabolic mirror at one end of the bench is used to produce a collimated beam of light which is parallel to the ways. A target assembly is also instrumented on the ways. By determining the back and front focal lengths of a lens with the nodal slide bench apparatus, the inter-nodal separation can be determined. Distortions as small as 2 microns have been determined by this method, therefore very accurate nodal separation determinations are possible. A nodal slide bench located at the U.S. Geological Survey (USGS) is capable of measuring inter-nodal separations to an accuracy of 0.1 mm. The accuracy of such a determination would be more than adequate for the purpose of relating the GPS antenna phase center to the entrance node. Unfortunately the USGS nodal slide bench is not large enough to handle the RC-10 lens system.

### A Poor Man's Nodal Slide Bench

The determination of the inter-nodal separation of a large lens system such as the RC-10 lens cone can be determined without a nodal slide bench and still not suffer a significant loss of accuracy. The lens is rested on its side (optical axis parallel to the floor) at an elevation above the floor such that approximately half of the lens diameter is above the level of a convenient table. The table is covered by a piece of paper which is long enough to overhang the table by approximately 1 foot. The lens (objective lens first) is slid up against the edge of the table pressing the overhanging paper between the lens and table. An observer stations himself behind the image plane of the lens approximately centered in the image space. A helper sticks a pin through the paper and into the table approximately 1 foot from the objective lens. A second pin is pushed through the paper approximately 2 feet from the objective lens on range with the first pin as determined by the observer. The observer must be careful not to change his

position during the process of placing the pins on range. In this case, the observer viewed the placement of the pins through a Wild T2 theodolite. The observer shifts to one side of the image space and the process is repeated with a second set of pins. This process is repeated for five or more different observation points in the image space. The pins should begin to form a fan-like array. Once enough sets of pins are position to satisfy the observer, the lens is carefully slid back away from the table. The overhanging paper is raised even with the table and properly supported. The rays of pins can now be graphically extended until they intersect at a common point. This point will be the entrance node. The lens cone can be measured from the vertical plane that came in contact with the table to the film plane. The distance from the intersection of rays on the paper to the fold in the paper where it overhung the table is measured and subtracted from the distance measured on the lens cone. The algebraic difference is the distance from the film plane to the entrance node. This determination was made for the NOAA B and G Cone lens. In both instances the distance was measured as 283 mm +/- 5 mm. Assuming a nominal focal length of 153 mm, the internodal separation is 130 mm for each lens. This compares to 121 mm scaled off a drawing supplied by Wild. The 5 mm accuracy estimate is based on the size of the small circle of intersections formed by the various rays.

# APPENDIX C

## NOAA Film Processing Specifications

## SPECIFICATIONS AND REQUIREMENTS

A. General Specifications

All photographic items produced by the contractor shall be:

1. Professional quality, contrast and density appropriate to NOS requirements, exact focus, precise indicated scale.

2. From material required to perform a task as listed on NOAA Form 76-16.

3. Aerial roll film, unprocessed and processed, shall be stored in accordance with manufacturer's specifications (reference Kodak Professional Black and White Films Manual F-5, Kodak Data for Aerial Photography Manual M-29) and in a secure area approved by NOS.

B. Specific Quality Standard, Specifications and Requirements

In addition to General Specifications, all photographic products are subject to specific quality standards that define the parameters necessary to establish an acceptable visual and measurable level of performance consisting of:

1. Residual Silver Test - A residual silver test shall be performed to verify thorough fixation of photographic black and white material. A test solution, Kodak Residual Silver Test Solution ST-1, or equivalent, shall be used (reference Kodak Data for Aerial Photography Manual M-29). The test shall be performed on the emulsion side in a clear area of the processed material. Tests that indicate insufficient fixation shall be cause for rejection of the task.

2. Archival Assurance Test - To verify that the wash of photographic material is sufficient to meet archival quality, a test shall be performed on the emulsion side in a clear area of processed photographic black and white material using Kodak Test Solution HT-2 and a Kodak Hypo Estimator or their equivalent (reference Kodak Data for Aerial Photography Manual, M-29). Tests that indicate insufficient wash shall be cause for rejection of the task.

3. Dimensional Stability

   a. Aerial Film (Original) - Changes in dimensional stability due to processing and drying of aerial roll film is determined by comparing the differential change of the focal plane dimensions (fiducials as reference points) as stated in the Camera Calibration Report, compared to the same points as recorded on the film. This differential change shall not exceed 0.1 mm.

b. Print materials - Change in dimensional stability due to processing (i.e., excessive time or temperature in developing, fix, wash, or drying) of the print material shall not exceed the dimensional characteristics specified by, and measured according to, the manufacturer for the product used (see Kodak data supplied in each box of materials.)

4. Distortion - Distortion induced in printing on film or other stable base material is determined by comparing the differential change of distance between points on original as compared to the distance between identical points on the reproduction. Distortion shall not exceed 10 micrometers.

5. Fiducial Marks - Each print or transparency shall show the fiducial marks on each exposure. The marks are located in each corner of the format and at the center of each side. All of these fiducial marks and other marks intended for precise measuring, such as recorded reseau marks on the geodetic camera, shall be clear and well-defined on the prints or transparencies and shall be printed so that the standard deviation of repeated readings of the coordinates of each made on the comparator shall not exceed 3 micrometers. Both the radial and the tangential resolution on the prints will be considered.

6. Border Mask

a. Border requirements for black-and-white contact prints and transparencies:

The B/W paper contact prints may be required to have a white border. When required, it will be created by the use of a mask extending not more than 1/16 inch inside the outer edge on three sides of the format but not obscuring the fiducials, title, or recorded information (RC-10 exposure number). The fourth side shall extend 1/2 inch outside the format to expose recorded Wild RC-8 camera data, exposure number, level bubble, etc. Wild RC-10 camera information that is recorded outside the format area is not required on NOS prints and shall be ignored.

A border mask is not required on film positives, direct negatives, or black and white negatives from color. A mask, if used, must be placed either on top of the platen surface, or on the bottom surface of the glass printing stage of the printer. The printing surface of the platen and the glass stage plate shall be clear of any tape, mask, or any material that prevents a direct uniform pressure between the printer platen, film stock, film original and the glass stage plate. No mask material shall be sandwiched between any of these surfaces while printing film stock material.

b. Border requirements for color contact prints and transparencies:

An opaque mask shall be placed on the underside of the glass stage plate of the electronic automatic dodge printer. The mask shall be so positioned that no printing light falls outside the film area nor shall the mask extend inside the picture to block the fiducials or title information.

c. Requirements for ratio prints (enlargements):

All tasks, with the exception of Code G, shall have a border mask outside of the four sides of the format area.

Code G - Photograph to be masked to show area specified on marked (cropped) print accompanying NOAA Form 76-16.

7. Film Titling - Newly processed aerial film shall be delivered to the COTR for inspection and upon acceptance the film will be returned to the contractor for titling. Titling data obtained from the NOAA Form 76-15 accompanying each roll shall be in the picture area and not less than 1/8 inch nor more than 1/4 inch from the format border. No titling shall be in the fiducial area. All titling shall be printed on the film base (non-emulsion side) and the pressure adjusted so as to prevent film deformations. The title shall consist of NOS (agency), date, lens code, film identifier, and exposure number. Film identifier shall be:

| Film | Identifier |
|---|---|
| Panchromatic | P |
| Color MS | C |
| Black & White Infrared | R |
| Aerochrome Infrared | CR |
| Color Negative | CN |

Sample - NOS 12-20-81 EP 2946

Exposure number titled on each frame shall be the number recorded on the film for that frame. In the event that the numbering sequence is repeated during the calendar year an A shall be prefixed to the ensuing numbers. The lens identifier is the capital letter notation in the box "Camera/Drive Unit No," on NOAA Form 76-15.

RC-8 (Wild) exposed film - title so that exposure number is located inside top right corner of frame as viewed with related instruments (clock, exposure number) to the right of the frame.

RC-10 (Wild) exposed film - title so that exposure number is located inside top right corner of frame as viewed with recorded exposure number at the top left side of frame.

8. Codes and Related Specifications - A code category (A through L) system is used by NOS to enable the laboratory technician to produce a product in accordance with NOS requirements and specifications. The code category for each task will be noted in the code category block appearing in the top portion of the NOAA Form 76-16, or in the QC column located on the bottom portion of the computer/ telephone hookup requisition.

All densitometric values will be obtained outside of areas containing sun spots, snow, or dense shadows unless otherwise stated on NOAA Form 76-16.

Codes and related specifications are as follows:

Code A - Photographs to be of generally good photographic quality for general distribution and not for a specified NOS requirement. Color and Black & White prints or diapositives as compared to the original, having a shift of not more than 0.10 correction will be accepted.

| B&W | D Minimum | D Maximum |
|---|---|---|
| Prints | 0.25 | 1.30 |
| Diapositives | 0.25 | 1.35 |
| Color | | |
| Prints | 0.15 | 1.90 |
| Diapositives | 0.15 | 1.90 |

Code B - Color prints or transparency to match original film. Change in color balance (fidelity) compared to original not to exceed the value of a 0.05 color correction.

"V" D minimum not less than 0.15
"V" D maximum not to exceed 1.90

Code C - Color print or transparency with color fidelity to be improved over original (i.e., remove a general color overcast, or, for infrared color,accent the reds, etc.). Desired correction may be stated on NOAA 76-16

Code D - Photographs to be used for shoreline delineation, sharp contrast between water and beach, holding detail in beach. B&W infrared contact prints shall be made on an electronic printer set in a no-dodge mode. B&W infrared ratio prints shall be made with no dodging. B&W infrared - water portions outside of any sun spot area shall range in density from an average of V 2.61 (step 18) to a density of V 0.50 (± 0.15) in white sand or beach. These specifications are valid only when read on print film on a transmission densitometer.

Specific user requirements may cause a variation in the above specified print densities.

Code E - Color photographs to be used for water penetration; maximum detail in underwater areas. A color shift equal to the value of a 0.05 color correction or as specified, will be acceptable.

| | | WATER | LAND |
|---|---|---|---|
| ITEM | D MIN. | D MAX. | D MAX. |
| CONTACT PRINTS | 0.7 | 1.00 | 1.50 |
| DIAPOSITIVES | 0.5 | 0.90 | 1.40 |

D minimum shall not be less, nor D maximum more, than specified.

Code F - Photographs to be used for exhibit; highest photographic quality as to display requirements, uniform tone maximum image detail, normal color rendition, etc.

Code G - Special cropping of photograph is required, a copy of the photograph with the specifications will be sent with requisition.

Code H - Photograph requires special filtering to enhance specific details as per instructions on NOAA 76-16 (i.e., generally in producing black and white negative from color transparencies).

Code I - Prior to printing, consultation with user is requested.

Code J - Airport survey quality with maximum detail sharpness of trees, buildings, towers, runways, taxi strips, runway markings, etc. Runway numbers must be visible. Individual tall images must be retained.

| Material | D MIN. | D MAX. |
|---|---|---|
| B/W contact prints | 0.20 | 1.30 |
| B/W diapositives | 0.25 | 1.40 |
| B/W ratio prints | 0.20 | 1.30 |

D minimum shall not be less, nor D maximum exceed, that specified.

Code K - Paper negatives from color transparencies; Paper negative contrast and density shall be such as to present a reasonable paper negative, not for reproduction purpose, but used to photo-identify general land features for checking flight line coverage.

Code L - Aerial Film Processing to be in accordance to instructions stated on NOAA Form 76-15 and NOS requirements and specifications.

9. Aerial Film Processing, Requirements and Specifications

a. Exposed, unprocessed aerial film shall be shipped directly to the contractor for processing. The film will be in a sealed container as supplied by the film manufacturer. Each container will have listed on the manufacturer's label the camera identification letter and a number corresponding to the consecutive number identifying the NOAA Form 76-15 Photographic Flight Report (see Attachment II) accompanying each roll. Each roll of processed film shall be returned to NOS in its original container. Film rolls shall not be interchanged or placed in new containers without authorization by the NOS COTR. The Flight Report will accompany each roll and shall be returned as a part of the processed film shipment to NOS. The COTR will assign the "SPOT NUMBER" (file locator number) to processed roll before it is returned to the contractor.

b. The contractor will furnish any labels he deems necessary for NOS to affix to film containers listing preprocessing information.

c. Aerial film shall be processed in chemistry formulated as stipulated by the film manufacturer (Kodak Data for Aerial Photography Manual M-29). No change to an alternate formula shall be made by the contractor unless approved by the NOS COTR or an authorized representative.

d. Determination of the exposure setting for film used by NOS is based on strictly controlled processing to produce a specified gamma for black and white film, or a specified density range for color film. The formula and time (through speed) for development and processing temperature used to obtain the given processed film specifications shall be defined as a "Standard" for processing a particular film type. Processing to a standard applies to color films only. A deviation from this standard may be requested by NOS to adjust for over or under exposure of the aerial film and shall be so stated in the Photographic Flight Report under "Recommendations" and on the contractor's labels. The exception to this is Aerocolor Negative 2445, where testing and extended development is not permitted. Black and white aerial films are processed to developed sensi-strips that the lab technician has cut from unexposed film at the trailing end of the roll. The through speed and temperature are derived from this sensi-strip that renders the specified gamma for the particular black and white film type. This sensi-strip will be returned as part of the processed film shipment.

e. Prior to processing a roll of aerial film the contractor shall expose a controlled calibrated sensitometric gray scale, having a minimum of eleven steps, on the film leader of each roll. Length of unexposed leader for this purpose will be noted in the Photographic Flight Report accompanying each roll.

f. Extra exposures for test development purposes (excluding Aerocolor 2445) may be exposed on the trailing end of the roll by the aerial photographer. The number of extra exposures, if any, will be noted in the Photographic Flight Report. If the roll contains no extra exposures the film will be processed under "standard" conditions unless stated otherwise under Recommendations, Photographic Flight Report. On rolls containing extra exposures the contractor, before processing an entire roll, shall cut as many of the extra exposures as needed to process as test samples for processing control. The samples shall be inspected and the contractor at his discretion will adjust the processing procedure to obtain a product meeting NOS specifications, or, the best possible product under circumstances of extreme over or under exposure by the photographer. Samples shall be taped to end of roll and delivered as a part of the roll to the COTR.

g. Aerial Film Processing Record, Laboratory Development Section, NOAA Form 76-15 shall be completed by the contractor.

h. Densitometric Specifications - Original aerial roll film shall be processed to the following:

1. Black and White (Standard)

| Film | Base Fog Not to Exceed | D Minimum Above Base Fog | D Maximum Not to Exceed | Gamma |
|---|---|---|---|---|
| 2402 | 0.10 | 0.20 ± 0.10 | 1.35 | 0.9 ± 0.05 or 1.2 ± 0.05 |
| 150PE | 0.12 | 0.20 ± 0.10 | 1.35 | 1.2 ± 0.05 |
| 2424 | 0.18 | 0.20 ± 0.10 | 1.45 | 1.9 ± 0.05 |

2. Color

| | STANDARD DEVELOPMENT | | | | | | FORCED DEVELOPMENT | | | |
|---|---|---|---|---|---|---|---|---|---|---|
| | BASE ± 0.10 | | | | SCENE "V" READOUT | | BASE ± 0.10 | | | |
| Film | V | C | M | Y | MIN | MAX | V | C | M | Y |
| 2443 | 2.87 | 2.85 | 2.85 | 3.05 | 0.16 | 2.05 | 2.70 | 2.70 | 2.55 | 2.65 |
| | | | | | 0.10 | 0.10 | | | | |
| | | | | | -0.05 | -0.10 | | | | |
| 2448 | 3.25 | 3.27 | 3.12 | 3.00 | 0.20 | 1.95 | 3.02 | 3.00 | 2.95 | 2.90 |
| | | | | | 0.10 | 0.10 | | | | |
| | | | | | -0.05 | -0.10 | | | | |
| 2445 | 0.25 | 0.24 | 0.25 | 0.20 | 0.20 | 1.46 | | | | |
| | | | | | 0.10 | 0.10 | | | | |
| | | | | | -0.05 | 0.10 | | | | |

Proper allowances will be made for the presence of sun spots, dark water bodies, deep shadows or snow fields if, in the opinion of the COTR, the contractor has exercised reasonable care to assure that the negatives (or positives) meet the requirements of density.

i. Residual Silver Test and Archival Assurance Test (reference Kodak Data for Aerial Photography Manual M-29) shall be made by the contractor and retained as a part of the roll. Negative test result shall be cause for rejection of the task.

C. Equipment Specifications/Description

1. Glass Surfaces - Stage plates for contact prints and negative carrier surfaces for enlargers shall be clean, free of dirt, dust, fingerprints, scratches or matter that would cause photo image deformation or film damage.

2. Contact Printer

a. Shall be an electronic automatic dodge and exposure printer with the capability to print in a no-dodge mode.

b. Platen pressure shall be adjusted to ensure positive contact over entire printing surface. (Note - a micro-flat glass sandwiched between airbag and print

medium must be used to ensure proper contact to film for the printing of all diapositives.

c. Glass printing surface (Stage plate) induced distortion not to exceed 10 micrometers measured diagonally across the printed surface.

d. Printing light source (Cathode ray tube) as dictated by printing material. (Note - full spectrum light source shall be used to produce black and white negatives from color transparencies.)

3. Ratio printer (Enlarger)

a. 10 x 10 format negative carrier.

b. Negative Carrier free of heat that would damage negative (transparency).

c. Distortion free, color corrected lens - Schneider Componon 300 mm or equivalent.

d. Lens axis perpendicular to negative carrier and easel.

e. Negative carrier parallel to easel.

f. Vacuum easel to take up to, and including, 40" x 40" stock.

g. Vacuum easel flat within 0.5 mm over whole surface.

h. .9X to 5X enlarging capability.

i. Accuracy of ratio scale to 0.01X and interpolated to within ±0.001X.

j. Ratio printer shall be free of building and equipment induced vibration.

4. Aerial film processing equipment

a. Film processed in an approved system that meets photogrammetric standards (i.e., low torque, controlled drying, uniform development, etc.).

b. Capability for adjusting development to compensate for over/under exposure.

5. Densitometer - The densitometer for reading black and white and color values shall be calibrated and maintained to equipment manufacturer's specifications. The equipment shall have a range of 0 to 3.00 with an accuracy of ±0.02.

6. Film Titling Machine - To title aerial film, a mechanical ink drafting device approved by the COTR, shall be used. This device must not cause any deformation to the film. A heat imprinting machine is not an acceptable technique. Height of character(s) not to exceed 3/16 inch.

D. Photographic Printing Material

Materials are to be the brand name as listed, or equivalent.

1. Paper Prints - black and white
   a. Kodak Kodabrome II or Kodak Polyfiber DW N (semi-matt)
   b. Kodak Kodabrome II or Kodak Polyfiber DW F (glossy)
   c. Kodak Panalure

2. Print Film
   a. Dupont Cronapaque or
   b. Eastman Type S0191

3. Film
   a. Kodak Aerographic Duplicating Type 4421
   b. Kodak Direct Negative Type LPD-4
   c. Kodak Separation Negative type 4131/4133

4. Color
   a. Ciba Print P-3 CPS 462
   b. Ciba transparency CTD 661
   c. Kodak Ektacolor Plus
   d. Kodak Vericolor Print Film
   e. Kodak Ektacolor print Film
   f. Kodak Aerochrome Duplicating
   g. Kodak Duratrans

5. Aerial film supplied by NOS, processed by contractor
   a. Plus X type 2402, 250' roll
   b. Agfa 150 PE, 250' roll
   c. Infrared type 2424, 250' roll
   d. Color M. S. Type 2448, 125' roll and 200' roll
   e. Color Infrared type 2443, 125' roll
   f. Color Aerocolor Negative Film, Type 2445, 125' roll and 200' roll.

6. Additional photographic materials for Special Projects activities may differ from the materials listed above. These materials will be furnished by NOS.

# APPENDIX D

## B and G Cone Lens Calibration

Camera Calibration Report Wild RC10 SN 1777 (B)

Camera type: Wild RC10 Camera serial no. 1777 (B)

Lens type: Wild Universal Aviagon II Lens serial no. UAg II 3043

Nominal focal length: 153 mm Maximum aperture: f/4

Effective date: June, 1988 Test aperture: f/4

| Fiducials: | No. | Xf (microns) | Yf(microns) |
|---|---|---|---|
| | F001 | 106000 | 105996 |
| | F002 | 105992 | -106003 |
| | F003 | -106003 | -106000 |
| | F004 | -106000 | 106000 |
| | F005 | 0 | 109989 |
| | F006 | 109996 | -7 |
| | F007 | -3 | -110001 |
| | F008 | -109999 | -1 |

| | | | |
|---|---|---|---|
| Principal distance: | | 152717.9 | +/- 3.0 |
| Principal point coordinates | Xp | 0.0 | +/- 2.1 |
| | Yp | 0.0 | +/- 3.3 |

Radial lens distortion:

| | | |
|---|---|---|
| K1 = | -0.57870819D-13 | +/- 0.85032550D-14 |
| K2 = | 0.58376533D-23 | +/- 0.10616050D-23 |
| K3 = | -0.18880698D-33 | +/- 0.37862235D-34 |

Tangential lens distortion:

| | | |
|---|---|---|
| K4 = | -0.13530654D-10 | +/- 0.88711529D-10 |
| K5 = | -0.20687093D-20 | +/- 0.36265628D-20 |
| PHI = | 068 42 05.6510 | +/- 039 34 41.7837 |

Standard deviation of unit weight: +/-0.75
Degrees of freedom: 197

Format and fiducials:

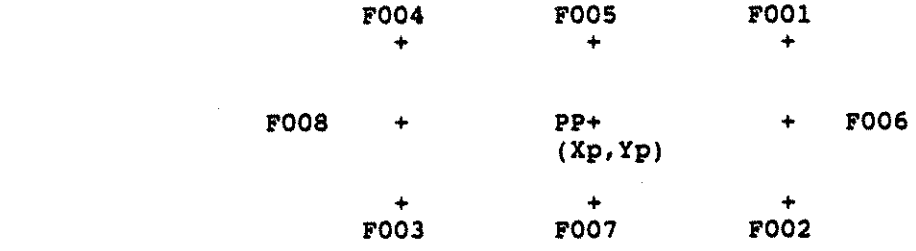

NOAA G CONE 15/4
CAMERA ORIENTATION PARAMETER DATA
ORIENTATION ANGLES FROM PRE STARS

| | ALPHA (GRADS) | OMEGA (GRADS) | KAPPA (GRADS) |
|---|---|---|---|
| ORIGINAL PARAMETERS | 0.1579292+000 | 0.1999144+003 | 0.8507176+002 |
| COMPUTED PARAMETERS | 0.1582592+000 | 0.1993100+003 | 0.8507767+002 |
| WEIGHTS (DIAGONAL) | 0.0000000 | 0.0000000 | 0.0000000 |
| RESIDUALS | 0.0000000 | 0.0000000 | 0.0000000 |
| CORRECTIONS | 0.3252718-003 | -0.6154995-003 | 0.5214792-002 |
| MEAN ERRORS OF UNKNOWNS | 0.1927410-003 | 0.1831462-003 | 0.1461923-003 |

ORIENTATION ANGLES FROM POST STARS

| | ALPHA (GRADS) | OMEGA (GRADS) | KAPPA (GRADS) |
|---|---|---|---|
| ORIGINAL PARAMETERS | 0.1579292+000 | 0.1999144+003 | 0.8507176+002 |
| COMPUTED PARAMETERS | 0.1574488+000 | 0.1993112+003 | 0.8507690+002 |
| WEIGHTS (DIAGONAL) | 0.0000000 | 0.0000000 | 0.0000000 |
| RESIDUALS | 0.0000000 | 0.0000000 | 0.0000000 |
| CORRECTIONS | -0.4853970-003 | -0.1833943-003 | 0.5138056-002 |
| MEAN ERRORS OF UNKNOWNS | 0.1081006-003 | 0.1790528-003 | 0.1284698-003 |

ORIENTATION ANGLES FROM EVENT STARS

| | ALPHA (GRADS) | OMEGA (GRADS) | KAPPA (GRADS) |
|---|---|---|---|
| ORIGINAL PARAMETERS | 0.1573232+000 | 0.1999144+003 | 0.8507176+002 |
| COMPUTED PARAMETERS | 0.1578377+000 | 0.1999109+003 | 0.8507712+002 |
| WEIGHTS (DIAGONAL) | 0.0000000 | 0.0000000 | 0.0000000 |
| RESIDUALS | 0.0000000 | 0.0000000 | 0.0000000 |
| CORRECTIONS | -0.9145425-004 | -0.4545146-003 | 0.5363863-002 |
| MEAN ERRORS OF UNKNOWNS | 0.1864759-003 | 0.1789757-003 | 0.1241678-003 |

| | EPSILON(GRADS) | XP | YP | CX | CY |
|---|---|---|---|---|---|
| ORIG PARAM | 0.4899689-003 | 0.1518662-004 | -0.8383916-005 | 0.1533035+000 | 0.1533039+000 |
| COMP PARAM | 0.4868770-003 | 0.1529726-004 | -0.8695521-005 | 0.1532992+000 | 0.1532998+000 |
| WEIGHTS | 0.0000000 | 0.0000000 | 0.0000000 | 0.0000000 | 0.0000000 |
| RESIDUALS | 0.0000000 | 0.0000000 | 0.0000000 | 0.0000000 | 0.0000000 |
| CORR'TNS | -0.3091945-005 | 0.1196374-006 | -0.3016052-006 | -0.4742670-005 | -0.4022529-005 |
| MEAN ERR | 0.1343000-003 | 0.5000330-006 | 0.5251150-006 | 0.1509016-005 | 0.1500497-005 |

| | DELTA X | DELTA Y | K1 | K2 | K3 |
|---|---|---|---|---|---|
| ORIG PARAM | 0.0000000 | 0.0000000 | -0.3037093-001 | 0.2642819+001 | -0.7242471+002 |
| COMP PARAM | -0.1016710-020 | -0.3853800-025 | -0.2600510-001 | 0.2200431+001 | -0.5842135+002 |
| WEIGHTS | 0.1000000+022 | 0.1000000+022 | 0.0000000 | 0.0000000 | 0.0000000 |
| CORR'TNS | 0.0000000 | 0.0000000 | 0.4365834-002 | -0.4423081+000 | 0.1394326+002 |
| MEAN ERR | 0.9698081-016 | 0.9680881-016 | 0.3433167-002 | 0.3608717+000 | 0.1212901+002 |

# APPENDIX E

## Final Iteration of G Cone System Calibration

CAMERA CALIBRATION OF THE NOAA G CONE CAMERA
NO. OF PHOTOS: 10
NO. OF CONTROL POINTS: 30
DEGREES OF FREEDOM: 253
NO. OF CYCLES: 10
VARIANCE OF UNIT WEIGHT = 0.86791E+00

RESULTS
INTERIOR ORIENTATION

| | X | Y | Z |
|---|---|---|---|
| | 0.105503E-01 | 0.260380E-01 | -0.153220E+03 |
| STD ERR | 0.573182E-02 | 0.586389E-02 | 0.505075E-02 |
| WEIGHT | 0.000000E+00 | 0.000000E+00 | 0.000000E+00 |
| | K1*10**-6 | K2*10**-12 | K3*10**-18 |
| | 0.105497E-01 | 0.342287E+00 | -0.143612E+02 |
| STD ERR | 0.128249E-01 | 0.151198E+01 | 0.533850E+02 |
| WEIGHT | 0.000000E+00 | 0.000000E+00 | 0.000000E+00 |
| | P1*10**-6 | P2*10**-12 | P3*10**-18 |
| | -0.275275E+00 | -0.363645E+06 | -0.382223E+14 |
| STD ERR | 0.171840E+00 | 0.158873E+06 | 0.896076E+13 |
| WEIGHT | 0.000000E+00 | 0.000000E+00 | 0.000000E+00 |

COVARIANCE/VARIANCE/CORRELATION COEFFICIENT MATRIX

ROW 1

| | | | |
|---|---|---|---|
| 0.100000E+01 | 0.154644E+00 | 0.778342E-01 | -0.139224E+00 |
| 0.184875E+00 | -0.220379E+00 | -0.823857E+00 | -0.371919E-01 |
| 0.309142E+00 | -0.126318E+00 | 0.160524E+00 | -0.110062E+00 |
| 0.533257E-02 | 0.583703E+00 | 0.674828E+00 | -0.118842E+00 |
| 0.220210E+00 | -0.606652E-02 | 0.318072E-01 | 0.588462E+00 |
| 0.672335E+00 | -0.414460E-01 | 0.923730E-01 | 0.297156E-01 |
| -0.191914E+00 | 0.580564E+00 | 0.668269E+00 | 0.956603E-02 |
| 0.793816E-01 | 0.649453E-01 | -0.138162E+00 | 0.584451E+00 |
| 0.668986E+00 | 0.336796E-01 | -0.456705E-01 | -0.133025E+00 |
| 0.223694E+00 | -0.470351E+00 | -0.673756E+00 | 0.552897E-01 |
| -0.399508E-01 | -0.317209E-01 | 0.168346E+00 | -0.488121E+00 |
| -0.652823E+00 | 0.701045E-01 | -0.740240E-01 | 0.909743E-01 |
| 0.832955E-01 | -0.487143E+00 | -0.630234E+00 | -0.944971E-02 |
| 0.100894E-01 | 0.108856E-01 | 0.188669E+00 | 0.560044E+00 |
| 0.679951E+00 | -0.182539E-01 | 0.327260E-01 | 0.295399E-01 |
| 0.193588E+00 | 0.552778E+00 | 0.680443E+00 | -0.215070E-01 |
| -0.183070E-01 | 0.256861E-01 | 0.140233E+00 | 0.556487E+00 |
| 0.666733E+00 | | | |

ROW 2

| | | | |
|---|---|---|---|
| 0.519768E-05 | 0.100000E+01 | -0.104980E+00 | 0.150835E+00 |
| -0.171798E+00 | 0.186239E+00 | -0.119436E-01 | -0.780823E+00 |
| 0.456254E+00 | -0.173855E+00 | -0.111444E+00 | -0.779005E-01 |
| 0.146057E+00 | 0.744134E+00 | -0.416805E+00 | -0.193885E+00 |
| -0.156376E+00 | -0.781535E-01 | 0.561001E-01 | 0.745352E+00 |
| -0.420551E+00 | -0.738475E-01 | -0.742900E-01 | -0.909967E-01 |
| -0.128460E+00 | 0.749544E+00 | -0.411346E+00 | -0.163340E-01 |
| -0.390595E-01 | -0.254201E-01 | -0.278675E+00 | 0.737384E+00 |
| -0.398913E+00 | 0.227896E-01 | 0.555252E-01 | 0.239927E-01 |
| 0.155774E+00 | -0.754239E+00 | 0.305778E+00 | 0.708926E-01 |
| 0.149664E-01 | 0.685399E-01 | -0.168709E-01 | -0.759912E+00 |
| 0.343387E+00 | 0.368083E-01 | -0.492369E-02 | 0.109275E-01 |
| -0.110063E+00 | -0.743167E+00 | 0.343074E+00 | -0.545127E-01 |
| -0.204100E-01 | 0.349653E-01 | 0.993416E-01 | 0.754454E+00 |
| -0.402330E+00 | -0.236430E-01 | -0.296598E-01 | 0.855318E-01 |
| 0.171646E-01 | 0.762751E+00 | -0.412329E+00 | -0.212784E-01 |
| 0.219722E-01 | 0.186469E-01 | -0.111029E+00 | 0.748108E+00 |
| -0.408107E+00 | | | |

ROW 3

| | | | |
|---|---|---|---|
| 0.225330E-05 | -0.310919E-05 | 0.100000E+01 | -0.910614E+00 |
| 0.829700E+00 | -0.759570E+00 | -0.787779E-01 | 0.354945E-01 |
| -0.102915E+00 | -0.296270E-01 | -0.200597E-01 | -0.520108E-01 |
| -0.134813E-01 | -0.592628E-01 | 0.136878E+00 | 0.236947E-01 |
| -0.727587E-02 | -0.103243E+00 | 0.410550E-02 | -0.368654E-01 |
| 0.139619E+00 | 0.127849E-02 | 0.242633E-01 | -0.103685E+00 |
| 0.421273E-02 | -0.403420E-01 | 0.118165E+00 | 0.602352E-02 |
| 0.228916E-01 | -0.538864E-01 | -0.851536E-02 | -0.358423E-01 |
| 0.116189E+00 | 0.199578E-01 | -0.372135E-01 | -0.114068E+00 |
| 0.202347E-01 | 0.651823E-01 | -0.768691E-01 | -0.463987E-01 |
| 0.119897E-01 | -0.673780E-01 | 0.627944E-01 | 0.296378E-01 |
| -0.971381E-01 | 0.100396E-01 | 0.147852E-01 | -0.681458E-01 |
| 0.370411E-01 | 0.469722E-01 | -0.112579E+00 | 0.235084E-01 |
| -0.232639E-01 | -0.129613E+00 | 0.270117E-02 | -0.210511E-01 |
| 0.122481E+00 | -0.629412E-02 | -0.135446E-01 | -0.141938E+00 |
| 0.220307E-01 | -0.381509E-01 | 0.115884E+00 | -0.167924E-01 |
| 0.453595E-02 | -0.123442E+00 | 0.838676E-02 | -0.418690E-01 |
| 0.111382E+00 | | | |

```
 ROW  4
-0.102344E-04   0.113434E-04  -0.589855E-04   0.100000E+01
-0.977652E+00   0.936268E+00   0.146280E+00  -0.415932E-01
 0.106497E+00   0.377448E-01   0.238316E-01  -0.986796E-01
 0.203460E-01   0.570941E-01  -0.221034E+00  -0.350288E-01
 0.735241E-03  -0.629927E-01   0.178906E-02   0.230501E-01
-0.220517E+00  -0.408240E-02  -0.255702E-01  -0.270784E-01
-0.316862E-02   0.330508E-01  -0.188235E+00  -0.527113E-02
-0.299172E-01  -0.260153E-01  -0.701576E-02   0.326259E-01
-0.174133E+00  -0.349495E-01   0.479148E-01   0.634993E-01
-0.251136E-01  -0.809767E-01   0.142000E+00   0.389606E-01
-0.135234E-01   0.175097E-01  -0.660448E-01  -0.441127E-01
 0.169789E+00  -0.132355E-01  -0.203941E-01  -0.288944E-02
-0.524417E-01  -0.559587E-01   0.183263E+00  -0.361385E-01
 0.254756E-01   0.229839E-01  -0.170467E-01   0.174811E-01
-0.197591E+00   0.133149E-01   0.104663E-01   0.521543E-01
-0.285392E-01   0.447614E-01  -0.192767E+00   0.146392E-01
 0.508852E-02   0.374034E-01  -0.191860E-01   0.459748E-01
-0.185836E+00

 ROW  5
 0.160220E-02  -0.152318E-02   0.633613E-02  -0.189578E-01
 0.100000E+01  -0.988042E+00  -0.189106E+00   0.657198E-01
-0.998515E-01  -0.489612E-01  -0.305711E-01   0.967850E-01
-0.211080E-01  -0.544755E-01   0.278926E+00   0.344533E-01
 0.493178E-03   0.731318E-01  -0.364356E-02  -0.125938E-01
 0.275566E+00  -0.542734E-02   0.182842E-01   0.288562E-01
-0.163579E-02  -0.286849E-01   0.240460E+00   0.631286E-02
 0.182572E-01   0.247646E-01   0.152951E-01  -0.225613E-01
 0.227017E+00   0.370910E-01  -0.640443E-01  -0.703940E-01
 0.305651E-01   0.791046E-01  -0.175248E+00  -0.356262E-01
 0.676566E-02  -0.394015E-01   0.684970E-01   0.424328E-01
-0.211894E+00   0.106018E-01   0.178123E-01   0.169093E-01
 0.583395E-01   0.476618E-01  -0.226160E+00   0.510597E-01
-0.187849E-01  -0.159663E-01   0.303710E-01  -0.447509E-02
 0.239326E+00  -0.157311E-01  -0.457050E-02  -0.678951E-01
 0.342816E-01  -0.408056E-01   0.240003E+00  -0.358284E-02
-0.131557E-01  -0.233254E-01   0.288221E-01  -0.335163E-01
 0.235628E+00

 ROW  6
-0.674344E-01   0.583010E-01  -0.204806E+00   0.641025E+00
-0.797521E+02   0.100000E+01   0.225259E+00  -0.858173E-01
 0.989937E-01   0.513800E-01   0.412219E-01  -0.961084E-01
 0.218645E-01   0.479980E-01  -0.326549E+00  -0.355565E-01
 0.864195E-03  -0.891783E-01   0.425864E-02   0.323134E-02
-0.319027E+00   0.904011E-02  -0.184686E-01  -0.282604E-01
 0.581631E-02   0.225586E-01  -0.277356E+00  -0.796357E-02
-0.143632E-01  -0.223400E-01  -0.212897E-01   0.132544E-01
-0.265333E+00  -0.354702E-01   0.698114E-01   0.764241E-01
-0.347523E-01  -0.741438E-01   0.205887E+00   0.297439E-01
-0.208521E-02   0.542912E-01  -0.705882E-01  -0.414954E-01
 0.244592E+00  -0.161102E-01  -0.107506E-01  -0.272618E-01
-0.612043E-01  -0.446606E-01   0.255585E+00  -0.616622E-01
 0.146646E-01   0.105799E-01  -0.410617E-01  -0.648439E-02
-0.271719E+00   0.200589E-01   0.150681E-02   0.800249E-01
-0.391357E-01   0.377604E-01  -0.276666E+00  -0.198716E-02
 0.180580E-01   0.169728E-01  -0.373138E-01   0.239654E-01
-0.272684E+00
```

```
 ROW  7
-0.811461E-03  -0.120349E-04  -0.683728E-04   0.322376E-03
-0.491332E-01   0.206645E+01   0.100000E+01   0.123398E-01
 0.322829E-02   0.473172E-01  -0.590339E-01   0.474679E-01
 0.182821E-01  -0.454930E+00  -0.715595E+00   0.246818E-01
-0.965999E-01  -0.462247E-01  -0.280914E-01  -0.460683E+00
-0.719084E+00  -0.145237E-01  -0.198907E-01  -0.207658E-01
 0.105039E+00  -0.448082E+00  -0.684474E+00  -0.317094E-01
-0.117312E-01   0.219791E-01   0.516905E-01  -0.442250E+00
-0.674160E+00  -0.113536E-01  -0.658324E-02   0.770982E-01
-0.128760E+00   0.345935E+00   0.681610E+00  -0.169867E-01
-0.332450E-02   0.262161E-01  -0.109262E+00   0.363273E+00
 0.659105E+00  -0.554026E-01   0.311724E-01  -0.497970E-01
-0.871407E-01   0.343191E+00   0.624396E+00  -0.268762E-01
 0.677437E-01  -0.422390E-01  -0.104119E+00  -0.423576E+00
-0.705852E+00  -0.527760E-01   0.597564E-01  -0.544631E-01
-0.135023E+00  -0.432045E+00  -0.709269E+00  -0.972867E-02
 0.555821E-01   0.278832E-01  -0.117538E+00  -0.415788E+00
-0.663031E+00

 ROW  8
-0.338680E+02  -0.727423E+03   0.284817E+02  -0.847474E+02
 0.157867E+05  -0.727853E+06   0.336883E+03   0.100000E+01
-0.102352E+00   0.832749E-01   0.747873E-01  -0.161835E-01
-0.490742E-01  -0.614270E+00   0.440223E+00   0.738638E-01
 0.817174E-01   0.391085E-02  -0.713067E-02  -0.620602E+00
 0.456808E+00  -0.347682E-01   0.450069E-02   0.107544E-02
 0.507596E-01  -0.632281E+00   0.444048E+00  -0.454672E-01
-0.235034E-01  -0.588998E-02   0.150199E+00  -0.609604E+00
 0.439707E+00   0.225111E-01  -0.157442E-01   0.831622E-02
-0.665183E-01   0.626068E+00  -0.334573E+00  -0.171314E-01
 0.205091E-01  -0.460639E-01   0.363881E-01   0.628398E+00
-0.372335E+00   0.778811E-02   0.229449E-01   0.284749E-01
 0.804610E-01   0.600128E+00  -0.360028E+00   0.174039E-01
-0.209457E-01   0.326428E-01  -0.488587E-01  -0.596524E+00
 0.413198E+00  -0.588957E-01  -0.231531E-01  -0.612409E-01
 0.894735E-02  -0.630893E+00   0.436697E+00  -0.283371E-01
-0.609295E-01   0.445644E-01   0.945449E-01  -0.602173E+00
 0.425232E+00

 ROW  9
 0.158780E+11   0.239738E+11  -0.465779E+10   0.122388E+11
-0.135284E+13   0.473556E+14   0.497097E+10  -0.145711E+18
 0.100000E+01  -0.306735E-01   0.426890E-01  -0.184889E-01
 0.116039E+00   0.483069E+00  -0.454733E-01  -0.324392E-01
 0.663123E-03  -0.635830E-01   0.587090E-01   0.490297E+00
-0.250074E-01   0.909731E-02   0.402978E-02   0.279551E-02
-0.163494E+00   0.466128E+00  -0.231509E-01   0.101738E-01
 0.257988E-01   0.243486E-01  -0.211734E+00   0.443532E+00
-0.205347E-01  -0.126410E-01   0.237801E-01   0.120588E-01
 0.188040E+00  -0.431118E+00  -0.278932E-01   0.370813E-02
 0.426504E-01   0.365435E-02   0.279112E-01  -0.452447E+00
-0.435753E-01  -0.728671E-01  -0.143454E-01  -0.561796E-02
-0.752345E-01  -0.486269E+00  -0.122783E-01   0.154936E-01
-0.101531E-01   0.371049E-01   0.137545E+00   0.458061E+00
-0.139743E-01  -0.560935E-01  -0.119402E-01  -0.365386E-01
 0.598132E-01   0.417840E+00  -0.312700E-02   0.172164E-01
-0.970727E-02   0.221703E-01  -0.195163E-01   0.446881E+00
-0.452668E-02
```

## EXTERIOR ORIENTATION

PHOTO NO. 1

| XO | YO | ZO | KAPPA | PHI | OMEGA |
|---|---|---|---|---|---|
| 6424.667 | 6042.129 | 2058.485 | 2.18766 | -0.01002 | 0.00048 |
| STD. ERROR | | | | | |
| 0.040 | 0.039 | 0.022 | 0.00001 | 0.00004 | 0.00004 |
| WEIGHT | | | | | |
| 400.000 | 400.000 | 625.000 | 0.00000 | 0.00000 | 0.00000 |

### RESIDUALS ON CONTROL POINTS
(PHOTO CO-ORDINATE UNITS)

| POINT NO. | RESIDUALS IN X | RESIDUALS IN Y |
|---|---|---|
| 24 | 0.229753E-02 | 0.149228E-02 |
| 9 | -0.103429E-02 | 0.353674E-02 |
| 23 | 0.685215E-03 | -0.291992E-02 |
| 8 | 0.391643E-02 | 0.344239E-02 |
| 17 | 0.465345E-03 | 0.995935E-02 |
| 16 | -0.211359E-02 | -0.486052E-02 |
| 15 | -0.159011E-02 | -0.697199E-02 |
| 26 | 0.223239E-02 | -0.456148E-02 |
| 13 | -0.271681E-02 | 0.154735E-02 |
| 25 | -0.231364E-02 | -0.919570E-03 |
| 2 | 0.147845E-02 | -0.232864E-02 |
| 3 | 0.174915E-02 | -0.224489E-02 |
| 4 | 0.217707E-02 | 0.133193E-02 |
| 5 | -0.217559E-02 | 0.350190E-02 |
| 6 | -0.751103E-03 | 0.195442E-02 |
| 18 | -0.462795E-02 | -0.182191E-03 |
| 20 | 0.902172E-03 | -0.288697E-03 |

## EXTERIOR ORIENTATION

PHOTO NO. 2

| XO | YO | ZO | KAPPA | PHI | OMEGA |
|---|---|---|---|---|---|
| 6144.426 | 6454.215 | 2058.058 | 2.18678 | -0.00247 | -0.00391 |
| STD. ERROR | | | | | |
| 0.039 | 0.037 | 0.021 | 0.00001 | 0.00004 | 0.00004 |
| WEIGHT | | | | | |
| 400.000 | 400.000 | 625.000 | 0.00000 | 0.00000 | 0.00000 |

### RESIDUALS ON CONTROL POINTS
(PHOTO CO-ORDINATE UNITS)

| POINT NO. | RESIDUALS IN X | RESIDUALS IN Y |
|---|---|---|
| 10 | -0.973267E-03 | -0.267082E-02 |
| 9 | -0.630546E-03 | 0.973358E-03 |
| 23 | 0.231214E-02 | -0.142277E-02 |
| 8 | 0.403432E-02 | 0.158044E-02 |
| 7 | 0.406123E-04 | 0.177591E-02 |
| 1 | -0.195183E-02 | -0.863360E-03 |
| 2 | 0.383470E-03 | -0.225546E-02 |
| 3 | 0.829492E-03 | -0.297151E-02 |
| 4 | 0.442927E-02 | 0.383158E-02 |
| 5 | 0.220297E-02 | -0.350231E-02 |
| 6 | 0.242770E-02 | 0.678013E-02 |
| 16 | -0.142614E-02 | 0.260583E-02 |
| 15 | -0.555712E-02 | 0.475954E-02 |
| 14 | -0.142461E-03 | -0.691305E-03 |
| 26 | 0.297325E-02 | 0.316412E-02 |
| 13 | 0.376313E-02 | -0.102487E-02 |
| 25 | -0.237755E-02 | -0.726885E-02 |
| 12 | -0.251800E-02 | -0.986216E-03 |
| 11 | -0.518122E-02 | 0.302626E-03 |
| 18 | -0.594905E-03 | -0.261913E-02 |

## EXTERIOR ORIENTATION

PHOTO NO. 3

| XO | YO | ZO | KAPPA | PHI | OMEGA |
|---|---|---|---|---|---|
| 5837.173 | 6910.082 | 2057.866 | 2.18034 | 0.00619 | -0.01009 |
| STD. ERROR | | | | | |
| 0.040 | 0.040 | 0.024 | 0.00001 | 0.00005 | 0.00004 |
| WEIGHT | | | | | |
| 400.000 | 400.000 | 625.000 | 0.00000 | 0.00000 | 0.00000 |

## RESIDUALS ON CONTROL POINTS
(PHOTO CO-ORDINATE UNITS)

| POINT NO. | RESIDUALS IN X | RESIDUALS IN Y |
|---|---|---|
| 10 | -0.140349E-02 | -0.310730E-02 |
| 24 | -0.346994E-03 | -0.383273E-02 |
| 9 | -0.115113E-02 | -0.223344E-02 |
| 8 | 0.268548E-02 | 0.218441E-02 |
| 7 | -0.102024E-02 | 0.232649E-02 |
| 15 | 0.404112E-02 | -0.172746E-02 |
| 14 | -0.165571E-02 | 0.519629E-02 |
| 26 | -0.769617E-03 | 0.238568E-02 |
| 13 | -0.487140E-02 | 0.118375E-02 |
| 25 | -0.262438E-03 | -0.217143E-02 |
| 12 | 0.504742E-02 | -0.173033E-02 |
| 11 | -0.195800E-02 | 0.100934E-02 |
| 22 | -0.110940E-04 | -0.866051E-02 |
| 21 | -0.162785E-02 | -0.105422E-02 |
| 20 | 0.351672E-03 | 0.515833E-02 |
| 19 | -0.178906E-03 | 0.251817E-02 |
| 2 | 0.392856E-02 | 0.441780E-03 |
| 4 | 0.192120E-02 | 0.193490E-02 |

## EXTERIOR ORIENTATION

PHOTO NO. 4

| XO | YO | ZO | KAPPA | PHI | OMEGA |
|---|---|---|---|---|---|
| 5554.979 | 7338.928 | 2056.570 | 2.1724 | 0.01014 | -0.01495 |
| STD. ERROR | | | | | |
| 0.043 | 0.041 | 0.027 | 0.00002 | 0.00005 | 0.00004 |
| WEIGHT | | | | | |
| 400.000 | 400.000 | 625.000 | 0.00000 | 0.00000 | 0.00000 |

## RESIDUALS ON CONTROL POINTS
(PHOTO CO-ORDINATE UNITS)

| POINT NO. | RESIDUALS IN X | RESIDUALS IN Y |
|---|---|---|
| 7 | 0.111121E-02 | -0.187839E-02 |
| 8 | -0.380287E-02 | -0.720119E-04 |
| 23 | -0.101323E-03 | -0.354908E-02 |
| 9 | 0.418124E-02 | 0.177323E-02 |
| 24 | 0.653727E-02 | -0.142850E-02 |
| 2 | -0.633249E-02 | -0.205665E-02 |
| 3 | -0.801822E-03 | 0.309909E-02 |
| 14 | 0.537243E-02 | -0.220559E-02 |
| 26 | -0.837097E-03 | 0.577349E-03 |
| 13 | 0.255396E-02 | 0.177665E-04 |
| 25 | 0.172915E-02 | -0.718395E-02 |
| 12 | 0.746699E-03 | -0.266830E-02 |
| 11 | -0.296967E-02 | 0.378103E-02 |
| 21 | -0.603723E-02 | 0.663783E-04 |
| 20 | -0.444641E-02 | 0.936835E-02 |

## EXTERIOR ORIENTATION

PHOTO NO. 5

| XO | YO | ZO | KAPPA | PHI | OMEGA |
|---|---|---|---|---|---|
| 6500.205 | 7498.652 | 2055.832 | -1.04739 | 0.02117 | -0.00780 |
| STD. ERROR | | | | | |
| 0.053 | 0.053 | 0.027 | 0.00002 | 0.00005 | 0.00004 |
| WEIGHT | | | | | |
| 236.686 | 236.686 | 625.000 | 0.00000 | 0.00000 | 0.00000 |

## RESIDUALS ON CONTROL POINTS
(PHOTO CO-ORDINATE UNITS)

| POINT NO. | RESIDUALS IN X | RESIDUALS IN Y |
|---|---|---|
| 28 | 0.124480E-03 | -0.167642E-02 |
| 29 | -0.173936E-03 | 0.589931E-03 |
| 7 | -0.211217E-02 | -0.276789E-02 |
| 8 | 0.615066E-02 | 0.108776E-03 |
| 24 | 0.488007E-03 | -0.625152E-02 |
| 10 | -0.604541E-02 | 0.375519E-02 |
| 5 | -0.141279E-02 | 0.211917E-02 |
| 4 | 0.213801E-02 | -0.437689E-03 |
| 3 | -0.201635E-02 | 0.464876E-03 |
| 1 | 0.435865E-02 | 0.452122E-02 |

## EXTERIOR ORIENTATION

PHOTO NO. 6

| XO | YO | ZO | KAPPA | PHI | OMEGA |
|---|---|---|---|---|---|
| 6778.145 | 7065.045 | 2055.558 | -1.03757 | 0.01679 | -0.00782 |
| STD. ERROR | | | | | |
| 0.052 | 0.054 | 0.025 | 0.00002 | 0.00005 | 0.00005 |
| WEIGHT | | | | | |
| 236.686 | 236.686 | 625.000 | 0.00000 | 0.00000 | 0.00000 |

## RESIDUALS ON CONTROL POINTS
(PHOTO CO-ORDINATE UNITS)

| POINT NO. | RESIDUALS IN X | RESIDUALS IN Y |
|---|---|---|
| 29 | 0.184241E-03 | -0.559266E-03 |
| 30 | 0.354418E-03 | -0.382592E-02 |
| 10 | 0.342230E-02 | 0.423402E-02 |
| 9 | 0.503131E-02 | 0.433765E-03 |
| 23 | 0.329343E-02 | -0.259375E-02 |
| 8 | -0.211372E-02 | 0.541999E-02 |
| 7 | -0.603727E-02 | 0.122859E-02 |
| 1 | -0.590362E-03 | -0.187142E-02 |
| 4 | 0.495308E-02 | -0.192599E-02 |
| 6 | -0.435124E-02 | 0.312108E-03 |

## EXTERIOR ORIENTATION

PHOTO NO. 7

| XO | YO | ZO | KAPPA | PHI | OMEGA |
|---|---|---|---|---|---|
| 7052.102 | 6642.316 | 2056.414 | -1.03532 | -0.00262 | 0.00180 |
| STD. ERROR | | | | | |
| 0.052 | 0.054 | 0.028 | 0.00002 | 0.00005 | 0.00005 |
| WEIGHT | | | | | |
| 236.686 | 236.686 | 625.000 | 0.00000 | 0.00000 | 0.00000 |

## RESIDUALS ON CONTROL POINTS
(PHOTO CO-ORDINATE UNITS)

| POINT NO. | RESIDUALS IN X | RESIDUALS IN Y |
|---|---|---|
| 28 | -0.108729E-03 | 0.171418E-02 |
| 30 | -0.353565E-03 | 0.389612E-02 |
| 10 | -0.122761E-02 | -0.714025E-02 |
| 24 | -0.113095E-02 | -0.676556E-02 |
| 9 | 0.212424E-02 | -0.213007E-04 |
| 8 | 0.120936E-02 | 0.147869E-02 |
| 2 | -0.187029E-02 | 0.441137E-02 |
| 3 | 0.262512E-02 | -0.495519E-02 |
| 4 | 0.862826E-03 | 0.579799E-02 |
| 5 | 0.287877E-02 | 0.370092E-02 |
| 6 | -0.381441E-02 | 0.661827E-05 |

## EXTERIOR ORIENTATION

PHOTO NO. 8

| XO | YO | ZO | KAPPA | PHI | OMEGA |
|---|---|---|---|---|---|
| 5435.434 | 5683.054 | 2057.602 | 2.15605 | -0.00944 | -0.00408 |
| STD. ERROR | | | | | |
| 0.042 | 0.042 | 0.024 | 0.00002 | 0.00005 | 0.00004 |
| WEIGHT | | | | | |
| 400.000 | 400.000 | 625.000 | 0.00000 | 0.00000 | 0.00000 |

## RESIDUALS ON CONTROL POINTS
(PHOTO CO-ORDINATE UNITS)

| POINT NO. | RESIDUALS IN X | RESIDUALS IN Y |
|---|---|---|
| 27 | 0.309854E-03 | 0.165127E-02 |
| 18 | 0.184078E-03 | -0.487084E-02 |
| 19 | -0.317566E-02 | 0.330095E-02 |
| 20 | 0.136806E-02 | 0.307155E-02 |
| 21 | 0.393846E-02 | 0.966094E-03 |
| 17 | 0.540029E-02 | -0.186741E-02 |
| 16 | -0.333579E-02 | 0.328163E-02 |
| 15 | -0.413417E-02 | -0.323321E-02 |
| 14 | -0.179536E-02 | -0.445037E-02 |
| 26 | -0.122032E-02 | 0.205131E-02 |
| 25 | -0.115058E-02 | 0.171421E-02 |
| 12 | -0.221415E-03 | -0.148826E-02 |
| 10 | -0.178948E-03 | 0.580965E-02 |
| 9 | 0.269544E-02 | -0.486408E-02 |
| 23 | -0.327782E-02 | -0.229727E-02 |

## EXTERIOR ORIENTATION

PHOTO NO. 9

| XO | YO | ZO | KAPPA | PHI | OMEGA |
|---|---|---|---|---|---|
| 5162.097 | 6121.975 | 2056.853 | 2.16163 | -0.01311 | 0.00023 |
| STD. ERROR | | | | | |
| 0.041 | 0.040 | 0.024 | 0.00001 | 0.00005 | 0.00004 |
| WEIGHT | | | | | |
| 400.000 | 400.000 | 625.000 | 0.00000 | 0.00000 | 0.00000 |

## RESIDUALS ON CONTROL POINTS
(PHOTO CO-ORDINATE UNITS)

| POINT NO. | RESIDUALS IN X | RESIDUALS IN Y |
|---|---|---|
| 27 | -0.328096E-03 | -0.165445E-02 |
| 18 | -0.597261E-02 | -0.225264E-02 |
| 19 | 0.585363E-03 | -0.228240E-03 |
| 20 | 0.115664E-02 | -0.234041E-02 |
| 21 | -0.220066E-02 | -0.246687E-02 |
| 22 | 0.366003E-02 | 0.135190E-02 |
| 11 | 0.527937E-04 | -0.204390E-02 |
| 12 | -0.356038E-02 | 0.370855E-02 |
| 25 | 0.233157E-02 | 0.107827E-02 |
| 13 | -0.877914E-02 | -0.313714E-04 |
| 26 | -0.574176E-02 | 0.662621E-02 |
| 16 | 0.151597E-02 | 0.165432E-02 |
| 10 | 0.183964E-02 | 0.440457E-03 |
| 9 | 0.444432E-02 | 0.358123E-02 |
| 23 | 0.450488E-02 | 0.504869E-02 |
| 8 | 0.855416E-03 | -0.270771E-02 |
| 7 | 0.276926E-02 | -0.851703E-02 |

## EXTERIOR ORIENTATION

PHOTO NO.10

| XO | YO | ZO | KAPPA | PHI | OMEGA |
|---|---|---|---|---|---|
| 4882.293 | 6565.074 | 2055.297 | 2.167 | -0.01238 | 0.00369 |
| STD. ERROR | | | | | |
| 0.043 | 0.044 | 0.028 | 0.00002 | 0.00005 | 0.00004 |
| WEIGHT | | | | | |
| 400.000 | 400.000 | 625.000 | 0.00000 | 0.00000 | 0.00000 |

## RESIDUALS ON CONTROL POINTS
(PHOTO CO-ORDINATE UNITS)

| POINT NO. | RESIDUALS IN X | RESIDUALS IN Y |
|---|---|---|
| 10 | 0.142308E-02 | 0.132925E-02 |
| 9 | -0.200741E-03 | 0.173337E-04 |
| 23 | -0.617757E-02 | 0.588826E-02 |
| 8 | 0.134285E-03 | -0.113887E-02 |
| 7 | 0.128644E-02 | 0.111081E-02 |
| 11 | 0.669256E-03 | 0.470922E-02 |
| 25 | -0.129854E-02 | -0.380968E-02 |
| 13 | 0.453345E-03 | -0.106371E-02 |
| 26 | 0.129606E-02 | -0.263233E-02 |
| 19 | -0.302873E-02 | -0.444097E-02 |
| 20 | -0.545067E-02 | 0.290244E-02 |
| 21 | 0.678442E-02 | 0.987067E-03 |
| 22 | 0.456697E-02 | -0.577690E-02 |

FINAL VALUES FOR SURVEY CONTROL

| POINT # | X | Y | Z |
|---|---|---|---|
| 1 | 6213.772 | 7964.092 | 292.805 |
| 2 | 6457.532 | 7577.147 | 292.001 |
| 3 | 6698.477 | 7188.155 | 291.157 |
| 4 | 6938.629 | 6799.692 | 290.310 |
| 5 | 7179.437 | 6410.582 | 289.425 |
| 6 | 7419.990 | 6021.772 | 288.481 |
| 7 | 5428.687 | 7404.845 | 293.429 |
| 8 | 5671.005 | 7017.396 | 291.310 |
| 9 | 5911.397 | 6628.465 | 289.911 |
| 10 | 6152.042 | 6239.414 | 291.720 |
| 11 | 4928.876 | 7177.343 | 294.932 |
| 12 | 5169.826 | 6779.583 | 294.096 |
| 13 | 5410.111 | 6390.716 | 293.284 |
| 14 | 5658.320 | 6007.852 | 292.233 |
| 15 | 5891.641 | 5612.963 | 291.502 |
| 16 | 6137.505 | 5226.899 | 290.457 |
| 17 | 6372.890 | 4835.211 | 289.612 |
| 18 | 5611.381 | 5123.288 | 299.041 |
| 19 | 5303.796 | 5585.525 | 300.734 |
| 20 | 5017.521 | 6013.422 | 296.557 |
| 21 | 4738.956 | 6452.871 | 293.782 |
| 22 | 4480.963 | 6887.125 | 295.081 |
| 23 | 5791.109 | 6822.845 | 290.169 |
| 24 | 6031.783 | 6434.064 | 290.046 |
| 25 | 5290.011 | 6585.251 | 293.712 |
| 26 | 5534.184 | 6199.252 | 292.779 |
| 27 | 4001.179 | 5960.130 | 305.059 |
| 28 | 7113.317 | 8095.682 | 289.281 |
| 29 | 7786.494 | 7520.720 | 287.891 |
| 30 | 7858.398 | 6859.957 | 289.704 |

| PARTIAL | CORRELATION COEFFICIENT | C/Z |
|---|---|---|
| 1 | 12 -0.34570E+00 | |
| 2 | 18 -0.34109E+00 | |
| 3 | 24 -0.29008E+00 | |
| 4 | 30 -0.27574E+00 | |
| 5 | 36 -0.18248E+00 | |
| 6 | 42 -0.19667E+00 | |
| 7 | 48 -0.18515E+00 | |
| 8 | 54 -0.23084E+00 | |
| 9 | 60 -0.24918E+00 | |
| 10 | 66 -0.20799E+00 | |

CAMERA CALIBRATION OF THE NOAA G CONE CAMERA
NO. OF PHOTOS: 10
NO. OF CONTROL POINTS: 30
DEGREES OF FREEDOM: 249
NO. OF CYCLES: 10
VARIANCE OF UNIT WEIGHT = 0.93624E+00

RESULTS
INTERIOR ORIENTATION

| | X | Y | Z |
|---|---|---|---|
| | 0.248793E-03 | 0.971624E-02 | -0.153220E+03 |
| STD. ERR | 0.578757E-02 | 0.604185E-02 | 0.526738E-02 |
| WEIGHT | 0.000000E+00 | 0.000000E+00 | 0.000000E+00 |

| | K1*10**-6 | K2*10**-12 | K3*10**-18 |
|---|---|---|---|
| | 0.355604E-01 | 0.173156E+01 | 0.401192E+02 |
| STD. ERR | 0.133519E-01 | 0.157508E+01 | 0.556748E+02 |
| WEIGHT | 0.000000E+00 | 0.000000E+00 | 0.000000E+00 |

| | P1*10**-6 | P2*10**-12 | P3*10**-18 |
|---|---|---|---|
| | -0.242619E+00 | -0.354803E+06 | -0.406937E+14 |
| STD. ERR | 0.178914E+00 | 0.164400E+06 | 0.101037E+14 |
| WEIGHT | 0.000000E+00 | 0.000000E+00 | 0.000000E+00 |

Case 4 solution using image coordinates corrected only for refraction

## LIST OF REFERENCES

American Society of Photogrammetry, (1980), *Manual of Photogrammetry*, Fourth Edition, Banta Publishing Company, New York, New York.

Andersen, Oystein, (1989), "Experience With Kinematic GPS During Aerial Photography in Norway," Unpublished paper, Department of Surveying, Agricultural University of Norway, As, Norway.

Bender, Lee U., (1971), "Analytical Photogrammetry, A Collinear Theory", RADC-TR-71-147.

Bertram, S., (1966), "Atmospheric Refraction", *Photogrammetric Engineering*, Vol. 32, No. 1, pp. 76-84.

Brown, D.C., (1966), "Decentering Distortion of Lenses", *Photogrammetric Engineering*, Vol. 32, No. 5.

Brown, D.C., (1969), "Advanced Methods for the Calibration of Metric Cameras", presented at the Symposium on Computational Photogrammetry, SUNY, Syracuse University, New York.

Chin, M. Miranda, (1988), "ARGO User's Guide," Unpublished National Geodetic Survey Manual, Rockville, Maryland.

Coker, Clayton, and Clynch, James R., and Brock, Chris, (1989), "Calibration of the Exposure Status Signal from the Wild RC20 Aerial Camera," Technical Report, Applied Research Laboratories, The University of Texas, Austin, Texas.

Curry, Sean and Baumrind, Sheldon, (1986), "Calibration of an Array Camera," *Photogrammetric Engineering and Remote Sensing*, Vol. 52, No. 5, pp. 627-635.

Dixon, Wilfrid J, and Massey, Frank J., Jr, (1969), *Introduction to Statistical Analysis*, McGraw-Hill Book Company, New York, New York.

Easton, R. L. (1980), "The Navigation Technology Program," *Global Positioning System*, Volume 1, Papers published in "Navigation," The Institute of Navigation, Washington, D.C.

Fraser, C. S., (1980), "Multiple Focal Setting Self-Calibration of Close-Range Metric Cameras," *Photogrammetric Engineering and Remote Sensing*, Vol. 46, No. 9, pp. 1161-1171.

Goad, Clyde, (1989), "GPS Lecture Notes," Unpublished, Department of Geodetic Science and Surveying, The Ohio State University, Columbus, Ohio.

Gruen, A., (1978), "Experience With Self-Calibrating Bundle Adjustment," *Proceedings of the American Society of Photogrammetry*, February-March, Washington D.C.

Halliday, David, and Resnick, Robert, (1966), *Physics*, Parts I and II, John Wiley and Sons, Inc., New York, New York.

Hamilton, Walter Clark, (1964), *Statistics in Physical Science*, The Ronald Press Company, New York, New York.

Kenefick, John F., (1971), "Ultra-Precise Analytics,"*Photogrammetric Engineering*, Vol. 37, No. 11, pp. 1167-1187.

Kenefick, John F., (1972), "Analytical Self-Calibration,"*Photogrammetric Engineering*, Vol. 38, No. 11, pp. 1117-1126.

King, Michael and Durboraw, I. Newton III, (1988), "A Detailed Description of Signal Processing in Motorola's Eagle GPS Receiver," Unpublished Proprietary Report, Motorola Inc., Tempe, Arizona.

King, R. W., Masters, E. G., Rizos, C., Stolz, A., and Collins, J., (1985), *Surveying With GPS*, Monograph 9, School For Surveying, The University of New South Wales, Kensington, N.S.W. Australia.

Lapine, Lewis A., (1990), "Practical Photogrammetric Control By Kinematic GPS," *GPS World*, Vol. 1, No. 3, pp. 44-49.

Lucas, James R., (1963), "Differentiation of the Orientation Matrix by Matrix Multipliers," *Photogrammetric Engineering*, Vol. 29, No. 7, pp. 708-715.

Lucas, James, R., (1987), "Aerotriangulation Without Ground Control" *Photogrammetric Engineering and Remote Sensing*, Vol. 53, pp. 311-314.

Lucas, James, R., (unpublished), "Photogrammetric Evaluation of Airborne GPS,"

Lucas, James R. and Mader, Gerald L., (1988), "Recent Advances in Kinematic GPS Photogrammetry," *GPS 88 - Engineering Application of GPS Satellite Surveying Technology Proceedings*, American Society of Civil Engineering Symposium, Nashville, Tennessee.

Lucas, James R., (1989), "GPS-Assisted Phototriangulation Package (GAPP) User's Guide, Version 1.02," *NOAA Technical Memorandum NOS CGS 2*, Geodetic Information Center, NOAA, Rockville, Maryland.

Mader, Gerald L., (1986), "Dynamic Positioning Using GPS Carrier Phase Measurements," *Manuscripta Geodaetica*, No. 11, pp. 272-277.

Mader, Gerald L., (1990), "OMNI Users Guide," Unpublished National Geodetic Survey Manual.

Merchant, Dean C., (1971), "Metric Calibration of the Aerial Photographic System by the Method of Mixed Ranges," Department of Geodetic Science and Surveying, The Ohio State University, Columbus Ohio.

Merchant, Dean C., (1973), *Elements of Photogrammetry*, Part I - Geometric Photogrammetry, Department of Geodetic Science, The Ohio State University, Columbus, Ohio.

Merchant, Dean C., (1973), *Elements of Photogrammetry*, Part II - Computational Photogrammetry, Department of Geodetic Science, The Ohio State University, Columbus, Ohio.

Merchant, Dean C., (1988), *Analytical Photogrammetry Theory and Practice*, Fourth Edition, Parts I and II, Department of Geodetic Science, The Ohio State University, Columbus, Ohio.

Merchant, Dean C., (1989) "Positioning the Photo Aircraft by the Global Positioning System, Photogrammetric Promises and Challenges," Proceedings of the ACSM/ASPRS Spring Convention, 1989.

Merchant, Dean C., (1990), "Aerial Photographic System Calibration," Department of Geodetic Science and Surveying, The Ohio State University, Columbus, Ohio.

Mikhail, Edward M. and Ackerman, F., (1976), *Observations and Least Squares*, University Press of America Inc., Lanham, Maryland.

Mikhail, Edward M. and Gracie, Gordon, (1981), *Analysis and Adjustment of Survey Measurements*, Van Nostrand Reinhold Company, New York, New York.

Moffit, Francis H., (1967), *Photogrammetry*, Second Edition, The International Textbook Company, Scranton, Pennsylvania.

Oberg, Erik, and Jones, Franklin D., Editors, (1935), *Machinery's Handbook*, Fifth Edition, Tenth Printing, The Industrial Press, New York, New York.

Olsen, Jon, (1984), "A Systematic Error in High Altitude Photography,", Unpublished paper, Geodaetisk Institut,

Operating and Service Manual, "5316A 100Mhz Universal Counter", Hewlett Packard Corporation.

Remondi, Benjamin William, (1984), "Using the Global Positioning System (GPS) Phase Observable for Relative Geodesy: Modeling, Processing, and Results," Doctoral Dissertation, Center for Space Research, University of Texas, Austin, Texas.

Remondi, Benjamin William, (1984), "Performing Centimeter-Level Surveys in Seconds with GPS Carrier Phase: Initial Results," *NOAA Technical Memorandum NOS NGS 43*, Geodetic Information Center, NOAA Rockville, Maryland.

Saastamoinen, J., (1972), "Refraction," *Photogrammetric Engineering*, Vol. 38, No. 8, pp. 799-810.

Saastamoinen, J., (1974), "Local Variation of Photogrammetric Refraction," *Photogrammetric Engineering*, Vol. 40, No. 3, pp. 295-301.

Schut, G.H., (1969), "Photogrammetric Refraction", *Photogrammetric Engineering*, Vol. 35, No. 1, pp. 79-86.

Spilker, J. J., Jr., (1980), "GPS Signal Structure and Performance Characteristics," *Global Positioning System*, Volume 1, Papers published in "Navigation," The Institute of Navigation, Washington, D.C.

Taylor, Eugene A., (1963), "Optical Tracking System for Space Geodesy," *The Use of Artificial Satellites for Geodesy*, Proceedings of The First International Symposium on the Use of Artificial Satellites for Geodesy, North-Holland Publishing Company, Amsterdam, Holland, pp. 187-192.

Taylor, Eugene A., (1964), "Calibration of the Coast and Geodetic Survey Satellite-Tracking System," Invited Papers, The International Society for Photogrammetry, Technical Commission V, Lisbon, Portugal, pp. 13-36.

Tudhope, Robert Lorne (1988), "Dynamic Aerial Camera Calibration Combining Highly Convergent and Vertical Photography," M.S. Thesis, Department of Geodetic Science and Surveying, The Ohio State University, Columbus, Ohio.

Uotila, U. A., (1973), "Useful Statistics for Land Surveyors," *Surveying and Mapping*, March, 1973, pp. 67-77.

Uotila, U. A., (1986), *Adjustment Computation Notes*, Department of Geodetic Science, The Ohio State University, Columbus, Ohio.

User's Manual, (1984), "Wild Aviolyt BC1," Release 3.20, Wild Heerburg Limited, Switzerland.

User's Manual, (1987), "Eagle Mini-Ranger Global Positioning System Receiver," Motorola Document Number: 68-P29027U, Motorola Inc., Tempe, Arizona.

Wells, David, Editor, (1986), *Guide to GPS Positioning*, Canadian GPS Associates, The University of New Brunswick Graphic Services, Fredericton, New Brunswick.